RESONANCE RAMAN STUDIES OF MILK XANTHINE OXIDASE AND RAMAN STUDIES OF MOLYBDENUM (VI) MODEL COMPLEXES FOR MOLYBDOENZYMES

Lawrence Jack Willis
B.S., Oregon State University, 1970
M.S., Wright State University, 1977

A dissertation submitted to the faculty
of the Oregon Graduate Center
in partial fulfillment of the
requirements for the degree
Doctor of Philosophy
in
Inorganic Chemistry

June, 1982

The dissertation "Resonance Raman Studies of Milk Xanthine Oxidase and Raman Studies of Molybdenum (VI) Model Complexes for Molybdoenzymes" by Lawrence Jack Willis has been examined and approved by the following Examination Committee:

T. M. Loehr, Thesis Advisor
Professor

J. K. Hurst
Professor

W. L. Pengelly
Assistant Professor

J. F. Pankow
Associate Professor

ACKNOWLEDGMENTS

I wish to express my thanks to my research advisor, Professor Thomas M. Loehr, for helpful guidance, comments, and suggestions in my work and preparation of this dissertation. I also wish to thank Dr. William Keyes and Dr. Thomas Thamann for their instruction and discussions on running the spectrometer and computer programs. Thanks are due to Dr. Edward Stiefel for providing the molybdenum complexes which are a major part of this dissertation and to Dr. Mary Taylor and her friends at Thomas' Dairy for providing the raw buttermilk for the xanthine oxidase preparation. Also, thanks go to Steve Conradson for assistance in enzyme preparation at Stanford University. Special thanks go to Nancy Christie for typing this dissertation.

A very large measure of appreciation goes to my wife Barbara for her support over these last several years which has enabled me to finish my studies.

TABLE OF CONTENTS

Page

ACKNOWLEDGMENTS iii

LIST OF TABLES vi

LIST OF FIGURES viii

ABSTRACT xi

INTRODUCTION 1

EXPERIMENTAL 14

- I. Preparation of Milk Xanthine Oxidase 14
- II. Activity Assay for Milk Xanthine Oxidase 16
- III. Molybdenum Model Complexes 17

RESULTS AND DISCUSSION 19

- I. Molybdenum (VI) Model Complexes 19
  - A. Solid State Vibrational Studies 21
    - 1. Complexes A, B, C, D, F, and G 22
    - 2. Complexes E and I 30
    - 3. Complex H 34
    - 4. Complexes J, K, and L 35
    - 5. Complexes M and N 38
  - B. Solution Raman Studies 40
    - 1. Complexes A, B, C, D, F, and G 40
    - 2. Complexes E and I 45
    - 3. Complex H 45
    - 4. Complexes J, K, and L 47
    - 5. Complexes M and N 54

Page

C. Normal Coordinate Analysis 54

1. Complex C 55

2. Complex H 60

D. Other Ligand Vibrational Frequencies 62

E. Oxygen Isotopic Substitutions 63

1. Complex A 64

2. Complex C 73

3. Complex F 76

4. Complex J 79

5. Complex K 82

II. Xanthine Oxidase 84

A. Flavin Adenine Dinucleotide (FAD) 84

B. Fe_2S_2 and Mo Groups 93

CONCLUSIONS 114

REFERENCES 120

APPENDIX I
RAMAN AND INFRARED SPECTRA OF THE MOLYBDENUM COMPLEXES . . 127

APPENDIX II
SOLUTION RAMAN SPECTRA OF THE MOLYBDENUM COMPLEXES 168

APPENDIX III
RESONANCE RAMAN SPECTRA OF COMPLEX K IN CH_2Cl_2 SOLUTION . . 194

BIOGRAPHICAL NOTE 203

LIST OF TABLES

Page

Table I. Chemical and Structural Formulas of the 14 Molybdenum Complexes 20

Table II. Assignment of Raman Frequencies for Complexes A, B, C, D, F, and G 23

Table III. Assignment of Raman Frequencies for Complexes E, I, H, J, K, and L 26

Table IV. Assignment of Raman Frequencies for Complexes M and N 39

Table V. Electronic Absorption Spectral Results for the Molybdenum Complexes in Solution 41

Table VI. Comparison of Solid State and Solution Raman Frequencies (cm^{-1}) for Complexes A, B, C, D, F, and G 43

Table VII. Comparison of Solid State and Solution Raman Frequencies for Complexes E, I, H, J, K, L, M, and N 46

Table VIII. Normal Coordinate Analysis Results for ν(Mo-S) from Complex C 59

Table IX. Comparison of Raman and Infrared Bands of the ^{18}O Isotopically Substituted Molybdenum Complexes . 66

Table X. Normal Coordinate Analysis Results for Complex A having a single Mo=O Force Constant (FC) 69

Table XI. Normal Coordinate Analysis Results of Complex A with two Mo=O Force Constants 72

Table XII. Assignments for some Vibrational Frequencies of the Isoalloxazine Ring System 87

Table XIII. Resonance Raman Peaks of Xanthine Oxidase and FAD . 89

Table XIV. Group Theory Classification of Vibrational Bands for Fe_2S_2(S-cys)$_4$ in D_2h Symmetry 99

Page

Table XV. Resonance Raman Peaks of Xanthine Oxidase, Deflavo Xanthine Oxidase, and Desulfo Xanthine Oxidase 110

LIST OF FIGURES

Page

Figure 1. Structure of $MoCl(tox)_2$ 7

Figure 2. Absorption spectra of native and deflavo xanthine oxidase displayed as molar extinction coefficient ($M^{-1}cm^{-1}$) per unit of molecular weight of 181,000 9

Figure 3. Absorption difference spectrum between xanthine oxidase inhibited by allo-xanthine and native xanthine oxidase expressed as $\Delta\varepsilon$ per molecule of flavin 10

Figure 4. Molecular structure of complex C, $MoO_2(CH_3NHCH_2C(CH_3)_2S)_2$ 25

Figure 5. Molecular structures of complex K, $MoO_2((SCH_2CH_2)_2NCH_2CH_2SCH_3)$ (top) and complex J, $MoO_2((SCH_2CH_2)_2NCH_2CH_2N(CH_3)_2)$ (bottom) 36

Figure 6. Molybdenum EXAFS spectral comparisons for complexes J (top) and K with sulfite oxidase and xanthine oxidase 37

Figure 7. Resonance Raman spectra of complex K in CH_2Cl_2 solution as a function of excitation wave length 48

Figure 8. Resonance Raman enhancement profiles for the 927- (O) and 950-cm^{-1} peaks of complex K in CH_2Cl_2 solution 49

Figure 9. Electronic absorption spectrum of complex K, saturated solution in CH_2Cl_2; $\varepsilon_{477} \sim 1.4X10^4$ $M^{-1}cm^{-1}$ 51

Figure 10. Infrared spectra of complex K in the ν(Mo=O) region 52

Figure 11. Raman spectrum of complex C from 50-550 cm^{-1} (bottom) and 500-1000 cm^{-1} (top) 56

Figure 12. Raman spectra of complex A (a) and ^{18}O-labeled A (b) 65

Page

Figure 13. Raman spectra of complex C (a) and ^{18}O-labeled C (b) 74

Figure 14. Raman spectra of complex F (a) and ^{18}O-labeled F (b) 77

Figure 15. Raman spectra of complex J (a), ^{17}O, ^{18}O-labeled J (b), and ^{18}O-labeled J (c) 81

Figure 16. Raman spectra of complex K (a) and ^{18}O-labeled K (b) 83

Figure 17. Infrared spectra of complex K (a) and ^{18}O-labeled K (b) 85

Figure 18. Structure of flavin isoalloxazine ring system with conventional numbering system. 37

Figure 19. Resonance Raman spectrum of FAD (1.2×10^{-4}M + KI for fluorescence quenching) from 100 cm^{-1} to 1700 cm^{-1} 88

Figure 20. Resonance Raman spectrum of xanthine oxidase in H_2O from 300-1700 cm^{-1} 91

Figure 21. Raman spectrum of aqueous deflavo xanthine oxidase 92

Figure 22. Resonance Raman spectra of putidaredoxin, adrenodoxin, and spinach ferredoxin obtained by 441.6 nm excitation 94

Figure 23. Resonance Raman spectrum of deflavo xanthine oxidase, sample 1, with 457.9 nm excitation 95

Figure 24. Resonance Raman spectrum of deflavo xanthine oxidase, sample 2, with 476.5 nm excitation 97

Figure 25. Resonance Raman spectrum of deflavo xanthine oxidase with 406.7 nm excitation 100

Figure 26. Resonance Raman spectrum of deflavo xanthine oxidase with 457.9 nm excitation 101

Figure 27. Resonance Raman spectrum of deflavo xanthine oxidase with 476.5 nm excitation 102

Page

Figure 28. Resonance Raman spectrum of deflavo xanthine oxidase with 488 nm excitation 103

Figure 29. Raman spectrum of deflavo xanthine oxidase with 514.5 nm excitation 104

Figure 30. Resonance Raman spectrum of desulfo xanthine oxidase 106

Figure 31. Resonance Raman spectrum of xanthine oxidase . . . 108

Figure 32. Resonance Raman spectrum of desulfo-deflavo xanthine oxidase 109

ABSTRACT

Resonance Raman Studies of Milk Xanthine Oxidase
and Raman Studies of Molybdenum (VI)
Model Complexes for
Molybdoenzymes

Lawrence Jack Willis, Ph.D.
Oregon Graduate Center, 1982

Supervising Professor: Thomas M. Loehr

Milk xanthine oxidase (E.C. 1.2.3.2) is an enzyme which depends on three different cofactors for activity: a molybdenum center, two distinct iron-sulfur centers, and a flavin adenine dinucleotide (FAD) group. This oxido-reductase has been studied by resonance Raman spectroscopy. The vibrational spectrum of FAD has been identified in the native enzyme; its spectrum was absent in the deflavo form of the enzyme. The vibrational spectrum of the Fe_2S_2 centers was also observed in the 280-400 cm^{-1} region, and appears to be identical to those reported for the Fe_2S_2 centers in adrenodoxin. Additional bands were identified in this region which are attributable to either the iron-sulfur centers or possibly to the molybdenum site. However, no unambiguous evidence was obtained by Raman spectroscopy for the molybdenum active site in xanthine oxidase.

Fourteen molybdenum (VI) complexes with oxygen, sulfur, and nitrogen ligands were studied by Raman spectroscopy from 50-1000 cm^{-1} as model compounds for the Mo site in the oxidase. The position of the molybdenum-oxygen stretching vibrations between 850 and 950 cm^{-1} was used to distinguish between two structures identified for these complexes. Values below 900 cm^{-1} are indicative of a skew-trapezoidal bipyramid structure with *cis* sulfurs in a possible partial disulfide bond. Values above 900 cm^{-1} indicate a distorted octahedral structure with *trans* sulfurs. Solution Raman spectra of the fourteen complexes indicate that the octahedral structure is preferred once the complexes are dissolved. Five of the complexes were substituted with ^{18}O allowing a study of the isotopic shift of the Mo-O frequencies. The shifts were studied by Normal Coordinate Analysis and the results were interpreted as $^{16}O/^{16}O$, $^{16}O/^{18}O$, $^{18}O/^{16}O$, and $^{18}O/^{18}O$ pairs in these dioxo Mo(VI) complexes. However, Normal Coordinate Analysis could not successfully match the entire set of metal-ligand stretching vibrations for the two complexes for which complete x-ray crystallographic structures have been published. Presumably, the intermolecular interactions in the solid state cannot be adequately treated by limitations in the force fields employed in this analysis.

INTRODUCTION

Xanthine oxidase (E.C. 1.3.2.3) is one of a small number of enzymes which require the trace element molybdenum.[1] Nature's use of molybdenum in biological systems is thought to be due to the ability of this element in high oxidation states to undergo a two electron reduction with a proton transfer.[1] In xanthine oxidase this property of molybdenum is used to catalyze the reaction of hypoxanthine to xanthine and xanthine to uric acid in animal livers. Knowledge of the ligands and coordination geometry of the molybdenum active site of xanthine oxidase would greatly enhance understanding the mechanism of catalysis.

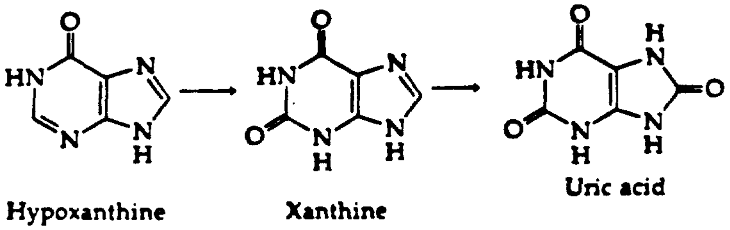

Other cofactors essential to enzyme function are two two-iron-two-sulfur groups and a flavin group (as FAD). Each enzyme molecule has two separate sets of these cofactors. The substrate reacts at the molybdenum site and the enzyme is reoxidized at the FAD site, converting O_2 into H_2O_2.

Xanthine oxidase has a molecular weight of ≈283,000.[2] Each molecule has two separately operating active catalytic units which show no activity when the molecule is divided into its two subunits. No evidence for allosteric interactions between the two catalytic units per molecule has been observed. However, one half of the enzyme can be fully active while the other half is inactivated in a form called demolybdo xanthine oxidase wherein the molybdenum is absent.[1]

Chemical modification of xanthine oxidase has helped to clarify the functions of the cofactors. The flavin moiety can be easily and reversibly removed. Such a deflavo enzyme reacts with xanthine until it is fully reduced. Other oxidizers such as ferricyanide or ferricytochrome c can then be used to restore activity toward xanthine.[3]

The iron-sulfur centers have been well characterized by their electron paramagnetic resonance (EPR) spectra. At liquid helium temperatures two different Fe/S signals are detected and are used to identify each iron-sulfur center. Fe/S system I has a g_{avg} of 1.95 while Fe/S system II has a g_{avg} of 2.01. Each Fe/S center ". . . accounts for one electron per half xanthine oxidase molecule in the fully reduced enzyme."[2] These properties are similar to plant ferredoxins and, therefore, it is presumed that each of the two types of Fe/S centers is a two-iron-two-labile-sulfur (Fe_2S_2) system. This has been confirmed by other methods.[4,5] There are a total of four Fe_2S_2 units in xanthine oxidase, each dimer containing one Fe/S type I center and one Fe/S type II center. Removal of the iron-sulfur centers appears not to be reversible.

Whereas the flavin and iron-sulfur centers are known and well understood, molybdoenzymes are few in number and their molybdenum sites are not well characterized. Removal of molybdenum from xanthine oxidase is irreversible and destroys enzyme activity.[2]

Based upon EPR work, molybdenum is believed to cycle from Mo(VI) in the resting enzyme to Mo(IV) upon reaction with xanthine, whereupon two electrons are transferred to either the Fe/S centers or FAD, reconverting molybdenum to Mo(VI). Since both Mo(VI) and Mo(IV) are diamagnetic, having d^0 and d^2 electronic configurations respectively, the EPR signals must arise from intermediate Mo(V) states during turnover, as no free radicals are thought to be associated with this enzyme. Four main Mo(V) EPR signals have been identified for xanthine oxidase by Bray.[2] These are called Very Rapid, Rapid, Inhibited and Slow. All four signals are observed in the range $g_{avg} = 1.971 \pm 0.006$. The Very Rapid signal changes to the Rapid signal with the uptake of a proton during enzyme turnover. The Slow signal is generated by dithionite reduction of an inactive form of the enzyme, desulfo xanthine oxidase. This form of the enzyme occurs upon storage but the formation is inhibited by addition of salicylate to the storage buffer. Desulfo xanthine oxidase can be generated by addition of cyanide to active enzyme, removing a sulfide as thiocyanate from resting enzyme, but not reduced xanthine oxidase. Active enzyme can be regenerated with sulfide treatment.

The nature of this cyanolyzable sulfur in the enzyme has been the subject of much speculation. It was widely believed to result from a persulfide group in the enzyme but the existence of such a group in xanthine oxidase has never been confirmed. In recent studies, the cyanolyzable sulfur has been replaced with isotopically labeled ^{33}S.[6] Electron paramagnetic resonance showed that the Very Rapid Mo(V) signal has strong coupling to the sulfur nucleus indicating that this sulfur is a ligand to molybdenum, and not a hydrolyzable persulfide group.

The Inhibited EPR signal arises from the reaction product of xanthine oxidase with methanol or formaldehyde. It is proposed that a formyl residue, -CHO, binds to the active center near the molybdenum since a proton is observed to be coupled to this Mo(V) EPR signal. Mo(V) is apparently stabilized in this air stable product whereas the other EPR signals are transient. When inhibited in this manner, it is not possible to generate desulfo xanthine oxidase. Likewise, this inhibited form cannot be generated from desulfo xanthine oxidase.

Demolybdo xanthine oxidase, another inactive form of the enzyme, was discovered when different preparations of xanthine oxidase yielded varying ratios of molybdenum to flavin.[2] It has been determined that demolybdo xanthine oxidase is naturally secreted along with active enzyme in amounts varying with the nutritional status of the animals. Demolybdo xanthine oxidase is more likely to be denatured by salicylate, thus providing a good method of minimizing its quantity during preparation.

The nature of the ligands of molybdenum in xanthine oxidase and several other molydoenzymes has recently been clarified by use of the relatively new technique of extended x-ray absorption fine structure (EXAFS). With this technique it is not only possible to identify the nearest atom neighbors of a given atom, but also to obtain accurate distances to those neighboring atoms. Less accurate, however, is the number of each kind of neighbor. Cramer et al.[7] have investigated the EXAFS spectra of a variety of molybdenum complexes to define the parameters necessary in an analysis of molybdenum complexes of unknown composition.

Applying these parameters to molybdenum in the enzymes xanthine oxidase and nitrogenase, Tullius et al.[8] were able to show that molybdenum in nitrogenase contains no double bonded oxygen ligands whereas it does in xanthine oxidase. Such oxo-ligands are a common feature of the chemistry of molybdenum. In addition, the ligands to molybdenum in xanthine oxidase were identified as one or two oxo-ligands at 1.71 Å, approximately two sulfurs at 2.54 Å, and one sulfur at 2.84 Å. The shorter bond length for the two sulfurs suggests they are thiolate sulfurs while the longer sulfur is suggested to be a thioether. Their data were not clear enough to establish the presence or absence of additional ligands such as nitrogen. The thiolate ligands were proposed to be *trans* to the oxo groups since the *trans* effect of oxo groups could explain the slightly longer bond lengths over those of model complexes.

Prior to the EXAFS information, the ligands to molybdenum in xanthine oxidase were presumed to be sulfur, oxygen, and nitrogen based upon their biological availability. Electron paramagnetic resonance studies seemed to implicate one or more sulfur ligands.[9]

Consequently, synthesis of molybdenum complexes with these ligands has flourished to model the molybdenum site in xanthine oxidase as well as other molybdoenzymes. Early models contained molybdenum dimer complexes since the chemistry of Mo(VI) favors μ-oxo and di-μ-oxo bridges.[10-22] These are not acceptable models, however, since all known molybdoenzymes incorporate monomeric molybdenum at their active sites.

Since the richest data on characterizing molybdenum in enzymes has come from EPR spectroscopy, the matching of these EPR signals to those from model complexes has been a primary focus of studies of Mo in enzymes. One complex that most closely matches the EPR signal parameters of xanthine oxidase is *cis*-oxochlorobis(8-mercaptoquinolinato)-molybdenum(V), $MoOCl(tox)_2$ Figure 1. It is interesting to note the presence of two thiolate and two nitrogen ligands in addition to the oxo and one chloro ligand. The chloro group may well play the role of the ubiquitous second *cis*-oxo group. Many Mo(VI) and Mo(V) complexes have now been synthesized with sulfur and nitrogen ligands and studied by EPR and x-ray crystallography to determine their potential as models for molybdoproteins.[24-34]

Until this work, only EPR and EXAFS were used to compare the molybdenum site in xanthine oxidase with Mo complexes.[35] Resonance Raman spectroscopy holds the potential for probing the molybdenum site in xanthine oxidase as well as the other co-factors, FAD and the Fe/S centers. Whereas infrared spectroscopy of proteins is not readily feasible due to the overlap of the multitude of protein vibrational modes and the strong absorption by aqueous solvents, resonance Raman

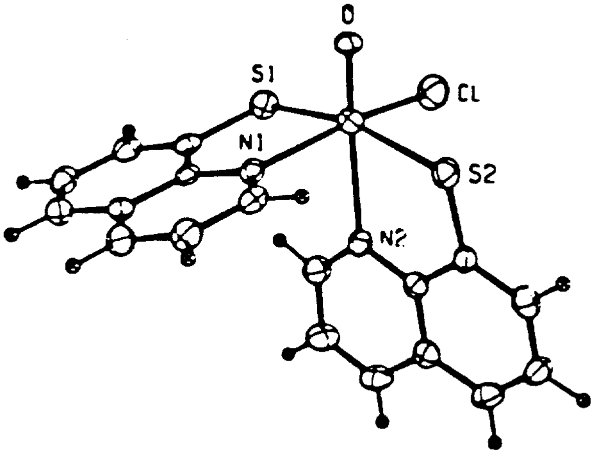
O
S1
Cl
N1
S2
N2

Figure 1. Structure of MoOCl(tox)$_2$.

{Taken from reference 23}

spectroscopy is capable of viewing the vibrational structure of only the chromophore sites involved in a protein. In xanthine oxidase, the FAD and Fe/S centers are strong chromophores and should possess resonance Raman spectra. The visible absorption spectra of native and deflavo xanthine oxidase are shown in Figure 2. The difference spectrum, also shown, is typical of the absorption spectrum for FAD.[2] The molybdenum site, however, does not have a well defined electronic absorption due to the strong masking effect of the FAD and Fe/S chromophores. Yet evidence exists for the presence of molybdenum absorptions. When molybdenum is locked into the Mo(IV) oxidation state by the inhibitor allopurinol, a difference spectrum is obtained as shown in Figure 3.[36] This shows an absorption with λ_{max} at ~ 380 mn for Mo(IV). Excitation of appropriate xanthine oxidase samples near this wavelength might yield a resonance enhanced Raman spectrum for the molybdenum active site.

To ascertain any resonance Raman spectral contributions due to the Mo-site in xanthine oxidase, it will be necessary to compare vibrational frequencies with known complexes of molybdenum. Since complete infrared or Raman spectra from model complexes are seldom published, it was necessary to study the Raman spectra of suitable molybdenum complexes in conjuction with the enzyme studies. Dr. Edward I. Stiefel and coworkers at the Charles F. Kettering Research Laboratories in Yellow Springs, Ohio, have synthesized a number of Mo(VI) complexes with oxygen, sulfur, and nitrogen ligands as potential models for molybdenum enzymes and agreed to collaborate with this researcher for the Raman studies of these complexes. Fourteen Mo(VI)

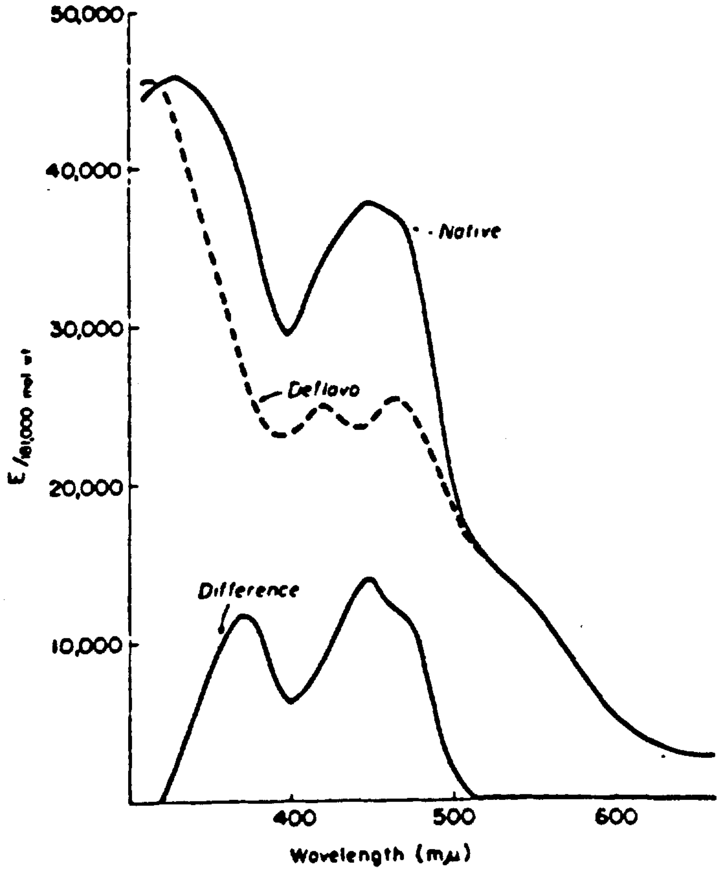

Figure 2. Absorption spectra of native and deflavo xanthine oxidase displayed as molar extinction coefficient ($M^{-1}cm^{-1}$) per unit of molecular weight of 181,000. The calculated difference spectrum between native and deflavo xanthine oxidase is displayed in the lower curve. {Reproduced from reference 3}. The currently accepted molecular weight of xanthine oxidase is 283,000.[2]

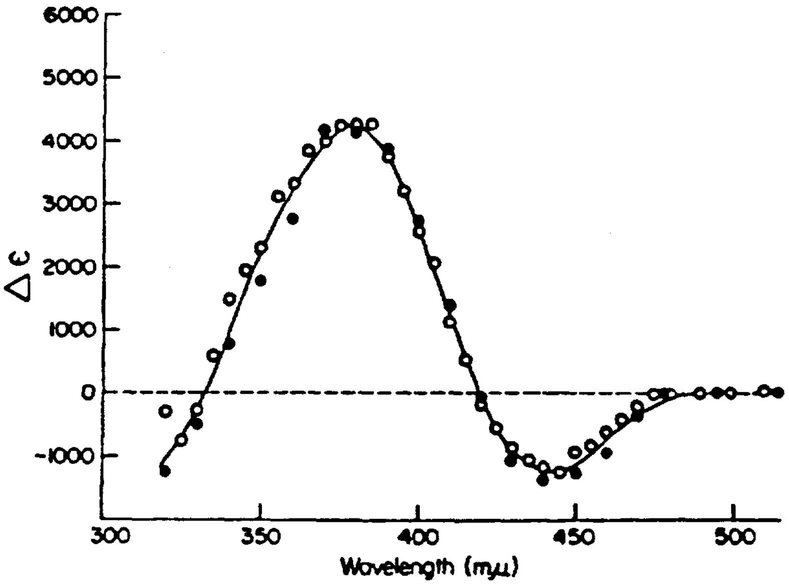

Figure 3. Absorption difference spectrum between xanthine oxidase inhibited by allo-xanthine and native xanthine oxidase expressed as Δε per molecule of flavin. {Reproduced from reference 36}

complexes were analyzed by Raman spectroscopy in both the solid state and in solution.

An additional study was performed on two of the complexes for which the x-ray crystallographic structures have been published. Normal coordinate analysis (NCA) of metal ligand vibrational frequencies was carried out to establish a better understanding of these vibrations in these complexes. Although x-ray crystal structures have been determined for four of the fourteen complexes, only two contain sufficient structural information for setting up normal coordinate analyses.

Normal coordinate analysis uses masses, structural coordinates, and vibrational force constants to calculate frequencies of vibration. If frequencies of vibration are known, NCA can then be used to calculate force constants. The F and G matrix method of Wilson[37] expresses the relation between force constants and vibrational frequencies in the following equation:

$$|FG - E\lambda| = 0.$$

The determinant on the left side of the equation contains three matrices, F, G, and E, and the scalar λ which relates to vibrational frequency via the following equation:

$$\lambda = 4\pi^2\nu^2c^2.$$

In this equation, ν is the frequency of vibration in cm^{-1} and c is the speed of light in cm/sec. The F matrix contains the force constants. The G matrix contains reciprocal masses and terms relating atoms through bonding interactions. E is a unit matrix.

For a nonlinear molecule with N atoms the F and G matrix method requires that a determinant of order 3N - 6 must be solved. Computer programs are necessary to solve such large equations. Schachtschneider[38] developed a set of programs which were modified[39] to three programs used in these calculations. These three programs are described below:

1. CART: This program converts the input structural data (bond lengths, angles, masses) into cartesian coordinate system and defines each atom's coordinates.

2. GMAT: This program calculates the G matrix with an option to symmetrize the G matrix if an appropriate U matrix, which transforms internal coordinates into symmetry coordinates, is provided for the molecular point group.

3. FPERT: This program calculates the F matrix, symmetrizes the F matrix on the basis of symmetry coordinates, if appropriate, solves the secular equation in internal coordinates, and optionally refines a calculated set of force constants to a given set of experimental frequencies.

Within a molecule there are many interactions to be considered such as bond stretching, bond angle bending, and non-bonded atom repulsions. Each interaction has its own force constant and the collection of force constants defines a force field. The general quadratic potential function,[37] $2V = \sum_{tt'}^{3N-6} F_{tt'} S_t S_{t'}$, where S_t and $S_{t'}$ are internal coordinates, N is the number of atoms in the molecule, and $F_{tt'}$ are the force constants, is the most complete and accurate model force field. However, it involves $(3N - 6)^2$ force constants many of which are insignificant interactions between separated atoms in a molecule and can rapidly use up valuable computer time for large molecules. To alleviate this problem, simpler force field models are considered.

The general valence force field (GVFF) model uses force constants only for stretching and bending vibrations. Interactions between non-bonded atoms are not considered. Another commonly used model is the Urey-Bradley force field (UBFF).[40] This model adds repulsive force constants between non-bonded atoms to the GVFF model. For the NCA calculations in this dissertation, only the GVFF model was used since the stretching vibrations were of primary interest.

The aim of the research described in this dissertation is an investigation of the enzyme xanthine oxidase by resonance Raman spectroscopy. The FAD cofactor spectra are to be compared with the spectra of known samples of FAD. The spectra of the Fe_2S_2 centers are to be compared with spectra from other known Fe_2S_2 containing proteins. The spectra of Mo(VI) complexes are to be studied to aid in identifying the Mo site vibrations in xanthine oxidase spectra.

EXPERIMENTAL

I. Preparation of Milk Xanthine Oxidase

Xanthine oxidase was prepared following the method of Massey et al.[41] with a modification of their final step. Freshly churned buttermilk in approximately 2 liter lots was treated with 0.2 g/L of sodium salicylate, 0.3 g/L of cysteine HCl, 0.37 g/L of EDTA, and 15.8 g/L of $NaHCO_3$ titrated to pH 7.5 with 2N NaOH. In a water bath, the temperature of the solution was elevated to 37°C and 1.6 g/L of pancreatin was added. The solution was stirred at 37°C for 3.5 hours and set to cool overnight in a refrigerator.

With vigorous stirring, 170 mL of *n*-butanol (cooled to -20°C) per liter of solution was added followed by 190 g/L of ammonium sulfate. After stirring for 30 min., the mixture was centrifuged at 650 x g. The lower aqueous layer was separated (by suction) from the precipitate in the upper organic phase and its volume measured. The precipitate was discarded. Ammonium sulfate was added to the aqueous solution, then placed in a refrigerator for two hours to allow the protein to precipitate and rise to the surface. The lower aqueous layer was removed by siphon and the protein precipitate was centrifuged at 10,000 x g for 30 min. All liquid layers were discarded and the protein precipitate was suspended in ~ 100 mL of 0.1 M phosphate buffer, pH 6.3, with 3×10^{-4} M EDTA and 10^{-3} M salicylate. The suspension was dialyzed overnight against three changes of three liter volumes of this same buffer.

The dialyzed solution was centrifuged at 15,000 x g for one hour at 4°C and then decanted from any further precipitate. The solution was passed onto a calcium phosphate-cellulose column (10 x 90 cm) and was then washed by at least five bed volumes of the buffer solution. The enzyme was eluted with the same buffer containing 5% (w/v) ammonium sulfate using an Amicon TCM 10 ultrafiltration apparatus with a membrane having a 10^5 molecular weight cutoff. The concentrated enzyme was then passed through a column (2.5 x 200 cm) of Sephacryl S-300 and concentrated once again by ultrafiltration. The concentrated, reddish-brown xanthine oxidase stock solution was then stored at 5°C until further use.

Deflavo xanthine oxidase was prepared by the method of Kanda et al.[42] A 2 mL sample of xanthine oxidase stock solution was dialyzed for 12-16 hrs. against 3M KI in Tris-HCl buffer (0.15M, pH 8.5, with 0.005% EDTA and 1 mM sodium salicylate). For the next 3 hours, dialysis was continued against 0.5 M KI in Tris buffer followed by a final 3 hours of dialysis against 0.5 M KCl in Tris buffer. After removal of the flavin the reddish-brown samples were concentrated by ultrafiltration using Millipore PTHK membranes (10^5 MW cutoff) and stored in the refrigerator until use.

Desulfo xanthine oxidase was prepared by the method of Gutteridge et al.[43] Dialysis of a 2 mL xanthine oxidase stock sample at room temperature was carred out against 30 mM KCN in the above Tris buffer.

After approximately three hours of dialysis, the sample was passed through a (3 x 100 cm) column of Sephadex G-15, concentrated by Millipore ultrafiltration (PTHK), and stored in the refrigerator until use. The appearance of the desulfo enzyme was indistinguishable from the native and deflavo forms of xanthine oxidase.

II. Activity Assay for Milk Xanthine Oxidase and Protein Concentration

The activity of xanthine oxidase was measured by the method of Avis et al.[44] A pyrophosphate buffer and a xanthine solution were prepared and stored for future uses. The pyrophosphate buffer contained 17.83 g of $Na_4P_2O_7 \cdot 10H_2O$ plus 3.33 g of $Na_2H_2P_2O_7$ in a volume of 500 mL at pH 8 with 2.5 mL of chloroform added as a preservative. The xanthine solution consisted of 13.5 mg of xanthine, 1 mL of 2N NaOH and water to a final volume of 100 mL and a final pH of 9.5 The assay requires a buffered xanthine solution which is freshly made whenever an assay is carried out. It consists of 3 mL of xanthine solution, 3 mL of N/50 HCl, 7 mL of pyrophosphate buffer, and 7 mL of water.

A xanthine oxidase sample from the stock solution was diluted about 100 -fold with cold pyrophosphate buffer. Buffered xanthine (2.5 mL) was added to one cuvette, stoppered, and the solution was mixed by inverting once, and placed in the sample compartment of a Cary 15 or Cary 16 spectrometer. The second cuvette was used in the reference compartment. Absorbance at 295 nm was followed for 10 minutes to record the appearance of uric acid.

The slope of the graph ($\Delta A_{295}/\Delta t_{min}$) was used to calculate the activity using the formula #units/mL = 2.7083 FX where F is the dilution factor of the enzyme and X is the slope. This formula was derived from Avis et al.[44] and includes an extinction coefficient difference of 9.6×10^3 M^{-1} cm^{-1} between xanthine and uric acid at 295 nm.

The biuret reaction was used to measure protein concentration. All chemicals were reagent grade or biochemical grade. Xanthine oxidase samples displayed activity ranging from 1.36 units/mg to 6.3 units/mg. These values compare favorably with standard preparations of xanthine oxidase.[41]

The Raman spectra were obtained on a Jarrell-Ash 25-300 Raman spectrophotometer with a modified grating drive and slit drive from RKB Inc. This instrument was interfaced to a Computer Automation LSI-2 computer controlled through a Tektronix 4010-1 interactive graphics terminal. The operation of the spectrometer has been described elsewhere.[45]

III. Molybdenum Model Complexes

The molybdenum(VI) model complexes were prepared by Dr. Edward I. Stiefel and coworkers at the Charles F. Kettering Research Laboratory in Yellow Springs, Ohio. Infrared spectra of these complexes were provided with the samples, but some were remeasured on a Perkin-Elmer 621 Grating Infrared Spectrophotometer as Nujol mulls. Information on the visible and ultraviolet absorption spectra of these complexes were provided with the samples.

RESULTS AND DISCUSSION

I. Molybdenum(VI) Model Complexes

The fourteen molybdenum(VI) model complexes obtained for this investigation are listed in Table I. All but two are dioxo molybdenum complexes with nitrogen and sulfur multidentate ligands completing the six coordinate environment around the metal. The last two are dioxo Mo dimers having an additional bridging μ-oxo ligand. All the ligands are similar but include small structural alterations which add steric effects and, thus, introduce slight changes in the geometries and physical properties among the complexes. Several of the complexes were available with ^{18}O coordinated so that isotopic shifts could be observed. These isotopic complexes are identified in Table I.

The Mo(VI) complexes were studied by solid state Raman spectroscopy and infrared spectroscopy to identify the molybdenum-ligand stretching vibrations. The frequency of the antisymmetric O=Mo=O stretching vibration was used to assign the structure of the complex between two possible geometries, distorted octahedral and skew-trapezoidal bipyramidal. In solution, all complexes display ν(Mo=O) frequencies characteristic of the octahedral structure indicating the lack of stability of the skew-trapezoidal bipyramid once dissolved.

Normal coordinate analysis was applied to two of the complexes, C and H, for which the x-ray crystal structures have been solved. These computer calculations were used to assist in the assignment of the stretching vibrations of molybdenum to the oxygen, sulfur, and nitrogen ligands. NCA also was used to explain the complex set of

Table I. Chemical and Structural Formulas of the 14 Molybdenum Complexes

Molybdenum Complex	Formula	Structural Formula
A	$MoO_2(NH_2CH_2C(CH_3)_2S)_2$ & $Mo^{18}O_2L_2$	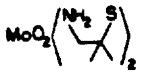
B	$MoO_2(C_6H_5CH_2NHCH_2C(CH_3)_2S_2$	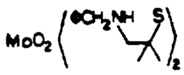
C	$MoO_2(CH_3NHCH_2C(CH_3)_2S)_2$ & $Mo^{18}O_2L_2$	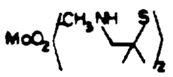
D	$MoO_2(CH_3NHC(CH_3)_2C(CH_3)_2S)_2$	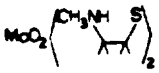
E	$MoO_2(SC(CH_3)_2CH_2NHCH_2CH_2NHCH_2C(CH_3)_2S)$	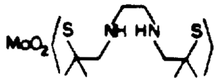
F	$MoO_2((CH_3)_2NCH_2C(CH_3)_2S)_2$ & $Mo^{18}O_2L_2$	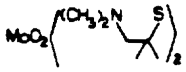
G	$MoO_2(NH_2CH_2CH_2S)_2$	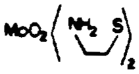
H	$MoO_2(tox)_2$[a]	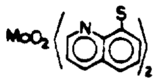
I	$MoO_2(SCH_2CH_2N(CH_3)CH_2CH_2N(CH_3)CH_2CH_2S)$	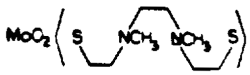
J	$MoO_2((CH_3)_2NCH_2CH_2N(CH_2CH_2S)_2)$ & $Mo^{17}O_2$ & $Mo^{18}O_2L$	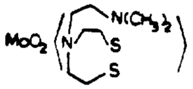
K	$MoO_2(CH_3SCH_2CH_2N(CH_2CH_2S)_2)$ & $Mo^{18}O_2L$	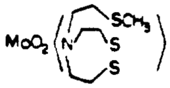
L	$MoO_2(NH_2CH_2CH_2N(CH_2CH_2S)_2)$	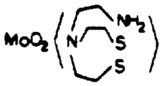
M	$Mo_2O_5((CH_3)_2NCH_2CH_2NHCH_2CH_2S)_2$	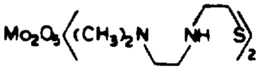
N	$Mo_2O_5((CH_3)_2NCH_2CH_2NHCH_2C(CH_3)_2S)_2$	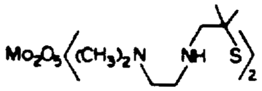

[a] tox = thiooxine = 8-mercaptoquinoline

Mo=O stretching vibrations seen in the infrared and Raman spectra of the five complexes with ^{18}O substitutions.

A. Solid State Vibrational Studies

A complete set of Raman and infrared spectra for all the complexes studied may be found in Appendix I. For ease of analysis, these complexes were separated into categories of similar ligand structure. The first category included the six complexes A, B, C, D, F and G which are derived from the 2-aminoethanethiol structure of G. The second category included complexes E and I which have linear tetradentate ligands derived from the ligands of A and G, respectively, by the addition of an ethylene bridge between the nitrogens. In addition, complex I has a methyl group on each nitrogen. Complex H, which has a bidentate ligand of a different structure, is similar to these above two categories but was analyzed separately. Complexes J, K, and L have tetradentate ligands with a tripod arrangement. Complexes M and N are molybdenum dimers with a μ-oxo bridge and a tridentate ligand. The complexes arrived in two shipments and were assigned letters arbitrarily; this accounts for complexes E and I being similar although alphabetically apart.

1. Complexes A, B, C, D, F, and G.

Whereas all of the Mo(VI) complexes studied are dioxo molybdenum compounds, the ligands in this first category are derived from the 2-aminoethanethiol structure found in complex G. Each complex has two of these bidentate ligands giving a coordination sphere of two oxygens, two nitrogens and two sulfurs.

Possible assignments of the stretching vibrations of these complexes are given in Table II. The molybdenum-oxygen stretching vibrations are known to fall in the 850-950-cm^{-1} range.[29, 46-53] Molybdenum-sulfur stretching vibrations ordinarily occur in the range 350-400 cm^{-1}.[46, 54-56] The molybdenum-nitrogen stretching vibration has rarely been characterized but in one complex is known to occur at 623 cm^{-1}.[55]

Molybdenum-nitrogen multiple bond formation is fairly common.[57-60] Multiple bond formation for Mo-N was observed for a nitrosyl complex due to π-backbonding, thus increasing the bond strength and accounting for the relatively high stretching frequency.[55] There is abundant structural information on molybdenum complexes with nitrogen ligands.[57-60] Bond lengths for Mo-N bonds vary from about 1.62 Å[58] to 2.55 Å,[60] showing a wide range of bond multiplicity.

In general, an octahedral coordination environment is expected around molybdenum with the oxo groups located in a *cis* arrangement. Steric interferences in the different ligands are expected to cause structural variation from one complex to another. Within this first group only complex C has a published x-ray crystallographic structure.[61]

Table II. Assignment of Raman Frequencies for Complexes A, B, C, D, F, and G

Molybdenum Complex	Structural Formula		Vibrational Frequencies (cm^{-1})		
			Mo=O	Mo-N	Mo-S
A	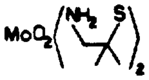	IR	907, 872	590, 539	404, 363
		R	906, 870	593	412, 362
B	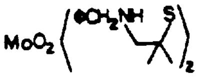	IR	923, 900	585, 560	405, 371
		R	924, 903	597, 566	414, 368
C	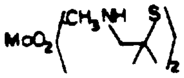	IR	882, 856	600, 555	378, 350
		R	877, 848	606	399, 360
D	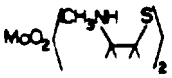	IR	878, 847	624, 557	408, 388
		R	876	631, 561	414, 380
F	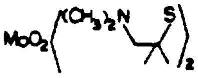	IR	893, 879	606, 562	373, 357
		R	891, 883	605, 555	376, 342
G	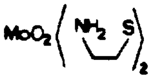	IR	888, 850		387, 351
		R	881, 852		356

It is reported to have the skew-trapezoidal bipyramid structure shown in Figure 4. A footnote to the structure paper states that complex F also has the skew-trapezoidal bipyramid structure. This structure is not octahedral but can be described by starting from a *trans* dioxo octahedral complex with *cis* N's and *cis* S's. Opening the N-Mo-N angle to 144° and closing the O-Mo-O angle to 122° between the nitrogens results in the observed structure. An unusual feature about this structure is the close S-S distance of 2.76 Å This is attributed to a partial disulfide bond which may have implications for enzyme mechanisms.

Stiefel et al.[61] proposed that the skew-trapezoidal bipyramid structure is responsible for the very low frequency of ν(Mo=O) in the infrared spectrum of complex C versus other molybdenum complexes known to be more nearly octahedral in structure. Table II lists infrared peaks for C at 882 and 845 cm^{-1} assignable to the symmetric and antisymmetric stretching vibrations of the MoO_2 unit. The corresponding Raman peaks are at 877 and 848 cm^{-1}. {Reasons for the Raman-infrared peak position discrepancy will be discussed in the isotope section, beginning on page 73}. Octahedral complexes H and J exhibit infrared peaks for ν(Mo=O) higher in frequency at (925, 895 cm^{-1}), respectively, as well as Raman peaks at (921, 891 cm^{-1}) and (919, 894 cm^{-1}) as listed in Tabel III. The lower frequencies of the skew-trapezoidal complex can be explained electronically as a result of its structure. The O-Mo-O angle at 122° is significantly larger than the more normal value of about 108° in octahedral complexes H and J. This larger

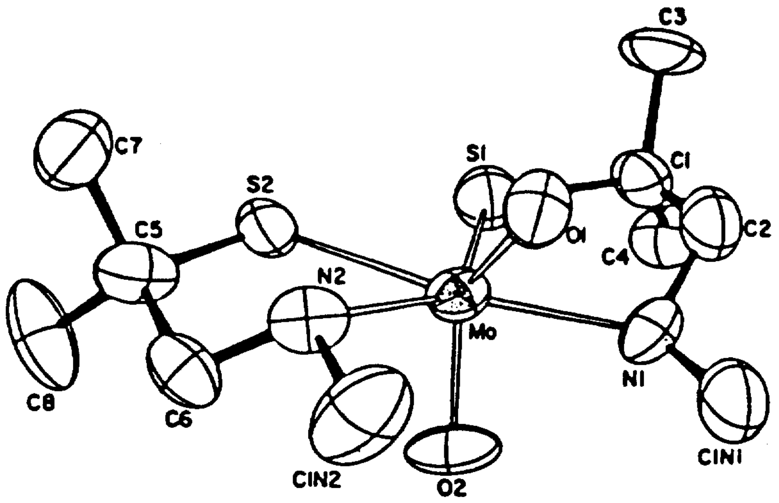
C3
C7
S1
C1
S2
C5
O1
C2
C4
N2
Mo
N1
C8
C6
CIN2
O2
CIN1

Figure 4. Molecular structure of complex C, $MoO_2(CH_3NHCH_2C(CH_3)_2S)_2$ {Reproduced from reference 60}.

Table III. Assignment of Raman Frequencies for Complexes E, I, H, J, K, and L

Molybdenum Complex	Structural Formula		Vibrational Frequencies (cm^{-1})		
			Mo=O	Mo-N	Mo-S
E	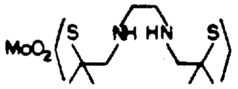	IR	901, 888, 866	592	392, 365
		R	905, $\underline{892}$,[a] 885, $\underline{866}$	593	392, 370
I	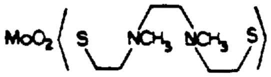	IR	923, 896	600, 541	401, 370
		R	909, 890	600, 532	407, 368
H	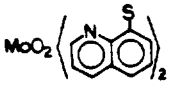	IR	925, 895	275	365, 342
		R	916, 891	276, 251	366, 342
J	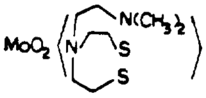	IR	923, 896	548, 526	412, 362
		R	919, 916, 894	545, 526	415, 366
K[b]	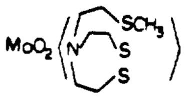	IR	923, 894	545	---
		R	922, 893	---	408, 370
L	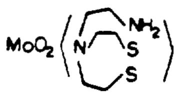	IR	913, 881	532	410, 365
		R	909, 884	---	407, 370

a) Underlined values are predominant Mo=O frequencies. Other values are secondary as explained in text.

b) The data for complex K are representative of a sample that may have experienced internal reduction of Mo. See text for details.

angle more closely approximates a *trans*-dioxo arrangement than the normal *cis*-dioxo Mo(VI) complexes. As the oxygens approach a *trans* configuration, they compete with each other to enter π-bonding with the same d-orbital on molybdenum. In a perfect *cis*-dioxo arrangement there is no such competition since each oxygen π-bonds with orthogonal d-orbitals. This competition lowers the amount or π-bonding to each and hence reduces bond strengths and vibrational frequencies.

Stiefel explains the unusual structure of complex C as a result of "unfavorable steric or electronic interactions" that would occur in a more normal octahedral environment.[61] With *trans* sulfurs *cis* to oxygens and *cis* nitrogens *trans* to oxygens (the octahedral structure), the methyl groups on the N atoms would sterically interfere with each other. An examination of this hypothesis was carried out using Fisher-Hirschfelder-Taylor atom models. These space filling models show steric interference when the optically active nitrogens are of the same configuration but not when the nitrogens are of opposite configurations. Three points then seem to favor the skew-trapezoidal bipyramid structure: the first is the presence of ligands with the same configuration around the optically active nitrogen (a racemic mixture should tend to favor an octahedral structure); the second is the absence of any groups *trans* to the oxo groups other than the other oxygen itself, which is as close to *trans* as has yet been discovered; the third is the possible formation of a partial disulfide bond between the *cis* sulfur atoms.

Complex B can be formed from complex C by the addition of a benzene ring to each of the methyl groups attached to nitrogen. These benzyl groups of B should create greater steric interferences than the methyl groups of C. On this basis one would predict low $\nu(Mo{=}O)$ frequencies for complex B, but this is not the case. These frequencies are higher and nearly identical to the "normal" octahedral complex H as can be seen in Tables II and III. Thus, by the criterion of its infrared and Raman frequencies, complex B is octahedral in structure, and the presence of a racemic ligand mixture is indicated.

Complex A, which has no substituents other than hydrogen, exhibits $\nu(Mo{=}O)$ frequencies between those of complex J and complex C. This indicates that the O-Mo-O angle is intermediate between the 122° of C and the 108° of J. Without x-ray crystal analysis it is not possible to determine which of the two structures it takes. It is possible that it might take yet another octahedral structure wherein the sulfurs are no longer *trans* to one another. Two structures are then possible wherein one or both sulfurs are *trans* to the oxygens. There is as yet no evidence to suggest structures for Mo(VI) complexes wherein thiolate ligands are *trans* to terminal oxygen ligands. A probable structure is a distortion of the "normal" octahedral structure wherein the O-Mo-O angle opens up to ~ 115° aided by hydrogen bonding with the nitrogen protons. This is supported by evidence showing the complex $MoO_2\{NH_2C(CH_3)_2CH_2S\}_2$ (not investigated here) to have infrared absorptions nearly identical to complex A.[61] This complex differs from A in that methyl groups are on the carbon next to nitrogen rather than next to sulfur. Stiefel cites nuclear magnetic resonance data of this complex having "two resonances for the CH_3 groups and AB patterns for the CH_2 and NH_2 protons, consistent with an octahedral structure with *trans* thiolate and *cis* amine donors."

As has already been mentioned, complex F is known to share the skew-trapezoidal bipyramid structure with C. The ν(Mo=O) frequencies of F are correspondingly low although not as low as those for complex C. Since the ligand of F contains only an additional methyl group on each of the nitrogens, one can see in Figure 4 that there is adequate space on each of the nitrogens for the additional methyl groups. The smaller O-Mo-O angle, as indicated by the slightly higher frequency, could be explained by small steric interaction between the new methyl groups and the oxygens, forcing the oxygens closer together.

Complex D exhibits ν(Mo=O) frequencies nearly identical to complex C. It is logical to assume that D also adopts the skew-trapezoidal bipyramid structure. The ligand of D differs from the ligand of C by two additional methyl groups on the other carbons connecting sulfur to nitrogen. An examination of Figure 4 shows that there is adequate room to accommodate the new methyl groups in this structural arrangement.

Complex G exhibits ν(Mo=O) frequencies comparable to complex F, also suggesting the skew-trapezoidal bipyramid structure. This is surprising since G has no methyl groups on the nitrogen of its ligand, a feature which has apparently been necessary to bring about the structural change from octahedral. However, G's ligand also has no methyl groups on the carbons connecting sulfur to nitrogen, a feature which is present in all complexes discussed so far and which apparently has no role in determining structure. Presumably ligand G is free to adopt either structure. The formation of a partial disulfide bond then seems to be the determining factor in the formation of the skew-trapezoidal bipyramid structure for complex G as suggested by the ν(Mo=O) frequencies.

2. Complexes E and I

The ligands of complexes E and I differ from each other principally by a methyl group on each of the nitrogens of ligand I. Both of these ligands are derived from the ligands of the group just discussed by a bridging ethylene group between the nitrogens making one tetradentate ligand out of two bidentate ligands. Ligand E is derived from ligand A and ligand I is derived from ligand C.

The ν(Mo=O) frequencies for these complexes are listed in Table III.

Complex E has low frequency Mo=O stretching vibrations similar to those of complexes F and G, suggesting a skew-trapezoidal bipyramid structure. Inspection of Figure 4 shows that linkage of the two methyl groups by a C-C bond would yield ligand E. However, this bridge would pass through the O-Mo-O angle and force this angle to widen while closing the N-Mo-N angle and opening the S-Mo-S angle, resulting in an as yet unknown *trans*-oxo Mo(VI) arrangement. This arrangement seems highly unlikely.

A space filling model aids our understanding of the structure of this complex. Each of the nitrogens is optically active, having four different substituents. Four different conformations of the ligand are therefore possible: dl, dd, ll and ld. In terms of coordination ability, the classifications span two cases, where the nitrogens are either the same (dd or ll) or different (dl or ld). When the nitrogens are of the opposite configurations, two coordination geometries are possible. The first places the sulfurs *trans* to each other. The nitrogens of necessity are *cis* to one another and oxygens are *cis* to one another and approximately *trans* to the nitrogens. There are steric constraints within the ligand in this configuration. The ethylene bridge between the two nitrogens has an eclipsed conformation with respect to its hydrogens. The amine hydrogens are forced close together, possibly creating interference with each other. Considerable space is allocated to the oxygens whereas the sulfurs and nitrogens are crowded into their coordination sites around molybdenum, resulting in a poor distribution of ligands.

The second geometry places the sulfurs *cis* to one another for possible disulfide bond formation. The nitrogens are again *cis* to one another as are the oxygens. The amine hydrogens point away from each other and may possibly hydrogen bond to the oxygens in such a way to increase the O-Mo-O angle. There is adequate room for the oxygens to separate to a little larger angle should hydrogen bonding occur. The nitrogen bridging ethylene backbone is well staggered. Structurally, this appears to be a favorable configuration.

When the nitrogens of ligand E are of the same configuration, the sulfurs can coordinate *cis* or *trans* to one another. In the *cis* sulfur arrangement there exists the possibility of a hydrogen bond from one amine nitrogen to one of the sulfurs. On the carbons adjacent to the sulfur atoms, one methyl group sterically interferes with one of the oxygens whereas a methyl group from the other sulfur sterically interferes with a possible disulfide bond. In the *trans* sulfur arrangement, however, the amine hydrogens no longer interfere with each other since they are now on opposite sides of the ligand backbone. Each can now hydrogen bond with its own nearby sulfur. The nitrogens are approximately *trans* to the oxygens. The bridging ethylene group is in a staggered conformation. There is one methyl from the carbon next to a sulfur which can sterically interfere with one of the oxygens.

Although two of the above-described structures seem possible, only one can explain the low ν(Mo=O) frequencies for complex E. When the nitrogens are of opposite configurations and the sulfurs are *cis* to one another, there are no apparent steric interferences. The O-Mo-O angle should widen because of hydrogen bonding, thus lowering the stretching frequency to those observed in the skew-trapezoidal bipyramid structure of complexes C, D, F, and G. The *cis* sulfur coordination also allows possible partial disulfide bonding as expected in complexes C, D, F, and G. The structure having *trans* sulfurs, with nitrogens of the same configuration would also be possible for complex E, but was ruled out due to the lower ν(Mo=O) frequencies. However, the Raman spectrum shows peaks of lesser intensity at 905 and 885

cm^{-1} that could be attributed to this geometry. Because this geometry has some steric interferences, it is quite appropriate that the intensities of these additional peaks are lower due to the presence of fewer molecules of this configuration.

Complex I displays ν(Mo=O) frequencies in the range expected for a more normal octahedral Mo(VI) complex. With N-methyl groups replacing the N-H, greater steric interactions come into play as demonstrated by space filling models. With the nitrogens of the same configuration, the sulfurs can coordinate either *cis* or *trans* to one another. In the *cis* arrancement, one N-Me group splits a possible partial disulfide bond, whereas the other N-Me group crowds one of the oxygens. One of the sulfurs is located *trans* to one of the oxygens, and the bridging ethylene group is in an eclipsed conformation. In the *trans* sulfur arrangement, the N-Me groups are on opposite sides of molybdenum and create no steric interactions. There is no crowding of the oxygens and the bridging ethylene group is in a staggered conformation.

With the nitrogens of ligand I in the opposite configurations, a *trans* sulfur arrangement is not possible. The N-Me groups are pushed into close proximity and prevent the ligand from twisting into an arrangement to allow this kind of coordination. The *cis* sulfur arrangement is possible, however. Here both N-Me groups crowd the oxygens and the bridging ethylene is forced toward a half-eclipsed conformation. With favorable sulfur coordination to molybdenum, the nitrogens are forced into poor coordination positions, making this an unsatisfactory configuration.

Thus, the *trans* sulfur with nitrogens of the same configuration appears to be the most favorable structure for complex I. This also approximates a normal octahedral Mo(VI) geometry and accounts for the higher ν(Mo=O) frequencies.

3. Complex H

Complex H has been well studied. The crystal structure of H reveals a near octahedral coordination geometry with *trans* sulfurs, *cis* nitrogens, and *cis* oxygens.[23] This is the usual Mo(VI) dithiolate structure. The ν(Mo=O) frequencies of 916 and 891 cm^{-1} nicely indicate this fact. The low frequency infrared spectrum of H has been analyzed by molybdenum isotopic substitutions and ν(Mo-S) and ν(Mo-N) have been established to be (375, 343 cm^{-1}) and 274 cm^{-1}, respectively.[62] However, the Raman data reported here differ from those of Zuika.[62] The two data sets are comparable except for a 375-cm^{-1} peak in Zuika's data and a 366-cm^{-1} peak reported here. Sample preparation may be the cause of this discrepancy. Zuika et al. obtained their Raman spectrum from a KBr disc, whereas in the present study, the spectrum of neat crystals was recorded. The pressure on the sample being mixed with KBr may have altered the structure, and hence the frequency of the Mo-S stretching vibration. Evidence that this may be the case comes from a comparison of the infrared data with the Raman data. Symmetric stretches tend to be strong in Raman spectra and weak in infrared spectra while antisymmetric stretches are weak in Raman spectra and strong in infrared spectra. In the infrared spectrum, the 343-cm^{-1} peak is strong and the 364-cm^{-1} peak is weak, whereas in the Raman spectrum the 342-cm^{-1} peak is weak and the 366-cm^{-1} peak is strong. If the 366-cm^{-1} feature were assigned to ν_{sym}(Mo-S) and the 343-cm^{-1} peak were assigned to ν_{asym}(Mo-S) then the intensities would match the expectation. Zuika's assignment of the 364-cm^{-1} peak to a bending vibration of the O-Mo-O angle can therefore be reassigned to ν(Mo-S). This will be discussed further in the section devoted to normal coordinate analysis.

4. Complexes J, K, and L

These three complexes have tripod ligands wherein a central nitrogen has three ethylene arms ending in nitrogen and sulfur making tetradentate ligands. One of the arms has its end group varied to change the nature of the complex.

Complex J has two tertiary nitrogens and two thiolate donors to molybdenum. Complex K has one tertiary nitrogen, one thioether, and two thiolate donors. These two complexes have been studied by x-ray crystallography and EXAFS.[35] The coordination geometries of both are the "normal" Mo(VI) dithiolate octahedral structure as shown in Figure 5. The thiolate sulfurs are *trans* to one another while the other two donors are *cis* to one another and *trans* to oxygen. The EXAFS spectrum of complex K with its thioether donor provides an excellent match to the EXAFS spectrum of sulfite oxidase, a molybdoenzyme that catalyzes the reaction of sulfite to sulfate. This comparison as well as that to xanthine oxidase and to complex J can be seen in Figure 6.

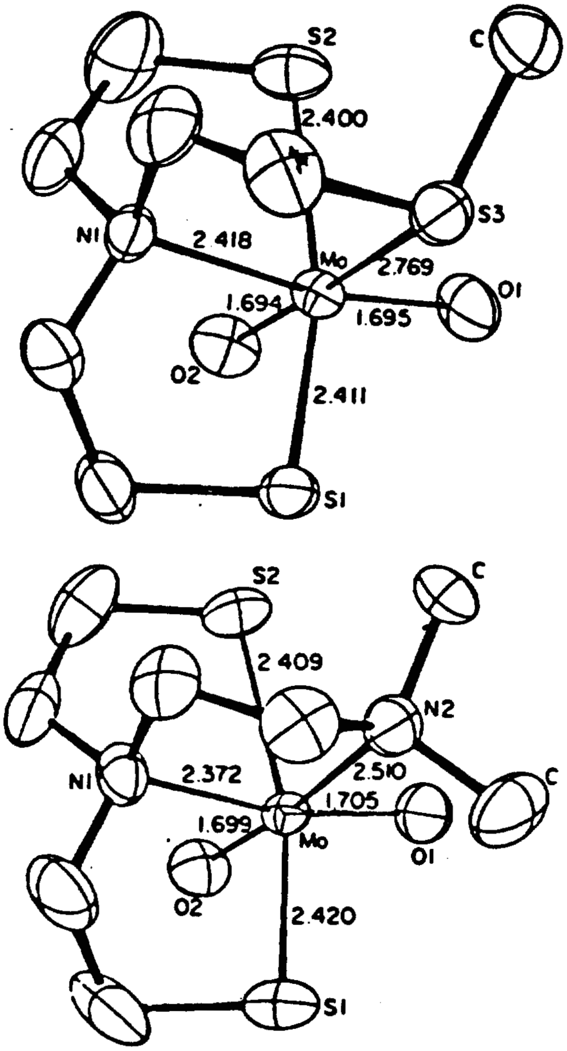
S2
C
2.400
S3
N1
2.418
Mo
2.769
O1
1.694
1.695
O2
2.411
S1
S2
C
2 409
N2
N1
2.372
2.510
C
1.705
1.699
Mo
O1
O2
2.420
S1

Figure 5. Molecular structures of complex K, $MoO_2((SCH_2CH_2)_2NCH_2CH_2SCH_3)$ (top) and complex J, $MoO_2((SCH_2CH_2)_2NCH_2CH_2N(CH_3)_2)$ (bottom). {Reproduced from reference 35}.

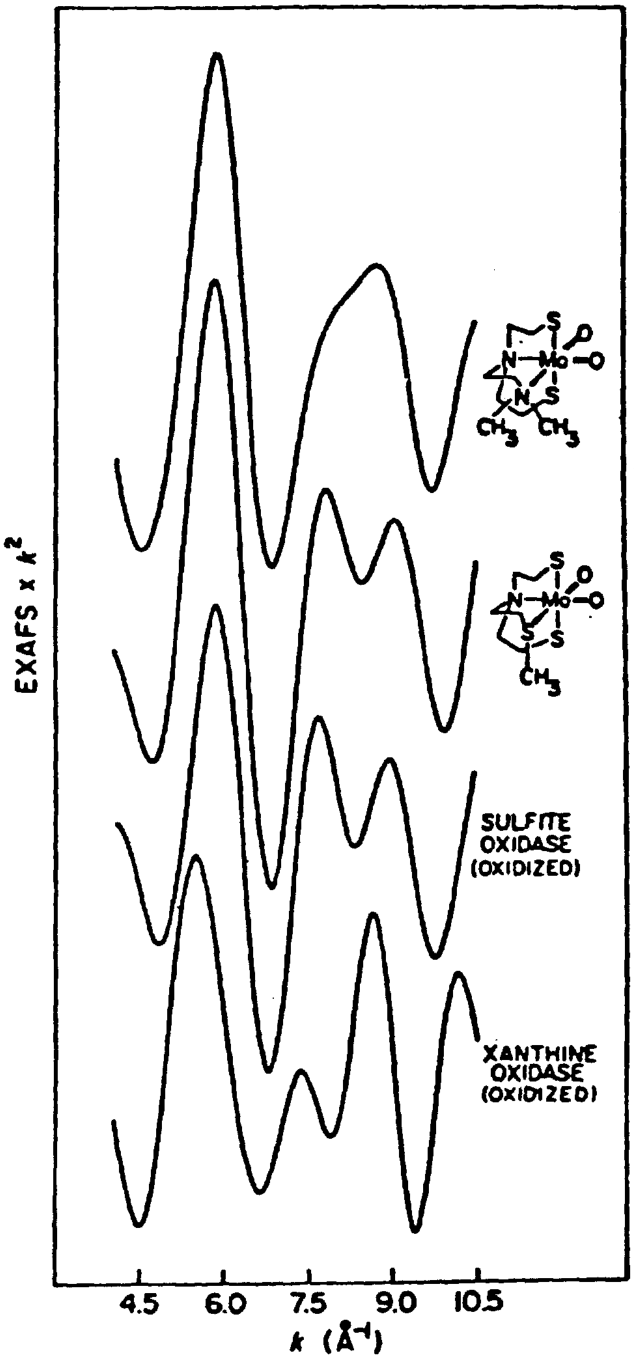

Figure 6. Molybdenum EXAFS spectral comparisons for complexes J (top) and K with sulfite oxidase and xanthine oxidase. {Reproduced from reference 35}.

Table III lists the ν(Mo=O) frequencies of these three complexes. Their high values also indicate that the structure in the normal Mo(VI) dithiolate structure, as confirmed by x-ray crystallography for complexes J and K. The frequencies for complex L, although still in the high range, are slightly lower than those for J and K indicating that some hydrogen bonding with the amine hydrogens or intermolecular hydrogen bonding may be occurring, causing the O-Mo-O angle to open. Complex K may have experienced internal reduction of Mo prior to its arrival at OGC. The data reported pertain to this possible reduced sample. This problem is discussed in detail in the section on solution data.

5. Complexes M and N

Complexes M and N are the only two dimeric molybdenum complexes considered in this study, where the two molybdenums are bridged by one oxygen atom. The bridging oxo group adds two new characteristic features to the vibrational spectrum at 750 and 450 cm^{-1}.[50, 53, 63, 64] These correspond to antisymmetric and symmetric stretching vibrations respectively, of the Mo-O-Mo bridge.[63] In complex M the appropriate bands appear at 715 and 460 cm^{-1}. In complex N only the antisymmetric band appears at 680 cm^{-1} in the infrared. The ν(Mo=O) frequencies are characteristic of octahedral Mo(VI) with normal *cis* oxo coordination. These frequencies are listed in Table IV.

The molybdenum-oxygen double bond stretching frequencies in the solid state Raman spectra of the fourteen Mo(VI) complexes can be used

Table IV. Assignment of Raman Frequencies for Complexes M and N

Molybdenum Complex	Structural Formula		Vibrational Frequencies (cm^{-1})			
			Mo=O	Mo-N	Mo-S	Mo-O-Mo
M	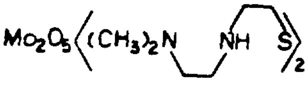	IR	918, 882	585, 520	370	715, 460
		R	914, 884	521	378	706, 462
N	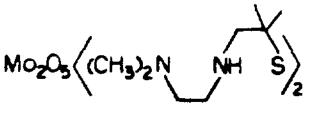	IR	916, 889	588, 520	375	680
		R	910, 883	---	382	---

as a guide to assigning structural types. When the antisymmetric ν(Mo=O) frequency is higher than ~ 900 cm^{-1}, the structure of the complex appears to be a distorted octahedron with *trans*-sulfurs and *cis*-oxygens. However, when the antisymmetric ν(Mo=O) frequency is below 900 cm^{-1}, the skew-trapezoidal bipyramid is the likely structure with *cis*-sulfurs and a possible partial disulfide bond.

B. Solution Raman Studies of Mo(VI) Model Complexes

Raman studies of solutions of the Mo(VI) complexes were carried out in three solvents: CH_2Cl_2, CH_3CN, and $(CH_3)_2SO$ (DMSO), over the range 800-1000 cm^{-1} to cover the ν(Mo=O) frequencies. DMSO was used for only a few complexes that were insoluble in CH_3CN and CH_2Cl_2. Because both CH_3CN and CH_2Cl_2 have Raman peaks within this range, it was necessary to run each complex in both solvents in order to see all Raman peaks due to the complexes. CH_2Cl_2 has a peak at ~ 899 cm^{-1} and CH_3CN has a peak at ~ 923 cm^{-1}. DMSO has a more complex Raman spectrum in this region with peaks at 899, 933, and 956 cm^{-1}. A complete set of solution Raman spectra and solvent spectra may be found in Appendix II. The electronic absorption spectral results obtained at the Kettering Research Laboratories are listed in Table V.

1. Complexes A, B, C, D, F, and G

Table VI lists the Raman ν(Mo=O) frequencies for this first group of complexes in both the solid state and in solution. Complexes A and B exhibit insignificant differences between their solid

Table V. Electronic Absorption Spectral Results for the Molybdenum Complexes in Solution [a)]

Complex	Structural Formula	Concentration (M)	Solvent	λ_{max} (nm)	Absorbance
A	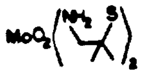	~ 1 × 10^{-4}	CH_3CN	355 260 226(sh)	0.68 0.75 0.83
B	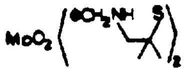	1.2 × 10^{-4}	CH_3CN	350 264(sh)	0.32 0.56
C	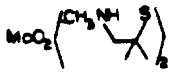	1.0 × 10^{-4}	CH_3CN	354 262(sh)	0.23 0.34
D	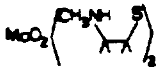	8.3 × 10^{-5}	CH_3CN	340(sh) 330 270(sh)	0.3 0.34 0.33
F	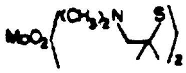	1.2 × 10^{-4}	CH_3CN	322(broad) 280(sh)	0.13 0.2
G	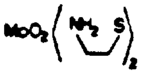	~ 1 × 10^{-4}	CH_3CN	354 272(sh) 246(sh) 230(sh)	0.51 0.59 0.64 0.75
E	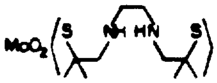	1.2 × 10^{-4}	CH_3CN	367 280 250 229(sh)	0.65 0.48 0.66 0.8
I	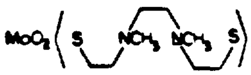	1.2 × 10^{-4}	CH_3CN	368 290 253 228	0.59 0.58 0.83 0.96
H	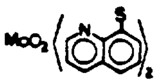	~ 9 × 10^{-4} ~ 9 × 10^{-5}	CH_3CN CH_3CN	412 253	0.6 0.38
J	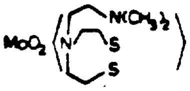	1.2 × 10^{-4}	CH_3CN	387(broad) 287 236	0.32 0.5 1.08

Table V (continued)

Complex	Structural Formula	Concentration (M)	Solvent	λ_{max} (nm)	Absorbance
K	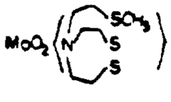	~ 1×10^{-4}	CH_3CN	326(broad)	0.26
				233	0.65
		1.2×10^{-4}	CH_2Cl_2	375	0.49
				235	1.48
L	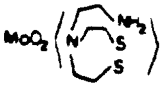	1.3×10^{-4}	CH_3CN	379(broad)	0.4
				286	0.69
				233	1.18
M	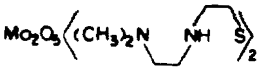	1.34×10^{-3}	CH_2Cl_2	420	0.58
		6.68×10^{-4}	CH_2Cl_2	350	1.0
				274	0.93
				229(sh)	1.18
N	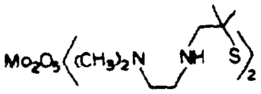	2.15×10^{-3}	CH_2Cl_2	418	0.8
		4.30×10^{-4}	CH_2Cl_2	350	0.74
				281	0.62
				228(sh)	0.82

a) Data obtained by Dr. E. T. Stiefel, Kettering Research Laboratory, Yellow Springs, Ohio.

Table VI. Comparison of Solid State and Solution Raman Frequencies (cm^{-1}) for Complexes A, B, C, D, F, and G

Molybdenum Complex	Structural Formula	Solid State	Solution		
			CH_3CN	CH_2Cl_2	DMSO
A	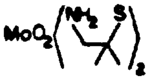	906 870			912 882
B	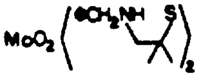	924 903	895	931	
C	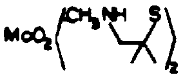	877 848	893	928	
D	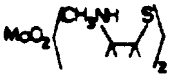	876	895	926	
F	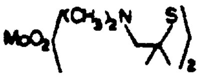	891 880	899[a]		
G	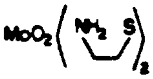	912 881 852			912 885 853

[a] Upon successive scans, the intensity of the 899-cm^{-1} peak decreases and no new peaks appear; Complex F seems to decompose in solution; see text.

state and solution spectra, suggesting that their structures retain the "normal" octahedral geometry. In complexes C and D, however, the frequency ν(Mo=O) shifts to higher frequency values, indicative of a change in coordination geometry upon dissolution. The solution values are those expected for a "normal" octahedral coordination geometry for Mo(VI). Complex F, however, appears to maintain its skew-trapezoidal bipyramid structure in solution. Complex G at first look appears to maintain its solid structure in solution. However, the peak at 912 cm^{-1} which is much smaller than the 881-cm^{-1} peak in the solid state, is much larger in solution than the 885-cm^{-1} peak. The intensity reversal upon solvation suggests a change in equilibrium from a predominantly skew-trapezoidal bipyramid species in the solid state (with only a small contribution of normal octahedral form) to mostly octahedral in the solution phase, with only a small amount of the skew-trapezoidal bipyramid structure. It appears that the "normal" octahedral geometry is preferred in solution.

Only complex F maintains its solid state structure in solution, but even then, only for a short period of time. The 899-cm^{-1} peak of complex F in CH_3CN which is prominent after one scan, disappears after ten scans and no peaks characteristic of the octahedral structure appear to replace it. Ligand F with its two methyl groups on nitrogen may not be stable in an octahedral geometry due to steric interferences. All of the skew-trapezoidal bipyramid complexes either decompose (as with sample F) or rearrange to octahedral upon solvation (as with examples C, D and G). These changes may be solvent dependent since all of these complexes were isolated from methanol solution in which nearly all of the complexes are insoluble.[65]

2. Complexes E and I

The Raman peak positions of the ν(Mo=O) frequencies for solid and solution samples are given in Table VII. In the solid state, complex E was determined to have predominantly *cis* sulfurs with nitrogens of opposite configuration allowing a large O-Mo-O angle and a consequent low ν(Mo=O) frequency. The DMSO solution data indicate that this geometry has changed to a *trans* sulfur arrangement wherein the O-Mo-O angle has decreased and ν(Mo=O) has increased. The minor *trans* component of solid E (Table III) has ν(Mo=O) values similar to those observed for E in DMSO solution. As is the case with complexes C, D, F, and G, the hypothesized partial disulfide bond is not stable in solution, the weakened S...S interaction gives rise to separate thiolate ligands. Complex I, however, displays no appreciable change of ν(Mo=O) upon solvation, indicating that the *trans* sulfur arrangement is preferred in solution as well as in the solid state.

3. Complex H

Table VII lists the ν(Mo=O) frequencies for complex H in both the solid and solution phases. The symmetric stretch appears at a slightly higher frequency in solution than in the solid state but the shift of ~ 10 cm^{-1} is not a large one. The geometry of H is relatively unchanged upon solvation as is evidenced by the ν(Mo=O) frequen-

Table VII. Comparison of Solid State and Solution Raman Frequencies for Complexes E, I, H, J, K, L, M, and N

Molybdenum Complex	Structural Formula	Solid State	Solution		
			CH_3CN	CH_2Cl_2	DMSO
E	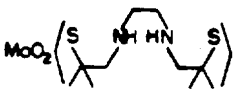	892			915
		866			888
I	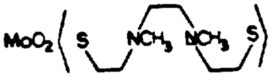	909		925	
		890	900		
H	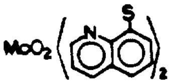	921		931	
		891	898		
J	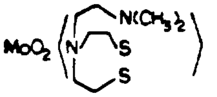	919, 916		930	
		894	900		
K	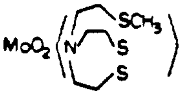	922			
		893		927	
L	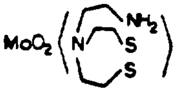	909			
		884		927	
M	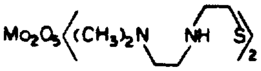	914		919	
		884	888	888	
N	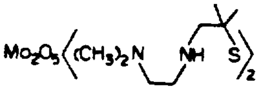	910		920	
		883	886	886	

cies.

4. Complexes J, K, and L

Table VII also lists the ν(Mo=O) frequencies for complexes J, K, and L. Complex J displays a small increase in these frequencies but is still characteristic of the normal octahedral Mo(VI) with *trans* sulfurs and *cis* nitrogens. Both complexes K and L display essentially the same frequencies as complex J. These observations indicate that the slight differences in structure which are apparent in the solid state are removed by solvent interactions, equalizing the Mo=O bond strengths in the dissolved complexes.

Employing CH_2Cl_2 as a solvent, the ^{18}O substituted complex K was used to extract a resonance enhancement profile of the ν(Mo=O) frequency at 927 cm^{-1}. Raman spectra were obtained with eight different excitation lines ranging from 406.7 nm to 647.1 nm over the frequency range from 800 - 1000 cm^{-1}. The spectral data were analyzed by fitting this region (840-980 cm^{-1}) with three component peaks: the solvent peak at 899 cm^{-1} served as an internal intensity standard; the symmetric O-Mo-O vibration is located at 927 cm^{-1}; the third peak at 950 cm^{-1} remains unassigned. A three-dimensional plot of six of these data sets are illustrated in Figure 7, and in Figure 8 the enhancement profiles for the peaks at 927 and 950 cm^{-1} are plotted. {The individual plots of these data showing the curve fitting analysis for each spectrum are given in Appendix III}. Both figures 7 and 8 clearly show a resonance enhancement maximum at approximately 480 nm.

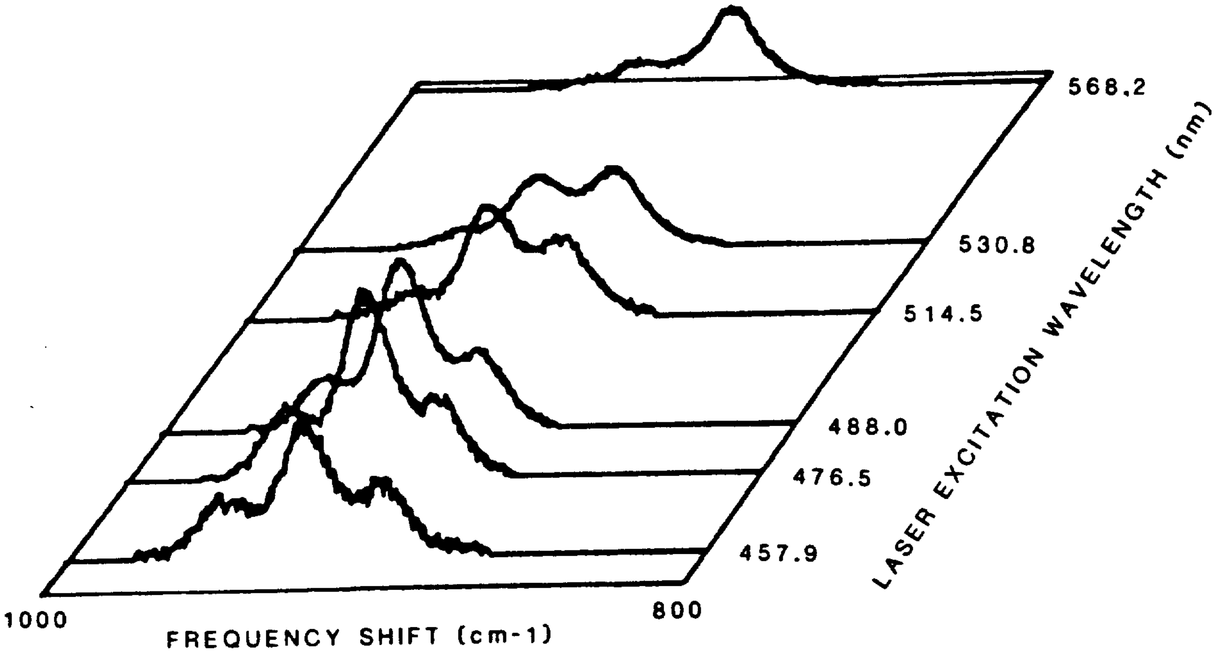

Figure 7. Resonance Raman spectra of complex K in CH_2Cl_2 solution as a function of excitation wavelength. The solvent peak at 899 cm^{-1} is used as an internal intensity standard for the excitation profile shown in Figure 8.

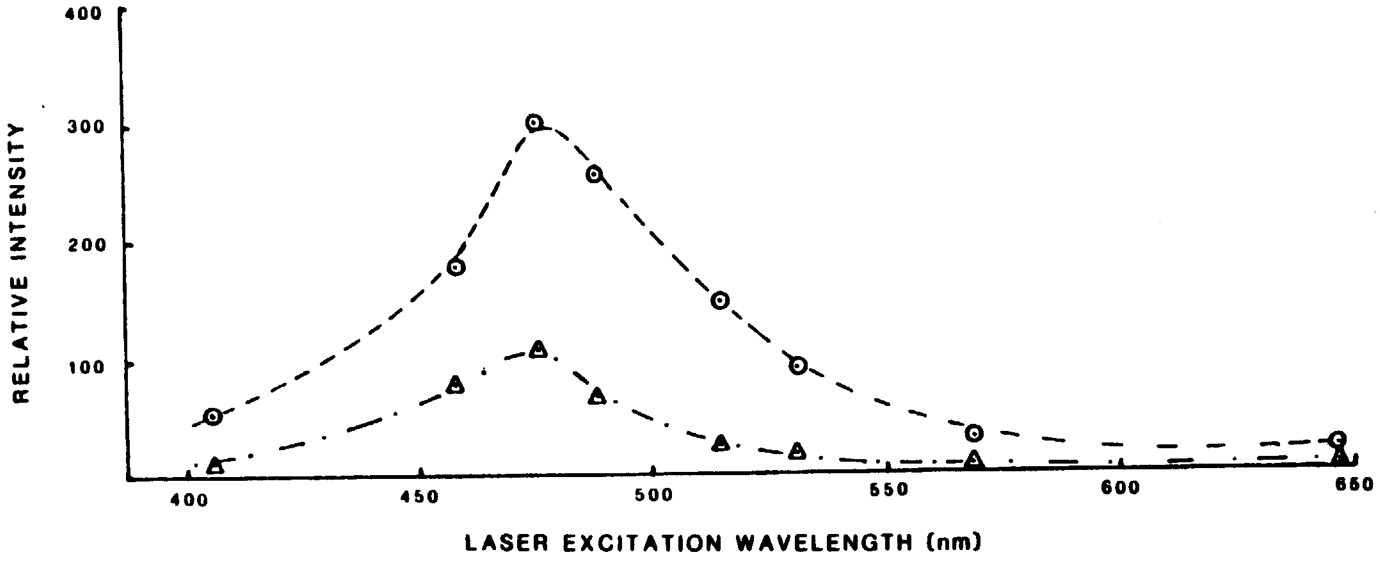

Figure 8. Resonance Raman enhancement profiles for the 927 (o) and 950cm^{-1} (Δ) peaks of complex K in CH_2Cl_2 solution. The lines are drawn as a visual aid.

Such a value is totally unexpected since complex K was reported to have absorption maxima at 375 nm and 235 nm in CH_2Cl_2 (Table V). To verify these diverse results, the electronic absorption spectrum of complex K was reinvestigated in CH_2Cl_2. The resulting spectrum shown in Figure 9, clearly reveals an absorption maximum at 477 nm in perfect agreement with the resonance Raman enhancement profile.

The marked difference between the electronic spectra shown in Figure 9 and the data for complex K presented in Table V helps to account for the similarly marked distinction between the infrared spectrum of complex K measured at the Oregon Graduate Center and that originally recorded in Ohio; these data are displayed in Figure 10. The infrared spectrum from Kettering Research Laboratories shows two very strong ν(Mo=O) peaks at 921 and 891 cm^{-1}, whereas in the OGC spectrum, these peaks are of weak and medium intensity, respectively. Both are overshadowed by a third peak at 941 cm^{-1} which is of weak to medium intensity in the Kettering spectrum. Clearly, either a change has occurred in the sample of complex K, or the Kettering infrared and electronic spectral data were obtained with a different preparation of this complex. Although the frequencies for ν(Mo=O) agree, their intensities as well as the electronic absorption spectra are not in accord. Furthermore, crystals of complex K are brown, whereas all of the other complexes are yellow or orange. The crystals on which the x-ray structural analyses were carried out (Figure 5) were described as yellow in color. It is possible that the sample, as received, is not a Mo(VI) complex but a form which has

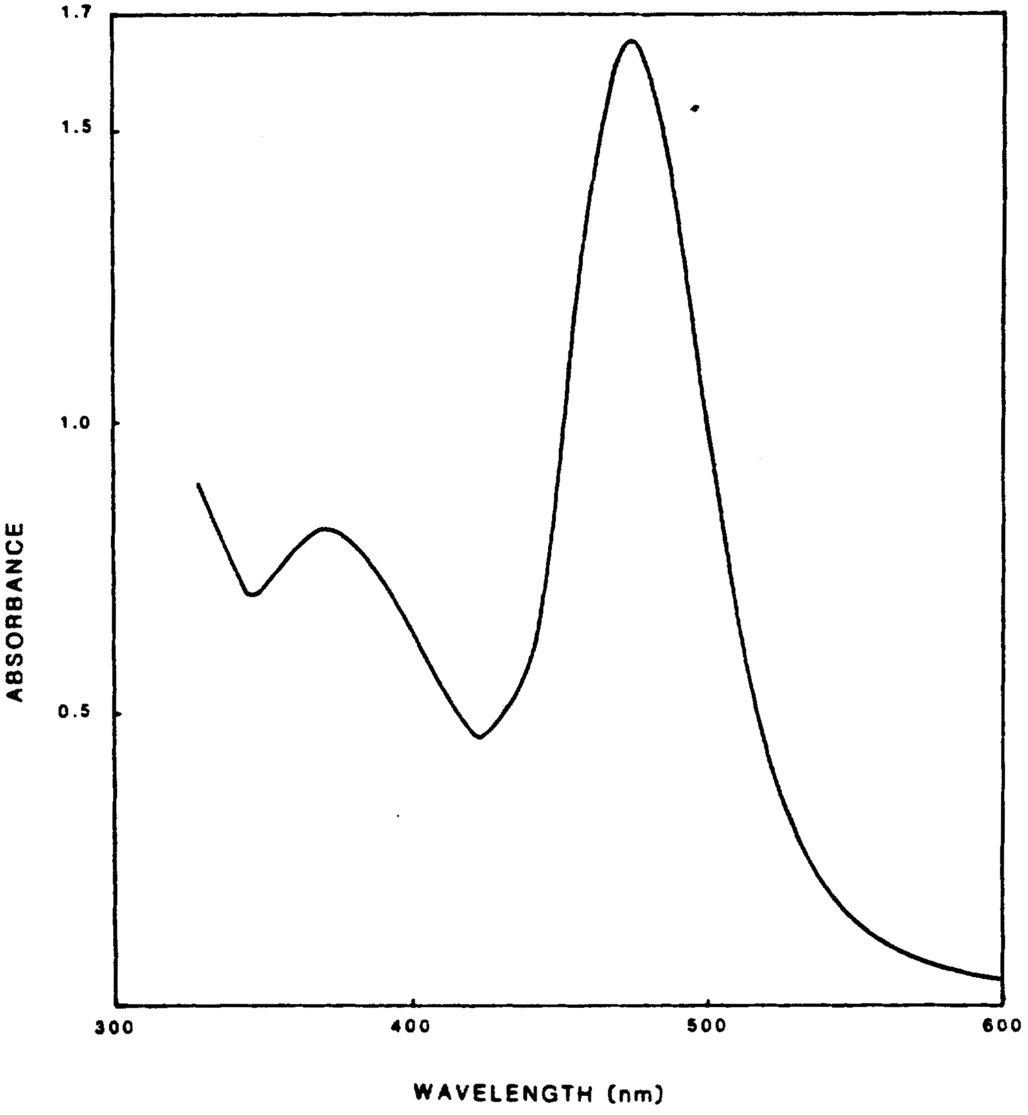

Figure 9. Electronic absorption spectrum of complex K, saturated solution in CH_2Cl_2; $\varepsilon_{477} \sim 1.4 \times 10^4\ M^{-1}cm^{-1}$.

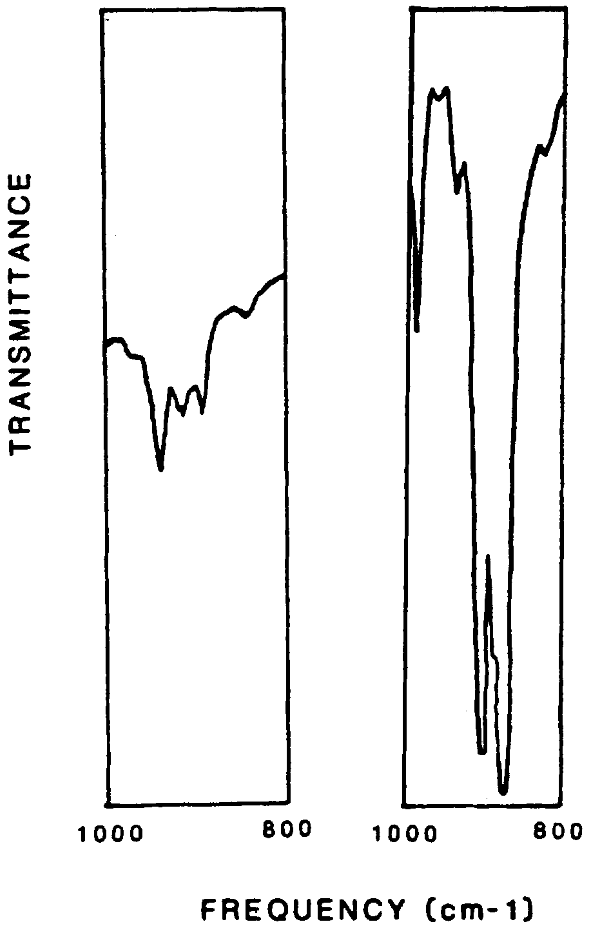

Figure 10. Infrared spectra of complex K in the ν(Mo=O) region. The spectrum on the left is from the sample as received and measured at the Oregon Graduate Center; the spectrum on the right was obtained at the Kettering Research Laboratories.

been reduced to Mo(V) or Mo(VI). Internal reduction is a severe problem noted by Stiefel in synthesizing complexes with three or four thiolate ligands on a MoO_2^{2+}core.[35] However, with two *trans* thiolate ligands and a thioether *cis* to both of these groups, the internal reduction may take longer to occur indicating that the ligand field can control the rate of reduction. If this reduction involves partial disulfide bond formation between the *cis*-oriented thiolate and thioether, then it follows that the less reactive thioether ligand should decrease the internal reduction rate. Such auto-reduction could explain the difference in spectra from the two laboratories.

Stiefel et al.[61] have suggested that the formation of a partial disulfide bond between sulfurs ligated to molybdenum may explain why Mo model complexes have not matched the redox, spectroscopic, and catalytic properties of molybdoenzymes. The delayed internal reduction of complex K shows how a controlled ligand field can affect the redox properties of Mo. The most recent EXAFS results on xanthine oxidase reveal that the ligand field in the enzyme probably contains the same sulfur ligands (2 thiolates and 1 thioether) as complex K. The active enzyme, however, differs in that it has only one terminal oxygen, but has a terminal sulfide ligand to replace the second terminal oxygen. There is also no evidence for the nitrogen ligand of complex K in the EXAFS data. The strong correlation of sulfur ligands between complex K and the xanthine oxidase EXAFS data and the internal reduction of complex K postulated to occur lend support to Stiefel's hypothesis of the role of partial disulfide bond in the enzyme mechanism.

5. Complexes M and N

The $\nu(Mo=O)$ frequencies for complexes M and N for solid and solution phases are also compared in Table VII. The frequency values are the same in two solvents for both complexes and very nearly the same for both in their solid states. These data indicate that no significant structural changes occur upon solvation.

6. Summary

The solution Raman studies of the Mo complexes have revealed that the distorted octahedral structure with *trans*-sulfurs and *cis*-oxygens is preferred in solution. Of the four complexes, C, D, F, and G, which adopt a skew-trapezoidal bipyramid structure in the solid state C, D, and G rearranged in solution and exhibited $\nu(Mo=O)$ characteristic of the normal octahedral structure; complex F decomposes in solution and loses its $\nu(Mo=O)$ frequency. The other ten complexes which are octahedral in the solid state retain this structure in solution. However, complex K exhibited a resonance Raman enhancement profile, an electronic absorption spectrum and infrared spectrum which support the appearance of a reduced Mo-center.

C. Normal Coordinate Analysis

Complexes C and H ($MoO_2(CH_3NHCH_2C(CH_3)_2S)_2$ and $MoO_2(tox)_2$) have both been structurally characterized by x-ray crystallography (Figures 4 and 1).[23, 61] The structural data provide a basis for normal coordinate analysis to assist in the assignment of the complex vibrational spectra. Although x-ray crystal structures have also been reported for complexes J and K,[35] (having tetradentate tripod ligands) the necessary atom positional parameters are not available, which precluded the use of normal coordinate analysis for these two complexes. Overall, NCA has been helpful in assigning vibrational bands of the Mo(VI) complexes.

1. Complex C

The model used for NCA of complex C was an atom set of $MoO_2S_2N_2$ with these atoms placed according to their published positional parameters.[61] Given an initial set of force constants for the Mo-O, Mo-S and Mo-N bonds from average literature values, successive iterations of the normal coordinate calculations were carried out to refine the force constants that would lead to a match of observed and calculated vibrational frequencies in the Raman and/or infrared spectra. For the Mo=O vibrations, the assigned values for the symmetric and antisymmetric stretches at 877 and 848 cm^{-1} were used for matching.

The selection of frequencies to provide a match for Mo-N stretches was not straightforward since only very few Mo-N stretches are assigned in the literature. Possible choices can be made from inspection of the Raman spectrum of complex C, shown in Figure 11. A doublet appears at 606 and 600 cm^{-1}. This doublet corresponds to a peak in the infrared spectrum at 600 cm^{-1}. Although a peak at this frequency is higher than for pure metal-ligand single bonds, nitrogen is known to form multiple bonds with molybdenum; on this basis, 600 cm^{-1}

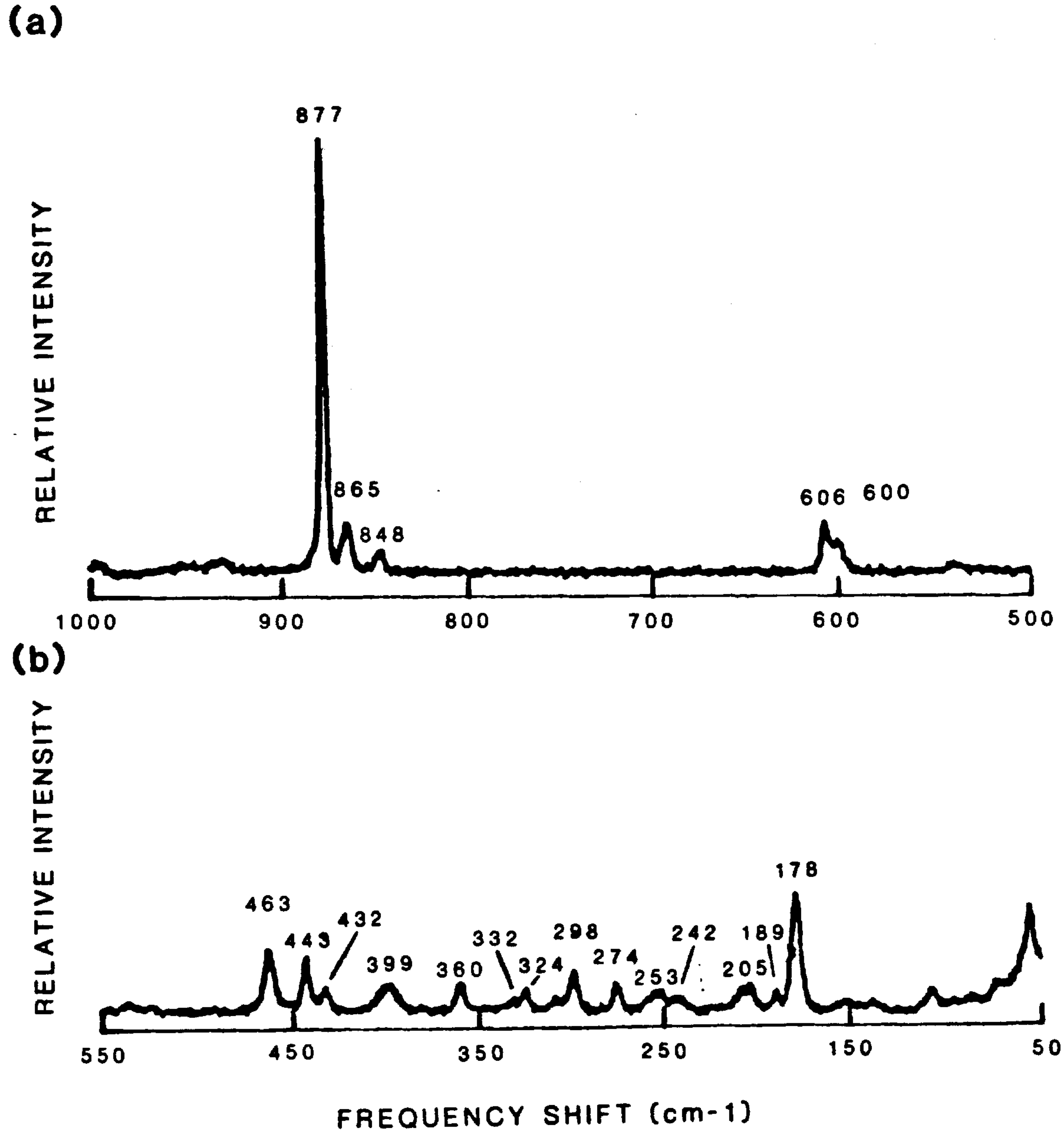

Figure 11. Raman spectrum of complex C from 50-550 cm^{-1} (bottom) and 500-1000 cm^{-1} (top). The scan parameters are as follows: Laser excitation, 568.2 nm, 40 mW; slits, 2.5 cm^{-1}; scan rate, 1.25 cm^{-1}/sec; number of scans, 2; 180 degree backscattering geometry; sample temperature, 77K.

would not be an unreasonable choice for ν(Mo-N). However, since both oxygens are already double bonded to molybdenum and since the nitrogens form an angle of 144° with molybdenum as well as angles near 140° with the sulfur ligands,[61] competition for π bonding among the ligands may lower the frequency of ν(Mo-N) thereby making the next lower frequency Raman peaks at 463, 443, and 432 cm^{-1} also potential candidates for these stretching vibrations. Combinations of all of these frequencies were attempted for ν(Mo-N) in the NCA calculations.

Stretching vibrations for ν(Mo-S) have been previously assigned at 390 cm^{-1}.[46] Raman peaks at 399 and 360 cm^{-1} are thus possible Mo-S frequencies for use with NCA. Alternatively, the higher frequencies at 463, 443, and 432 cm^{-1} could serve as possible Mo-S frequencies when the 600 cm^{-1} bands are selected for Mo-N stretches.

Matching of the O=Mo=O stretching vibrations was not very satisfactory. The two observed peaks are separated by 29 cm^{-1} (877 cm^{-1} and 848 cm^{-1}), but the best calculated values have a separation of 68 cm^{-1} (896 cm^{-1} and 828 cm^{-1}). The use of a general valence force field and the particular geometry of complex C couple these two frequencies so that they cannot be obtained with a smaller separation. The failure of NCA to generate more satisfactory frequencies for ν(Mo=O) may be due to extensive hydrogen bonding between molecules that occurs in the solid state.[61] Furthermore, the model used is oversimplified since only the atoms liganded to molybdenum were used.

Matching of the ν(Mo-N) and ν(Mo-S) frequencies provided some more interesting results. The peaks at 606 and 600 cm^{-1} could not be matched as the symmetric-antisymmetric pair of molybdenum-nitrogen stretching vibrations because the separation of 6 cm^{-1} between these peaks was much too small. However, a much closer match was obtained by using the 606-cm^{-1} peak and an infrared peak at 555 cm^{-1} for these Mo-N vibrations, as NCA calculated frequencies at 611 and 549 cm^{-1}.

If it is assumed that the 611/549 cm^{-1} pair is a satisfactory match for ν(Mo-N) assigned at 606/555 cm^{-1}, then a match for ν(Mo-S) must also be found. Five peaks are available in the Raman spectrum of complex C in the appropriate frequency range for molybdenum-thiolate vibrations, located at 463, 443, 432, 399, and 360 cm^{-1}. A series of NCA calculations was performed matching different pairs of these frequencies to obtain a best fit. The results of these calculations are listed in Table VIII. Although reasonable matches were obtained with all pairs of these numbers, only one pair resulted in an exact match. Using this criterion, the peaks at 399 and 360 cm^{-1} are assigned as the symmetric and antisymmetric S-Mo-S stretching vibrations for complex C. Furthermore, these values agree with the assignments of Ueyama et al.[46] who found the Mo-S stretching frequencies between 385-395 cm^{-1} in Mo-cysteine complexes.

The alternate possibility that ν(Mo-N) can be assigned to the 463, 443, or 432-cm^{-1} peaks was also explored. Because of their proximity to ν(Mo-S) at 399 and 360 cm^{-1}, considerable coupling of ν(Mo-S) with ν(Mo-N) resulted using these frequencies. In all three possible combinations of symmetric and antisymmetric pairs for these three frequencies, no adequate match could be calculated for ν(Mo-N). The

Table VIII. Normal Coordinate Analysis Results for ν(Mo-S) from Complex C

Experimental Peaks (cm^{-1})	Calculated Values [a] (cm^{-1})					
463	459	460				
443	440		443	440		
432		430	427		430	
399				398	398	399
360						360

a) Each column represents the results of a single calculation to match the pair of experimental peaks to the left.

coupling had the additional effect of giving a poorer match for ν(Mo-S). Therefore, it is proposed that ν(Mo-N) occurs at 606 cm^{-1} for the symmetric stretch and 555 cm^{-1} for the antisymmetric stretch.

2. Complex H

The model used for complex H was an atom set of $MoO_2N_2S_2$ in the coordinate positions as defined by the x-ray crystal structure. Because the nitrogen ligand is part of an aromatic ring system and not free to vibrate by itself, the mass used for nitrogen in these calculations was the mass of the double ring. This increased mass for a nitrogen ligand has been shown to be appropriate in work by Wright[66] and Cornilsen[67] in conjunction with pyridine and imidazole ligands respectively.

The assignments of ν(Mo=O), ν(Mo-N), and ν(Mo-S) have been discussed earlier and these results are listed in Table III. The calculated frequencies of 922 and 885 cm^{-1} match fairly closely with the experimental Raman values of 916 and 891 cm^{-1}. Coupling of these two vibrations in this geometry does not allow the separation between peaks to be made any smaller. Structural factors other than geometry and stretching force constants are probably involved, making this simple model inadequate to compute these frequencies more exactly. It is interesting to note that present results for complex H provide an exact match for the ν(Mo=O) frequencies of complex A (Table II). For this compound, the separation between the observed peaks assigned to symmetric and antisymmetric modes is 37 cm^{-1}, identical to the NCA calculated separation found for complex H. The agreement is most likely fortuitous, since the experimentally observed separation of ν(Mo=O) peaks for complex H is only 25 cm^{-1}.

The peak at 276 cm^{-1} was identified by Zuika et al.[62] as ν(Mo-N) but no second peak was assigned to the Mo-N vibrations. Since both symmetric and antisymmetric modes are expected, NCA has been used to identify the other component. Calculated values for complex H are at 276 and 251 cm^{-1} which match the experimental Raman values exactly and such an assignment is proposed for the symmetric and antisymmetric stretches for ν(Mo-N), respectively.

Calculation of ν(Mo-S) proved more difficult because the previously assigned values of 366 and 342 cm^{-1} (Table III and accompanying discussion) could not be matched by NCA. Whereas the frequencies and intensities of the Raman and infrared peaks make them good candidates for these assignments, their separation is only 24 cm^{-1}. The NCA program was unable to calculate a separation for the two components of the ν(Mo-S) modes below 100 cm^{-1}. The frequencies most closely matched are at 418 cm^{-1} and 328 cm^{-1} in the Raman data.

In an attempt to lower the calculated frequency from 418 cm^{-1} to 366 cm^{-1}, the mass of sulfur was increased some 50-100%. Since sulfur is bound to a large ring system, it is not unreasonable to expect a higher effective mass for the sulfur ligand. NCA calculations then produced a frequency at 367 cm^{-1}. Unfortunately, the second frequency for ν(Mo-S) was depressed to 330 cm^{-1} resulting in a 40 cm^{-1} spread and the frequencies for ν(Mo-N) were also shifted from their previously calculated values. These changes derive from significant coupling between ν(Mo-S) and ν(Mo-N), preventing the calculation of an entire set of four frequencies to match experimental values. Again the simplified model does not allow an accurate computational analysis of the system. Therefore, the values previously assigned for ν(Mo-S) at 366 and 342 cm^{-1} and for ν(Mo-N) at 276 and 251 cm^{-1} are proposed to be the best possible description of this system (Table III).

D. Other Ligand Vibrational Frequencies

The frequencies for ν(Mo=O) are readily identified in the Raman and infrared spectra of these complexes due to their intensity in a region normally free of other peaks. The same cannot be said for the frequencies of ν(Mo-S) and ν(Mo-N), however. ν(Mo-S) has been studied in a large number of complexes and the frequency range is known to be about 350-400 cm^{-1}.[46] The expected frequency range for ν(Mo-N) is not as well known. Normal coordinate analysis of complex C calculated a reasonable match to observed frequencies at 606 and 555 cm^{-1}. These values indicate that multiple bonding of nitrogen to molybdenum is occurring. This is expected for Mo-N bonds although the phenomenon has not been widely studied by infrared spectroscopy.[55, 58, 60] Where vibrational frequencies are known for ν(Mo-N), the multiple bonding produces stretching frequencies above 600 cm^{-1}.[55] Other complexes exhibit ν(Mo-N) at 553 and 528 cm^{-1}.[55] Based upon these reported values, ν(Mo-N) for amine-nitrogens can be expected over a wide range of frequencies from about 500 to 650 cm^{-1}.

Tables II, III, and IV list infrared and Raman peaks within the appropriate frequency ranges for ν(Mo=O), ν(Mo-N), and ν(Mo-S). The values listed for ν(Mo-N) and ν(Mo-S) are suggested assignments based only upon the expected frequency ranges for these vibrations. Often, the peaks listed for ν(Mo-N) are the only peaks visible in the 500-600-cm^{-1} region and the values observed in Raman spectra do not always correspond with the values in infrared spectra. In such cases, solid state effects or, possibly, local centers of symmetry for these vibrations may permit only the symmetric mode to appear in the Raman spectrum and only the antisymmetric mode to appear in the infrared spectrum. Positive identification of these modes would require a more detailed study involving isotopes of nitrogen and sulfur, a more detailed NCA using the full molecular structure, and a more sophisticated force field which takes non-bonded interactions into account.

E. Oxygen Isotopic Substitutions

Five of the complexes were available with ^{18}O substitution: A, C, F, J, and K. Based upon simple mass effects, any Mo=O frequency solely affected by the ^{18}O isotope should be shifted to 0.951 of its normal value. In all the cases examined, new peaks appeared only in the range of ν(Mo=O), but the spectra were far more complex than expected. Normal coordinate analysis was used to interpret these data. All lower frequency peaks are identical in position and intensity when comparing the two isotopic isomers, suggesting that oxygen-dependent deformation modes have little or no sensitivity to the mass change.

Below the Raman spectra of each of these isotopically-enriched complexes are discussed relative to the previously investigated ^{16}O-forms of the corresponding complexes.

1. Complex A

The spectra of complex A and its isotopic isomer are shown in Figure 12 and summarized in Table IX. There are two peaks of interest in complex A at 906 and 870 cm^{-1}. Simple mass effects would predict that these two peaks shift to 862 and 827 cm^{-1} respectively in the ^{18}O spectrum. If the isotopic substitution were not complete, then one would expect to see a superposition of all four peaks. However, the observed spectrum is still more complex despite the higher noise. In the ^{16}O isomer the 906-cm^{-1} peak is about three times as intense as the 870-cm^{-1} peak. Both of these peaks are present in the ^{18}O isomer but the 902-cm^{-1} peak is not quite twice as intense as the 870-cm^{-1} peak. The ^{16}O complex's 906-cm^{-1} peak is split into a 914-cm^{-1} and a 902-cm^{-1} peak in the ^{18}O spectrum. In a similar fashion the ^{16}O 870-cm^{-1} peak is split into an 881 and an 870-cm^{-1} peak in the ^{18}O spectrum. This can be explained by considering which site the ^{18}O occupies when only one ^{18}O is substituted. In a pure octahedron with *trans* sulfurs and *cis* nitrogens *trans* to *cis* oxygens, two mirror image isotopes are possible. The real complex is undoubtedly distorted from a pure octahedron but the two isomers are still possible. The oxygens are not in equivalent positions due to the nonsuperimposability of the two isomers. When one ^{18}O is substituted, two isomers

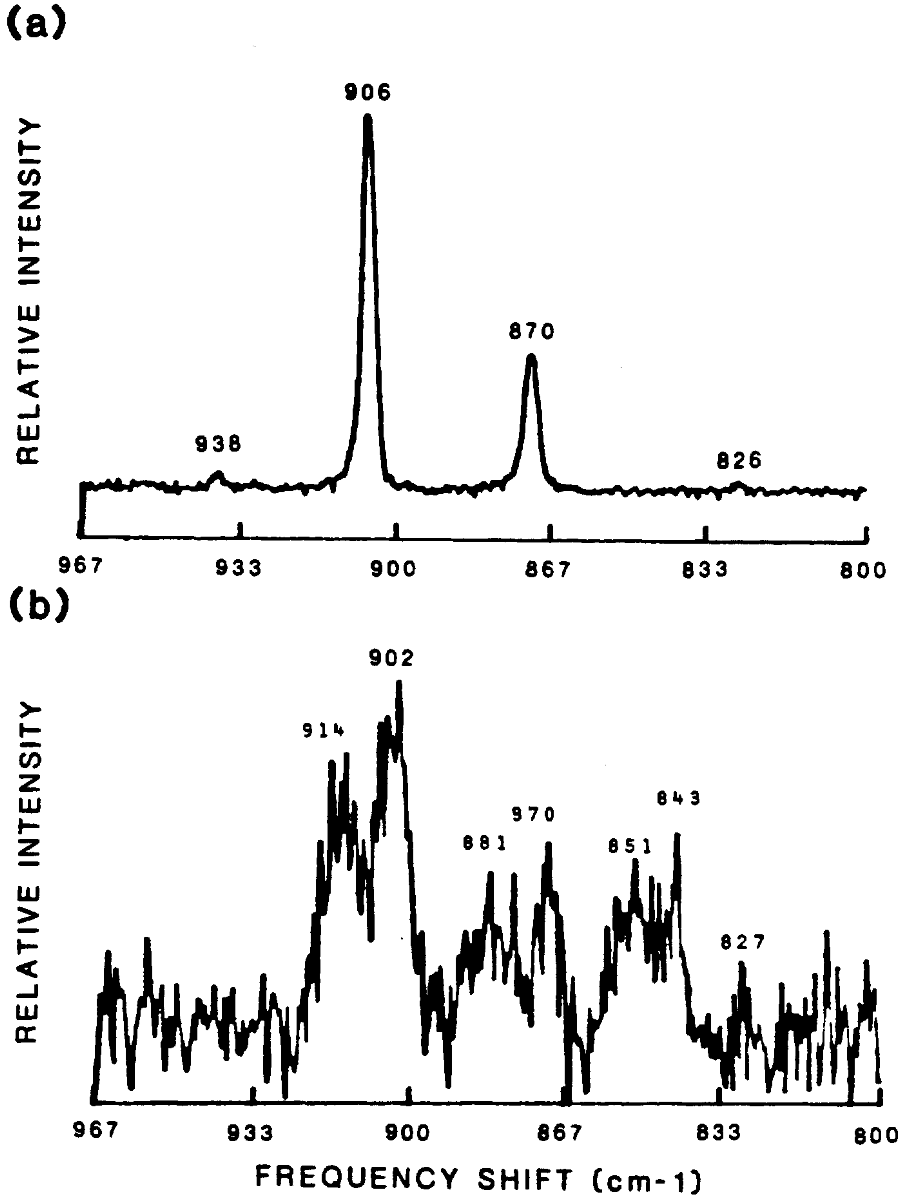

Figure 12. Raman spectra of complex A (a) and ^{18}O - labeled A (b). Scan parameters are as follows: laser excitation, 568.2 nm, 30 mW; slits, 2.5 cm^{-1}; scan rate, 2.5 cm^{-1}/sec; number of scans, 10; 180 degree backscattering geometry; sample temperature, 77K.

Table IX. Comparison of Raman and Infrared Bands of the ^{18}O Isotopically Substituted Molybdenum Complexes[a]

A 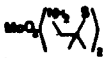				C 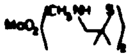				F 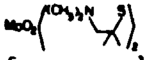				J 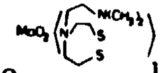						K 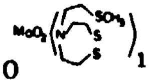			
^{16}O		^{18}O		^{16}O		^{18}O		^{16}O		^{18}O		^{16}O		^{17}O		^{18}O		^{16}O		^{18}O	
R	IR	R	IR	R	IR	R	IR	R	IR	R	IR	R	IR	R	IR	R	IR	R	IR	R	IR
		914	913		882		883	891	892	893	893	919	920	919	920	920	920	939	942	939	942
906	907			877		878				886	888	916	913	914	914	912	912	930		927	
		902	900			872	872	878	880	879	880			911		907	908	922	922		
		881	881									894	895	893	893	893	893	914	915	913	912
870	870	870	867	865		865			855	860	858		890						908		905
		851	847		855		859					876		878	880			893	894		898
		843	840	848		848	848			847			874	873		873	875				873
										840				859	860	860	861			860	
						834		839	836	838	838					856					855
						828	827						850			851	851				845

a) Frequencies are in cm^{-1}.

are possible for each mirror image. Each position would then have a different force constant, thus producing a splitting of frequencies as observed in Figure 12B. This splitting is not observed in the normal complex because the vibrations of the oxygens are coupled to one another. Calculating the mass effect on these new frequencies, 913 cm^{-1} would be predicted to shift to 868 cm^{-1}, and 881 cm^{-1} would shift to 838 cm^{-1}. Both of these calculated frequencies appear in Figure 12B, the 868-cm^{-1} frequency is seen at 870 cm^{-1} and 838-cm^{-1} frequency at 843 cm^{-1}. However, the 870-cm^{-1} feature also occurs in the ^{16}O spectrum. As mentioned previously, the intensity of this peak increased relative to that at 902 cm^{-1} indicating that two coincident peaks are likely to be present. The predicted 870 cm^{-1} to 827 cm^{-1} mass shift was not unambiguously observed due to the noise of the spectrum (Figure 12B) and the expected lower intensity of this peak, but a feature at ~ 827 cm^{-1} is discernible. However, a new peak at 851 cm^{-1} has not been explained.

The above argument is based on the assumption that each peak is independently shifted by isotopic substitution. However, the original two peaks in the ^{16}O spectrum at 906 cm^{-1} and 870 cm^{-1} represent the symmetric and antisymmetric stretching combinations of the two Mo=O bonds respectively. These two modes are coupled together and their frequency relationship must be considered to understand the vibrational results. Normal coordinate analysis provides a means for this understanding. This technique does require a specific crystal structure or structural model. Since the x-ray crystal structure for complex A is not yet available, it is necessary to use a model structure for the NCA calculations. As concluded previously, the structure for complex A is the normal octahedral ligand geometry for dioxo-molybdenum (VI) complexes. The x-ray crystal structure for complex H has been reported and is known to be of the normal octahedral geometry.[23] Therefore, the structure of complex H was chosen as a structural model for the NCA calculations of complex A. (The successful NCA match for the two Mo=O modes has been noted earlier.)

In the first calculation both oxygens were assigned a mass of 16. The Mo=O force constant was refined through iteration to match the given experimental frequencies of 906 and 870 cm^{-1}. The NCA matched these frequencies exactly with a force constant of 632 Newtons/meter. Since values for Mo=O force constants range from about 570 to 900Nm^{-1} [68] a value of 632 Nm^{-1} is reasonable. This force constant was then used to calculate the frequencies expected with one or two ^{18}O atoms. The results of these calculations are given in Table X. With one ^{18}O atom, the calculated frequencies are 896 and 840 cm^{-1} regardless of which ^{16}O is substituted with ^{18}O. The 896-cm^{-1} frequency is close to the 902-cm^{-1} value observed in the Raman spectrum of the mixed isotope complex. Similarly, the 840-cm^{-1} frequency is close to the experimental value of 843 cm^{-1}. In the case of two atoms of ^{18}O being substituted, the calculated frequencies are at 865 and 827 cm^{-1} for the same force constant of 632 Nm^{-1}. These are the values calculated previously by simple mass effects. Although 865 cm^{-1} is close to 870 cm^{-1}, there is only poor experimental evidence for an 827-cm^{-1}

Table X. Normal Coordinate Analysis Results for Complex A having a single Mo=O Force Constant (FC)[a]

Raman		Normal Coordinate Analysis							
A $^{16}O-^{16}O$	A $^{16}O-^{18}O$	$^{16}O-^{16}O^{b}$	$^{16}O-^{18}O^{c}$ FC 632	$^{18}O-^{18}O^{c}$ FC 632	$^{18}O-^{18}O^{d}$	$^{16}O-^{16}O^{e}$	$^{16}O-^{18}$ FC 646 [f]	$^{18}O-^{18}O$ FC 646 [f]	$^{18}O-^{18}O^{g}$
	914					915			
906		906					905		
	902		896						
	881					880			885
870	870	870			875			875	
				865					
	851						849		847
	843		840		837			837	
				827					

[a] Frequencies in cm^{-1}; force constants in Nm^{-1}.

[b] Force constant refined to 632 Nm^{-1} to match 906 and 870 cm^{-1}.

[c] FC held fixed during calculation.

[d] Force constant refined to 648 Nm^{-1} to match 870 and 843 cm^{-1}.

[e] Force constant refined to 644 Nm^{-1} to match 914 and 881 cm^{-1}.

[f] Average of 648 and 644 Nm^{-1}; FC held fixed during calculation.

[g] Force constant refined to 661 Nm^{-1} to match 881 and 851 cm^{-1}.

peak. Another calculation was then performed on the doubly substituted ^{18}O molecule in which the Mo=O force constant was refined for a still better fit. The result, as listed in Table X, is a pair of peaks at 875 cm^{-1} and 837 cm^{-1} with a force constant of 648 Nm^{-1}. The 875 cm^{-1} feature is now higher in frequency than the experimental 870-cm^{-1} peak, but the calculated 837-cm^{-1} frequency is closer to the 843-cm^{-1} experimental observed peak. The force constant increased from 632 Nm^{-1} to 648 Nm^{-1} but this remains a satisfactory value for a Mo=O bond.[68]

It is still necessary to explain the experimentally observed 914, 881, and 851 cm^{-1} peaks. Therefore, the double ^{16}O model force constant was refined to match the 914 cm^{-1} and 881 cm^{-1} peaks. The new force constant was calculated as 644 Nm^{-1}, a value very close to the 648 Nm^{-1} calculated in the double ^{18}O refinement. An intermediate value of 646 Nm^{-1} was then used to calculate the mixed isotope frequencies. As shown in Table X, these frequencies are 905 and 849 cm^{-1}, values that can be satisfactorily matched to the experimental 902 cm^{-1} and 851 cm^{-1} frequencies.

A last force constant refinement was carried out to match the 881 cm^{-1} and 851 cm^{-1} peaks to a double ^{18}O substituted molecule. The frequency match is good as seen in Table X, but the force constant is now higher at 661 Nm^{-1}. Although it is still a reasonable value for a Mo(VI)=O bond, it represents a third value for the system under study. As mentioned previously, the two oxygen atoms are not in equivalent positions in the complex; it is therefore not unreasonable for each Mo=O bond to have a different force constant, but a third value is not acceptable in this simple system.

The following discussion presents results attempting to fit these frequencies with two Mo=O force constants. Using the values of 646 and 632 Nm^{-1} obtained above as initial force constants, the double ^{16}O model was refined against the 914 and 881 cm^{-1} frequencies and against the 906 and 870 cm^{-1} frequencies to obtain a match with two new sets of force constants. These results are shown in Table XI. The first four columns of NCA calculations show the frequencies obtained with force constants of 650 Nm^{-1} for the first oxygen and 639 Nm^{-1} for the second oxygen. In this set of calculations, it makes a difference whether the first oxygen has a mass of 16 or 18 in the mixed isotope molecule. When one combines the results of these first four columns, all of the frequencies observed for the mixed isotope sample can be accounted for. The worst fit is the double ^{18}O isotope where the calculated 836-cm^{-1} value falls short of the experimental 843-cm^{-1} frequency and the calculated 874-cm^{-1} values falls short of the experimental 881-cm^{-1} frequency and also exceeds the experimental 870-cm^{-1} feature. Since these two calculated values do not appear in the experimental data, it is reasonable to suggest a low abundance of this composition in the sample.

The last four columns of Table XI represent the calculated frequencies using the force constants 635 Nm^{-1} and 626 Nm^{-1} for the two Mo=O bonds. Other than the double ^{16}O molecule, the calculated frequencies are not good matches for the experimental frequencies. The lower values of the force constants give frequencies lower than those

Table XI. Normal Coordinate Analysis Results of Complex A with two Mo=O Force Constants [a]

Raman		Normal Coordinate Analysis							
A ^{16}O-^{16}O	A ^{16}O-^{18}O	^{16}O-^{16}O[b]	^{16}O-^{18}O[c]	^{18}O-^{16}O[c]	^{18}O-^{18}O[c]	^{16}O-^{16}O[d]	^{16}O-^{18}O[e]	^{18}O-^{16}O[e]	^{18}O-^{18}O[e]
	914	916							
906			907			906			
	902			902			897	893	
	881	880							
870	870				874	870			
									865
	851			850					
	843		845		836		837	841	
									827

---

[a] Frequencies in cm^{-1}; force constants in Nm^{-1}.

[b] Two force constants refined to match 914 and 881 cm^{-1}. Final force constants and 639 Nm^{-1}.

[c] No refinement of force constants. Final force constants of 650 and 639 Nm^{-1} used in calculation.

[d] Two force constants refined to match 906 and 881 cm^{-1}. Final force constants are 635 and 626 Nm^{-1}.

[e] No refinement of force constants. Final force constants of 635 and 626 Nm^{-1} used in calculation.

observed in the Raman spectrum, it may be concluded that this set of force constants does not provide an accurate description of the mixed isotope system under study. However, it is necessary to explain the values for an ^{16}O only system where the ν(Mo=O) frequencies are strongly coupled together in the solid state. The best theoretical model that explains the vibrational data for complex A with an isotopic mixture of ^{16}O and ^{18}O has each oxygen with its own force constant (one at 650 Nm^{-1} and one at 639 Nm^{-1}) in a structural model equivalent to the published x-ray crystal structure of complex H. This model is represented by the first four columns of NCA calculations in Table XI.

2. Complex C

The Raman spectra of complex C and ^{18}O substituted C are displayed in Figure 13 and the data are tabulated in Table IX. Simple isotopic substitution predicts that the 877 cm^{-1} peak will shift to 834 cm^{-1}. As seen in Figure 13B, a new peak appears exactly at this value. The 877 cm^{-1} peak is split into two components at 878 and 872 cm^{-1}, demonstrating that the two oxygens are inequivalent. The new peak at 872 cm^{-1} is calculated to shift to 829 cm^{-1}; an experimental peak at 828 cm^{-1}matches this calculation almost exactly.

The 878-cm^{-1} peak in Figure 13B is the symmetric O-Mo-O stretching vibration. Yet it differs in position from the infrared peak which occurs at 882 cm^{-1}. An explanation for this difference can be found in solid state crystal effects. The x-ray crystal structure

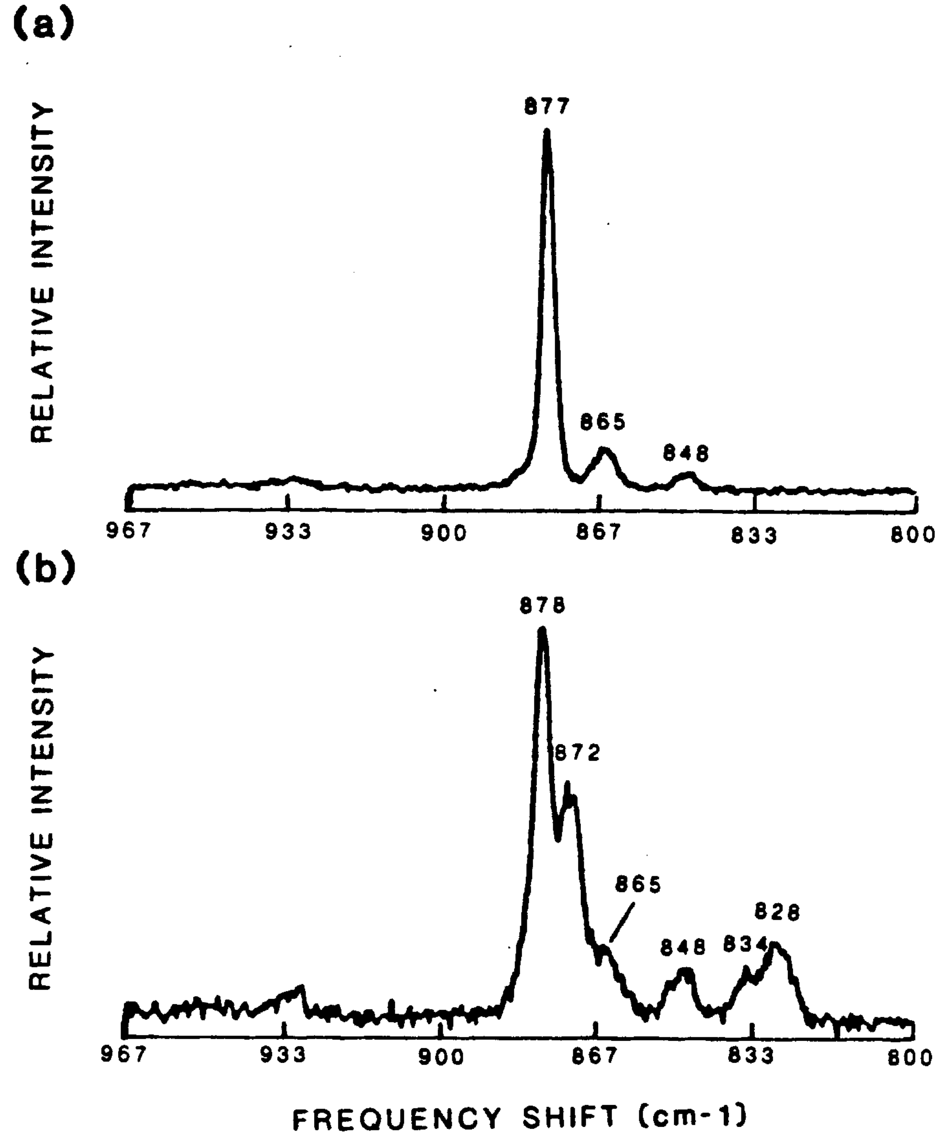

Figure 13. Raman spectra of complex C (a) and ^{18}O labeled C (b). Data have been expanded by a factor of 3. Scan parameters are as follows: laser excitation, 568.2 nm, (a) 40 mW, (b) 50 mW; slits, 2.5 cm^{-1}; scan rate, 1.25 cm^{-1}/sec; number of scans, (a) 2, (b) 21; 180 degree backscattering geometry; sample temperature, 77K.

paper describes the crystals as monoclinic in the $P2_1/c$ space group.[61] Although not stated explicitly in this paper, the number of molecules per unit cell must be 2 or 4, and is most likely 2.[69] Within the unit cell, vibrations of both molecules can be coupled, such that a vibration of molecule 1 of the unit cell can couple with the same vibration of molecule 2. This coupling of normal modes can be either symmetric or antisymmetric. The symmetric combination mode would be visible in the Raman spectrum whereas the antisymmetric mode would be visible in the infrared spectrum.

In the infrared spectrum, the antisymmetric O-Mo-O vibration appears at 855 cm^{-1} whereas in the Raman spectrum it appears at 848 cm^{-1}. A similar solid state effect can explain the difference in positions. In the Raman spectrum a further peak is noted at 865 cm^{-1}. It is also seen in the isotope enriched sample in the Raman spectrum but is not seen in either infrared spectrum. If the 865-cm^{-1} peak were assigned as a Mo=O stretching vibration, it would be expected to shift to 823 cm^{-1} upon isotopic substitution, however no peak is observed at 823 cm^{-1} to verify such an assignment. The 848-cm^{-1} peak, which is assigned as the antisymmetric O-Mo-O vibration, would be expected to shift to 806 cm^{-1} upon ^{18}O substitution. However, no such peak is observed to verify this assignment either. The 848-cm^{-1} peak is thus assigned on the basis of the similar frequency difference between symmetric and antisymmetric O-Mo-O vibrations as observed in the infrared spectrum. This difference in the infrared peak positions is 26 cm^{-1} . In the Raman, the difference between the 877 and the

865-cm $^{-1}$ peak positions is 12 cm $^{-1}$ but between the 877 and the 848-cm^{-1} peaks it is 29 cm $^{-1}$.

The lack of an observed isotopic shift for the 848 cm $^{-1}$ peak can be explained by reference to the normal coordinate analysis of complex A, where only the doubly ^{18}O-subsituted molecule showed the simple shift of the antisymmetric peak. Thus, if the concentration of doubly ^{18}O-substituted molecule is small then it is not likely to be observed in the vibrational spectrum. A normal coordinate analysis of complex C to resolve these isotopic substitution assignments could not be done due to the poor match of Mo=O stretching vibrations in the ^{16}O molecule as discussed above (page 57).

3. Complex F

The spectra of complex F and its ^{18}O-substituted isomer are shown in Figure 14. In the isotope enriched mixture, the oxygens were again inequivalent, and the symmetric absorption band was seen to be split from a single peak at 892 cm^{-1} to a doublet with peaks at 893 and 886 cm^{-1}. Simple isotopic substitution of ^{18}O predicts a shift of these two peaks to 849 and 843 cm^{-1}, respectively. A broad peak at 846 cm^{-1} could account for both of these shifts. The rest of the spectrum is complicated by a peak of unknown origin at 839 cm^{-1} and the difficulty of assigning the antisymmetric O-Mo-O vibration. Based upon the Raman spectrum in Figure 14A, the 878-cm^{-1} peak could be assigned as the antisymmetric vibration on the basis that it is farther away from the symmetric mode at 892 cm^{-1} than the feature at

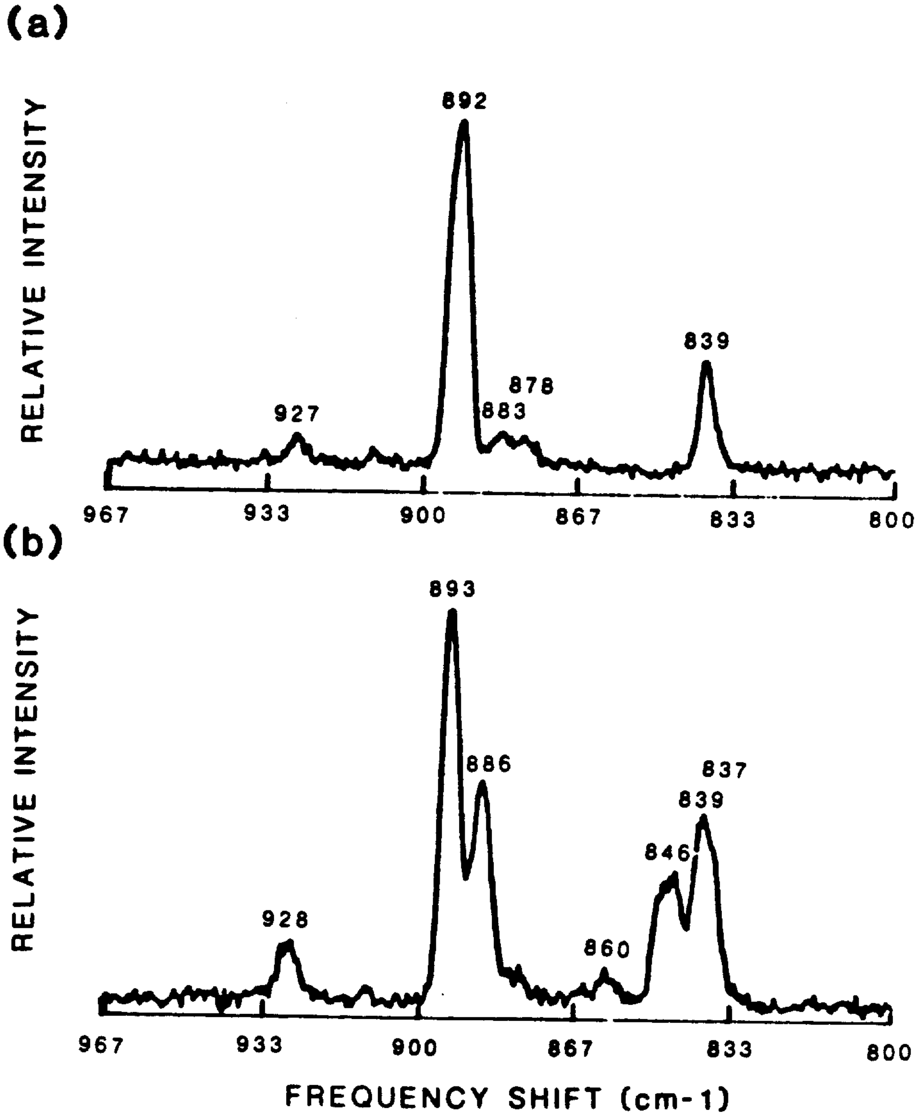

Figure 14. Raman spectra of complex F (a) and ^{18}O-labeled F (b). Scan parameters are as follows: laser excitation, 568.2 nm, 35 mW; slits, 2.5 cm^{-1}/; scan rate, (a) 2.5 cm^{-1}/sec, (b) 0.25 cm^{-1}/sec; number of scans, (a) 10, (b) 1; 180 degree backscattering geometry; sample temperature, 77K.

883 cm^{-1}; yet, their difference of 14 cm^{-1} is considerably smaller than the 30-40 cm^{-1} normally observed. If the 878 cm^{-1} frequency is shifted by isotopic substitution, it should then appear at 836 cm^{-1}. In Figure 14B, a shoulder on the 839-cm^{-1} peak is barely apparent at 837 cm^{-1} and might correspond with the predicted shift.

Based upon the infrared spectra, a peak at 855 cm^{-1} would be in a logical position to be the antisymmetric O-Mo-O stretching mode since the difference in frequency between this value and the symmetric mode at 892 cm^{-1} is 37 cm^{-1}. A peak exists in the Raman spectrum of the isotopic mixture at 860 cm^{-1}. Solid state symmetry effects that may have led to a vanishing intensity of this feature in the Raman spectrum of the ^{16}O structure, were removed by ^{18}O-substitution causing it to appear in the Raman spectrum of the isotopic mixture. The predicted isotopic shift for an 860-cm^{-1} peak would be to 818 cm^{-1}, but no feature is present in either the Raman or the infrared spectrum at that frequency. However, as explained for complexes C and A, a double ^{18}O-substituted molecule is required to observe such a shift, so that its absence is not entirely unexpected.

Based upon the NCA calculations of complex A, the Mo=O stretching modes of complex F are assigned as follows: symmetric ^{16}O-Mo-^{16}O 892 cm^{-1}, antisymmetric 860 cm^{-1}; symmetric ^{16}O-Mo-^{18}O 893 cm-1, anti symmetric 837 cm^{-1}; symmetric ^{18}O-Mo-^{16}O 886 cm^{-1}, antisymmetric 846 cm^{-1}. The first Mo=O bond is designated as having the higher force constant and, therefore, has a higher frequency assigned to it.

It is interesting to note that the weak Raman feature at 878 cm^{-1}

has a very strong infrared companion at 880 cm^{-1}. Due to their respective intensities in the Raman and infrared spectra, it is undoubtedly an antisymmetric vibration. The 878-cm^{-1} frequency was considered above as a candidate for the antisymmetric O-Mo-O vibration, but this assignment was discarded due to the small frequency difference between it and the symmetric vibration at 892 cm^{-1} and the ambiguous isotope shift. The 880-cm^{-1} peak remains strong in the infrared spectrum of the isotopic mixture, suggesting that it is not involved with the oxygen-molybdenum vibrations. A possible assignment for this band is the antisymmetric stretching vibration of the $N(Me)_2$ group. This spectral feature would not be present in complex C because nitrogen carries only one methyl group in that compound. In complex F, however, with two methyl groups, this absorption will be stronger since the dipole moment change will be greater. Assignment of the 880-cm^{-1} frequency as the antisymmetric Me-N-Me stretch leads to a search for the symmetric stretch which would be expected to be nearby. An excellent candidate for that mode is the 839-cm^{-1} peak which is present and unchanged in the spectra of both the ^{16}O compound and the ^{18}O-isotopic mixture in both infrared and Raman spectroscopy.

4. Complex J

Complex J is unique among these complexes in that two isotopic mixtures were available for study. The first contained substitution by a mixture of about 10% ^{17}O and about 7% ^{18}O while the second contained substitution with only ^{18}O. The three isomeric spectra are displayed in Figure 15. The list of peak positions is given in Table IX. In Figure 15A, the symmetric O-Mo-O vibration at 920 cm^{-1} has a companion at 916 cm^{-1} which is also assigned as the symmetric O-Mo-O vibration since it disappears together with 920 cm^{-1} in Figure 15C, the Raman spectrum of the ^{18}O substituted complex. The crystal structure of complex J explains this splitting. The unit cell contains four molecules of this complex.[35] This arrangement permits many more coupling combinations of these important vibrations than in a system with only two molecules per unit cell as postulated for complex C. Therefore, it is not surprising to see the main symmetric O-Mo-O vibration split into a doublet. The antisymmetric O-Mo-O vibration also shows signs of this splitting with a shoulder on the 894 cm^{-1} peak at 898 cm^{-1}.

For the ^{18}O isotope, the peaks at 920-916 cm^{-1} and 894 cm^{-1} are calculated to shift to 875-871 cm^{-1} and 850 cm^{-1} in the double oxygen exchange molecule. Peaks at these frequencies can be observed in Figure 15C. The 920 cm^{-1} and 894 cm^{-1} peaks have lost most of their intensity indicating that very few of the ^{16}O-Mo-^{16}O molecules exist in this sample. However, new peaks at 911 cm^{-1} and 906 cm^{-1} indicate that the mixed isotopes with inequivalent oxygens are present. The breadth of the peak from 850 to 860 cm^{-1} indicates that several vibrations are represented. This band is assigned as the antisymmetric O-Mo-O vibration for both of the mixed isotopes. The separation of about 50 cm^{-1} from the 911/906 cm^{-1} pair corresponds with the NCA calculated separation of the symmetric-antisymmetric pair in the mixed

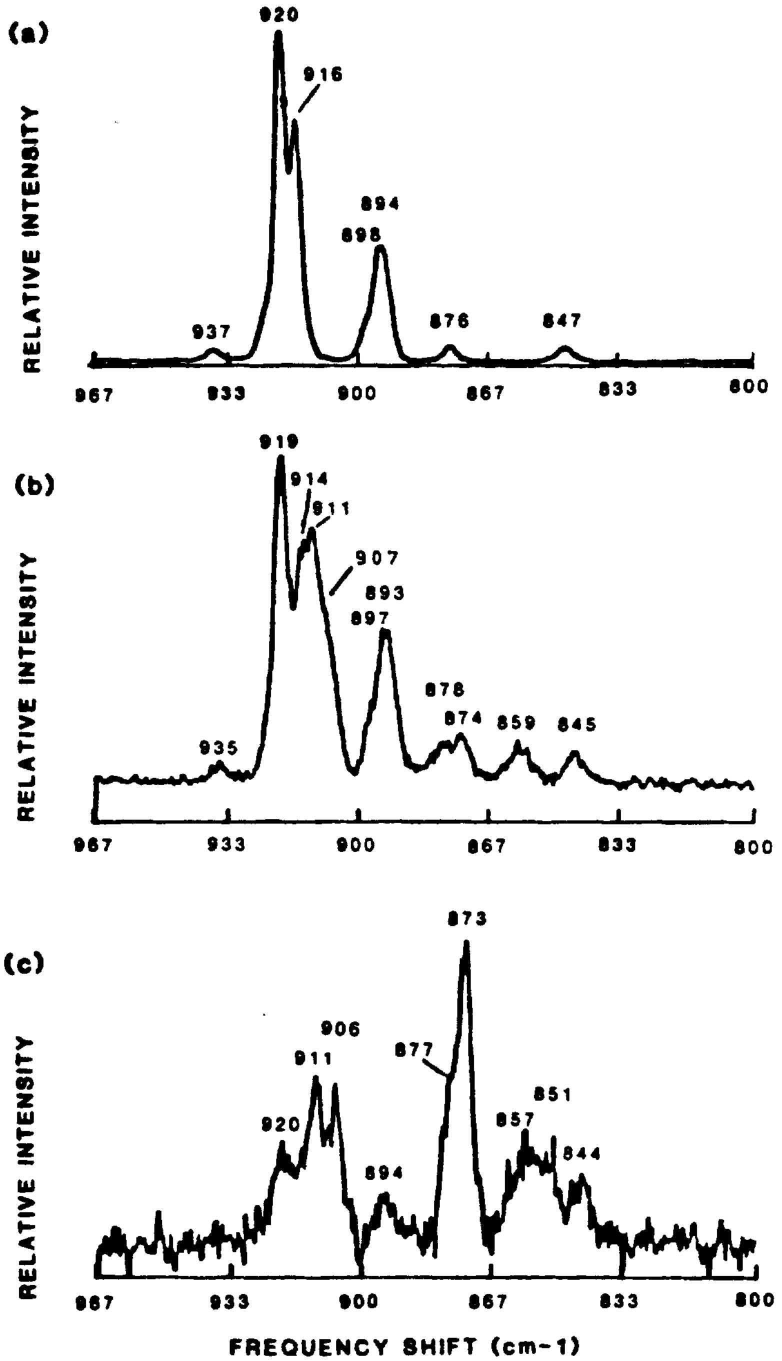

Figure 15. Raman spectra of complex J (a), ^{17}O, ^{18}O labeled J (b), and ^{18}O labeled J (c). Scan parameters are as follows: laser excitation, 568.2 nm, 36 mW; slits, 2.5 cm^{-1}; scan rate, 0.25 cm^{-1}/sec; number of scans, 1; 180 degree backscattering geometry; sample temperature, 77K.

isotope molecule of complex A.

Analysis of the ^{17}O-^{18}O isotopic mixture is more complicated due to the many combinations possible with three isotopes of oxygen into two inequivalent positions. Although the amounts of ^{17}O and ^{18}O available for substitution in the exchange reaction were small, substitution did occur as evidenced by Figure 15B. The splitting of the antisymmetric O-Mo-O vibration at 920 cm^{-1} into a 919, 911 cm^{-1} pair with a shoulder at 907 cm^{-1} in this isotopic mixture again demonstrates the inequivalence of the two oxygens. New peaks are observed at 878 and 859 cm^{-1} . All of these new peaks are identical to those observed in Figure 15C where only ^{18}O was substituted. Mass effect calculations for ^{17}O predict that the 920 cm^{-1} peak will shift to 896 cm^{-1} and the 894 cm^{-1} peak will shift to 871 cm^{-1}. However, there are already peaks present at these frequencies and contribution due to ^{17}O could not be resolved.

5. Complex K

The Raman spectra of complex K and its ^{18}O substituted isomer are shown in Figure 16. The peak positions are compiled in Table IX. The peak at 922 cm^{-1} is assigned as the symmetric O-Mo-O vibration since it disappears from the spectrum of the ^{18}O-substituted compound. The 922-cm^{-1} peak is predicted to shift to 877 cm . Although very small, a feature does appear at 878 cm (Figure 16B) which was not found in the unsubstituted sample (Figure 16A). Furthermore, a feature at

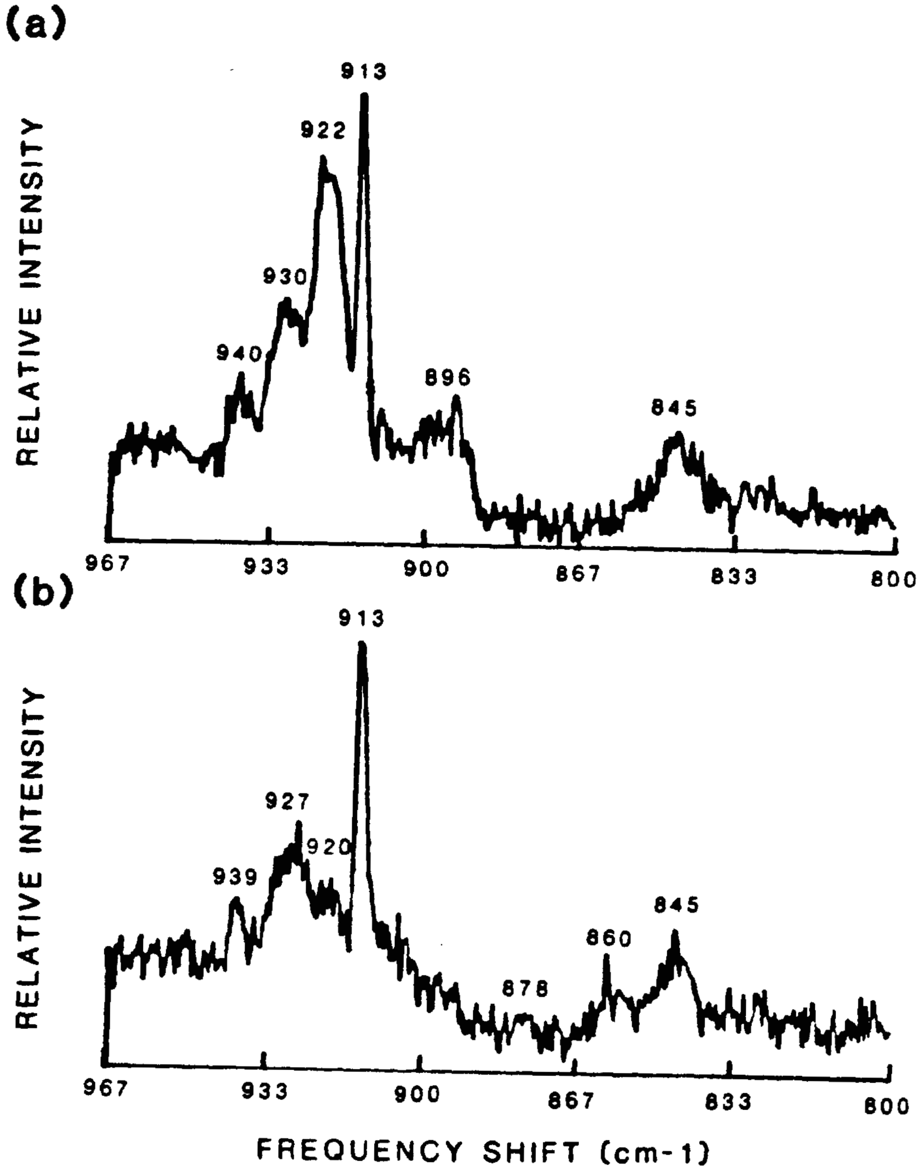

Figure 16. Raman spectra of complex X (a) and ^{18}O labeled X (b). Scan parameters are as follows: laser excitation, 568.2 nm, (a) 45 mW, (b) 60 mW; slits, 2.5 cm^{-1}; scan rate, 0.125 cm^{-1}/sec; number of scans, 2; 180 degree backscattering geometry; sample temperature, 77K.

896 cm^{-1} is observed to disappear upon ^{18}O substitution (Figure 16). This peak is predicted to shift to 852 cm^{-1}, and a new feature does appear in the Raman spectrum at 860 cm^{-1} indicating an antisymmetric O-Mo-O vibration. The noise level in the Raman spectra for complex K is rather high and apparently due to the scattering properties of the sample itself. To verify the Raman results, the infrared data for complex K (Figure 17) show that two peaks at 922 and 894 cm^{-1} have disappeared in the ^{18}O substituted spectrum, confirming their identification as the symmetric and antisymmetric O-Mo-O vibrations, respectively.

6. Summary

Using a model structure for complex A, the complex isotopic shifts of ν(Mo=O) have been explained by normal coordinate analysis as combinations of ^{18}O and ^{16}O singly substituted at inequivalent oxygen sites in these dioxo Mo(VI) complexes. The frequency differences between the symmetric and antisymmetric O-Mo-O vibrations has been identified for each of the combinations of ^{18}O and ^{16}O. The difference was important in understanding the variety of peaks present in a complex with unequal substitution of oxygens and was used as a basis for interpreting the spectra of ^{18}O-substituted complexes C, F, J, and K.

II. Xanthine Oxidase

A. Flavin Adenine Dinucleotide (FAD)

Resonance Raman spectral studies of FAD and flavin-contained cofactors and proteins have often been hampered by a strong fluores-

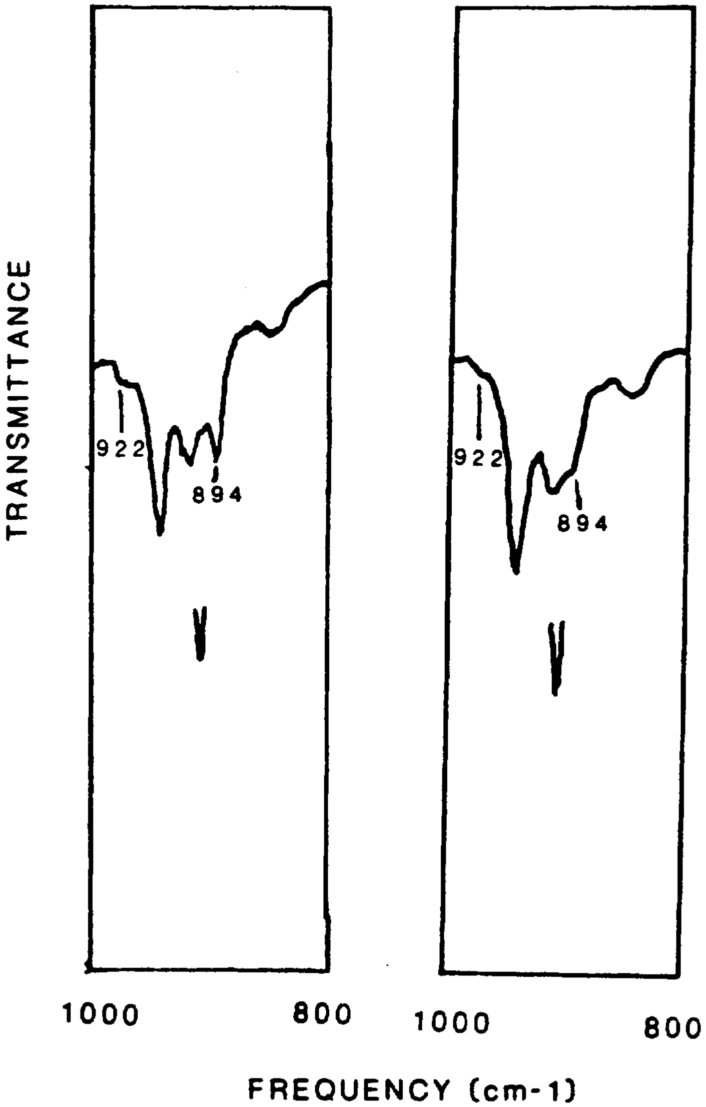

Figure 17. Infrared spectra of complex K (a) and ^{18}O labeled K (b). The polystyrene 906.7 cm^{-1} peak is displayed for calibration.

cence background tending to obscure the weak Raman signals. Recently, however, Raman spectra of FAD have been seccessfully obtained after quenching the fluorescence with potassium iodide or protein,[70] or by using the technique of Coherent Anti-Stokes Raman Scattering (CARS).[71, 72] Many FAD and FAD-derivative spectra have subsequently been obtained for a variety of proteins,[73-79] and several of the vibrational peaks have been tentatively assigned to structural features based on shifts of these frequencies when a new functional group is attached to a specific part of the ring system. The isoalloxazine ring system common to flavins and numbering scheme for the flavin molecule is shown in Figure 18, and Table XII lists resonance Raman frequencies which have been assigned. A drawback of many of these studies has been the limited range over which the Raman data have been collected. In most cases, 1100 cm^{-1} is the lower limit of the scan range although several low frequency spectra have been reported.[70, 74-77] Of these, only one is a study of FAD alone. The others report the spectra of FAD or FMN associated with a protein.

It is important to obtain spectra at much lower frequencies where metal-ligand vibrations exist. To distinguish between FAD peaks and metal-ligand vibrations in xanthine oxidase at low frequencies, the complete resonance Raman spectrum of FAD was examined. These data are displayed in Figure 19. The major peaks in FAD are listed in Table XIII and compared against published values.

With a knowledge of the spectrum of FAD, it is possible to compare it to the spectrum of xanthine oxidase, whose resonance Raman

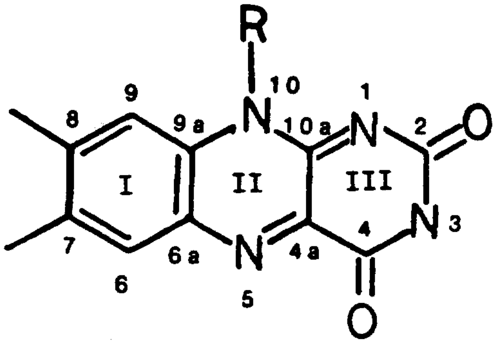

Figure 18. Structure of flavin isoalloxazine ring system with conventional numbering system. R represents rest of flavin structure, i.e., ribose (riboflavin), ribose 5'-phosphate (FMN), ribose 5'-diphosphoadenosine (FAD).

The three fused rings are numbered I, II, and III as seen from left to right.

Table XII. Assignments for some Vibrational Frequencies of the Isoalloxazine Ring System

Position (cm^{-1})	Assignment	Reference
1229	Ring I	75
1251	C(2)-N(3)/N(3)-H BEND	70
1356	C(4)-C(4a)-C(10a)	78
1407	Ring III	75
1583	N(5)-C(4a)-C(10a)-N(1)	78
1631	Ring I	74, 75

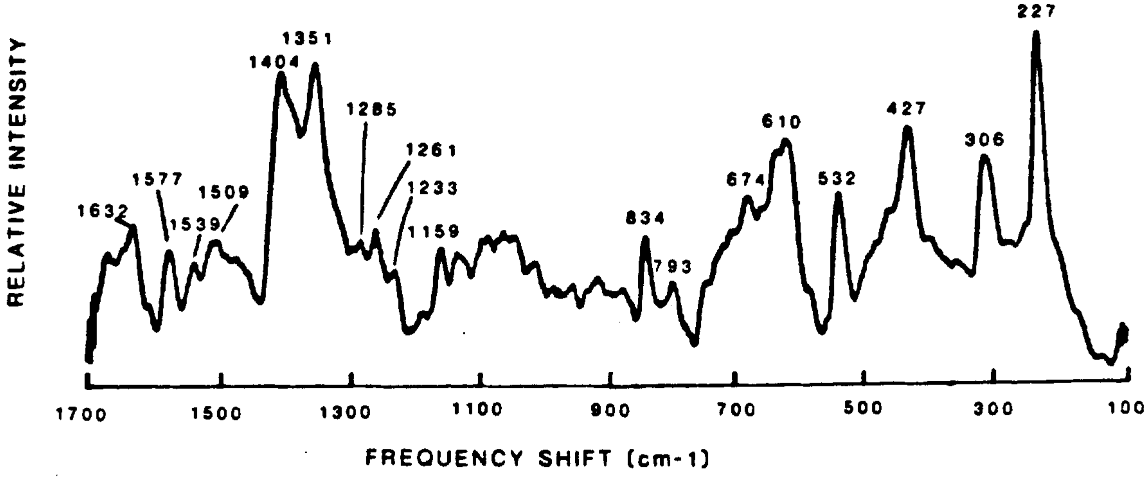

Figure 19. Resonance Raman spectrum of FAD (1.2x10^{-4}M + KI for fluorescence quenching) from 100 cm^{-1} to 1700 cm^{-1}. The peaks at 227 cm^{-1} and 306 cm^{-1} are due to ice in this frozen solution. Data have been subjected to a 25 point smoothing routine. Scan parameters: laser excitation, 488 nm, 25-40 mW; slits, 10 cm^{-1}; scan rate, 4 cm^{-1}/sec; number of scans, 56; 180 degree backscattering geometry; sample temperature, 77K.

Table XIII. Resonance Raman Peaks of Xanthine Oxidase and FAD

XO[a]	FAD[a]	XO[a]	FAD[a]	FAD[b]	FAD[c]
351		1164	1161	1161	1164
396				1182	1185
423	427	1233	1230	1228	1231
439		1269	1261	1253	1260
506		1287	1283		1277
527	523	1352	1351	1354	1359
585	582	1408	1403	1411	1416
617	613	1470			
687	673	1501		1508	1507
740		1546	1541		
760		1586	1579	1585	1584
790	791	1636	1631	1630	1635
832	833	1679	1672		
977					

[a] This work; frequencies in cm^{-1}

[b] Reference 70

[c] Reference 72

spectrum is displayed in Figure 20 and whose major peaks are listed along with those of FAD in Table XIII. The spectral peaks of xanthine oxidase correlate well with those of FAD. In the region above 790 cm^{-1}, all principal peaks in xanthine oxidase can be attributed to FAD. Below this value, all of the major FAD peaks are still seen in xanthine oxidase; however, a number of new features are also observed and will be discussed in the next section.

The resonance Raman spectrum of deflavo xanthine oxidase is displayed in Figure 21. Upon comparison with Figure 20, it is clear that removal of FAD from xanthine oxidase also removes the flavin contributions to the Raman spectrum. All of the major peaks have disappeared, leaving a noisy background spectrum with no distinct peaks except for the broad feature beneath ~ 1400 cm^{-1}. This feature corresponds to a fluorescence maximum at ~ 520 nm. The spectra in Figures 19 and 20 provide the first resonance Raman data of xanthine oxidase to show the FAD contribution.

None of the FAD peaks in the xanthine oxidase spectrum shows any significant shift in position, suggesting no preferential interaction of any part of the isoalloxazine system with the protein. Specific interactions have been proposed on the basis of shifts in the resonance Raman spectrum that have been noted in several protein-flavin studies.[71-78] Modes of vibration associated with rings I or II show significant changes in frequency when FMN binds to *D.gigas* flavodoxin.[78] However, Schopfer and Morris[79] showed that a modification of one part of the ring system affects peak positions in other parts of

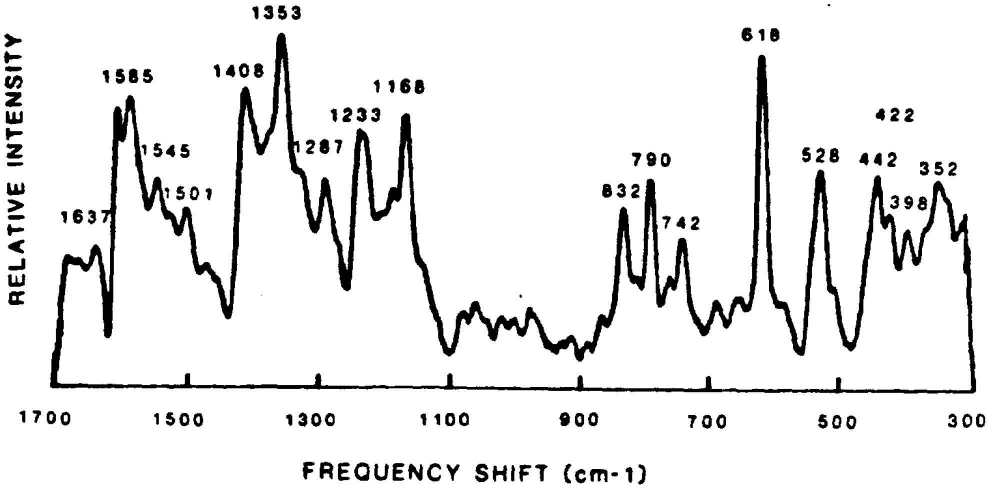

Figure 20. Resonance Raman spectrum of xanthine oxidase in H_2O from 300-1700 cm^{-1}. Data have been subjected to a 25-point smooth. Scan parameters: laser excitation, 488 nm, 20-25 mW; slits, 8 cm^{-1}; scan rate, 2 cm^{-1}/sec; number of scans, 90; 180-degree backscattering geometry; sample temperature, 77K. The baseline drop-off occurring between the 1585 and 1637 cm^{-1} peaks is due to the laser shutting off during an overnight run.

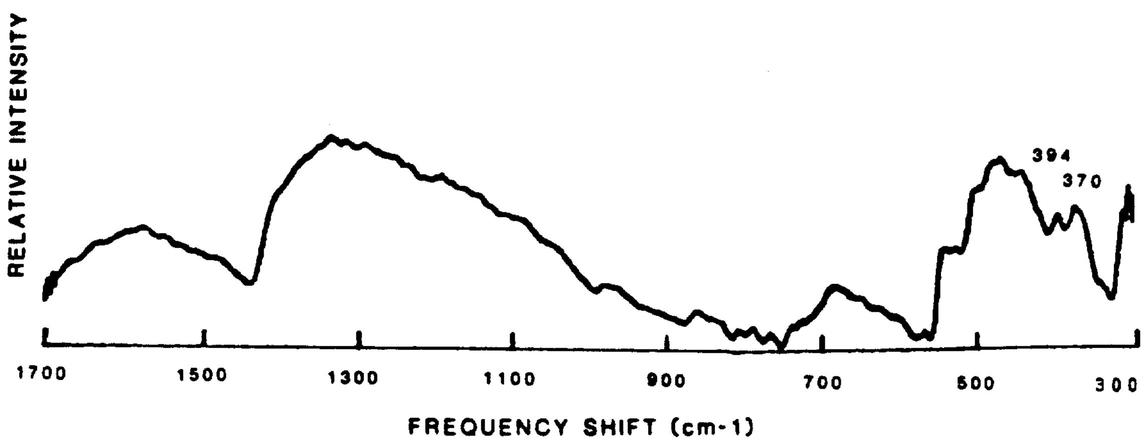

Figure 21. Raman spectrum of aqueous deflavo xanthine oxidase. The data have been subjected to a 25-point smooth. Scan parameters: laser excitation, 488 nm, 27-30 mW; slits, 10 cm^{-1}; scan rate, 2 cm^{-1}/sec; number of scans, 137; 180-degree backscattering geometry; sample temperature, 77K.

the ring system, and warn against overinterpretation of data. Due to the large 10 cm^{-1} slitwidth used in these experiments and a ± 3 cm^{-1} error in locating peak positions, a difference in peak positions of ≈ 6 cm^{-1} might not be observed between the xanthine oxidase and the FAD spectra.

B. Fe_2S_2 and Mo Groups

The electronic absorption spectrum of deflavo xanthine oxidase represents the spectrum of the iron-sulfur groups (see Figure 2). Laser excitation below 500 nm should give rise to a resonance Raman spectrum of these iron-sulfur groups in xanthine oxidase. Removal of the flavin from the protein should remove any low frequency flavin peaks that would interfere in the interpretation of the Fe_2S_2 Raman spectrum.

Resonance Raman spectroscopy has previously been attempted on deflavo xanthine oxidase, but high fluorescence caused a poor signal-to-noise ratio. Only a band at about 280 cm^{-1} was observed by Yamamoto,[80] who obtained better results with putidaredoxin, adrenodoxin, and spinach ferredoxin (Figure 22). All three of these two-iron-two-sulfur proteins exhibit three major bands at ≈ 280, 340, and 390 cm^{-1}. Since a 280 cm^{-1} band was observed in deflavo xanthine oxidase, it should be possible to observe the other bands if the signal-to-noise ratio is sufficiently increased.

The first detailed resonance Raman spectrum of the Fe_2S_2 centers of xanthine oxidase is displayed in Figure 23. Three strong bands

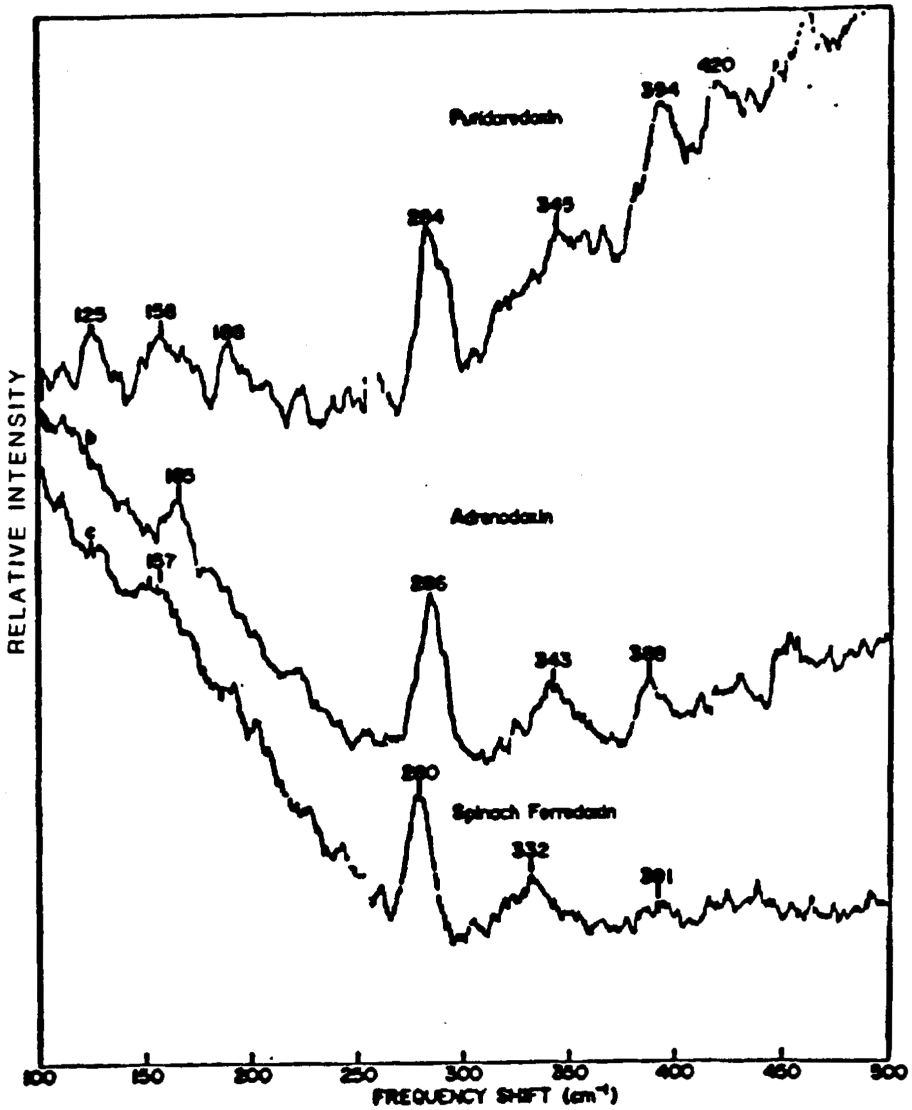

Figure 22. Resonance Raman spectra of putidaredoxin, adrenodoxin, and spinach ferredoxin obtained by 441.6 nm excitation. Reproduced from reference 80.

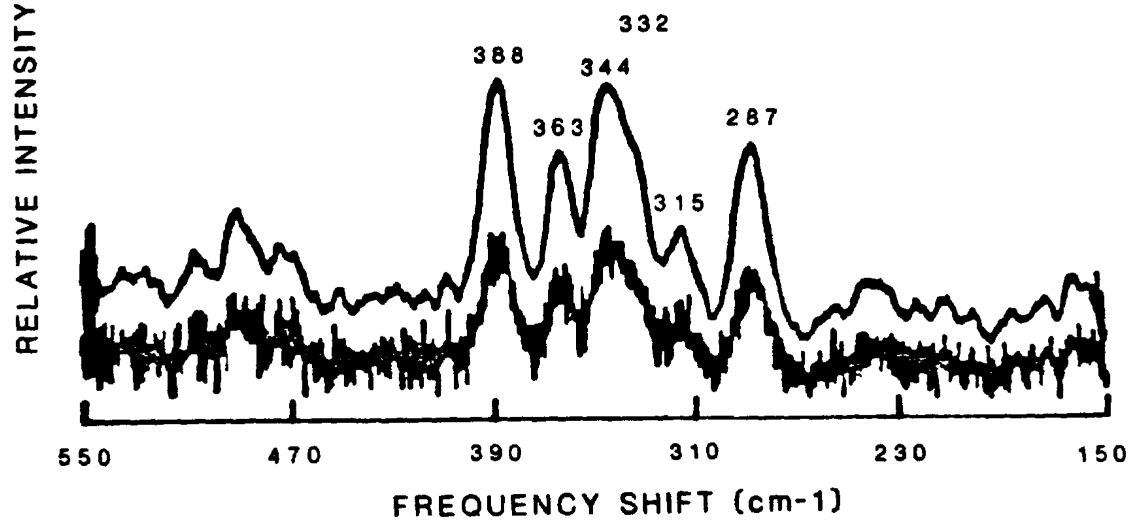

Figure 23. Resonance Raman spectrum of deflavo xanthine oxidase, sample 1, with 476.5 nm excitation. The upper trace results from a 25-point smooth applied to the raw data displayed in the lower trace, the two traces are shown with different vertical gains. Scan parameters: laser power, 55 mW; slits, 10 cm^{-1}; scan rate, 2 cm^{-1}/sec; number of scans, 239; 180-degree backscattering geometry; sample temperature, 4°C.

are observed at 287, 344 (broad), and 388 cm^{-1}. These occur at the same values as the three dominant peaks observed for the Fe_2S_2 group in adrenodoxin. In addition, three other features are observed at 315, ≈332 (shoulder), and 363 cm^{-1}. Resolution is improved in the resonance Raman spectrum of another sample of deflavo xanthine oxidase, as shown in Figure 24. The shoulder at 332 cm^{-1} is now decomposed into two peaks at 326 and 335 cm^{-1}, although the former is close to noise-limited.

Assignment of the 287, 344, and 388 cm^{-1} peaks appears to be straightforward in light of the correlation with the spectrum of adrenodoxin and the close agreement with the spectra of putidaredoxin and spinach ferredoxin. These three bands are assigned to the Fe_2S_2-(Cys)$_4$ structural group.[80] The other four peaks are not as easily assigned. Although there are two types of Fe_2S_2 centers in xanthine oxidase, EPR only distinguishes between them at liquid helium temperatures; it is, therefore, quite unlikely that their resonance Raman spectra will be significantly different, especially at 4°C, the temperature at which these spectra were taken. It is possible that all of these peaks are assignable to the Fe_2S_2 centers. Yamamoto's spectra show very broad bands at 332 (ferredoxin), 343 (adrenodoxin) and 345 cm^{-1} (putidaredoxin) as seen in Figure 22. The resolution and signal-to-noise ratio of her spectra are not sufficient to show the presence of these additional bands within the broad envelope of the 340 cm^{-1} band. A group theoretical analysis for an $Fe_2S_2(S\text{-}Cys)_4$ center with D_{2h} symmetry predicts the existence of 9 Raman active vibra-

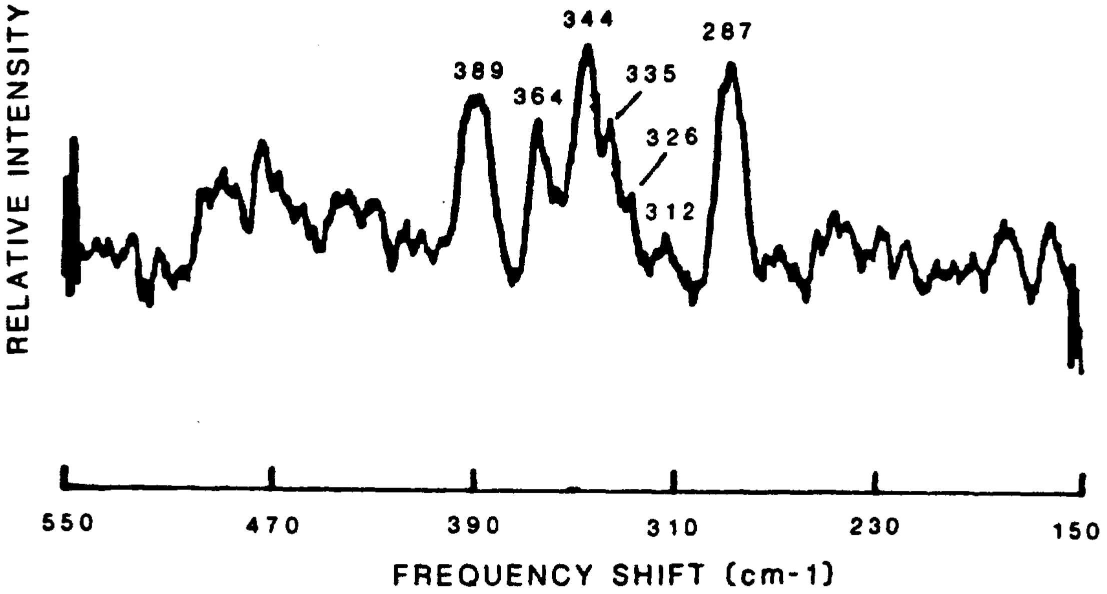

Figure 24. Resonance Raman spectrum of deflavo xanthine oxidase, sample 2, with 476.5 nm excitation. The data have been subjected to a 25-point smooth. Scan parameters: laser power, 45 mW; slits, 10 cm^{-1}; scan rate, 2 cm^{-1}/sec; number of scans, 280; 180-degree backscattering geometry; sample temperature, 4°C.

tions as indicated in Table XIV. Normal coordinate analysis on $Fe_2S_2S'_4$ assigned the three main bands to A_g symmetry and predicted the existence of a fourth A_g band at about 35 cm^{-1}.[80] That leaves the five B_g modes unassigned. If one assumes that the protein distorts the $Fe_2S_2(S\text{-}cys)_4$ center away from the centrosymmetric D_{2h} symmetry, then some of the infrared active bands could also appear in a Raman spectrum. Thus, it is reasonable to assume that the four bands in deflavo xanthine oxidase at 313, 327, 333 and 364 cm^{-1} might also be assignable to the Fe_2S_2 centers.

To examine the resonance enhancement of these Raman peaks, spectra were recorded with excitation by several different laser wavelengths. The results of this study are displayed in Figures 25-29. Only the spectrum obtained with green excitation (514.5nm) shows the Raman spectrum largely obscured by background noise. All of the spectra obtained with blue light excitation (457.9 nm, 476.5 nm, and 488.0 nm) show well defined Fe_2S_2 vibrational peaks in the 270 to 400 cm^{-1} region. As can be seen in Figure 2, all of the blue laser lines fall within the absorption envelope of deflavo xanthine oxidase whereas the green line at 514.5 nm is just outside the Fe_2S_2 absorption, thus accounting for the observed resonance enhancement behavior.

Of interest is the spectrum of Figure 25 obtained with violet excitation at 406.7 nm. Only the three major peaks at 290, 345, and 392 cm^{-1} are visible while the other four peaks at 313, 327, 333, and 364 cm^{-1} have disappeared. This indicates that these latter four peaks are no longer in resonance while the former three peaks are still in a resonance condition. Since the flavin has been removed, this raises

Table XIV. Group Theory Classification of Vibrational Bands for $Fe_2S_2(S\text{-cys})_4$ in D_2h Symmetry

Raman Active		Infrared Active		Inactive	
Ag	4	B_1u	3	Au	1
B_1g	1	B_2u	3		
B_2g	2	B_3u	2		
B_3g	2				
Totals	9		8		1

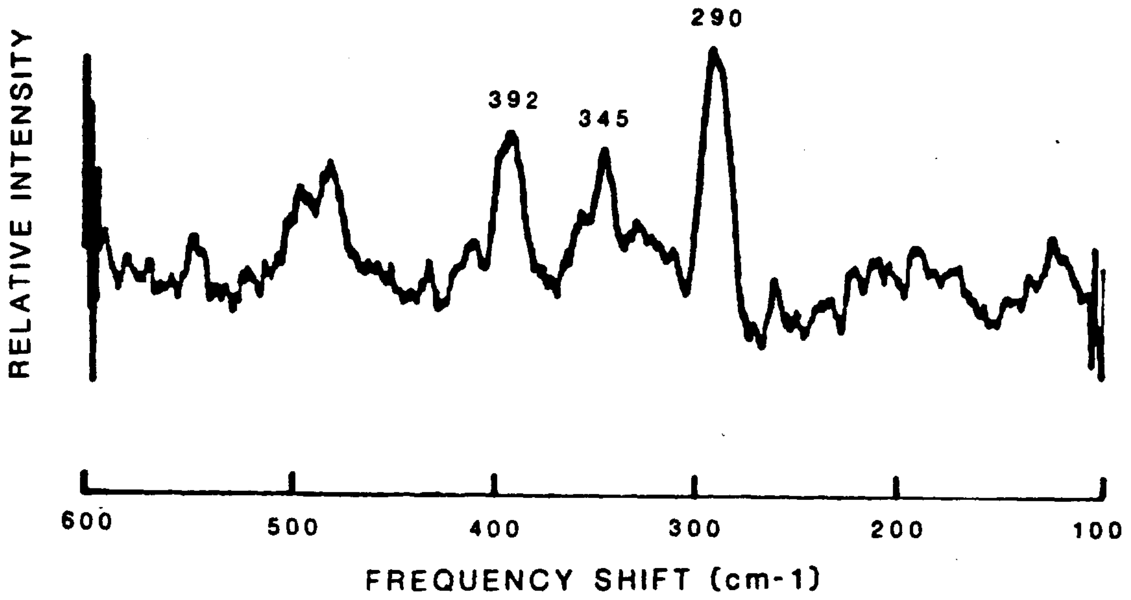

Figure 25. Resonance Raman spectrum of deflavo xanthine oxidase with 406.7 nm excitation. The data have been subjected to a 25-point smooth. Scan parameters: laser power, 20 mW; slits, 14 cm^{-1}; scan rate, 2 cm^{-1}/sec; number of scans, 86; 180-degree backscattering geometry; sample temperature, 4°C.

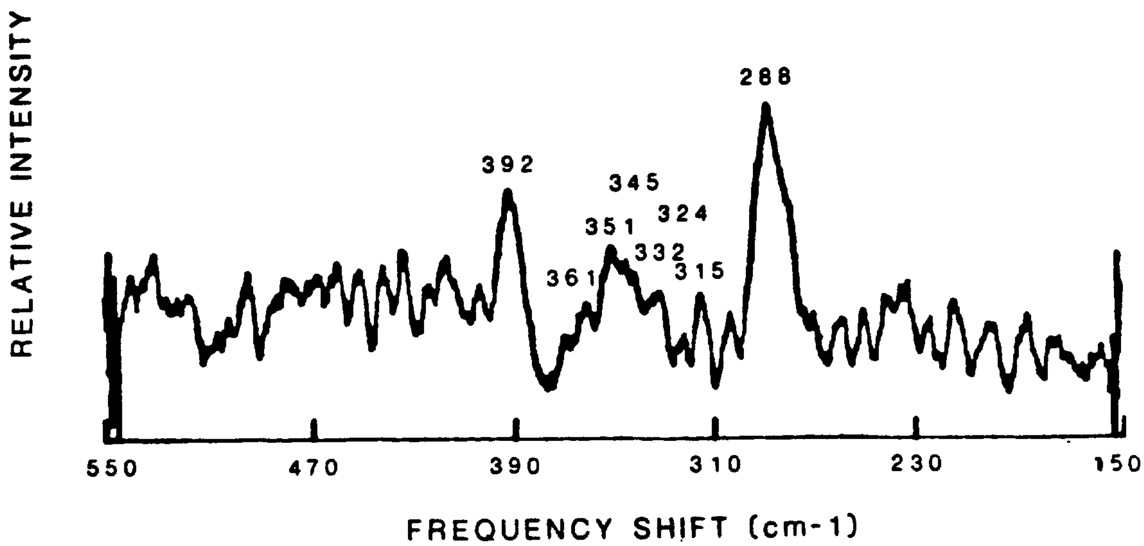

Figure 26. Resonance Raman spectrum of deflavo xanthine oxidase with 457.9 nm excitation. The data have been subjected to a 25-point smooth. Scan parameters: laser power, 20 mW; slits, 10 cm^{-1}; scan rate, 2 cm^{-1}/sec; number of scans, 330; 180-degree backscattering geometry; sample temperature, 4°C.

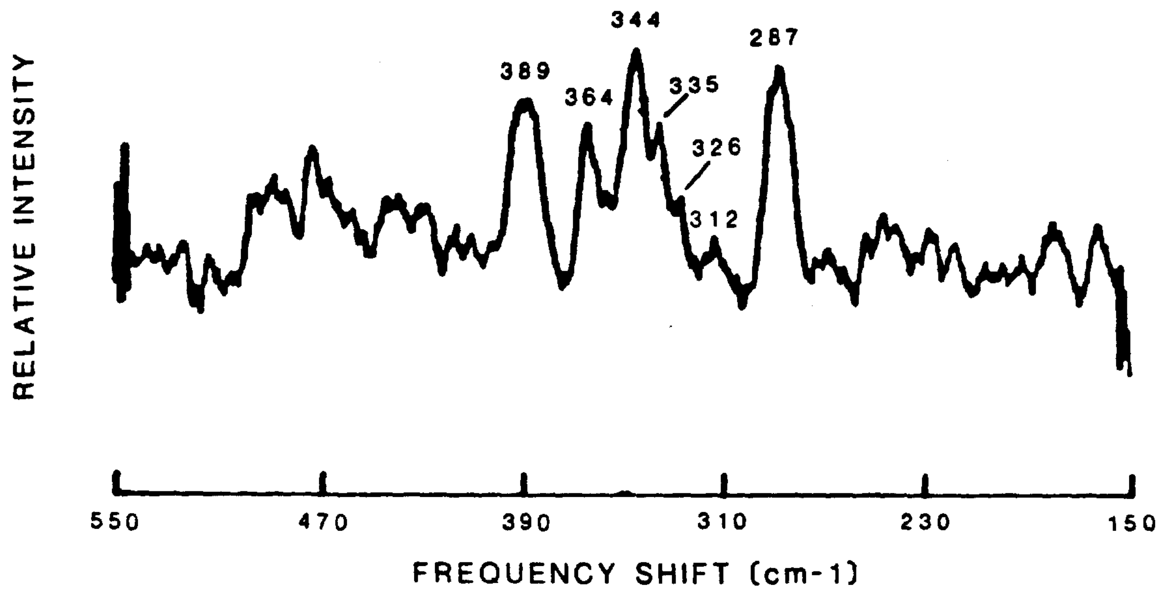

Figure 27. Resonance Raman spectrum of deflavo xanthine oxidase with 476.5 nm excitation. The data have been subjected to a 25-point smooth. Scan parameters: laser power, 45 mW; slits, 10 cm^{-1}; scan rate, 2 cm^{-1}/sec; number of scans, 280; 180-degree backscattering geometry; sample temperature, 4°C. (Same as Figure 24, but repeated for comparison in this series.)

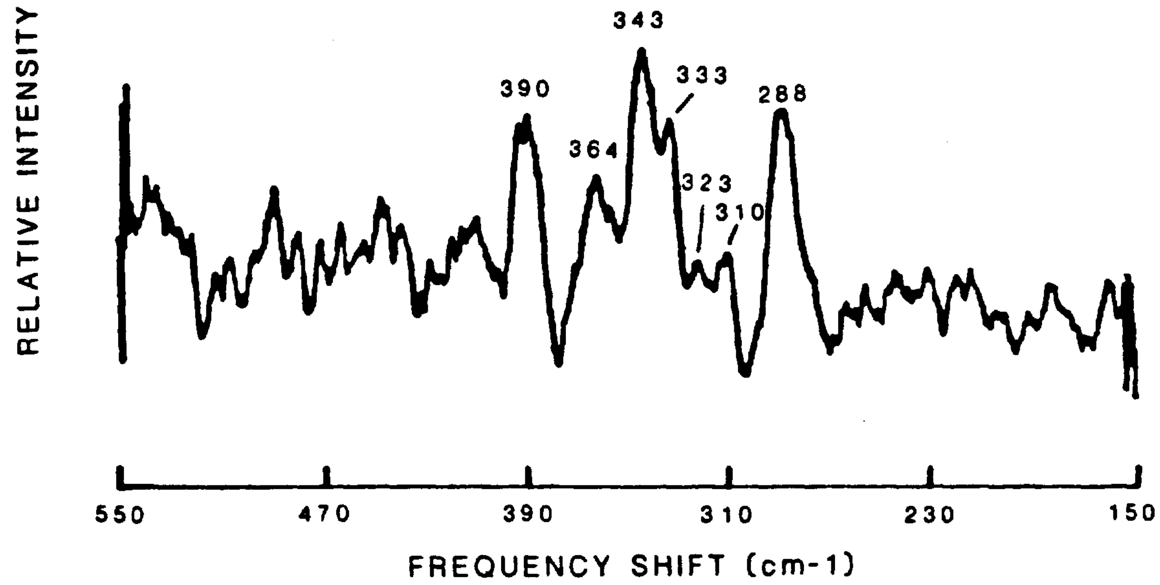

Figure 28. Resonance Raman spectrum of deflavo xanthine oxidase with 488 nm excitation. The data have been subjected to a 25-point smooth. Scan parameters: laser power, 35 mW; slits, 10 cm^{-1}; scan rate, 2 cm^{-1}/sec; number of scans, 330; 180-degree backscattering geometry; sample temperature, 4°C.

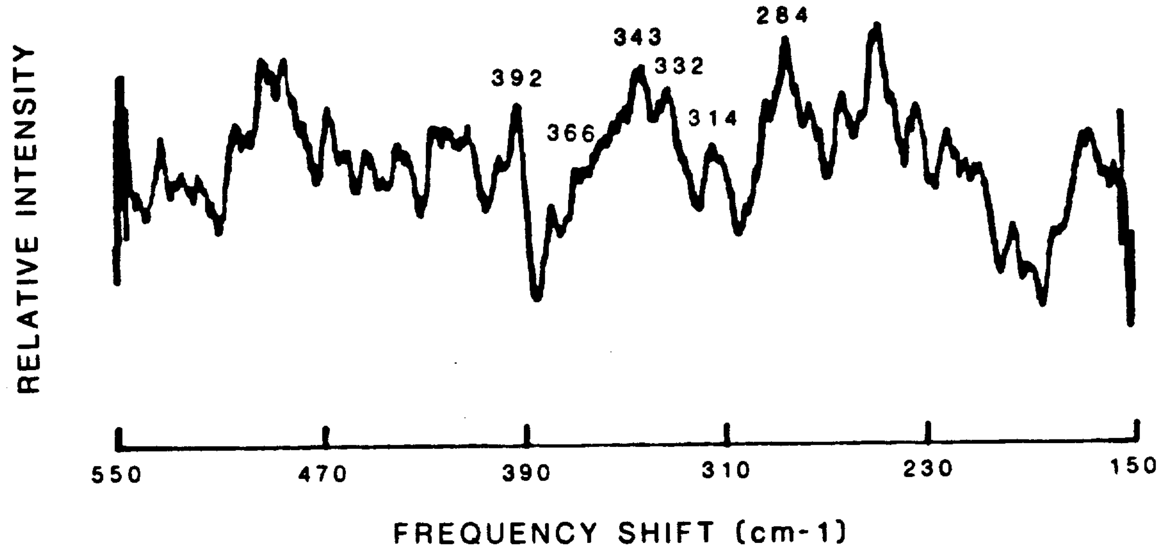

Figure 29. Raman spectrum of deflavo xanthine oxidase with 514.5 nm excitation. The data have been subjected to a 25-point smooth. Scan parameters: laser power, 60 mW; slits, 10 cm^{-1}; scan rate, 2 cm^{-1}/sec; number of scans, 366; 180-degree backscattering geometry; sample temperature, 4°C.

the possibility that the four frequencies arise from another chromophore, that is, molybdenum. A feature in Figure 25 at about 500 cm^{-1} looks significant. Similar features appear in Figures 27 and 29 but are absent in Figures 26 and 28. Because the feature at about 500 cm^{-1} is not totally reproducible as indicated in the data shown in this work and other data not included in this work, it is not considered to be important at this time.

To investigate the possibility that molybdenum is involved in these vibrational frequencies, the molybdenum site was altered by treatment with KCN to remove the terminal sulfide ligand.[6] If the resonance Raman spectrum is significantly altered by this treatment, then the participation of molybdenum in the vibrational motions can be assumed to be real. The spectrum of desulfo xanthine oxidase is displayed in Figure 30. All of the main features are present with the possible exception of the 327 cm^{-1} peak. That feature (326 cm^{-1} peak in Figure 24) was already very close to noise limited and its presence or absence is, therefore, not conclusive. A new peak is apparent at 378 cm^{-1} which might be attributed to a molybdenum-ligand vibration in the altered molybdenum ligand coordination sphere; however, a different sample of desulfo xanthine oxidase did not reveal a peak at this frequency, indicating that it may be due to random noise. Even though the 378 cm^{-1} peak is as strong as some of the other peaks observed, it is still just within the noise level of the spectrum. Although the other peaks are also close to the signal-to-noise level, they are nonetheless consistently reproduced in every

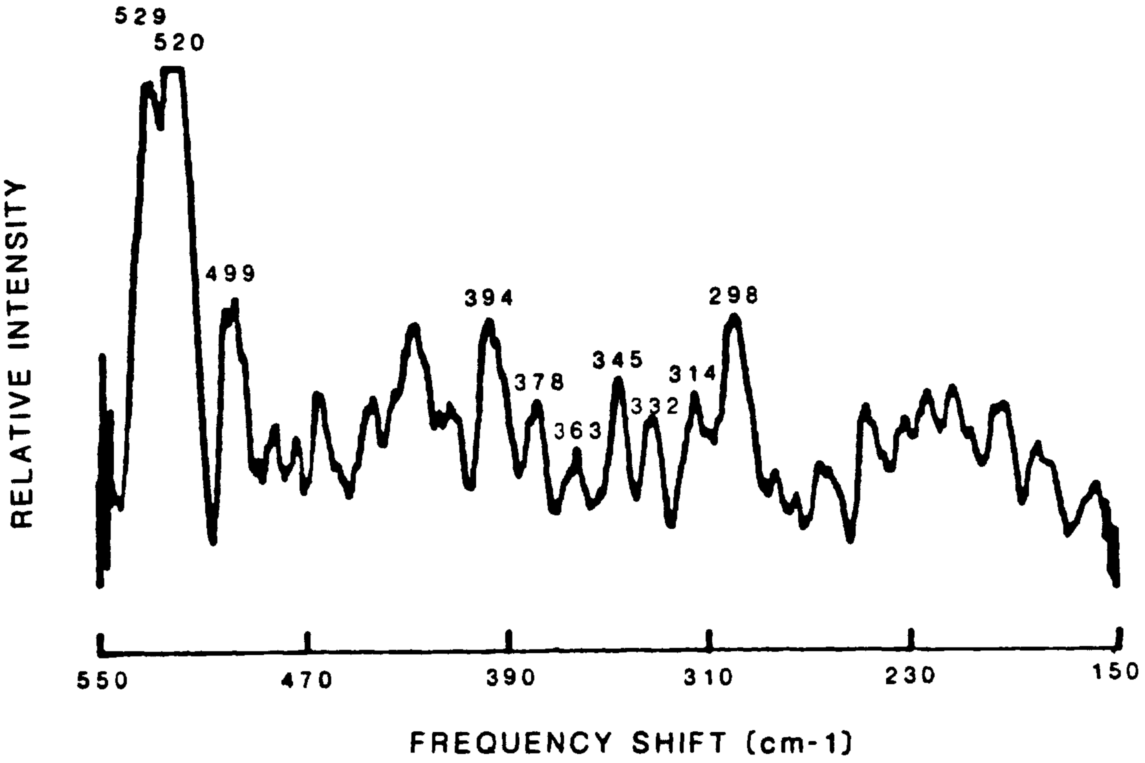

Figure 30. Resonance Raman spectrum of desulfo xanthine oxidase. The data have been subjected to a 25-point smooth. Scan parameters: laser excitation, 476.5 nm, 55 mW; slits, 10 cm^{-1}; scan rate, 2 cm^{-1}/sec; number of scans, 328; 180-degree backscattering geometry; sample temperature 4°C.

sample for which a spectrum was obtained. Thus, there is no hard resonance Raman evidence for a change in the coordination sphere of molybdenum upon cyanide treatment.

In other attempts to understand the nature of the four peaks differing from those found by Yamamoto,[80] the resonance Raman spectra of pure xanthine oxidase and a sample of desulfo-deflavo xanthine oxidase were investigated. The results of these two experiments are shown in Figures 31 and 32. To correlate these data, the Raman shift of the peaks from xanthine oxidase, deflavo xanthine oxidase, desulfo xanthine oxidase, and desulfo-deflavo xanthine oxidase are listed together in Table XV. Inspection of the data in this table shows that essentially all the peaks listed are observed in all four different samples of xanthine oxidase. In desulfo-deflavo xanthine oxidase as in desulfo xanthine oxidase, the already questionable 327 cm^{-1} is absent. However, an additional peak is noted in pure xanthine oxidase and desulfo xanthine oxidase at 299 cm^{-1} which is absent in deflavo and desulfo-deflavo xanthine oxidase. This 299-cm^{-1} peak appears to be present when flavin is present and absent when flavin is absent, so it can probably be assigned to some deformation mode of the FAD system. This peak was not observed previously in the FAD spectrum (Figure 19) because the data were collected at 77K and an ice band obscures that region of the spectrum.

The peak at 326 cm^{-1} is not visible in the desulfo and desulfo-deflavo xanthine oxidase samples. It may be present under slightly broadened 333-cm^{-1} peaks, but it is more likely to be truly absent in

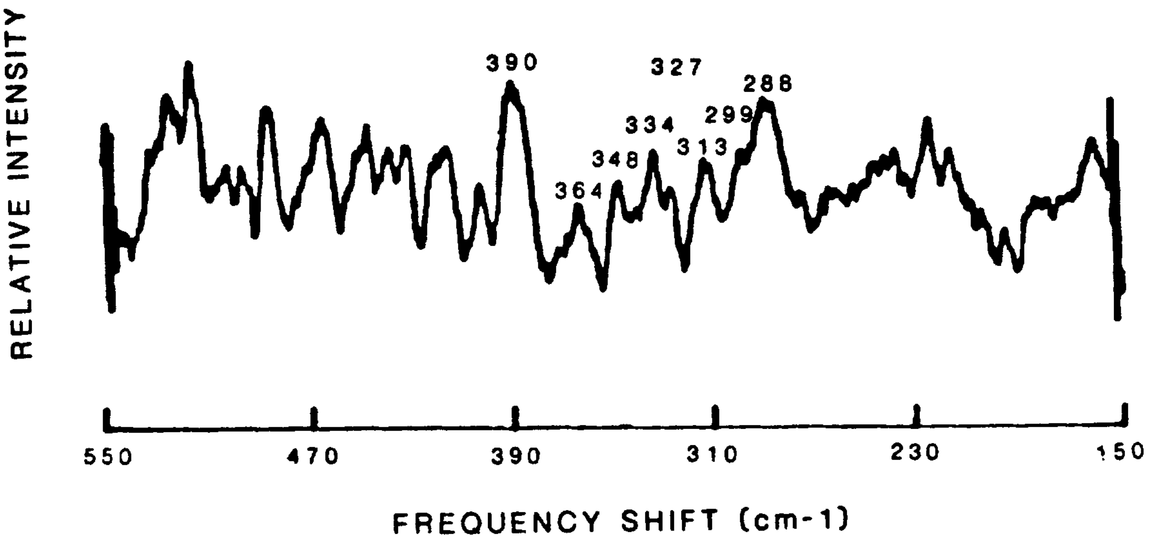

Figure 31. Resonance Raman spectrum of xanthine oxidase. The data have been subjected to a 25-point smooth. Scan parameters: laser excitation, 476.5 nm, 50 mW; slits, 10 cm^{-1}; scan rate, 2 cm^{-1}/sec; number of scans, 317; 180-degree back-scattering geometry; sample temperature, 4°C.

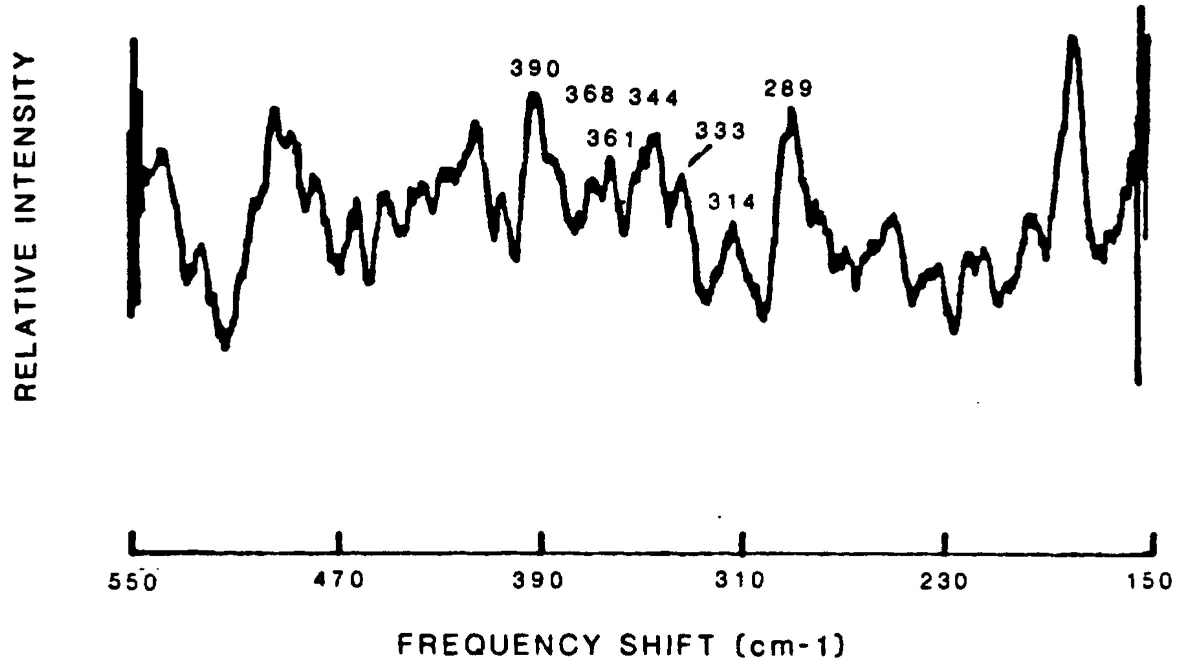

Figure 32. Resonance Raman spectrum of desulfo-deflavo xanthine oxidase. The data have been subjected to a 25-point smooth. Scan parameters: laser excitation, 476.5 nm, 60 mW; slits, 10 cm^{-1}; scan rate, 2 cm^{-1}/sec; number of scans, 615; 180-degree backscattering geometry; sample temperature, $4^{o}C$.

Table XV. Resonance Raman Peaks of Xanthine Oxidase, Deflavo Xanthine Oxidase, and Desulfo Xanthine Oxidase [a]

XO	Deflavo XO	Desulfo XO	Desulfo-Deflavo XO
288	288		290
299		298	
313	313	315	312
327	327		
334	333	331	333
348	344	344	344
363	364	362	361
390	389	395	391

[a] Frequencies in cm^{-1}.

these spectra. If this is the case, then it may be an indication of a molybdenum-ligand vibration since the desulfo form of the enzyme is common to both of these spectra. Evidence against the molybdenum-ligand hypothesis is seen in Figure 25 where the four additional peaks disappear with violet excitation (406.7 nm). Since Mo(VI) should absorb light more strongly in the ultraviolet, any molybdenum-ligand vibrations should be enhanced as excitation approaches the uv. The more likely possibility is that the 327 cm^{-1}-feature is a random noise peak, since its intensity is within the noise level of the spectra where it is seen. Data of better quality would be needed to determine with certainty the origin of the 327 cm^{-1} peak.

The molybdenum(VI) model complexes indicate the frequency regions where metal-ligand stretching vibrations are expected to occur. Molybdenum-oxygen stretching frequencies range from about 850-1000 cm^{-1}, molybdenum-sulfur around 350-400 cm^{-1}, and molybdenum-nitrogen can be found over a broad range from about 550-650 cm^{-1}. If the nitrogen is part of an inflexible ring system, the effective ligand mass is much greater and the frequency can be much lower. The search for molybdenum-ligand stretching vibrations in xanthine oxidase was not successful. Figures 20 and 21 show no bands in the 850-1000 cm^{-1} that are reproducible and assignable to ν(Mo=O). Several samples of different forms of xanthine oxidase produced the same negative results.

In the molybdenum(VI) complexes, the intensities of the peaks assigned to ν(Mo-S) and ν(Mo-N) were always less intense that those assigned to ν(Mo=O). Since the xanthine oxidase samples did not show evidence of molybdenum-oxygen stretching modes, the likelihood of seeing ν(Mo-S) or ν(Mo-N) is also small. Complicating this situation furthur, ν(Mo-S) is expected at ≈350-400 cm^{-1} where the peaks for the $Fe_2S_2(S\text{-}Cys)_4$ groups appear. But this consideration allows for the possibility that the occasionally observed peak at ≈378 cm^{-1} is due to ν(Mo-S) in xanthine oxidase since it is in the approximate frequency region expected.

Detection of ν(Mo-N) in xanthine oxidase is less likely due to the broad range available for this ligand. If the ligand is part of a heterocyclic aromatic functional group such as histidine or a pterin derivative (as has been identified as part of the molybdenum cofactor of xanthine oxidase and other molybdoenzymes[81]), the frequency could be quite low, at ≈250 cm^{-1}. If the nitrogen were an amine, a frequency range of about 500-600 cm^{-1} could be expected since multiple bonding is not unusual to molybdenum.[55, 58, 60] Complicating the search is the fact that nitrogen has not been identified as a ligand of molybdenum in xanthine oxidase. It has only been postulated as a ligand.[1, 43] Therefore, unambiguous identification of any spectral peak as a molybdenum-nitrogen stretching vibration is very difficult. No peaks identifiable as such have been observed in any of the Raman data on xanthine oxidase.

Observing the resonance Raman signals of molybdenum-ligand vibrations in xanthine oxidase is expected to be difficult. The resting enzyme contains Mo(VI), a d^0 ion, which has no bands due to any d-d transitions. Any ligand-metal charge transfer bands are expected in the ultraviolet, so that ultraviolet laser excitation would be necessary to enhance the intensity of vibrations associated with the atoms participating in electronic charge transfer. Full UV-Raman capability was not available in the laboratory during this research. Evidence exists for a Mo(IV) absorption at about 380 nm (See Figure 3) but since this is in the UV, resonance Raman behavior associated with this transition was not investigated.

Summary

The three main bands of the Fe_2S_2 groups of xanthine oxidase have been observed in four different forms of the enzyme at 288, 344, and 389 cm^{-1}. An additional four bands at 313, 327, 333, and 364 cm^{-1} have also been observed which lack the resonance enhancement with violet excitation (406.7 nm) of the three main bands, yet share resonance enhancement with blue excitation (457.9, 476.5, and 488.0 nm). The 327 cm^{-1} band lacks reproducibility in two forms of the enzyme in which a terminal sulfide is removed from molybdenum. Yet all four of these peaks lose enhancement where molybdenum ligands are expected to gain resonance enhancement (406.7 nm) and cannot therefore be considered as potential molybdenum-ligand vibrational frequencies. Since there are a number of other Raman active modes unaccounted for in this $Fe_2S_2(S\text{-}Cys)_4$ system of D_2h symmetry, it is most likely that these four additional bands arise solely from the Fe_2S_2 groups.

CONCLUSIONS

Xanthine oxidase has been studied by resonance Raman spectroscopy. The native enzyme displays the spectrum of the FAD moiety. There is a one to one correlation between the resonance Raman peaks of FAD in solution and the resonance Raman peaks of xanthine oxidase. Although other researchers have observed shifts in frequency of the isoalloxazine moiety of flavin attached to other flavoproteins,[71-78] none was observed in xanthine oxidase. This may be a result of experimental uncertainty in peak position due to the large slitwidth, the large number of scans, and the high noise level of the spectral signal. On the other hand, it may also be an indication that the FAD is not bound to the resting enzyme via isoalloxazine, but through the adenine portion of the molecule.

By removal of the flavin from xanthine oxidase, the resonance Raman signal of the Fe_2S_2 groups were observed. Three peaks of this signal coincided exactly in frequency with the resonance Raman signal of adrenodoxin. Additional peaks seen only in the xanthine oxidase spectrum may also be present in adrenodoxin but are not resolved from noise. These additional peaks in xanthine oxidase may also be attributed to the Fe_2S_2 groups with different resonance enhancement characteristics. They go out of resonance with excitation at 406.7 nm, indicating that they are associated with the absorption band due to Fe_2S_2 at 450-470 nm. The three main resonance Raman peaks remain in resonance through the violet at 406.7 nm to the blue at 488.0 nm. As the excitation wavelength continues into the green at 514.5 nm, resonance enhancement declines. The foregoing behavior indicates the association of the absorption envelope of the Fe_2S_2 groups with the Raman enhancements. Unambiguous evidence for resonance Raman peaks for the molybdenum center of xanthine oxidase could not be obtained. Excitation of enzyme samples with blue laser lines revealed no peaks attributable to ν(Mo=O), ν(Mo-S), or ν(Mo-N). One peak at about 378 cm^{-1} might be due to ν(Mo-S), but this peak was not consistently reproducible.

The Raman data for the 14 molybdenum(VI) complexes were analyzed along with infrared data and x-ray crystal structures of several of these complexes to make structural predictions about those complexes of unknown crystal structure. Two structural geometries are represented. The normal geometry for dioxo molybdenum(VI) complexes with two thiolate and two nitrogen ligands is represented by a distorted octahedron with *cis* oxygens, *trans* sulfurs each *cis* to the oxygens, and *cis* nitrogens each *trans* to an oxygen. This structure results in the symmetric O-Mo-O stretching vibration lying above 900 cm^{-1}. All but four of the complexes exhibit this approximate structure.

The other geometry as defined by the x-ray crystal structure of C, $MoO_2(CH_3NHCH_2C(CH_3)_2S)_2$, is a skew trapezoidal bipyramid. The interesting feature of this structure is the possible formation of a partial disulfide bond. The structure causes the O-Mo-O angle to decrease, resulting in a frequency below 900 cm^{-1} due to competition between the oxygens for the same Mo d orbitals involved in π bonding. The four complexes exhibiting this structural characteristic are D, $MoO_2(CH_3NHC(CH_3)_2C(CH_3)_2S)_2$, F,$MoO_2((CH_3)_2NCH_2C(CH_3)_2S)_2$, G,$MoO_2(NH_2CH_2CH_2S)_2$, and complex C mentioned above.

Two of the complexes, M, $Mo_2O_5((CH_3)_2NCH_2CH_2NHCH_2CH_2S)_2$ and N,$Mo_2O_5((CH_3)_2NCH_2CH_2NHCH_2C(CH_3)_2S)_2$, are molybdenum dimers with a single μ-oxo bridge. Both of these complexes exhibit the ν(Mo=O) frequencies of the normal distorted octahedral geometry. Complex E,$MoO_2(SC(CH_3)_2CH_2NHCH_2CH_2NHCH_2C(CH_3)_2S)$, although it is incapable of the skew trapezoidal bipyramid structure, exhibits both low frequency ν(Mo=O) of high intensity and high frequency ν(Mo=O) of much lower intensity. Space filling molecular models predict two possible geometries. The more favorable geometry involves close approach of the sulfurs for possible disulfide bond formation. This structure also allows room for the two oxygens to separate with the possible aid of hydrogen bonding from the amine protons, consequently lowering ν(Mo=O) below 900 cm^{-1}. The second geometry has some unfavorable, yet not prohibitive, steric constraint of a methyl group with an oxygen. In this arrangement the sulfurs are *trans* to each other and the oxygens are forced closer together, thus raising ν(Mo=O) in frequency above 900 cm^{-1}.

Complex I, $MoO_2(SCH_2CH_2N(CH_3)CH_2CH_2N(CH_3)CH_2CH_2S)$, which is similar to the above complex, has additional side chain methyl groups which create many more steric interferences. Therefore, it can only assume a configuration with *trans* sulfurs and *cis* oxygens with ν (Mo=O) above 900 cm^{-1}.

Within this group of complexes with similar ligands, a *cis* sulfur geometry gives the potential for disulfide bond formation and seems to result in a lowering of ν(Mo=O) below 900cm^{-1}. Disulfide bonds generate a larger O-Mo-O angle. When the sulfurs are *trans* to each other, the O-Mo-O angle is more normal and ν(Mo=O) is greater than 900 cm^{-1}. Factors influencing the formation of the partial disulfide bond could not be positively identified among the four complexes which exhibit this structural feature.

Two of the complexes, C, $MoO_2(CH_3NHCH_2C(CH_3)_2S)_2$ and H, MoO_2(8-mercaptoquinoline) , were subjected to normal coordinate analysis since their x-ray crystal structures were available. The O-Mo-O stretching vibrations of the former complex could not be matched by the simplified atom set $MoO_2N_2S_2$ with a general valence force field. The calculated peaks were 896 and 828 cm^{-1} while the observed peaks were at 877 cm^{-1} and 848 cm^{-1}. A good match for ν(Mo-N) was close to some experimental Raman peaks. The oversimplification of the model in conjunction with the simplest force field is inadequate to analyze this complex which has more complicated interactions such as intermolecular hydrogen bonding and solid state vibrational coupling.

The simple structural model for the latter complex resulted in close fits for ν(Mo=O) and ν(Mo-N), but not for ν(Mo-S). Again oversimplification of the model and a simple force field probably caused the inability to calculate a close fit to experimental data.

Normal coordinate analysis was successfully used to interpret the isotopic shifts of the five complexes available with ^{18}O substituted for ^{16}O. Applying the structure of the complex MoO_2(8-mercaptoquinoline)$_2$ as a model for the complex A, $MoO_2(NH_2CH_2C(CH_3)_2S)_2$, an exact match to the O-Mo-O stretching frequencies was achieved. By substituting ^{18}O for ^{16}O in the calculations, all experimental peaks were matched, thus describing the force field for this complex exactly. The inequivalence of the oxygen atoms predicted by the structural model was verified by the use of two separate force constants for the Mo=O band. It is important to note the separation between the symmetric and antisymmetric O-Mo-O vibrations when interpreting the isotopic Raman data. For this complex the separation is 37 cm^{-1} when both oxygens are ^{16}O. When only one oxygen is replaced with ^{18}O, the separation increases to 62 cm^{-1} when the weaker bonded oxygen is replaced and to 52 cm^{-1} when the stronger bonded oxygen is replaced. When both oxygens are replaced by ^{18}O, the separation is the same as for the unsubstituted molecule. This knowledge of separation was applied in the successful interpretation of the isotopic shifts of the other four complexes, C, $MoO_2(CH_3NHCH_2C(CH_3)_2S)_2$, F, $MoO_2((CH_3)_2NCH_2C(CH_3)_2S)_2$, J, $MoO_2((CH_3)_2NCH_2CH_2N(CH_2CH_2S)_2)$, and K, $MoO_2(CH_3SCH_2CH_2N(CH_2CH_2S)_2)$.

Application of the results of the molybdenum model complex studies to the interpretation of the xanthine oxidase results is not possible due to the lack of resonance Raman data on the molybdenum site of the enzyme. During the course of this research, additional information on the molybdenum site of xanthine oxidase by the technique of EXAFS was published,[82] indicating that these complexes are no longer totally appropriate to model the enzyme. It was discovered that the active enzyme probably has only one terminal oxo group, the second oxo group being replaced by a terminal sulfur atom.[82] Therefore, new model complexes should include a single terminal oxygen and a terminal sulfur atom. The other ligands of molybdenum in xanthine oxidase were not altered by these EXAFS studies. Also revealed by EXAFS studies was that in desulfo xanthine oxidase, the sulfur which is removed by cyanide is the terminal sulfur atom. It is replaced by a terminal oxygen, thereby leaving molybdenum with two terminal oxygens. This makes the molybdenum complexes studied in this dissertation possible models for the inactive desulfo form of molybdenum in xanthine oxidase. In order to obtain resonance Raman data on the molybdenum site of xanthine oxidase, samples must be excited by laser light in the ultraviolet to enhance vibrational intensities of the Mo(IV) chromophore at ≈380 nm.

REFERENCES

1. E. I. Stiefel, Progr. Inorg. Chem., 22, 1, (1977).
2. R. C. Bray in The Enzymes, 3rd ed., Vol. XII, pp. 299-419, Paul D. Boyer, ed., Academic Press, New York, 1975.
3. H. Komai, V. Massey, and G. Palmer, J. Biol. Chem., 244, 1692 (1969).
4. K. Garbett, R. D. Gillard, P. F. Knowles, and J. E. Stangroom, Nature, 215, 824 (1967).
5. G. B. Wong, D. M. Kurtz, Jr., R. H. Holm, L. E. Mortenson, and R. G. Upchurch, J. Am. Chem. Soc., 101, 3078 (1979).
6. J. P. G. Malthouse and R. C. Bray, Biochem. J., 191, 265 (1980).
7. S. P. Cramer, K. O. Hodgson, E. I. Stiefel, and W. E. Newton, J. Am. Chem. Soc., 100, 2748 (1978).
8. T. D. Tullius, D. M. Kurtz, Jr., S. D. Conradson, and K. O. Hodgson, J. Am. Chem. Soc., 101, 2776 (1979).
9. R. C. Bray and L. S. Meriwether, Nature, 212, 467 (1966).
10. A. Kay and P. C. H. Mitchell, Nature, 219, 267 (1968).
11. J. R. Knox and C. K. Prout, J. Chem. Soc. Chem. Commun., 1227 (1968).
12. J. R. Knox and C. K. Prout, Acta Crystallogr. Sect. B, 25, 1857 (1969).
13. L. R. Melby, Inorg. Chem. 8, 349 (1969).

14. A. Kay and P. C. H. Mitchell, J. Chem. Soc. A, 2421 (1970).

15. B. Jezowska-Trzebiatowska, M. F. Rudolf, L. Natkaniec, and H. Sabat, Inorg. Chem., 13, 617 (1974).

16. T. Glowiak, M. Sabat, H. Sabat, and M. F. Rudolf, J. Chem. Soc. Chem. Commun., 712 (1975).

17. B. M. Gatehouse, E. K. Nunn, J. E. Guerchais, and R. Kergoat, Inorg. Nucl. Chem. Lett., 12, 23 (1976).

18. W. E. Newton, G. J.-J. Chen, and J. W. McDonald, J. Am. Chem. Soc., 98, 5387 (1976).

19. C. D. Garner, R. Durant, and F. E. Mabbs, Inorg. Chem. Acta, 24, L29 (1977).

20. B. Jezowska-Trzebiatowska, T. Glowiak, M. F. Rudolf, M. Sabat, and J. Sabat, Russ. J. Inorg. Chem., 22, 1590 (1977).

21. W. Rittner, A. Müller, A. Neumann, W. Bäther, and R. C. Sharma, Angew. Chem. Int. Ed. Engl., 18, 530 (1979).

22. P. C. H. Mitchell and C. F. Pygall, J. Inorg. Biochem., 11, 25 (1979).

23. K. Yamanouchi & J. H. Enemark, Inorg. Chem., 18, 1626 (1979).

24. E. I. Stiefel, W. E. Newton, and N. Pariyadeth, in Proceedings of the Climax Second International Conference on the Chemistry and Uses of Molybdenum, p. 265, P. C. H. Mitchell and A. Seaman, eds., Climax Molybdenum Co., London, 1976.

25. N. Pariyadeth, W. E. Newton, and E. I. Stiefel, J. Am. Chem. Soc., 98, 5388 (1976).

26. O. A. Rajan, S. Adhikari, and A. Chakravorty, *Indian J. Chem. Sect. A.*, *15*, 337 (1977).

27. J. T. Spence, M. Minelli, P. Kroneck, M. I. Scullane, and N. D. Chasteen, *J. Am. Chem. Soc.*, *100*, 8002 (1978).

28. O. A. Rajan and A. Chakravorty, *Inorg. Chim. Acta*, *37*, L503 (1979).

29. W. E. Hill, N. Atabay, C. A. McAuliffe, F. P. McCullough, and S. M. Raxxoki, *Inorg. Chim. Acta*, *35*, 35 (1979).

30. V. Srinivasan, E. I. Stiefel, A. Elsberry, and R. A. Walton, *J. Am. Chem. Soc.*, *101*, 2611 (1979).

31. O. Bortolini, F. Di Furia, and G. Modena, *J. Am. Chem. Soc.*, *103*, 3924 (1981).

32. E. I. Stiefel, K. F. Miller, A. E. Bruce, N. Pariyadath, J. Heinecke, J. L. Corbin, J. M. Berg, and K. O. Hodgson, in *Molybdenum Chemistry of Biological Significance*, W. E. Newton ad S. Otsuka, eds., Plenum Press, New York, 1980.

33. K. Yamanouchi and J. H. Enemark, *Inorg. Chem.*, *17*, 1981 (1978).

34. W. S. Mialki, E. I. Stiefel, A. E. Bruce, and R. A. Walton, *Inorg. Chem.*, *20*, 1614 (1981).

35. J. M. Berg, K. O. Hodgson, S. P. Cramer, J. L. Corbin, A. Elsberry, N. Pariyadath, and E. I. Stiefel, *J. Am. Chem. Soc.*, 101, 2774 (1979).

36. V. Massey, H. Komai, G. Palmer, and G. B. Elion, *J. Biol. Chem.*, *245*, 2837 (1970).

37. E. B. Wilson, Jr., J. C. Decius, and P. C. Cross, Molecular Vibrations, McGraw-Hill Book Company, Inc., 1955.

38. J. H. Schachtschneider, Technical Report No. 57-65, Shell Development Co., Emeryville, CA 1966.

39. H. Fuhrer, V. B. Kartha, K. G. Kidd, P. J. Krueger, and H. H. Mantsch, Computer Programs for Infrared Spectroscopy, Bulletin No. 15, National Research Council of Canada, Ottawa, 1976.

40. M. C. Urey and C. A. Bradley, Phys. Rev., 38, 1969 (1931).

41. V. Massey, P. E. Brumby, H. Komai, and G. Palmer, J. Biol. Chem., 244, 1682 (1969).

42. M. Kanda, F. O. Brady, K. V. Rajagopalan, and P. Handler, J. Biol. Chem., 247, 765 (1972).

43. S. Gutteridge, S. J. Tanner, and R. C. Bray, Biochem. J., 175 887 (1978).

44. P. G. Avis, F. Bergel, and R. C. Bray, J. Chem. Soc., 1100 (1955).

45. T. M. Loehr, W. E. Keyes, and P. A. Pincus, Anal. Biochem., 96, 456 (1979).

46. N. Ueyama, M. Nakata, T. Araki, A. Nakamura, S. Yamashita, and T. Yamashita, Inorg. Chem., 20, 1934 (1981).

47. G. R. Hanson, A. A. Brunette, A. C. McDonell, K. S. Murray, and A. G. Wedd, J. Am. Chem. Soc., 103, 1953 (1981).

48. J. T. Spence, M. Minelli, and P. Kroneck, J. Am. Chem. Soc., 102, 4538 (1980).

49. J. P. Wilshire, L. Leon, P. Bosserman, and D. T. Sawyer, J. Am. Chem. Soc., 101, 3379 (1979).

50. R. M. Wing and K. P. Callahan, Inorg. Chem., 8, 871 (1969).

51. W. P. Griffith, J. Chem. Soc. A., 211 (1969).

52. N. Kim, S. Kim, P. A. Vella, and J. Zubieta, Inorg. Nucl. Chem. Lett., 14, 457 (1978).

53. W. E. Newton and J. W. McDonald, J. Less-Common Met., 54 51 (1977).

54. S. G. Murray and F. R. Hartley, Chem. Rev., 81, 365 (1981).

55. J. A. Broomhead and J. R. Budge, Aust. J. Chem., 32, 1187 (1979).

56. J. M. Chen and C. S. Wang, Solid State Commun., 14, 857 (1974).

57. B. Spivak and Z. Dori, Coord. Chem. Rev., 17, 99 (1975).

58. G. Butler, J. Chaff, W. Hussain, G. J. Leigh, and D. L. Hughes, Inorg. Chim. Acta, 30, L287 (1978).

59. J. Goubeau, Angew. Chem. Int. Ed., 5, 567 (1966).

60. J. C. J. Bart and V. Ragaini, Acta Crystallogr. Sect. B, 36, 1351 (1980).

61. E. I. Stiefel, K. F. Miller, A. E. Bruce, J. L. Corbin, J. M. Berg, and K. O. Hodgson, J. Am. Chem. Soc., 102, 3624 (1980).

62. I. V. Zuika, Yu. A. Bankovskii, and Ya. V. Ashak, Zh. Obshch. Khim., 46, 2287 (1976).

63. J. Hyde, K. Venkatasubramanian, and J. Zubieta, Inorg. Chem., 17, 414 (1978).

64. P. C. H. Mitchell, *Q. Rev.*, 20, 103 (1966).

65. E. I. Stiefel, personal communication, 1978.

66. P. G. Wright, P. Stein, J. M. Burke & T. G. Spiro, *J. Am. Chem. Soc.*, *101*, 3531 (1979).

67. B. C. Cornilsen & K. Nakamoto, *J. Inorg. Nucl. Chem.*, *36*, 2467 (1964).

68. F. A. Cotton & R. M. Wing, *Inorg. Chem.*, *4*, 867 (1965).

69. *International Tables for X-Ray Crystallography*, Vol. I, N. F. M. Henry and K. Lonsdale, eds., Kynoch Press, Birmingham, England, 1969, p. 99.

70. M. Benecky, T. Y. Li, J. Schmidt, F. Frerman, K. L. Watters, and J. McFarland, *Biochemistry*, *18*, 3471 (1979).

71. P. K. Dutta, J. R. Nestor, and T. G. Spiro, *Proc. Nat. Acad. Sci. USA*, *74*, 4146 (1977).

72. P. K. Dutta, J. Nestor, and T. G. Spiro, *Biochem. Biophys. Res. Commun.*, *83*, 209 (1978).

73. T. Kitagawa, Y. Nishina, K. Shiga, H. Watari, Y. Matsumura, and T. Yamano, *J. Am. Chem. Soc.*, *101*, 3376 (1979).

74. T. Kitagawa, Y. Nishina, Y. Kyogoku, T. Yamano, N. Ohishi, A. Takai-Suzuki, and K. Yagi, *Biochemistry*, *18*, 1804 (1979).

75. Y. Nishina, K. Shiga, K. Horiike, H. Tojo, S. Kasai, K. Yanase, K. Matsui, H. Watari, and T. Yamano, *J. Biochem.*, *88*, 403 (1980).

76. Y. Nishina, K. Shiga, K. Horiike, H. Tojo, S. Kasai, K. Matsui, H. Watari, and T. Yamano, *J. Biochem.*, *88*, 411 (1980).

77. P. K. Dutta and T. G. Spiro, *Biochemistry*, *19*, 1590 (1980).

78. R. M. Irwin, A. J. W. G. Visser, J. Lee, and L. A. Carreira, Biochemistry, 19, 4639 (1980).

79. L. M. Schopfer and M. D. Morris, Biochemistry, 19, 4932 (1980).

80. T. Yamamoto, Ph.D. Dissertation, University of Michigan, 1973.

81. J. L. Johnson, B. E. Hainline, and K. V. Rajagopalan, J. Biol. Chem., 255, 1783 (1980).

82. J. Bordas, R. C. Bray, C. D. Garner, S. Gutteridge, and S. S. Hasnain, Biochem. J., 191, 499 (1980).

APPENDIX I

RAMAN AND INFRARED SPECTRA OF THE MOLYBDENUM COMPLEXES

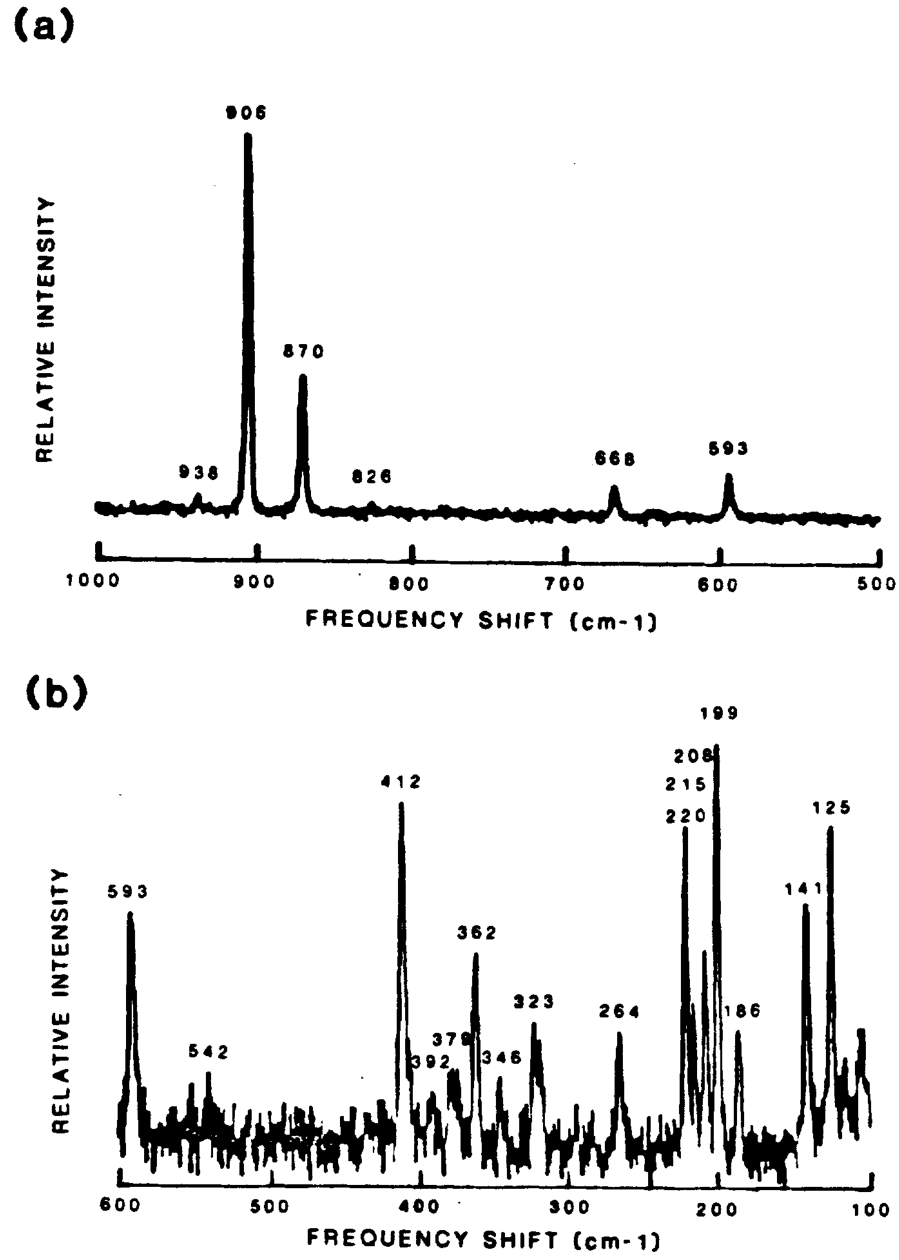

Figure I-1. Raman spectrum of complex A. Scan parameters: laser excitation, 568.2 nm; slitwidth, 2.5 cm^{-1}; scan rate, 2.5 cm^{-1}/sec; number of scans, 10; 180 degree backscattering geometry; sample temperature, 77K.

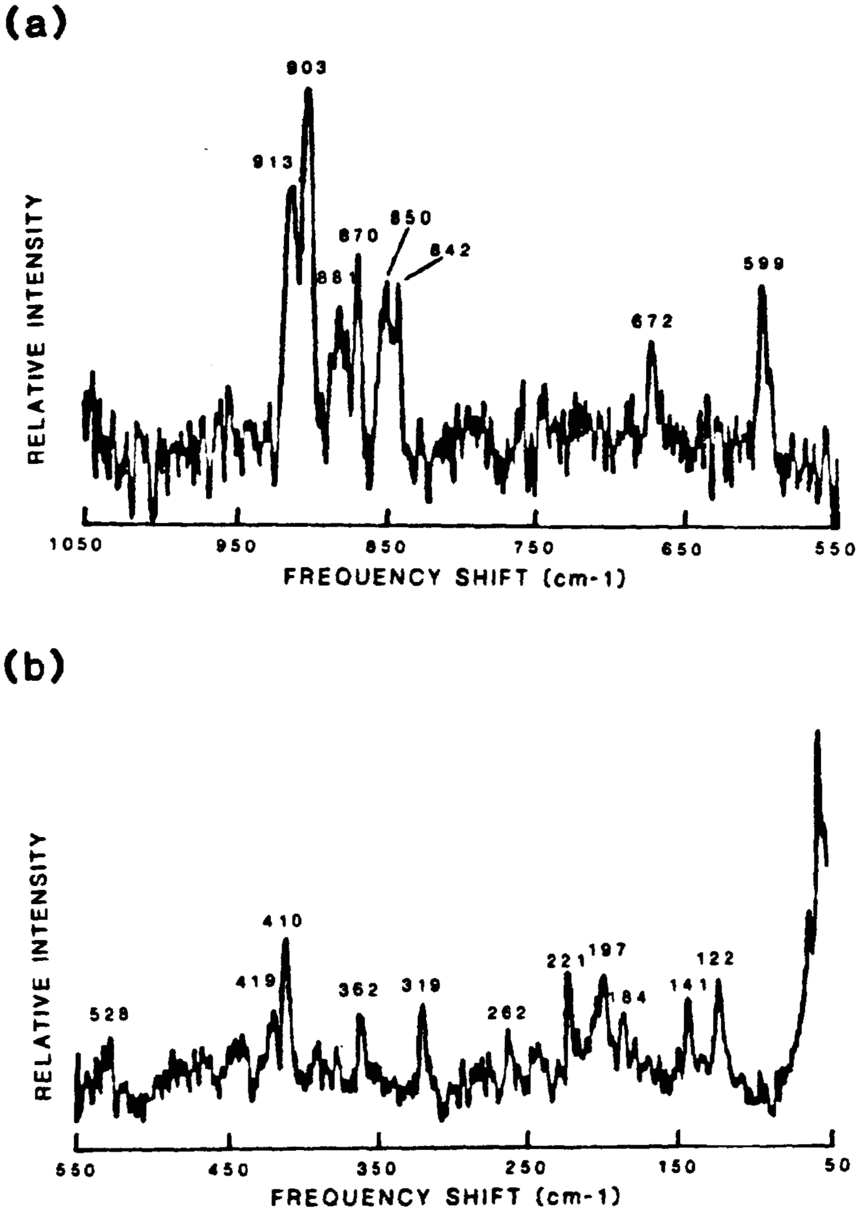

Figure I-2. Raman spectrum of ^{18}O substituted complex A. Scan parameters: laser excitation, 568.2 nm; slitwidth, 2.5 cm^{-1}; scan rate, 2.5 cm^{-1}/sec; number of scans, 10; 180 degree backscattering geometry; sample temperature, 77K; data subjected to 9 point smoothing routine.

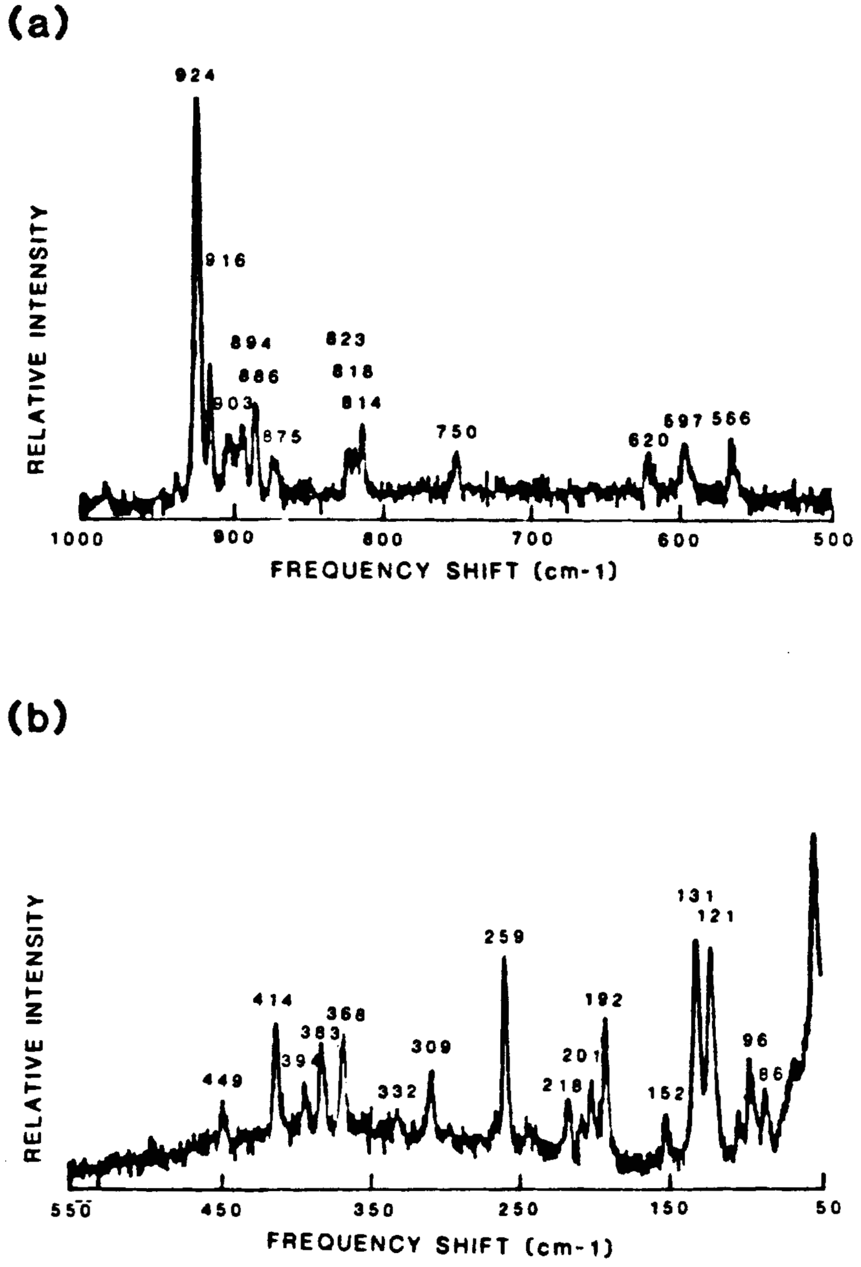

Figure I-3. Raman spectrum of complex B. Scan parameters: laser excitation, 568.2 nm; slitwidth, 2.5 cm^{-1}; scan rate, 2.5 cm^{-1}/sec; number of scans, 10; 180 degree backscattering geometry; sample temperature, 77K.

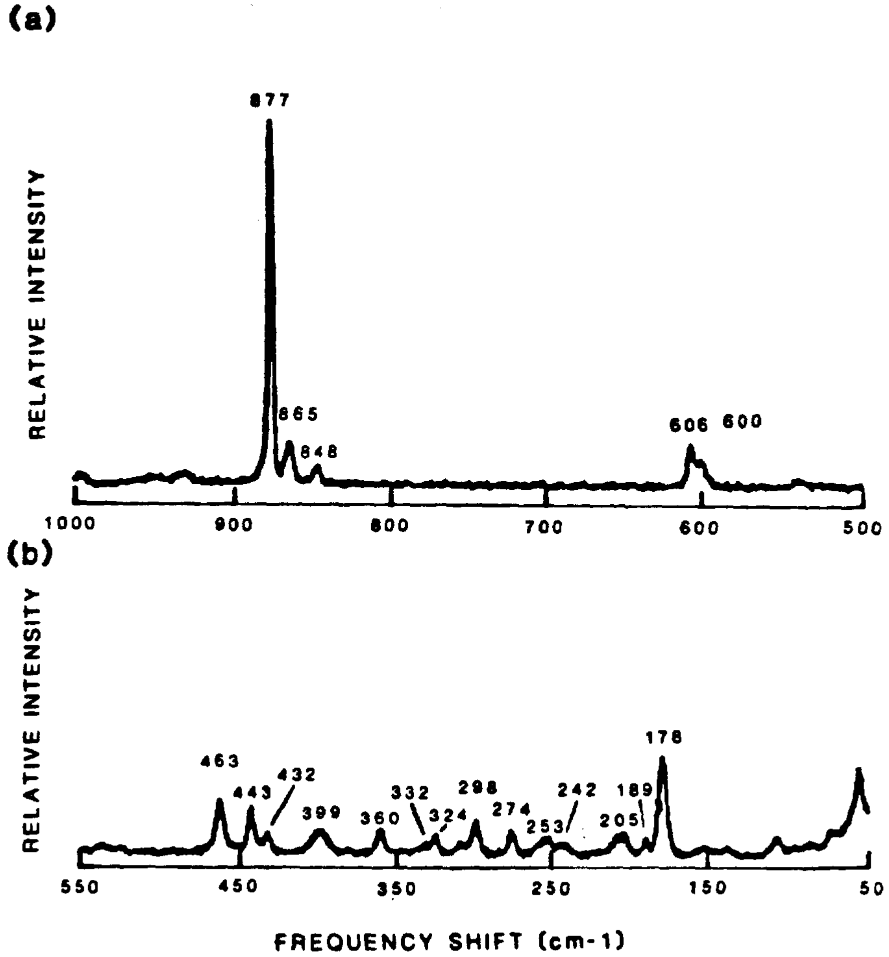

Figure I-4: Raman spectrum of complex C. Scan parameters: laser excitation, 568.2 nm; slitwidth, 2.5 cm^{-1}; scan rate, 2.5 cm^{-1}/sec; number of scans, 10; 180 degree backscattering geometry; sample temperature, 77K.

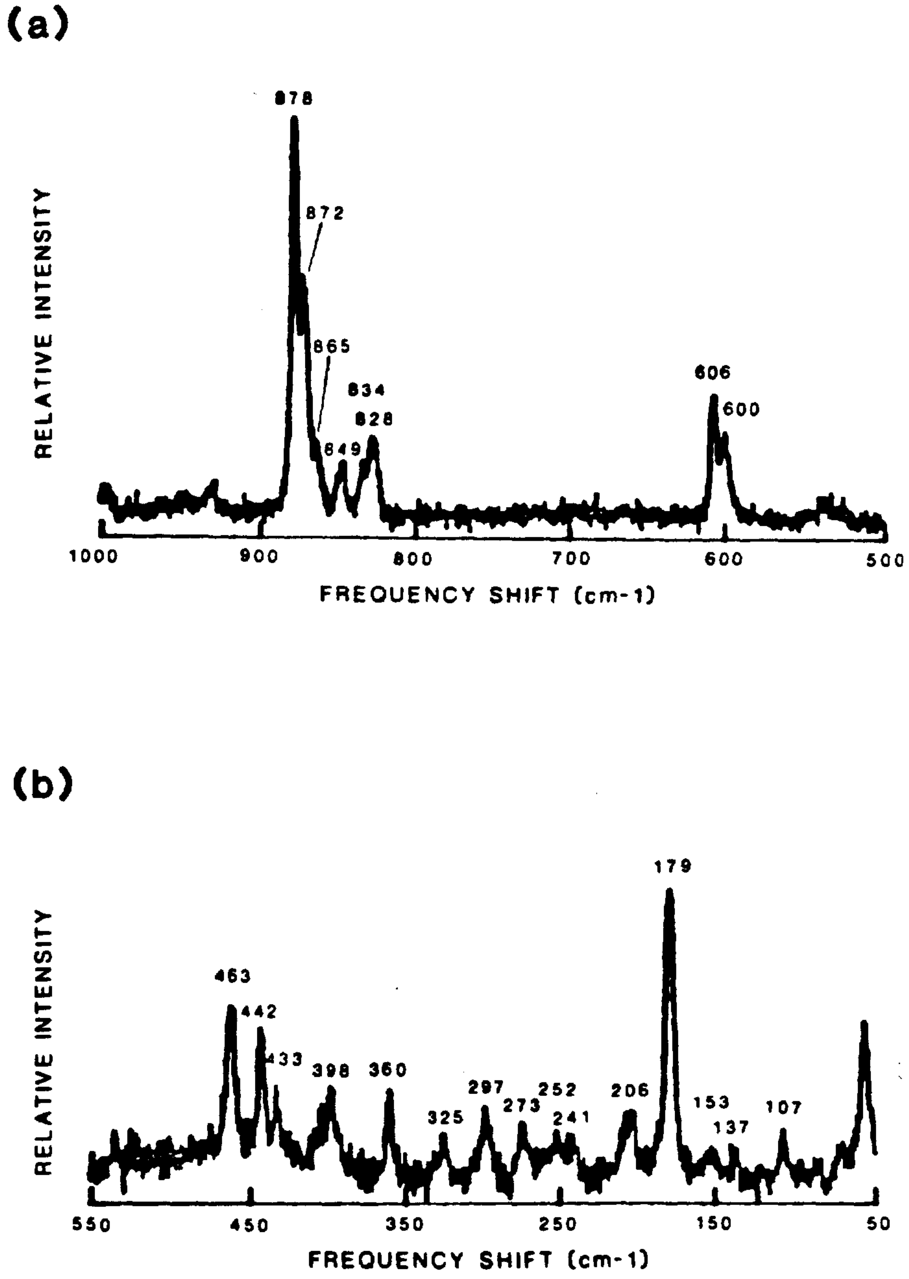

Figure I-5. Raman spectrum of ^{18}O substituted complex C. Scan parameters: laser excitation, 568.2 nm; slitwidth, 2.5 cm^{-1}; scan rate, 1.25 cm^{-1}/sec; number of scans, (a) 21, (b) 5; 180 degree backscattering geometry; sample temperature, 77K.

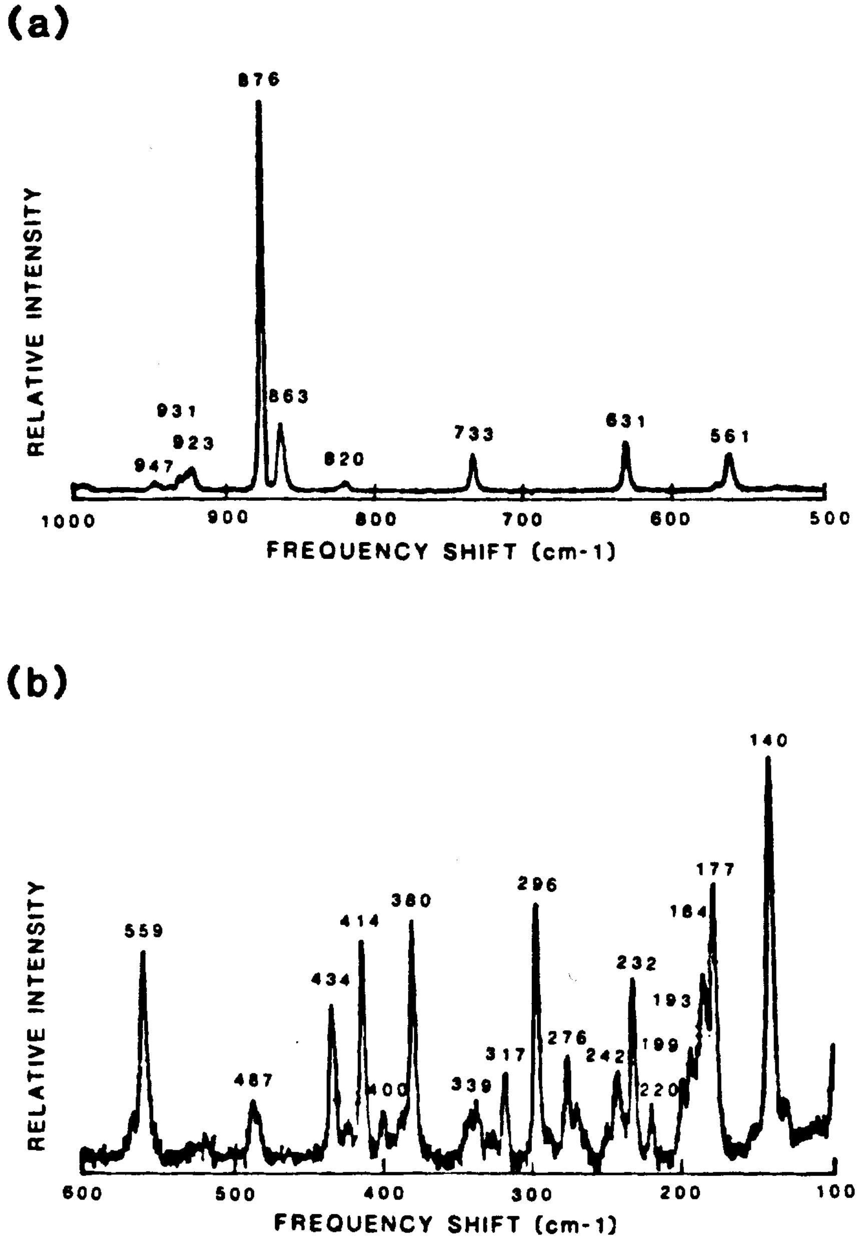

Figure I-6. Raman spectrum of complex D. Scan parameters: laser excitation, 568.2 nm; slitwidth, 2.5 cm^{-1}; scan rate, 2.5 cm^{-1}/sec; number of scans, 10; 180 degree backscattering geometry; sample temperature, 77K.

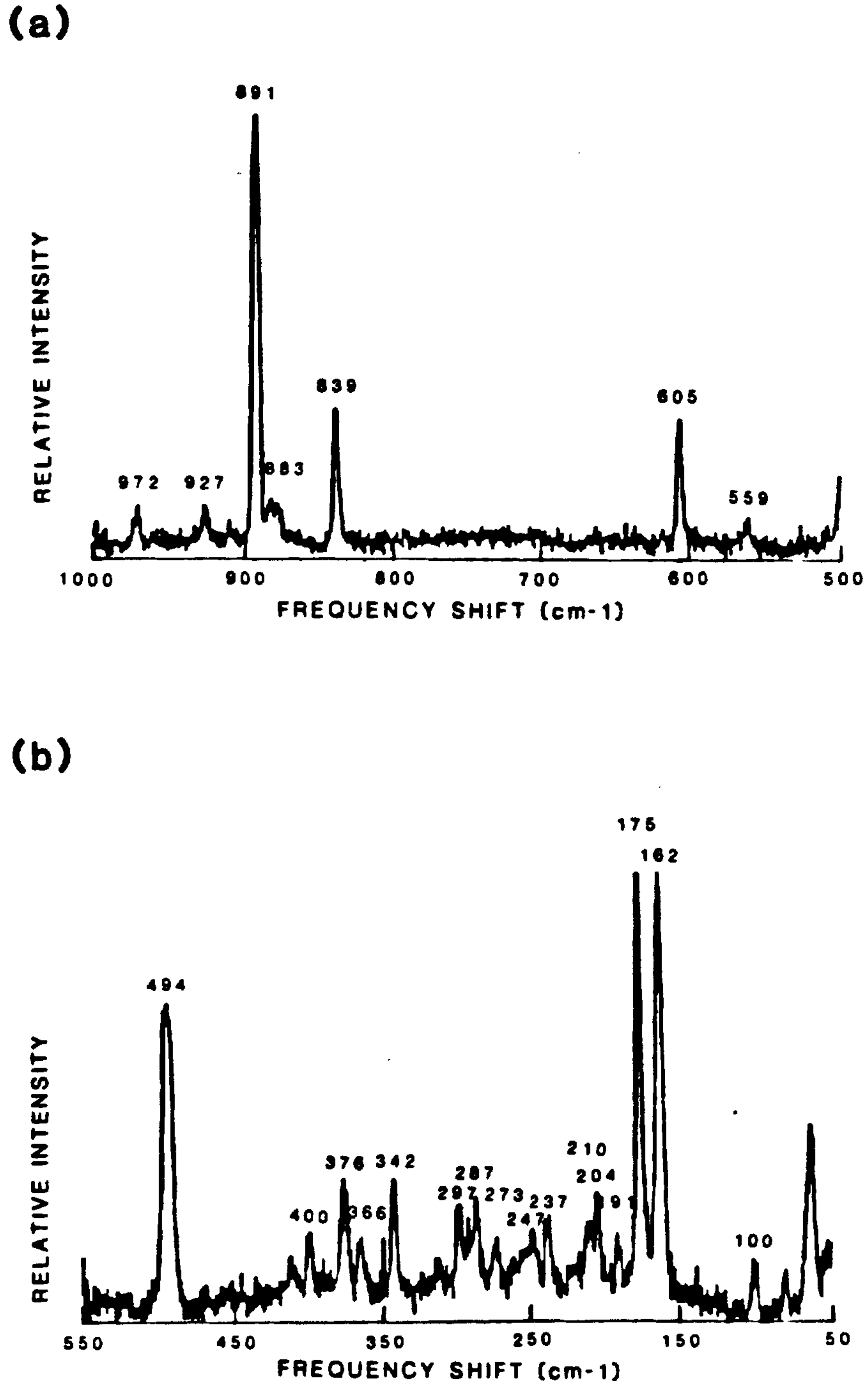

Figure I-7. Raman spectrum of complex F. Scan parameters: laser excitation, 568.2 nm; slitwidth, 2.5 cm^{-1}; scan rate, 2.5 cm^{-1}/sec; number of scans, 10; 180 degree back-scattering geometry; sample temperature, 77K.

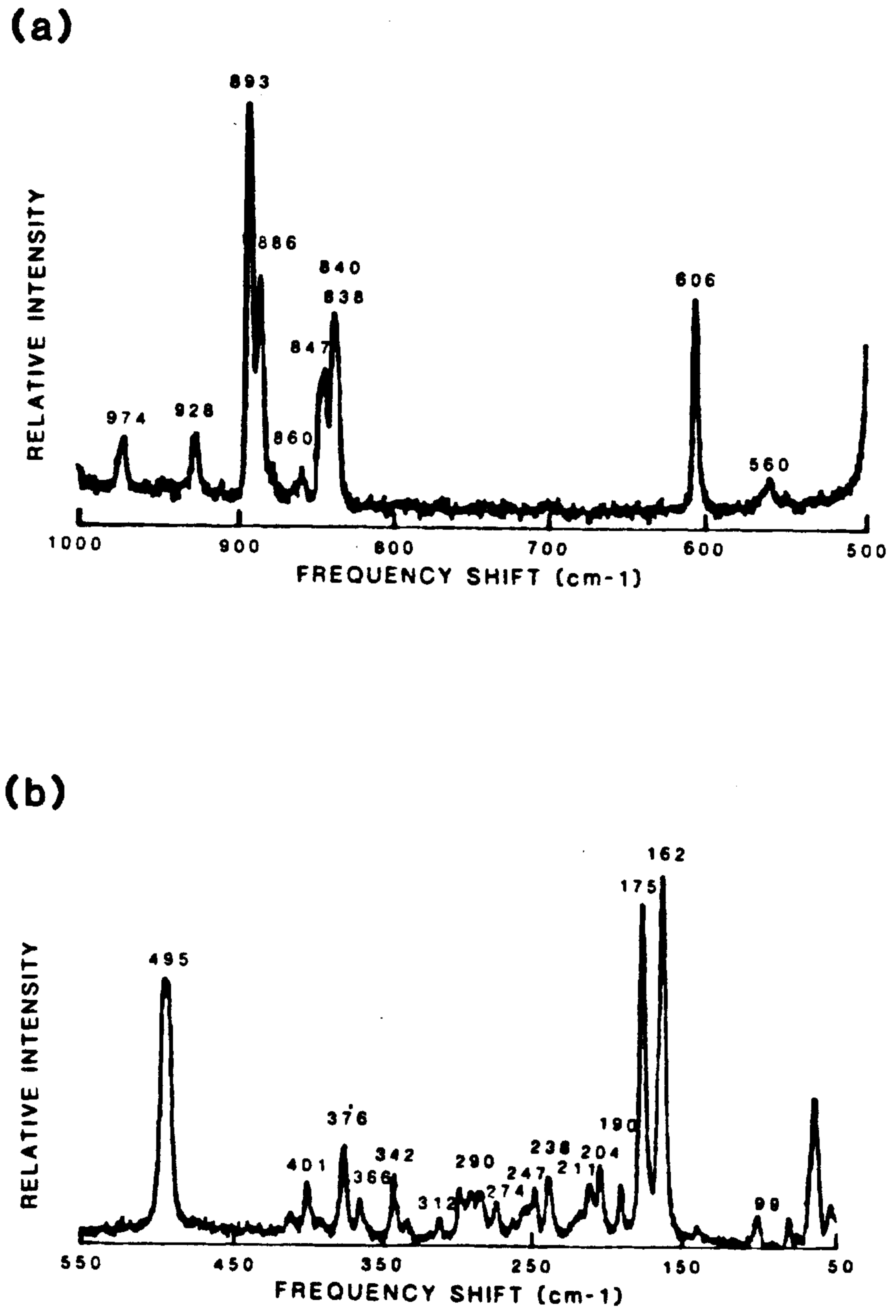

Figure I-8. Raman spectrum of ^{18}O substituted complex F. Scan parameters: laser excitation, 568.2 nm; slitwidth, 2.5 cm^{-1}; scan rate, 0.25 cm^{-1}/sec; number of scans, 1; 180 degree backscattering geometry; sample temperature, 77K.

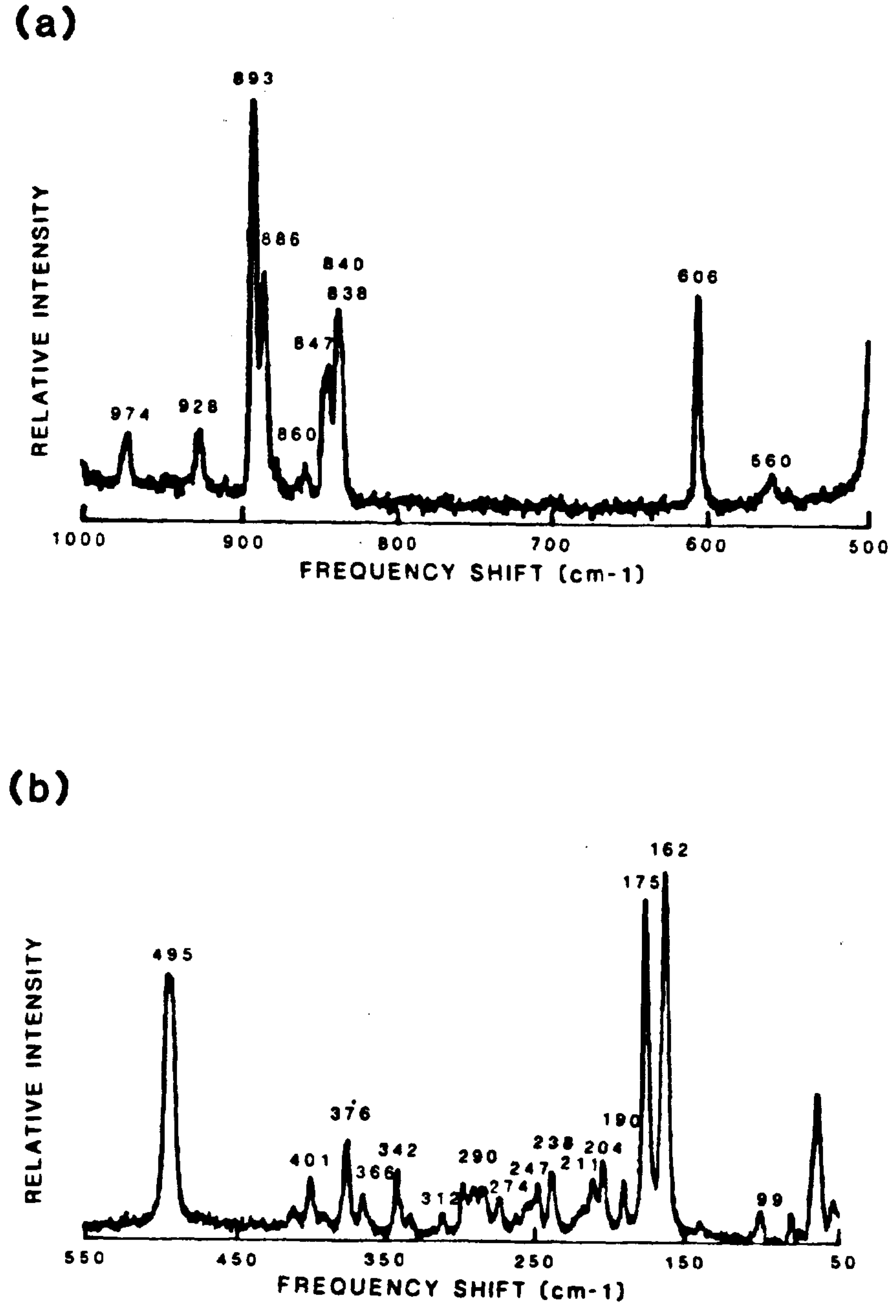

Figure I-8. Raman spectrum of ^{18}O substituted complex F. Scan parameters: laser excitation, 568.2 nm; slitwidth, 2.5 cm^{-1}; scan rate, 0.25 cm^{-1}/sec; number of scans, 1; 180 degree backscattering geometry; sample temperature, 77K.

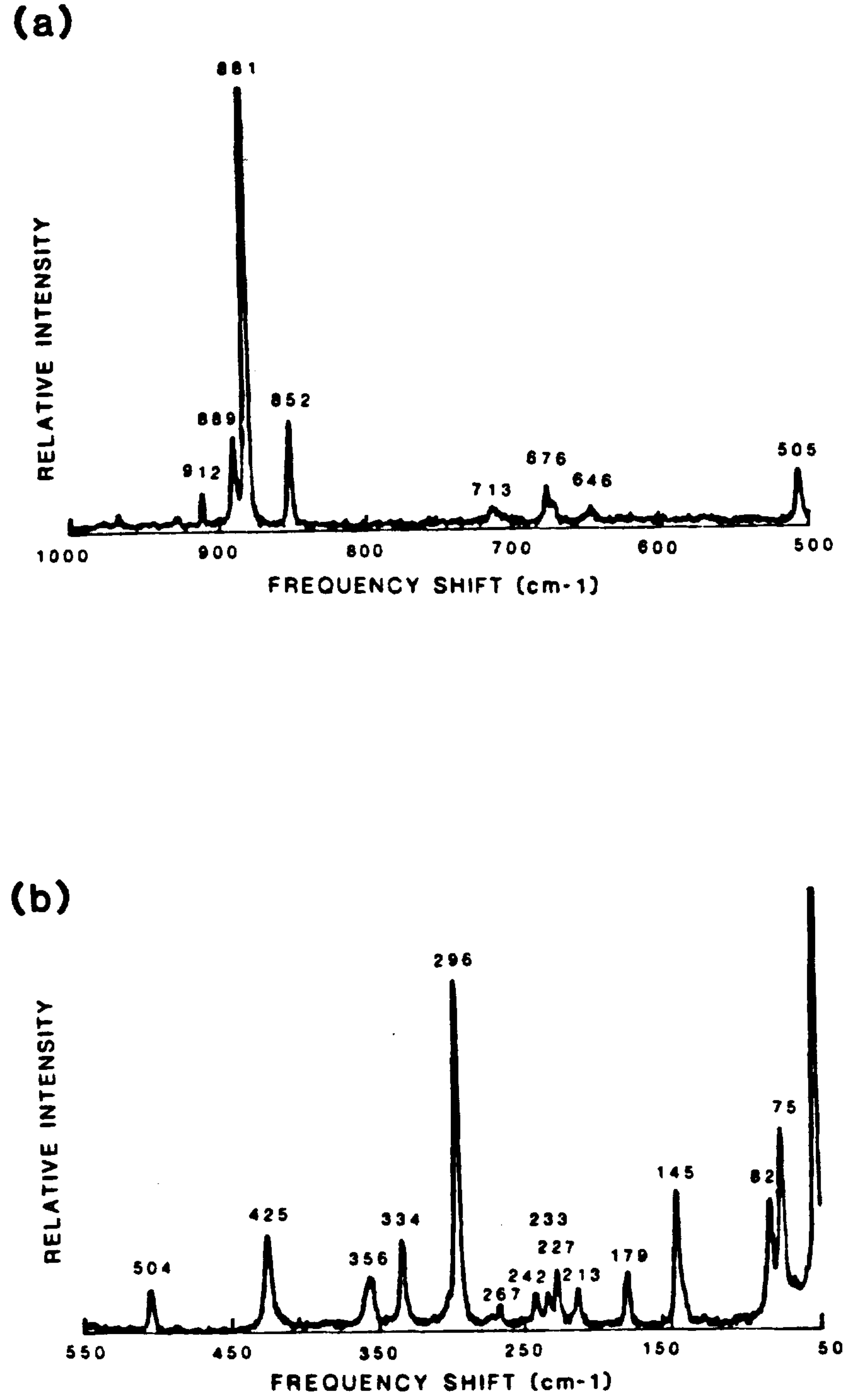

Figure I-9. Raman spectrum of complex G. Scan parameters: laser excitation, 568.2 nm; slitwidth, 2.5 cm^{-1}; scan rate, 0.25 cm^{-1}/sec; number of scans, 1; 180 degree backscattering geometry; sample temperature, 77K.

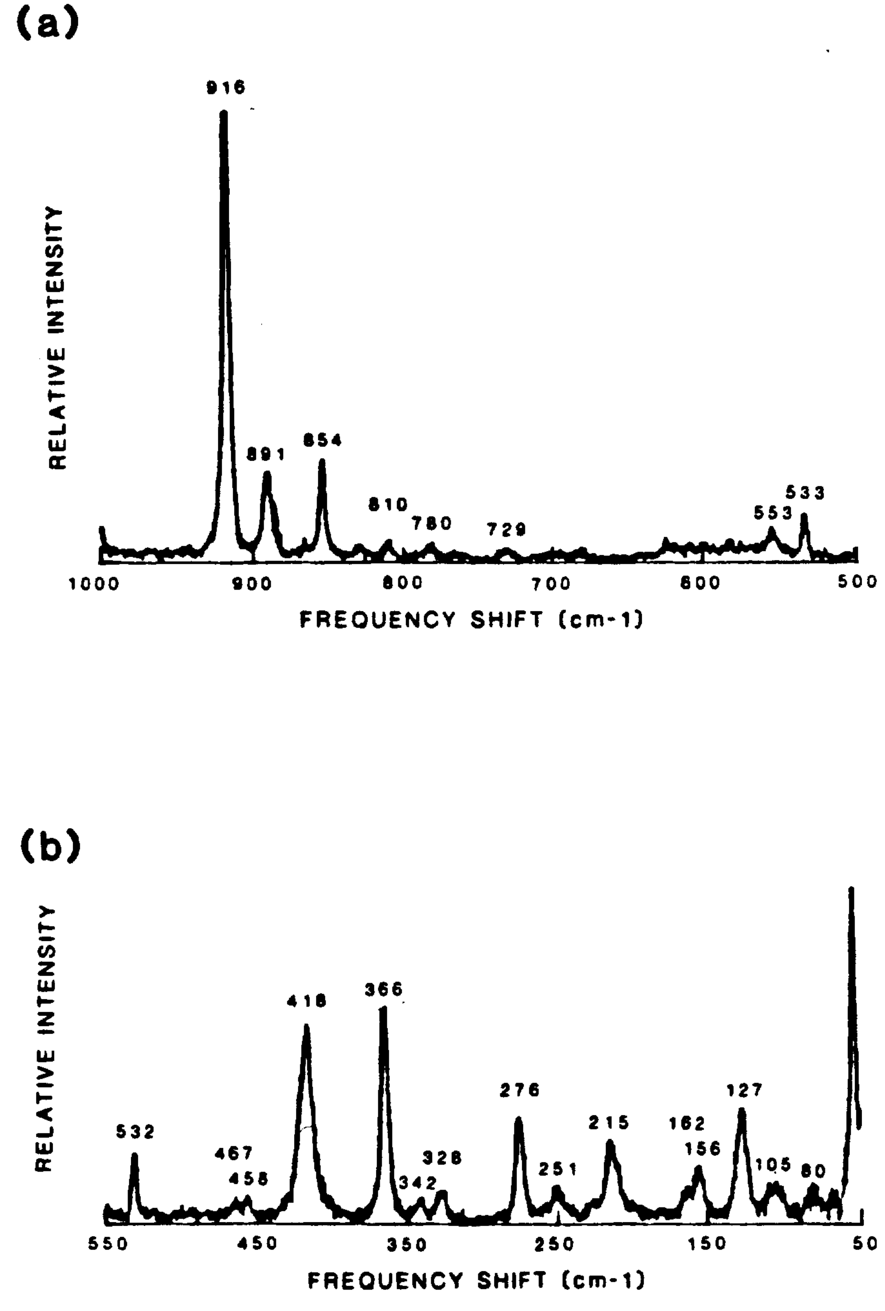

Figure I-10. Raman spectrum of complex H. Scan parameters: laser excitation, 568.2 nm; slitwidth, 2.5 cm^{-1}; scan rate, 0.25 cm^{-1}/sec; number of scans, 1; 180 degree back-scattering geometry; sample temperature, 77K.

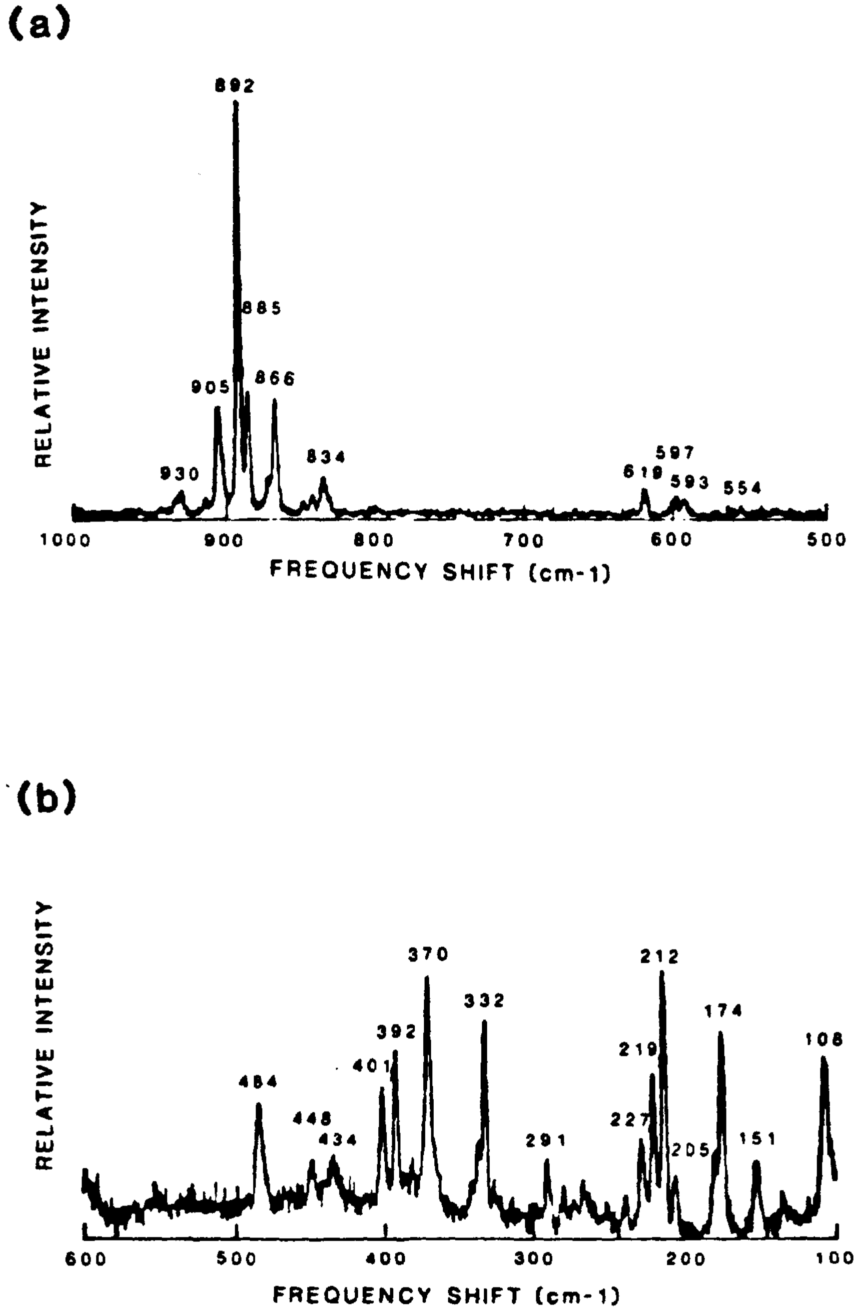

Figure I-11. Raman spectrum of complex E. Scan parameters: laser excitation, 568.2 nm; slitwidth, 2.5 cm^{-1}; scan rate, 2.5 cm^{-1}/sec; number of scans, 10; 180 degree backscattering geometry; sample temperature, 77K.

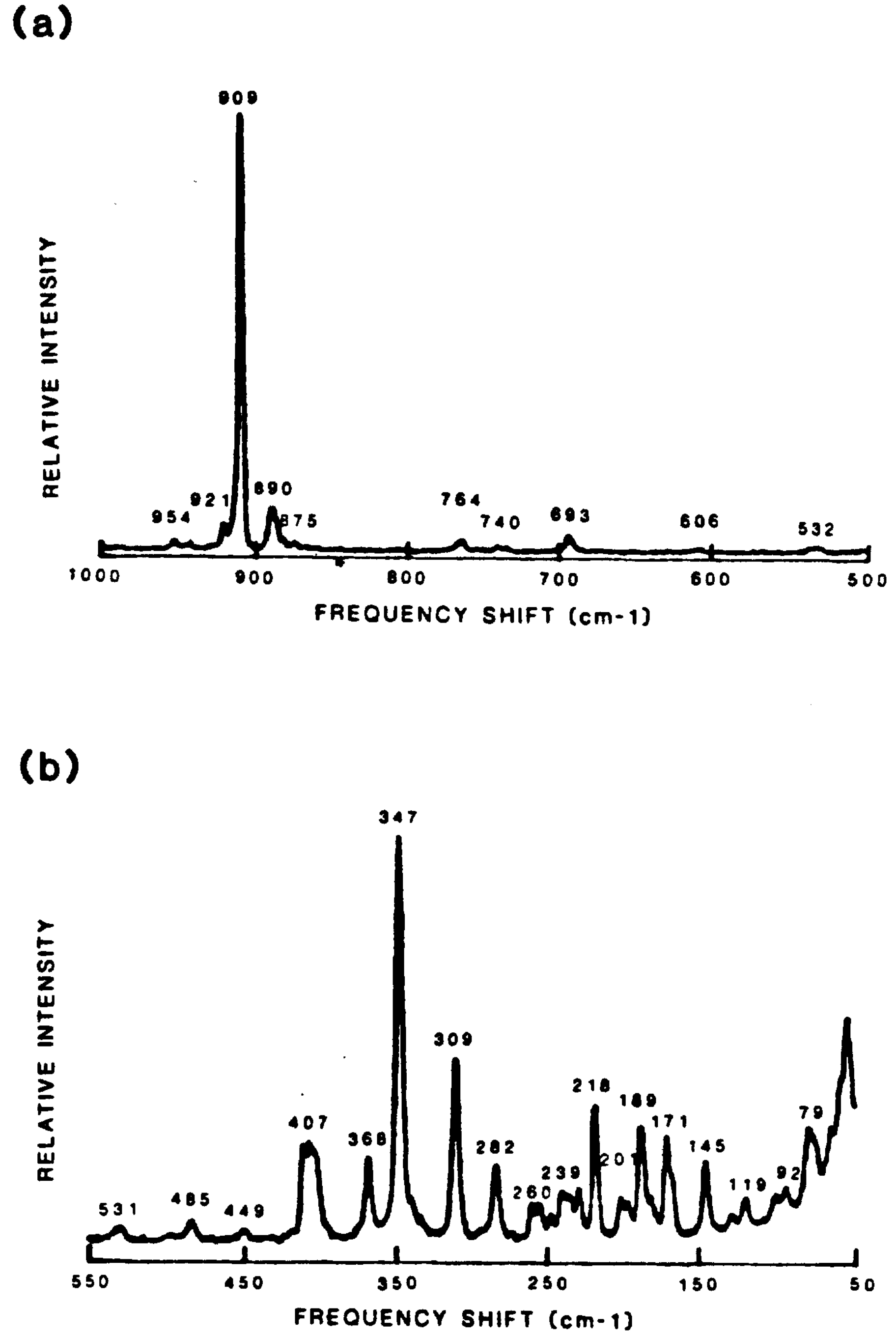

Figure I-12. Raman spectrum of complex I. Scan parameters: laser excitation, 568.2 nm; slitwidth, 2.5 cm^{-1}; scan rate, 0.25 cm^{-1}/sec; number of scans, 1; 180 degree backscattering geometry; sample temperature, 77K.

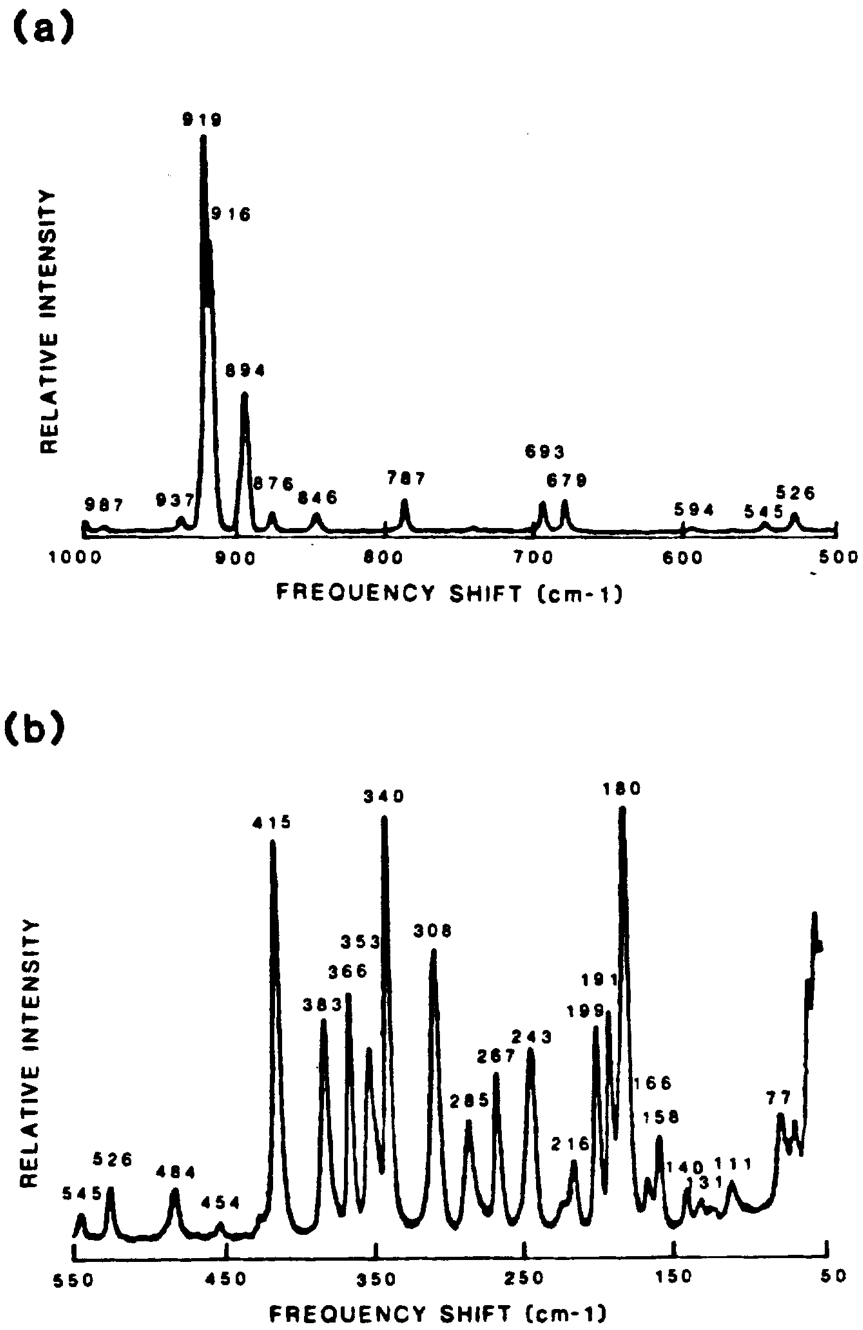

Figure I-13. Raman spectrum of complex J. Scan parameters: laser excitation, 568.2 nm; slitwidth, 2.5 cm^{-1}; scan rate, 0.25 cm^{-1}/sec; number of scans, 1; 180 degree backscattering geometry; sample temperature, 77K.

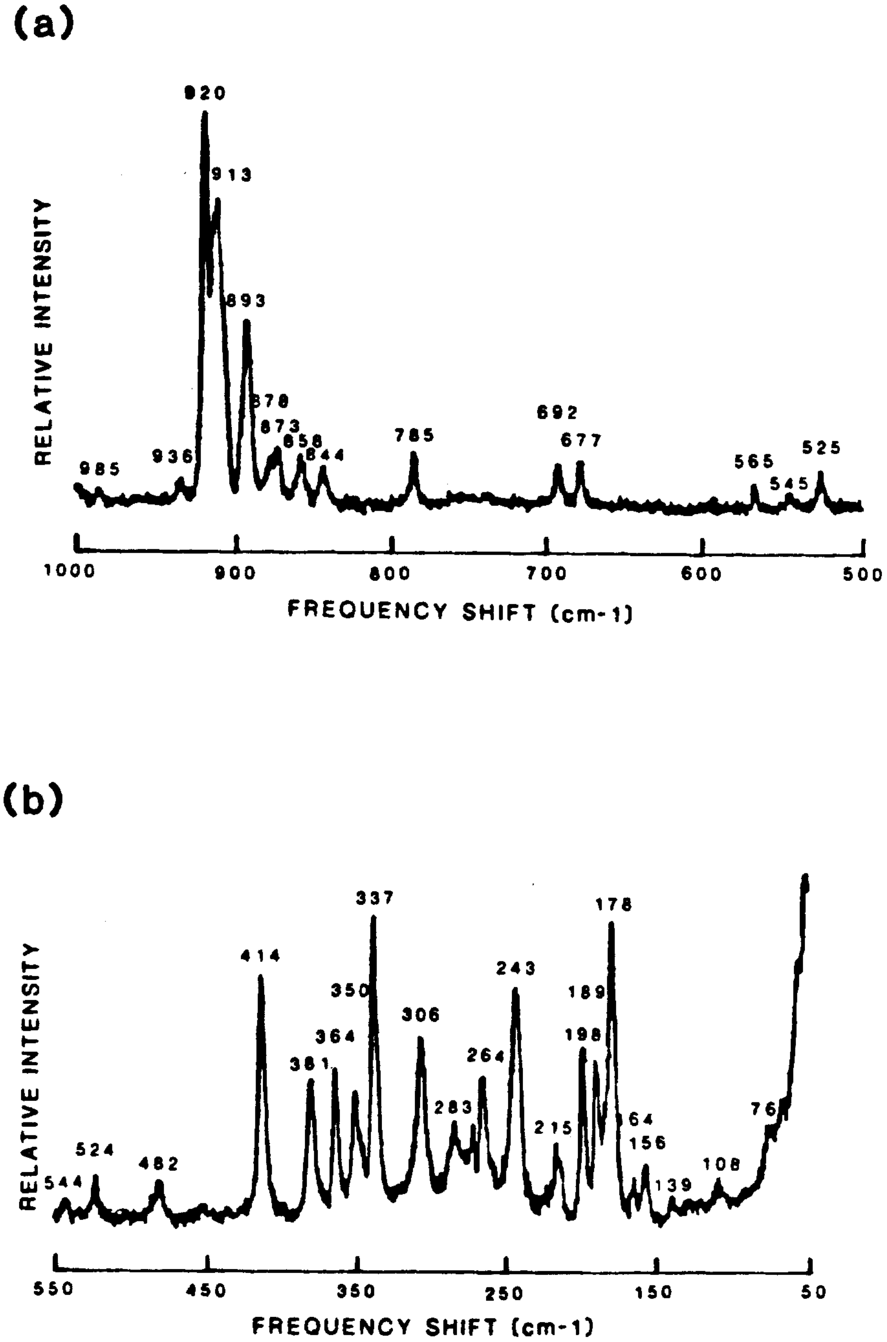

Figure I-14. Raman spectrum of ^{17}O, ^{18}O substituted complex J. Scan parameters: laser excitation, 568.2 nm; slitwidth, 2.5 cm^{-1}; scan rate, 0.25 cm^{-1}/sec; number of scans, 1; 180 degree backscattering geometry; sample temperature, 77K.

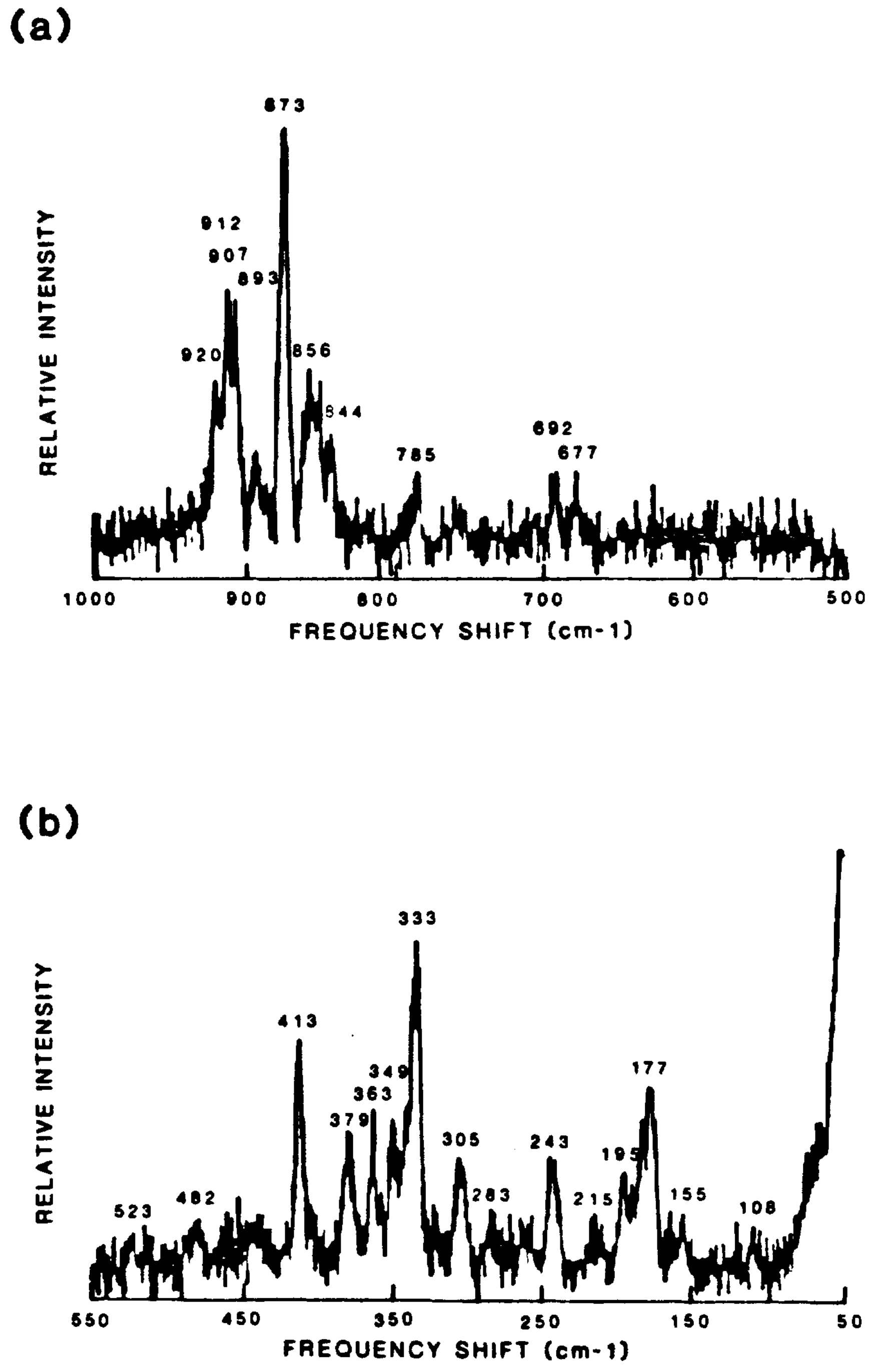

Figure I-15. Raman spectrum of ^{18}O substituted complex J. Scan parameters: laser excitation, 568.2 nm; slitwidth, 2.5 cm^{-1}; scan rate, 0.25 cm^{-1}/sec; number of scans, 1; 180 degree backscattering geometry; sample temperature, 77K.

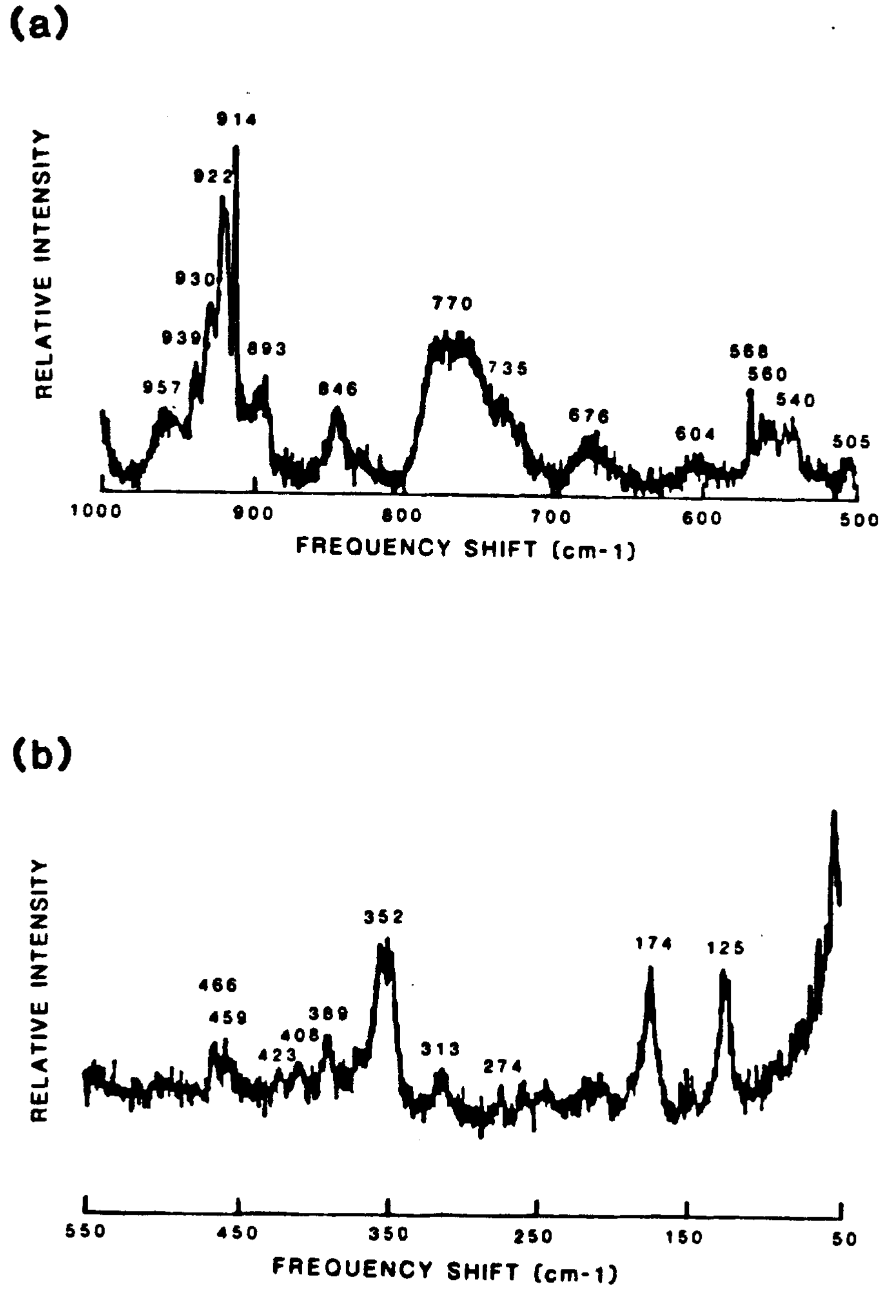

Figure I-16. Raman spectrum of complex K. Scan parameters: laser excitation, 568.2 nm; slitwidth, 2.5 cm^{-1}; scan rate, (a) 0.125 cm^{-1}/sec, (b) 0.25 cm^{-1}/sec; number of scans, (a) 2, (b) 1; 180 degree backscattering geometry; sample temperature, 77K.

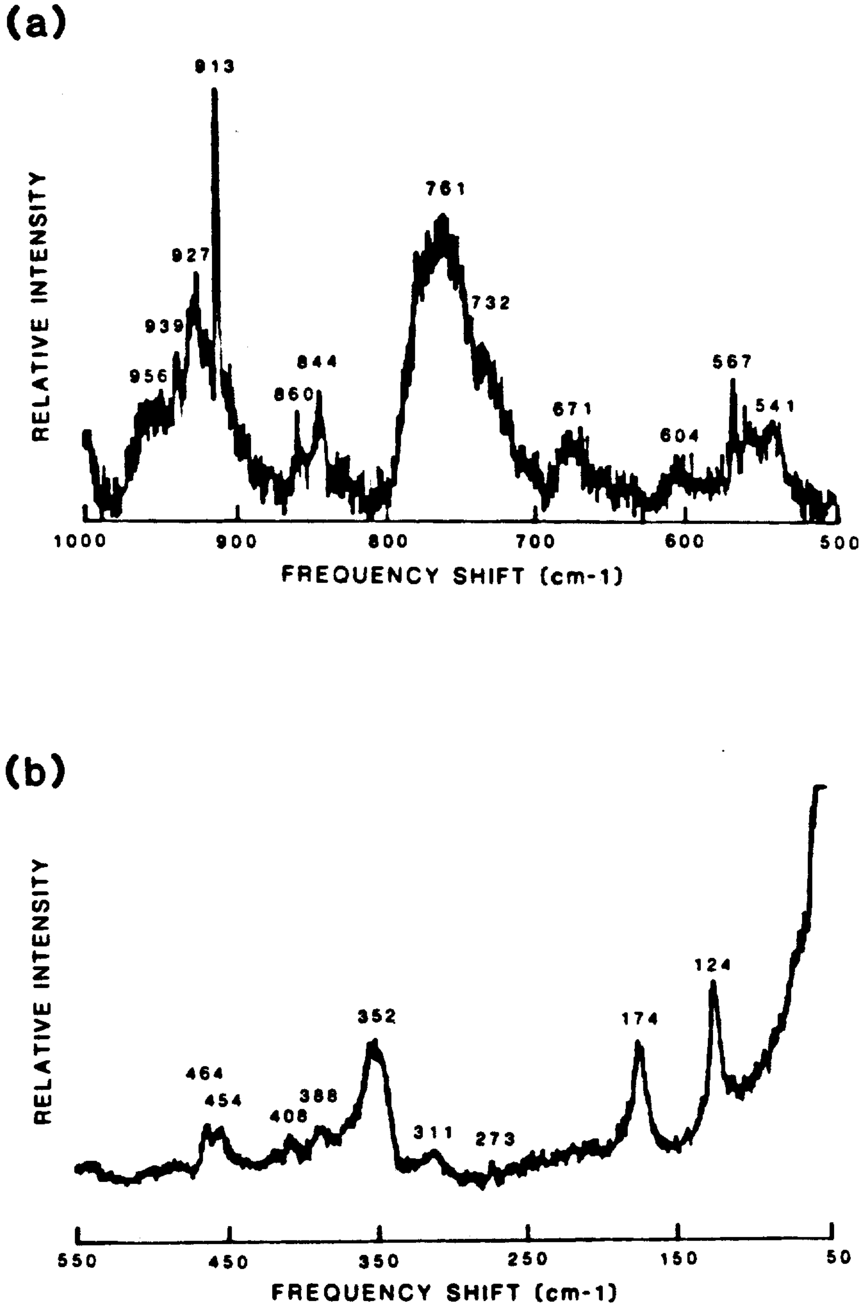

Figure I-17. Raman spectrum of ^{18}O substituted complex K. Scan parameters: laser excitation, 568.2 nm; slitwidth, 2.5 cm^{-1}; scan rate, 0.125 cm^{-1}/sec; number of scans, (a) 2, (b) 1; 180 degree backscattering geometry; sample temperature, 77K.

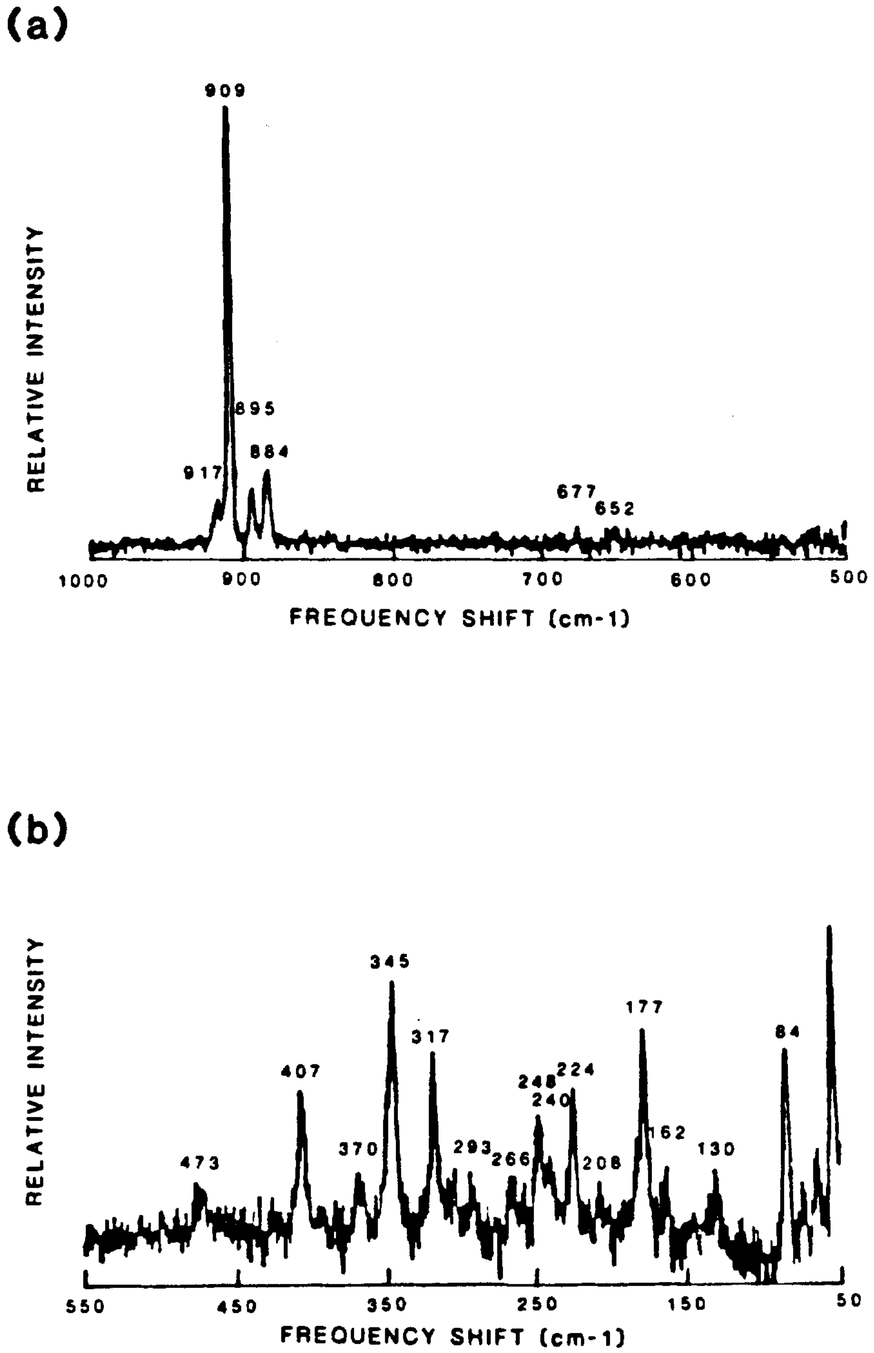

Figure I-18. Raman spectrum of complex L. Scan parameters: laser excitation, 568.2 nm; slitwidth, 2.5 cm^{-1}; scan rate, 0.25 cm^{-1}/sec; number of scans, 1; 180 degree back-scattering geometry; sample temperature, 77K.

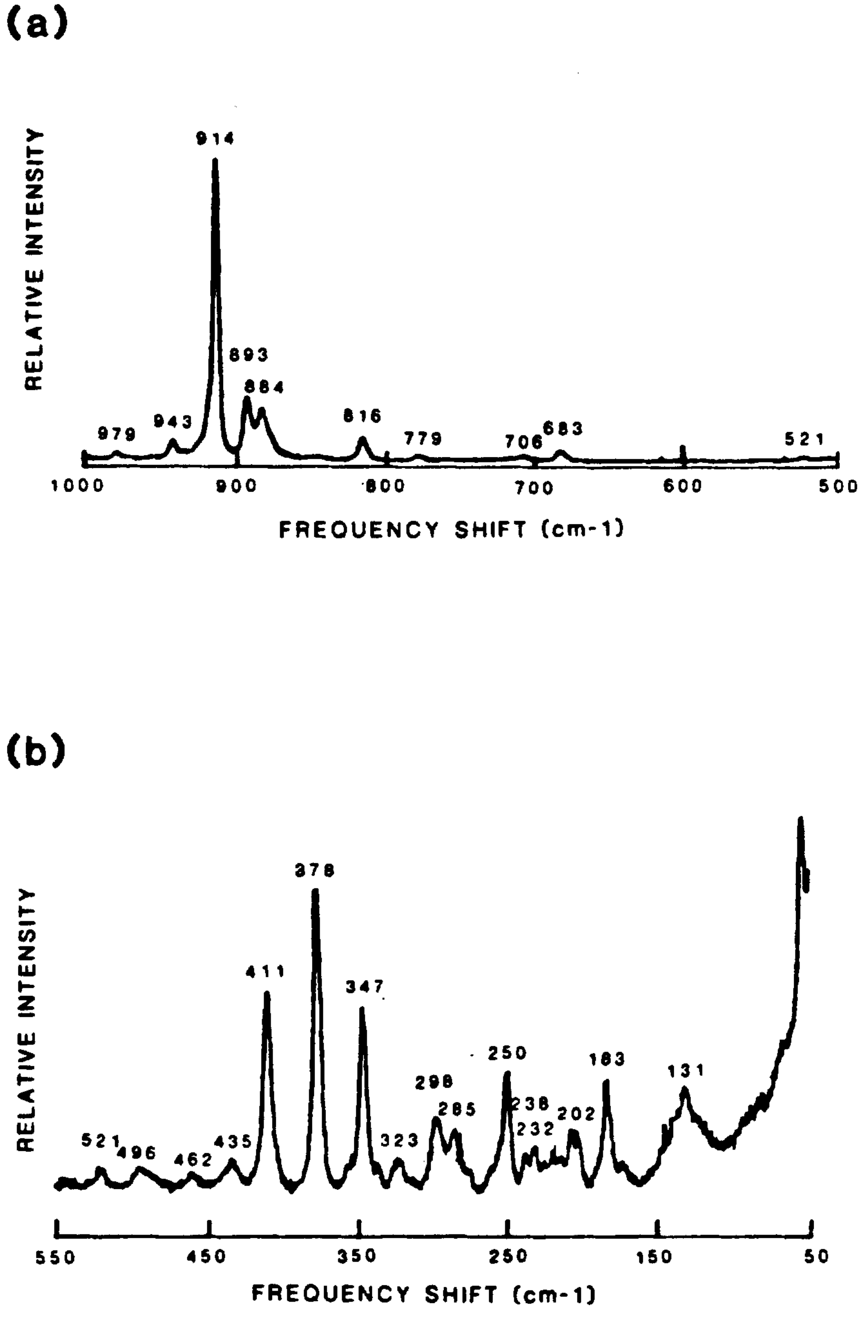

Figure I-19. Raman spectrum of complex M. Scan parameters: laser excitation, 568.2 nm; slitwidth, 2.5 cm^{-1}; scan rate, 0.25 cm^{-1}/sec; number of scans, 1; 180 degree back-scattering geometry; sample temperature, 77K.

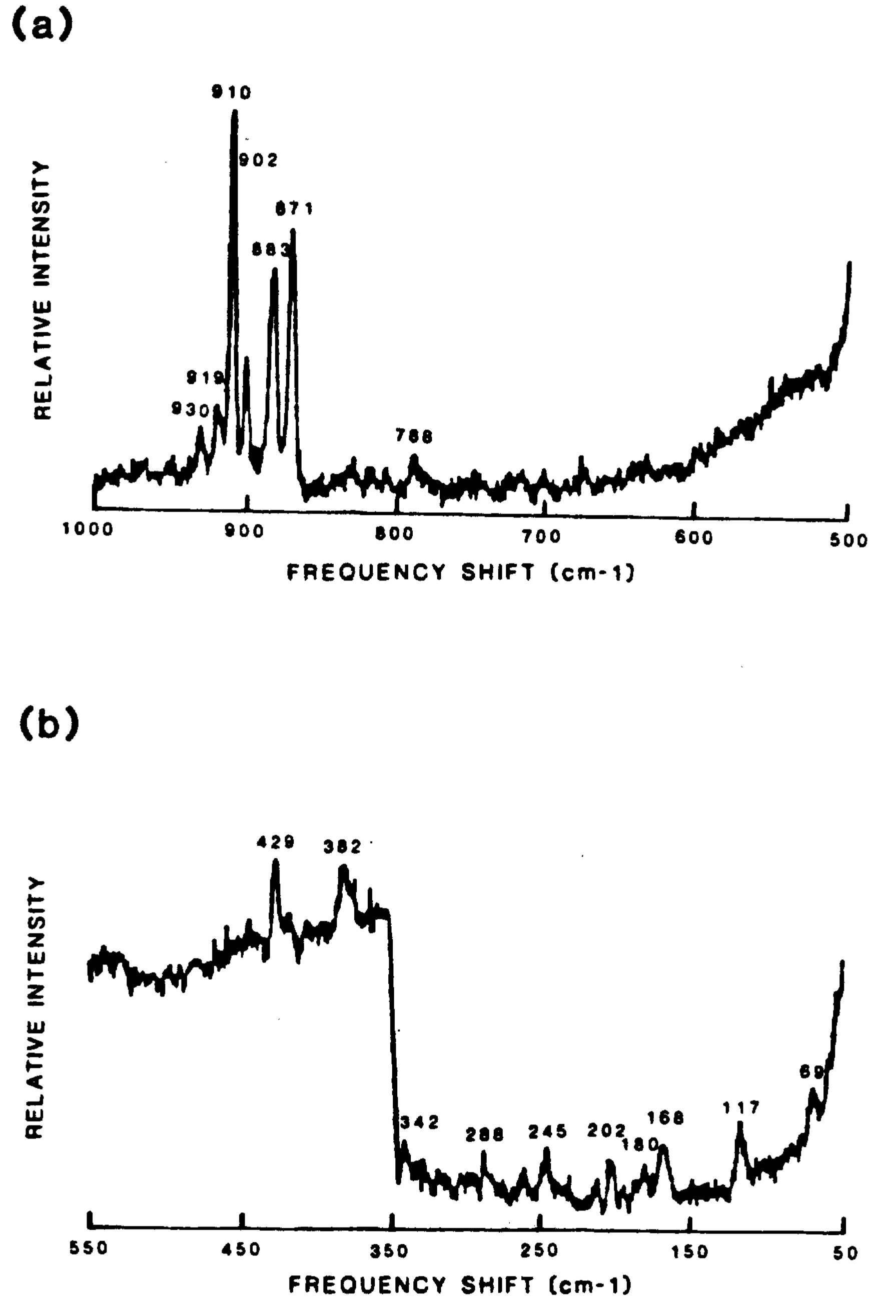

Figure I-20. Raman spectrum of complex N. Scan parameters: laser excitation, 568.2 nm; slitwidth, 2.5 cm^{-1}; scan rate, 0.25 cm^{-1}/sec; number of scans, 1; 180 degree backscattering geometry; sample temperature, 77K.

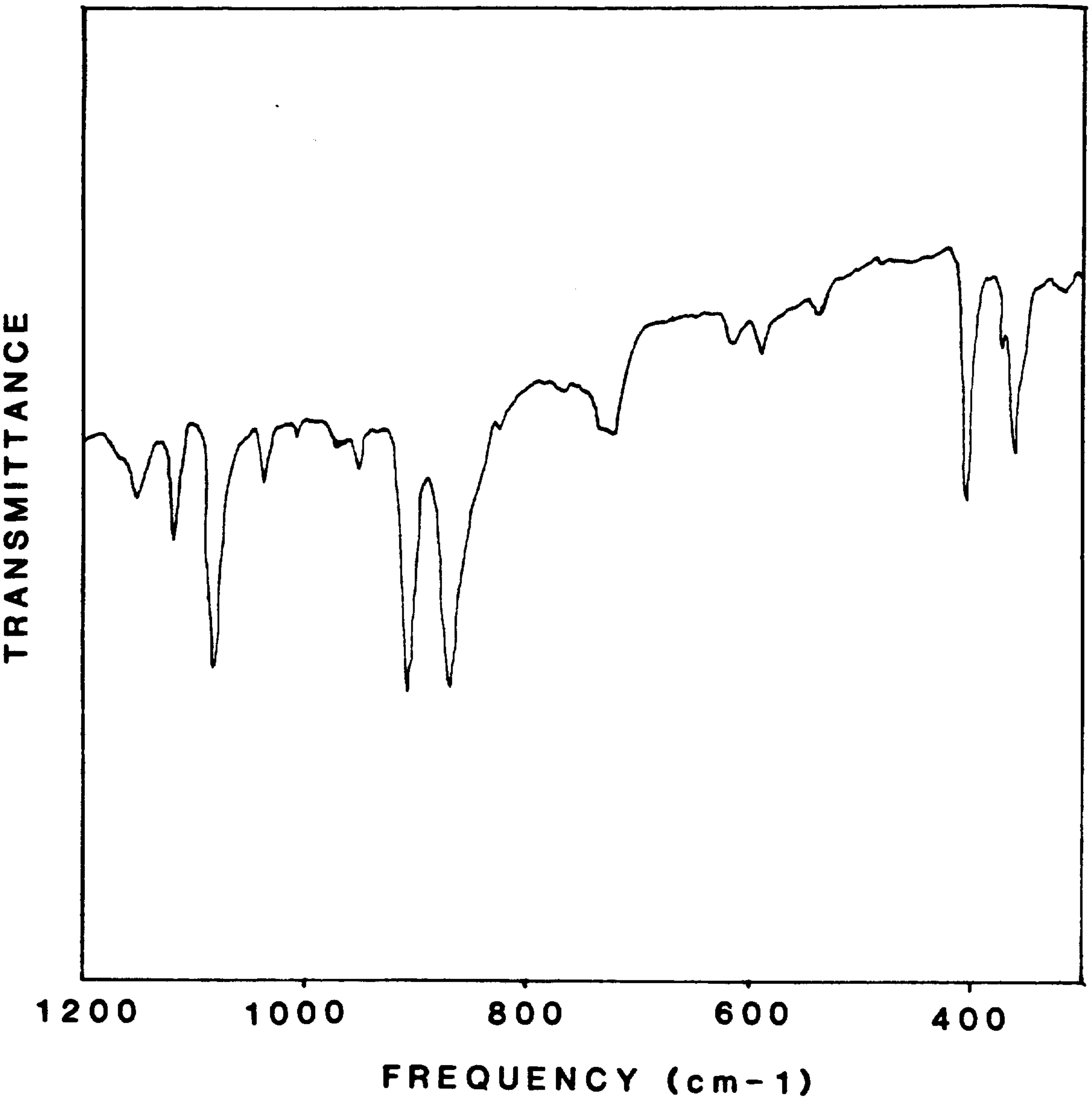

Figure I-21. Infrared spectrum of complex A.

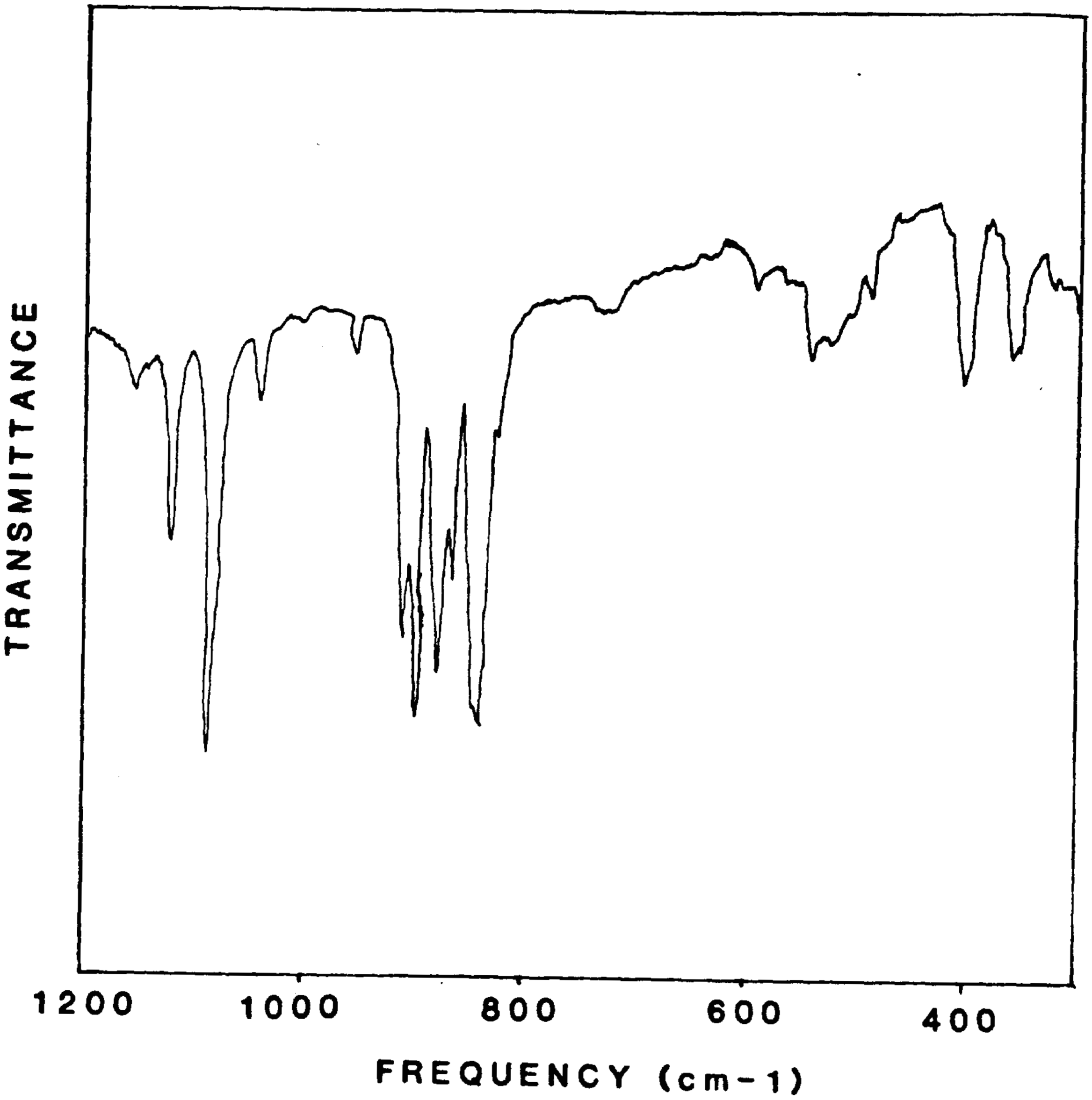

Figure I-22. Infrared spectrum of ^{18}O substituted complex A.

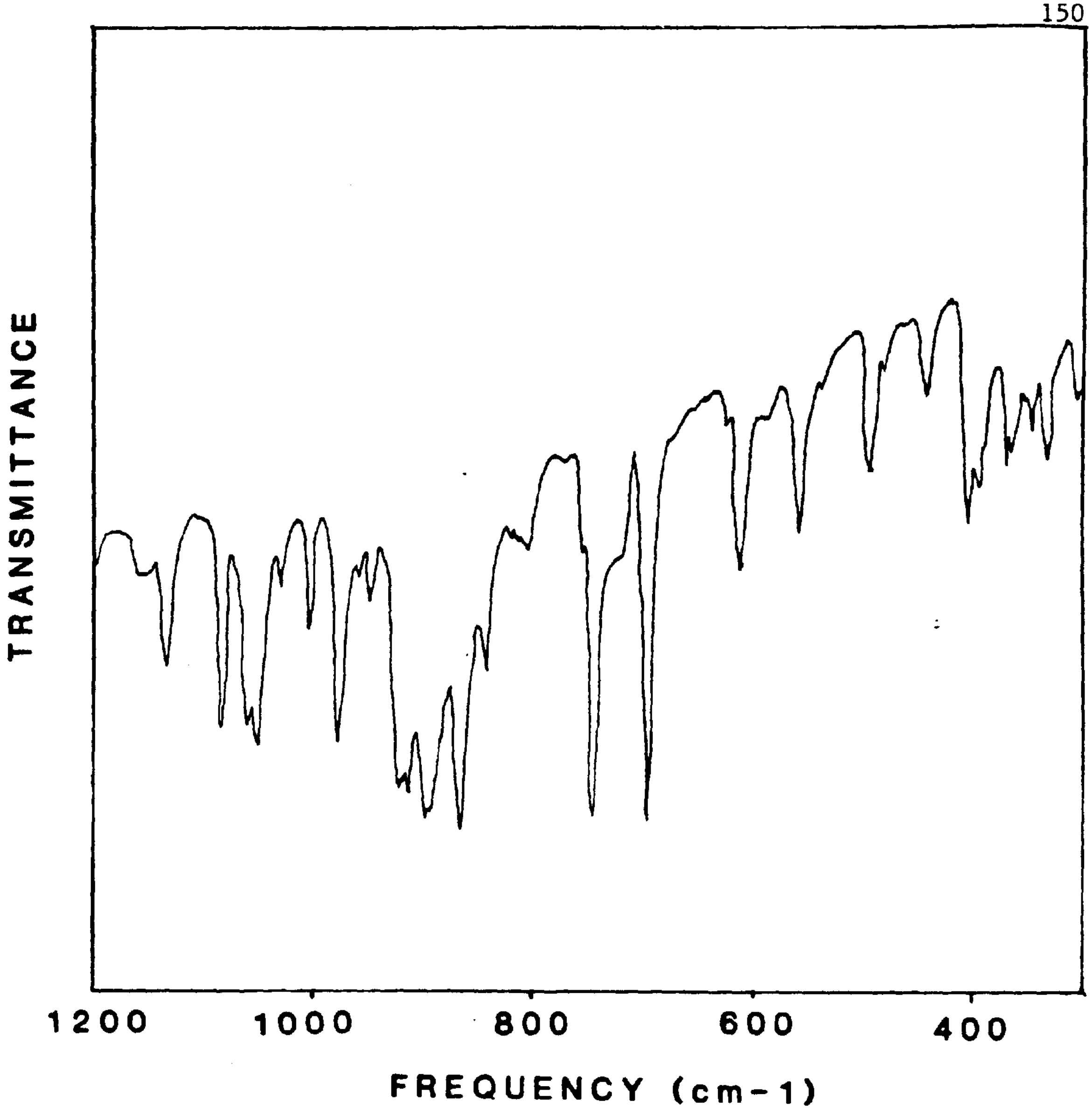

Figure I-23. Infrared spectrum of complex B.

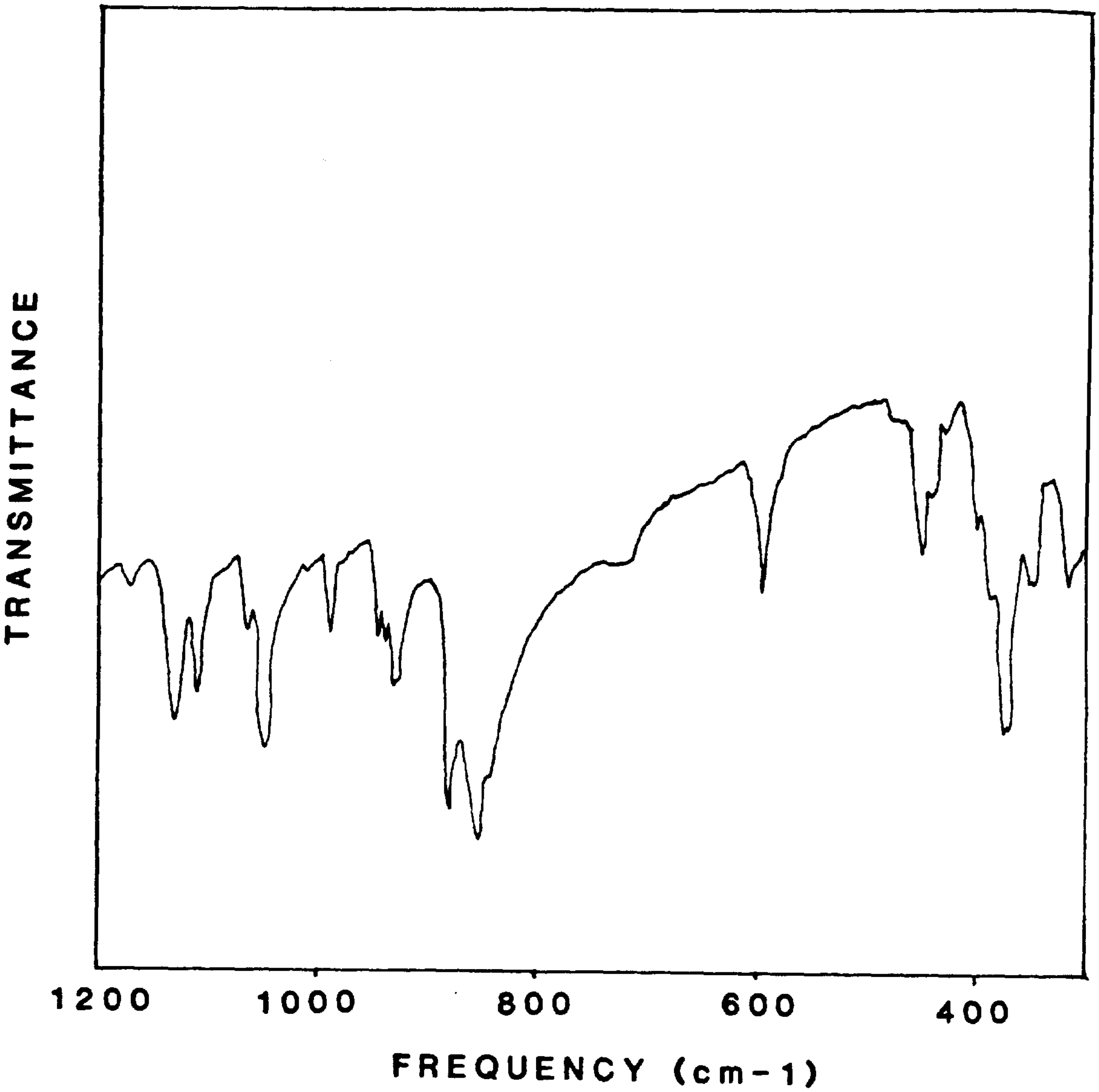

Figure I-24. Infrared spectrum of complex C.

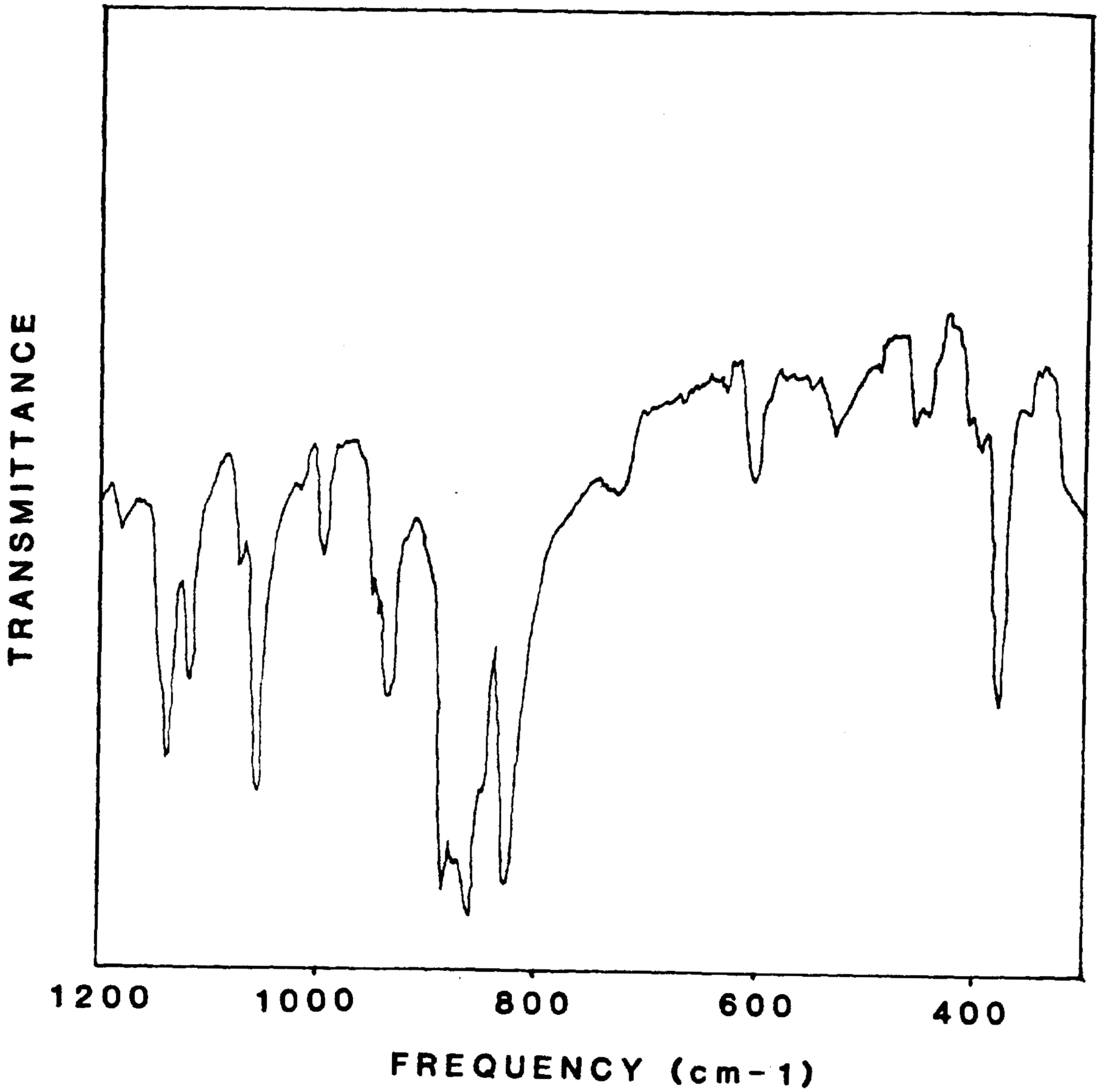

Figure I-25. Infrared spectrum of ^{18}O substituted complex C.

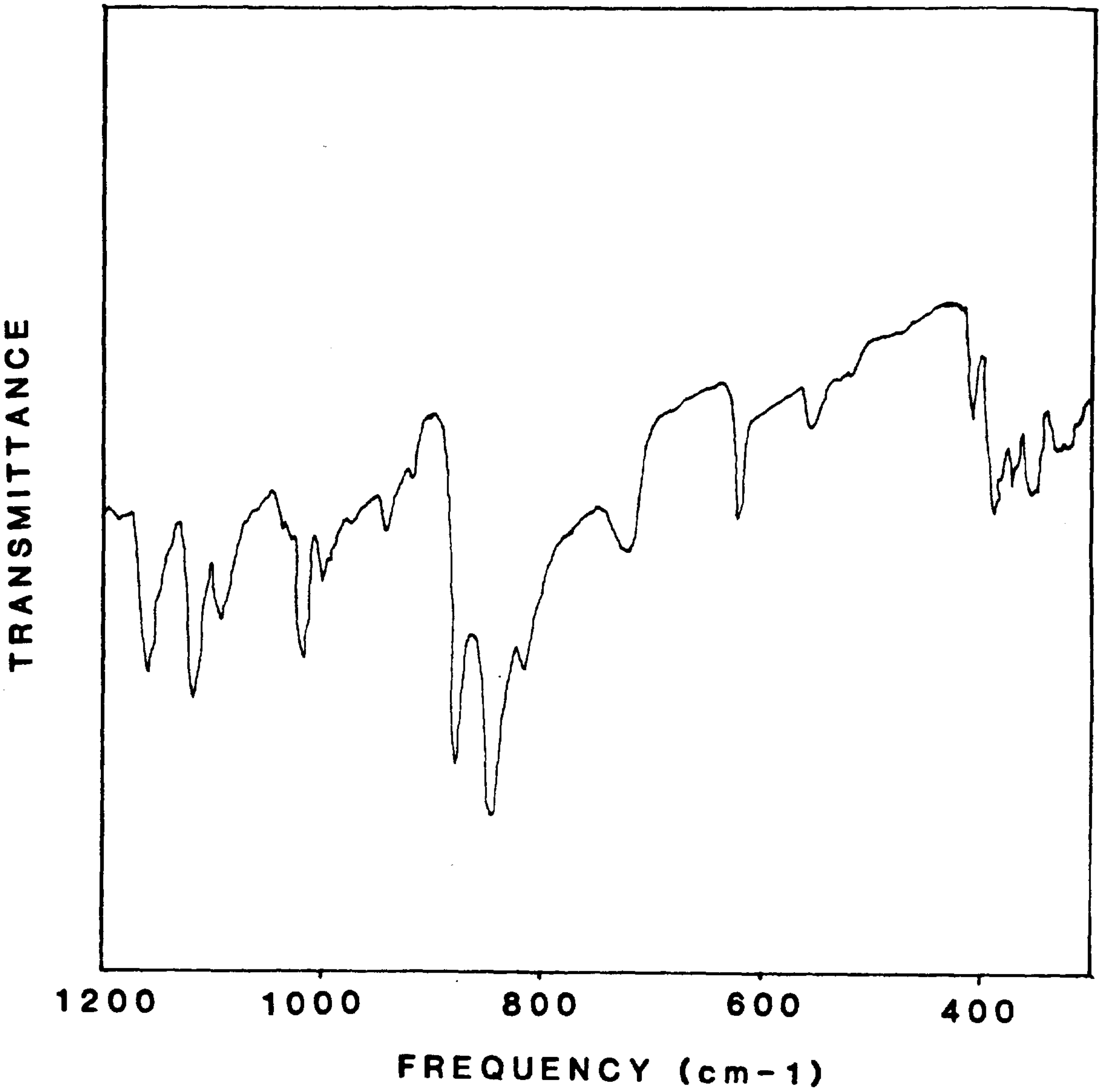

Figure I-26. Infrared spectrum of complex D.

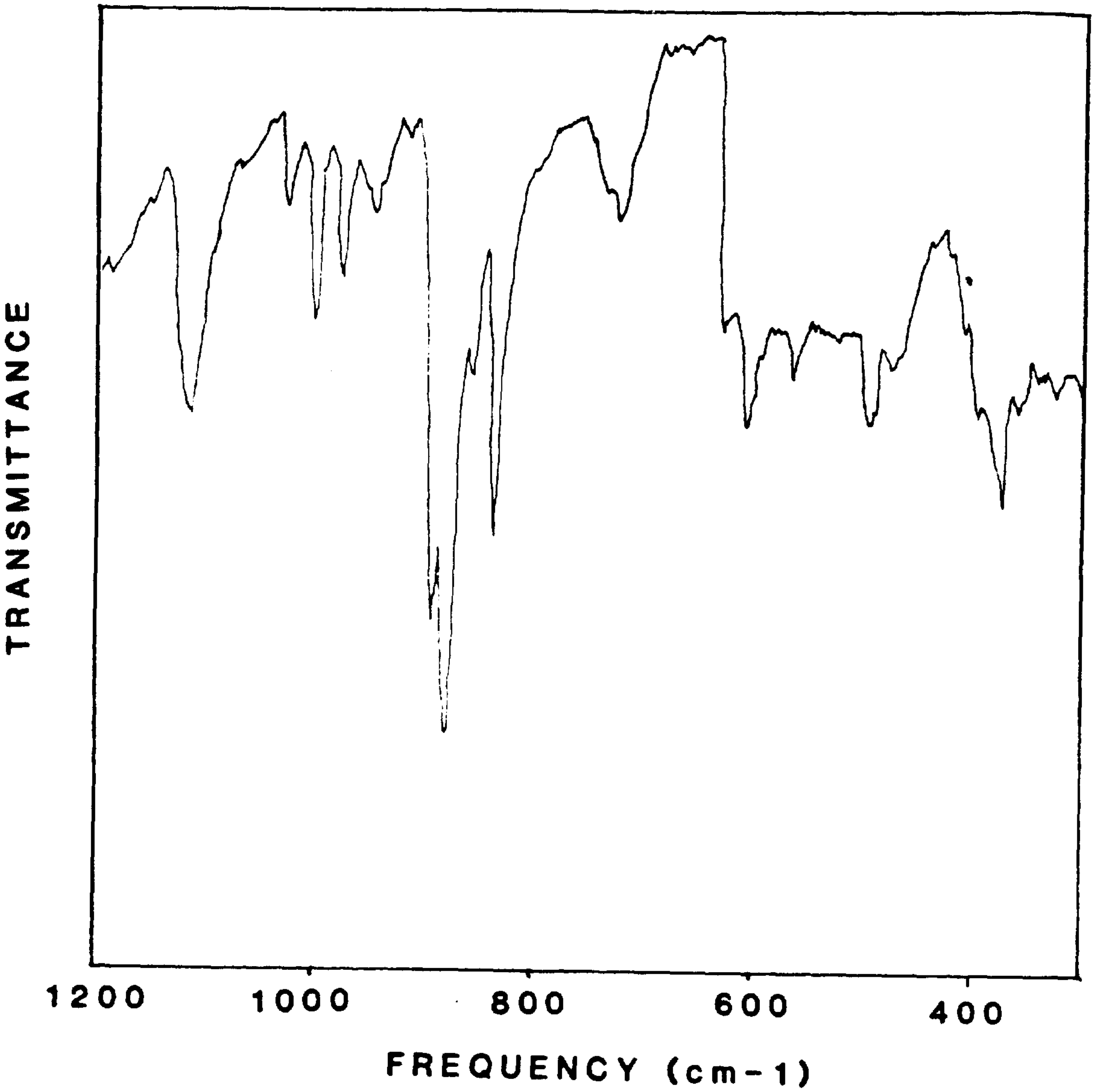

Figure I-27. Infrared spectrum of complex F.

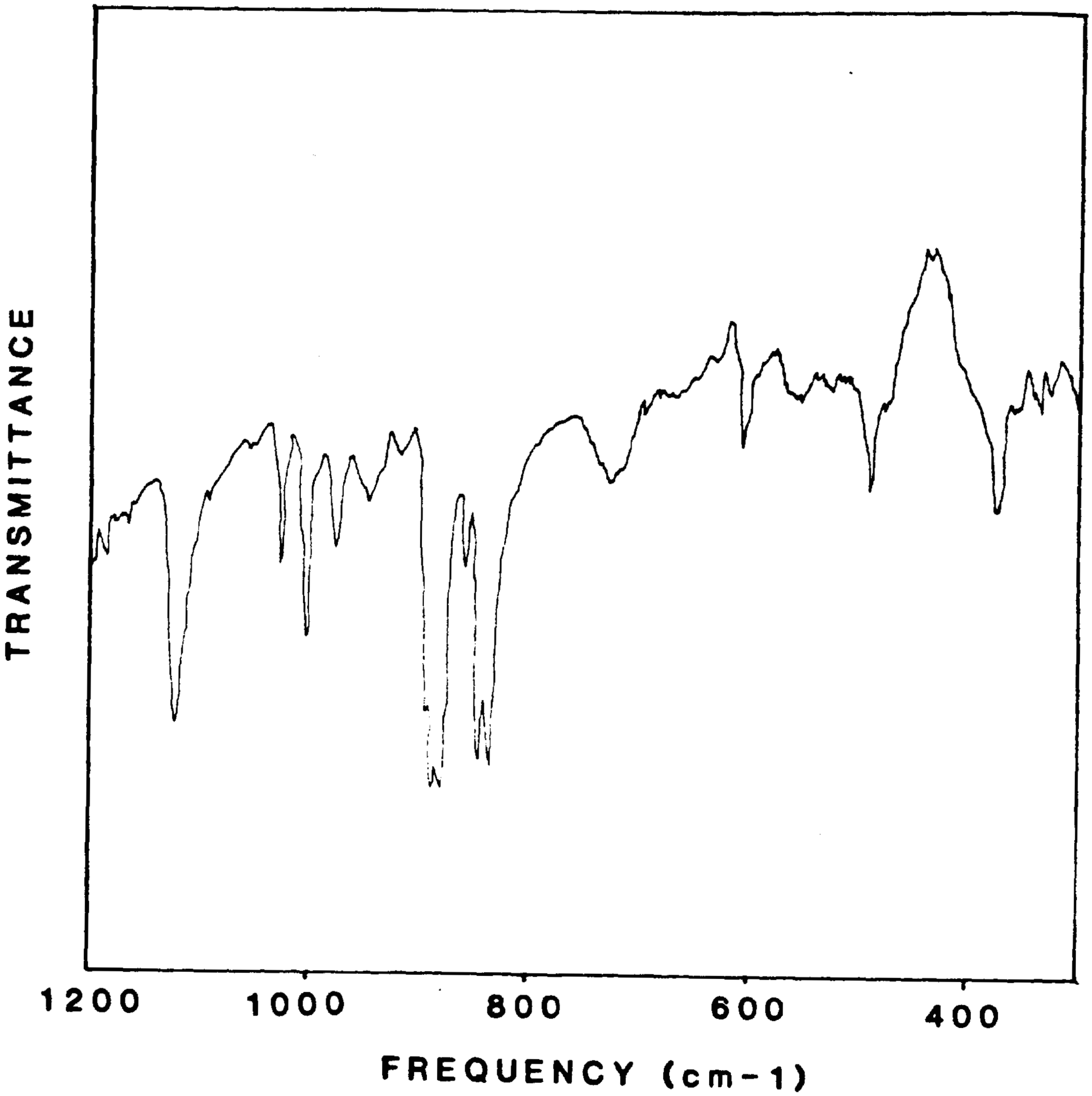

Figure I-28. Infrared spectrum of ^{18}O substituted complex F.

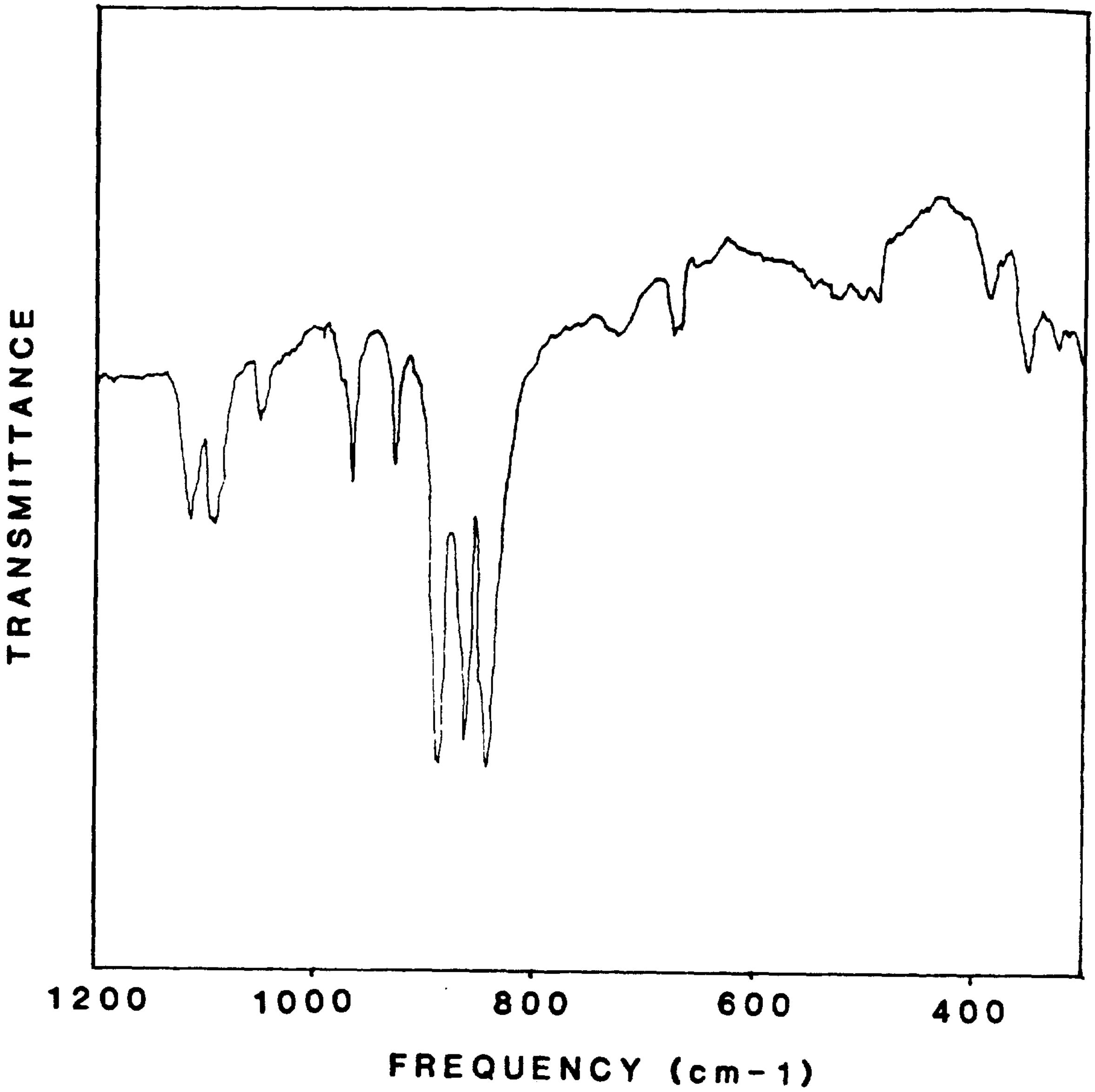

Figure I-29. Infrared spectrum of complex G.

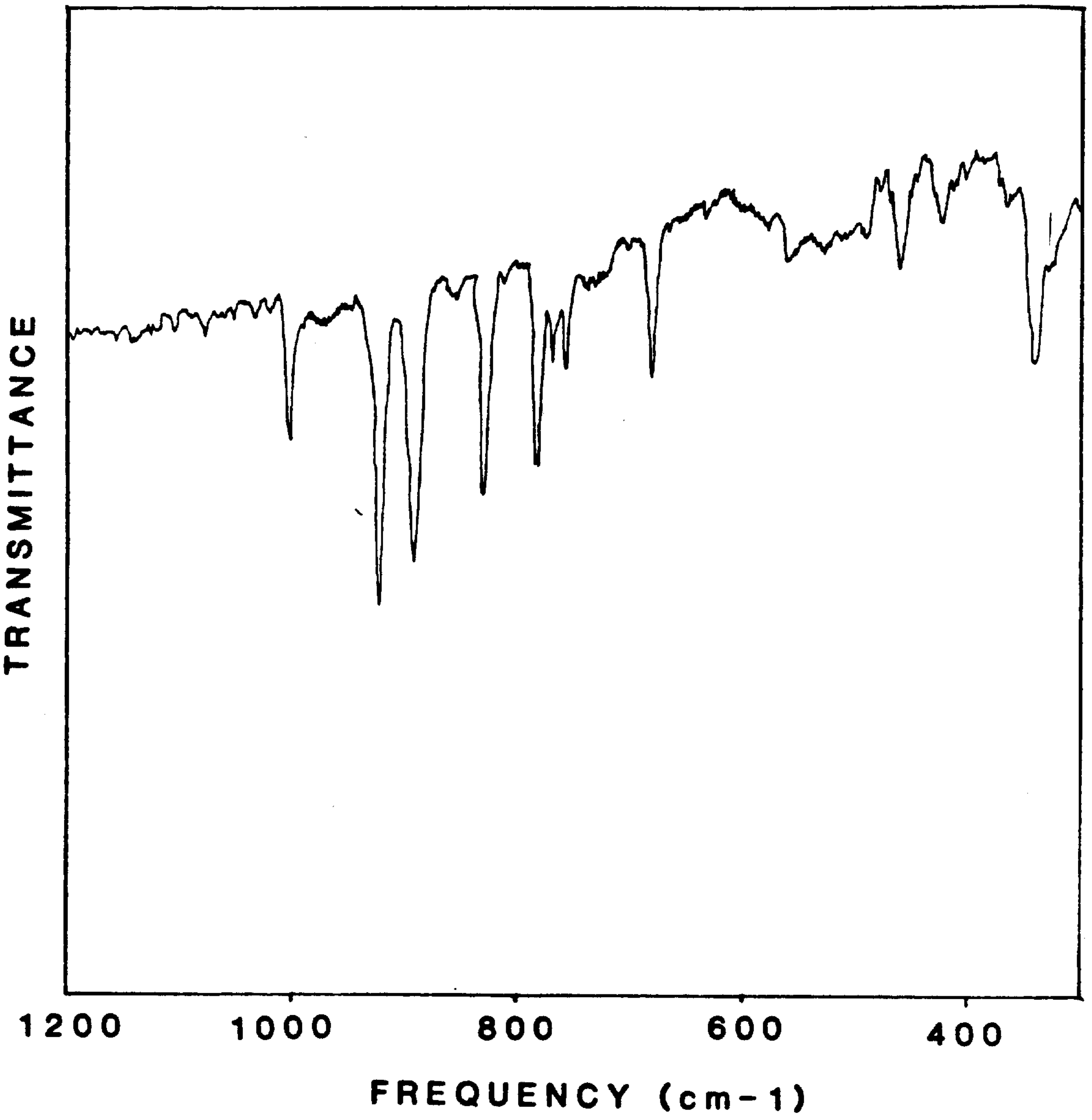

Figure I-30. Infrared spectrum of complex H.

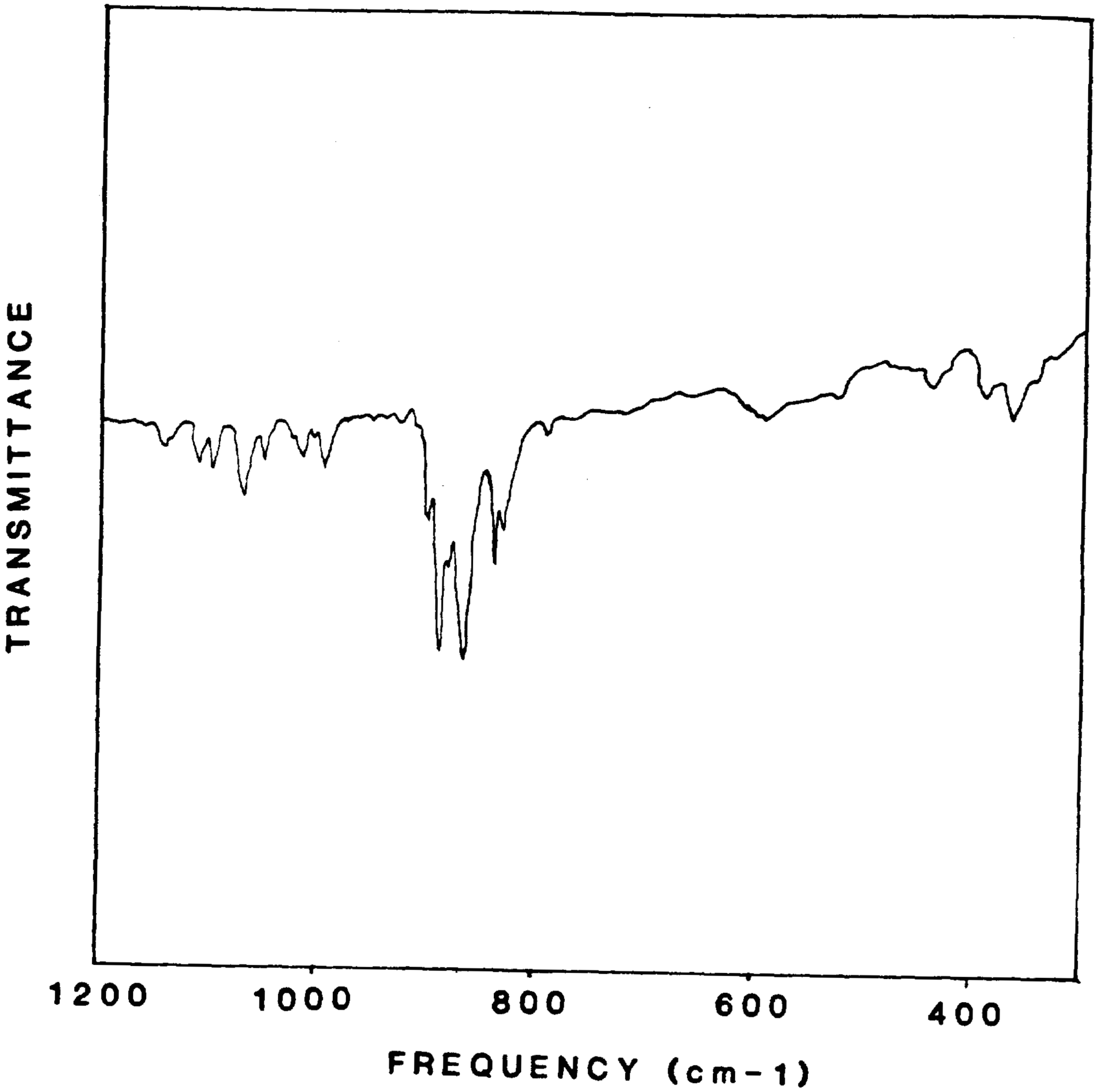

Figure I-31. Infrared spectrum of complex E.

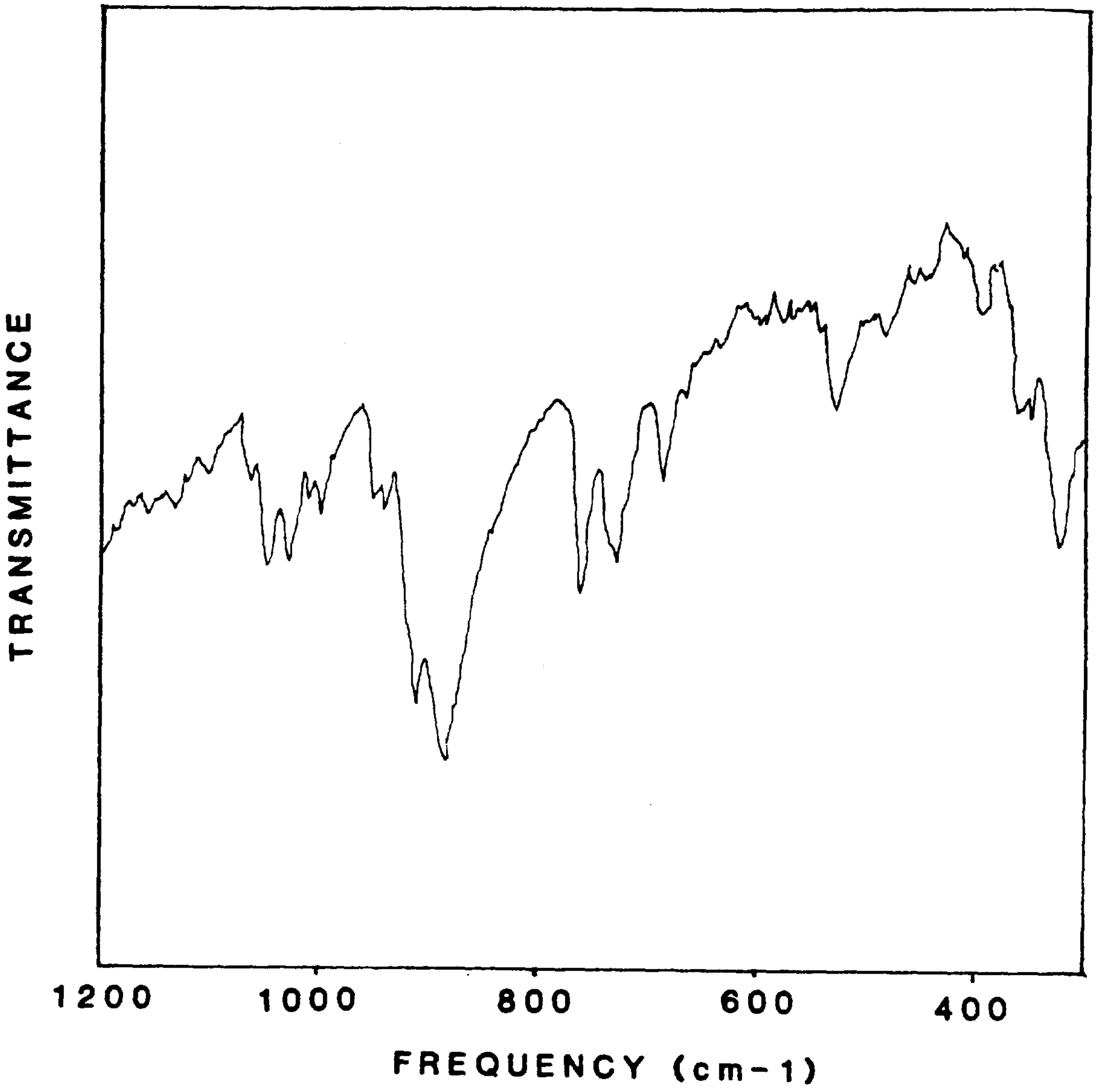

Figure I-32. Infrared spectrum of complex I.

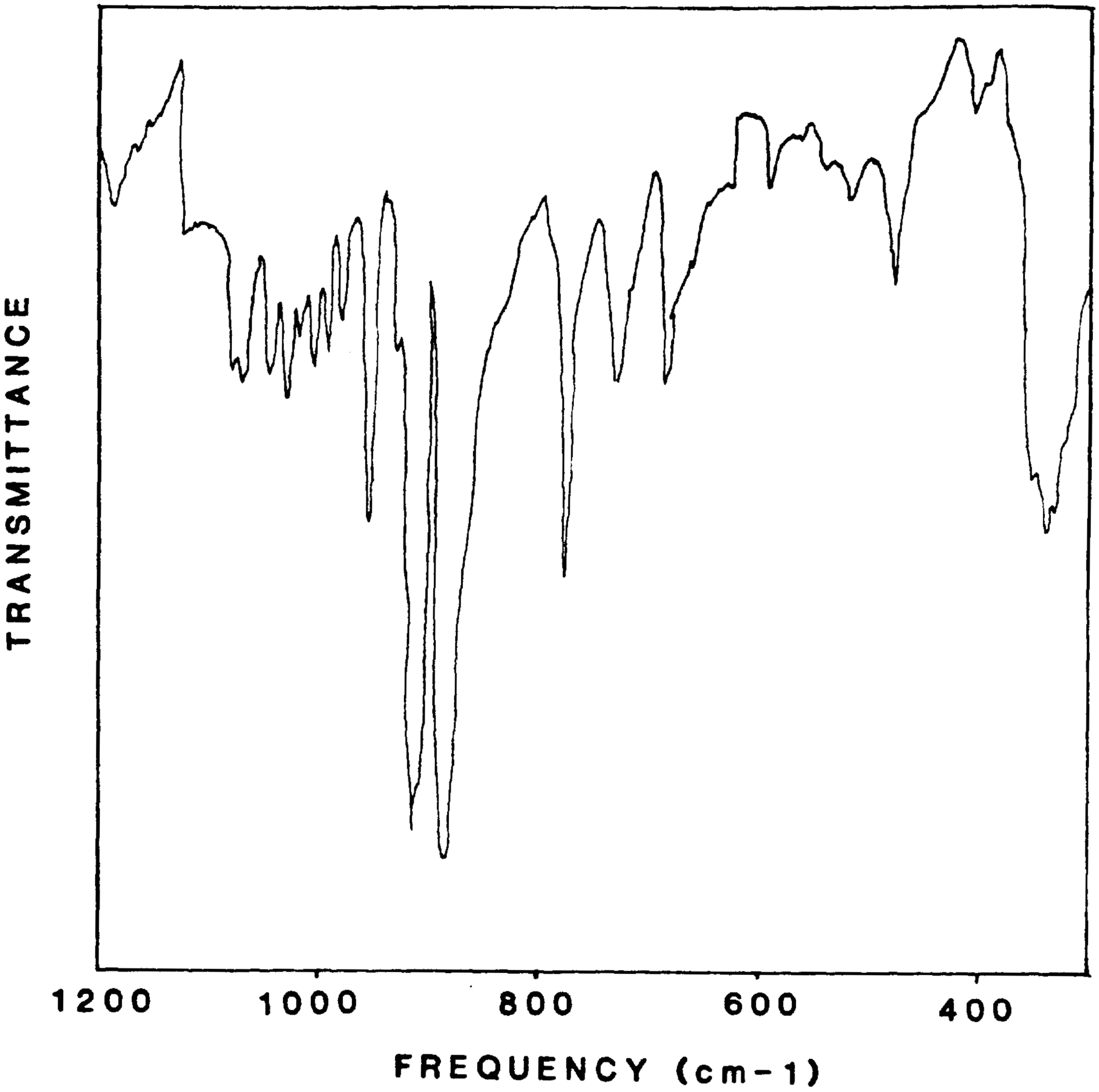

Figure I-33. Infrared spectrum of complex J.

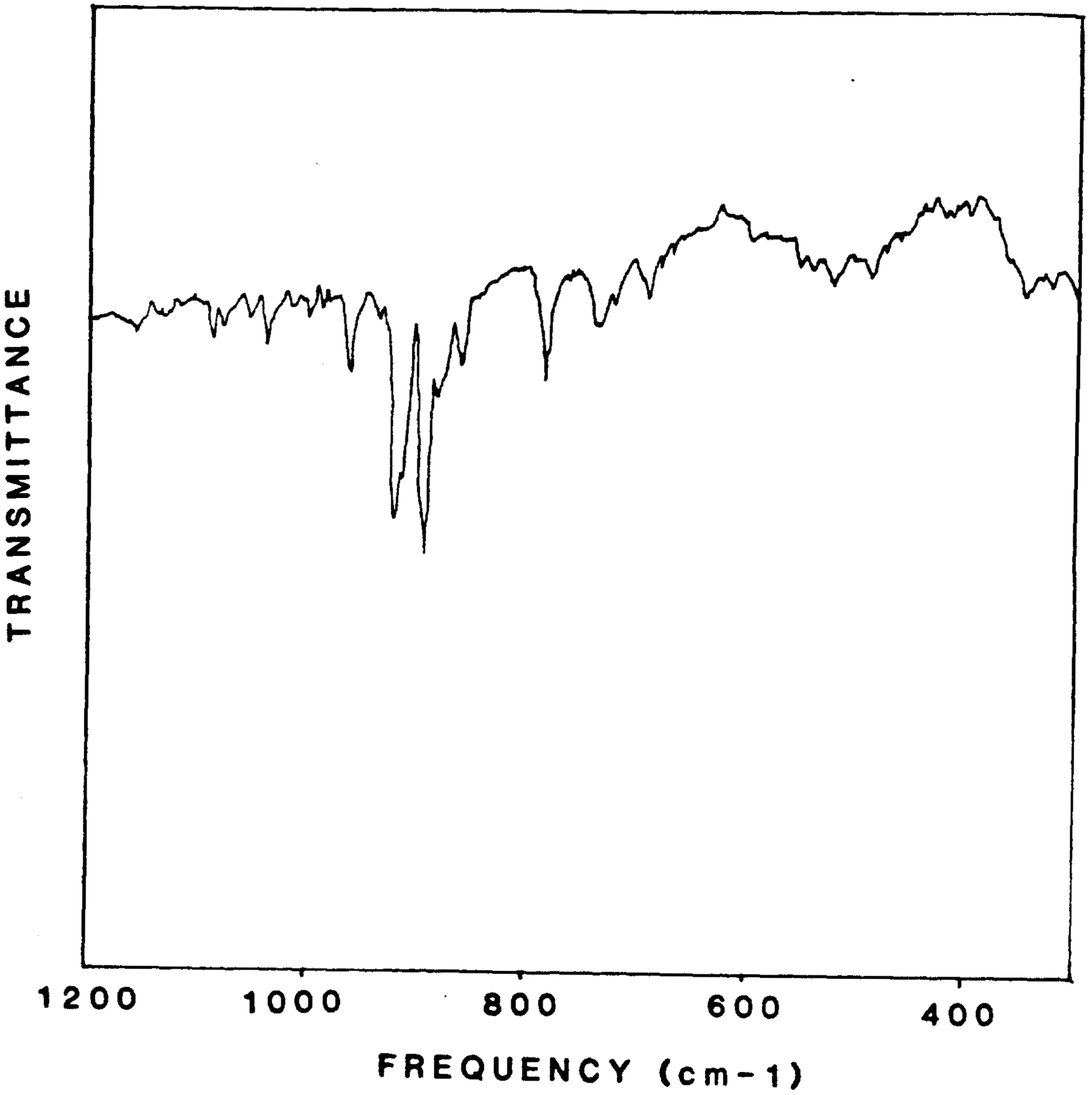

Figure I-34. Infrared spectrum of ^{17}O, ^{18}O substituted complex J.

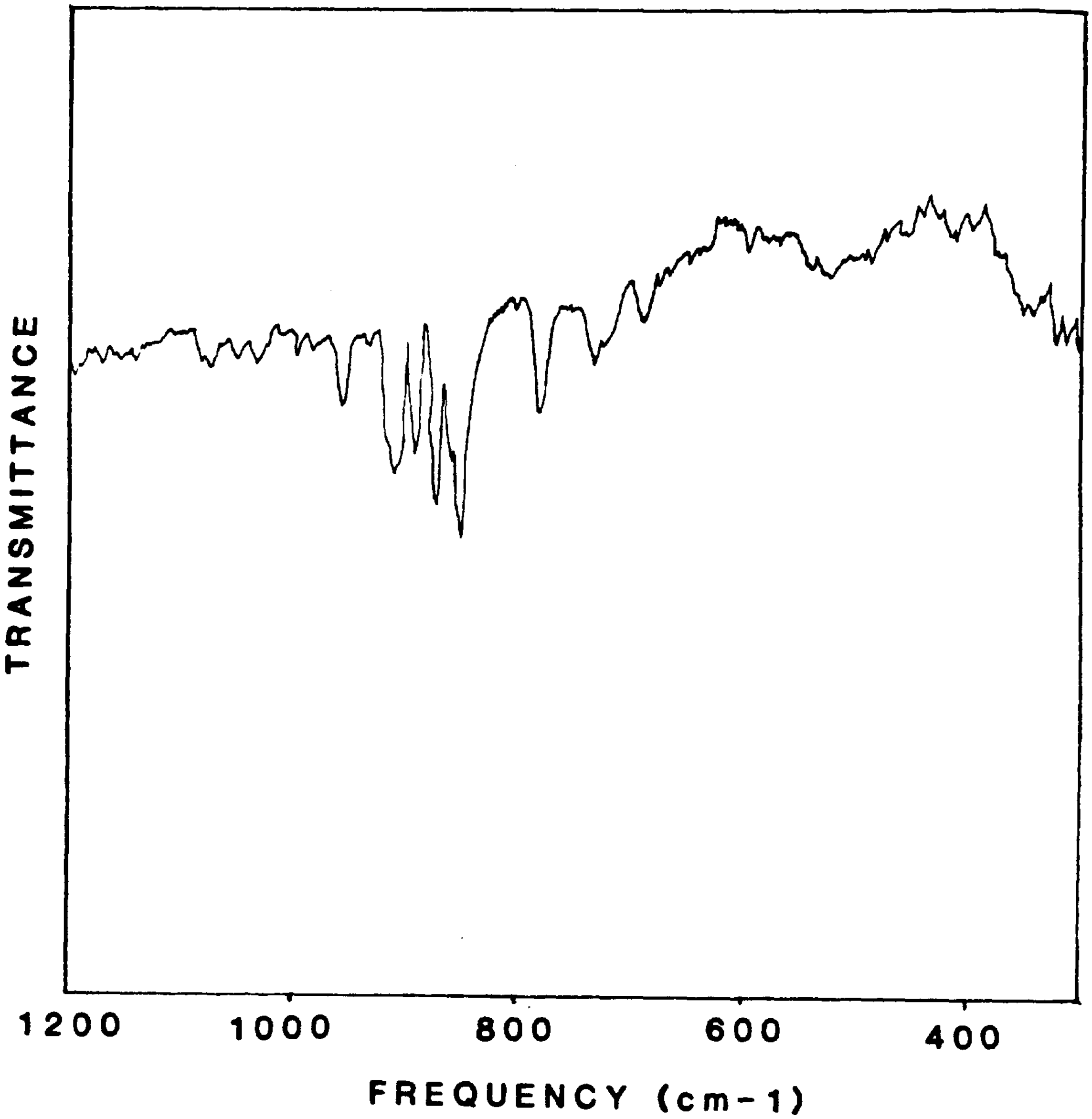

Figure I-35. Infrared spectrum of ^{18}O substituted complex J.

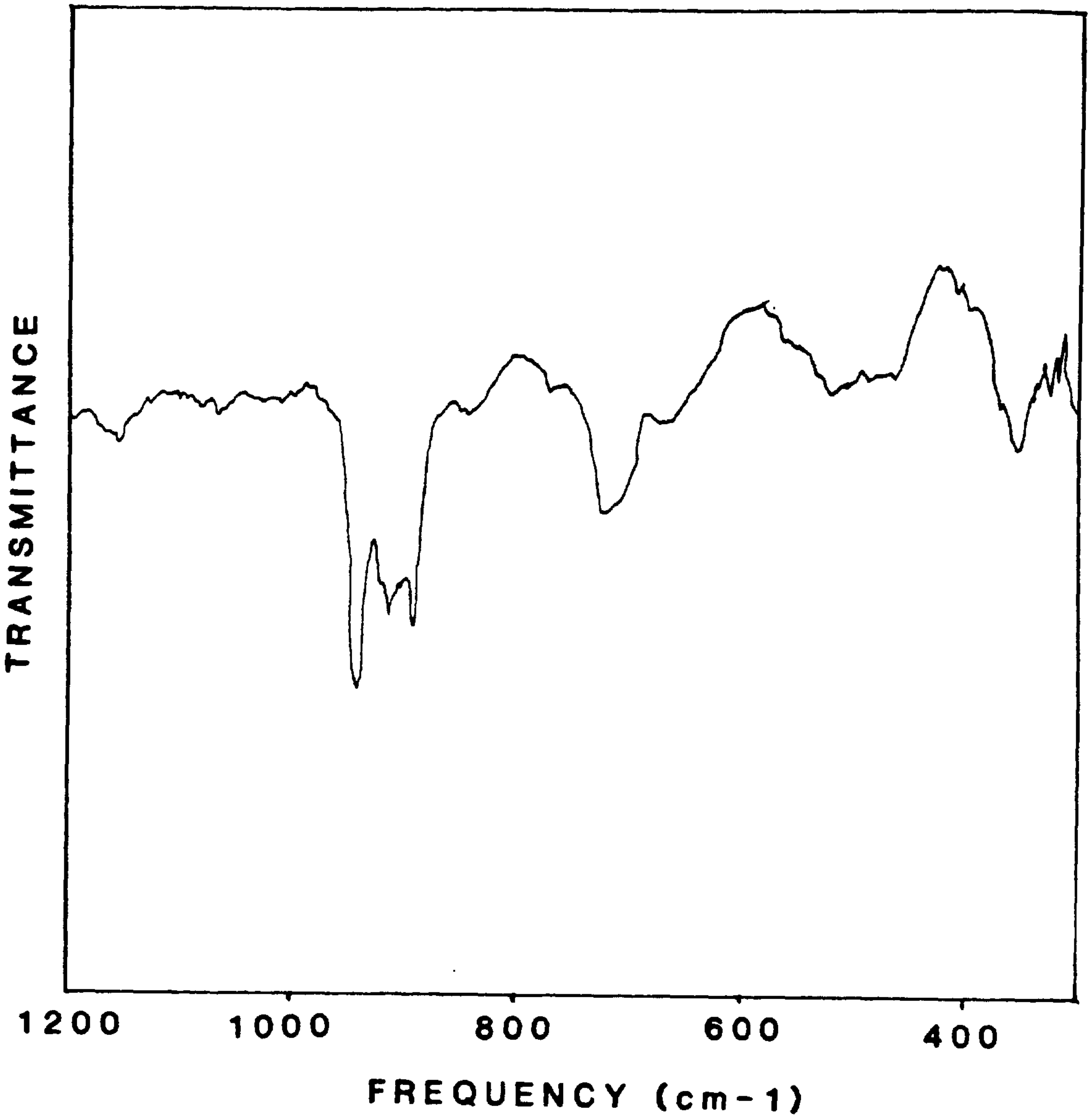

Figure I-36. Infrared spectrum of complex K.

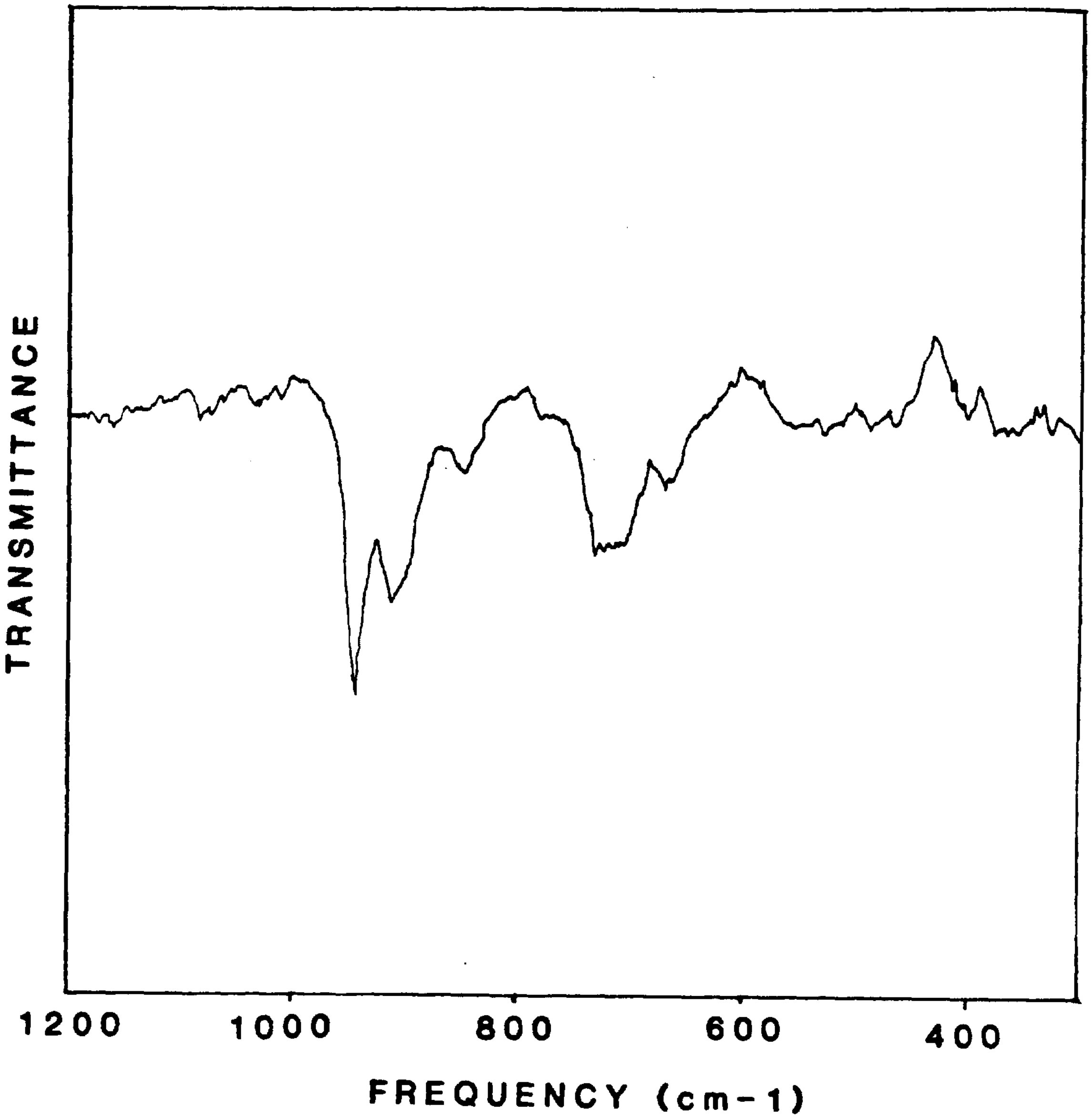

Figure I-37. Infrared spectrum of ^{18}O substituted complex K.

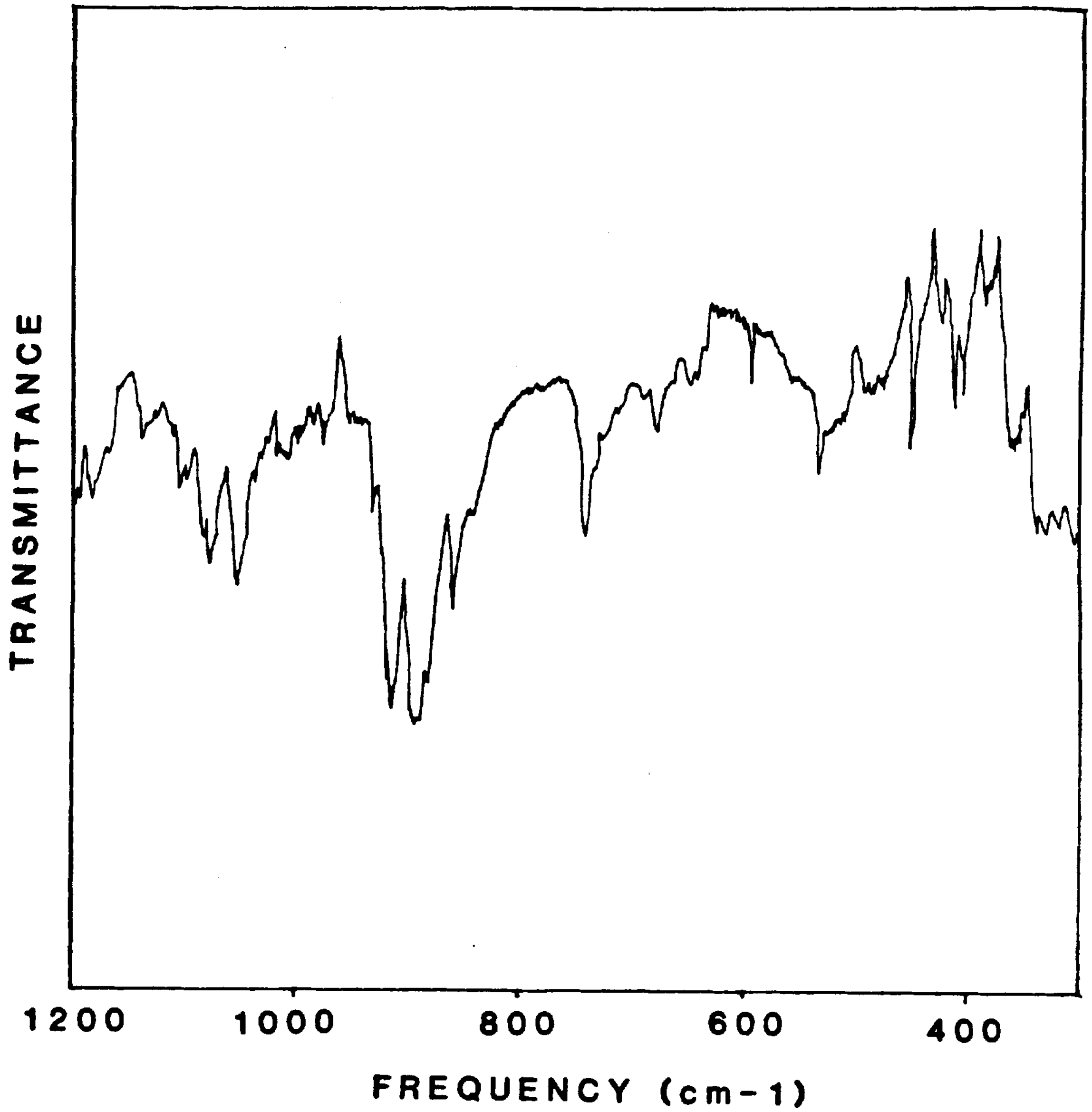

Figure I-38. Infrared spectrum of complex L.

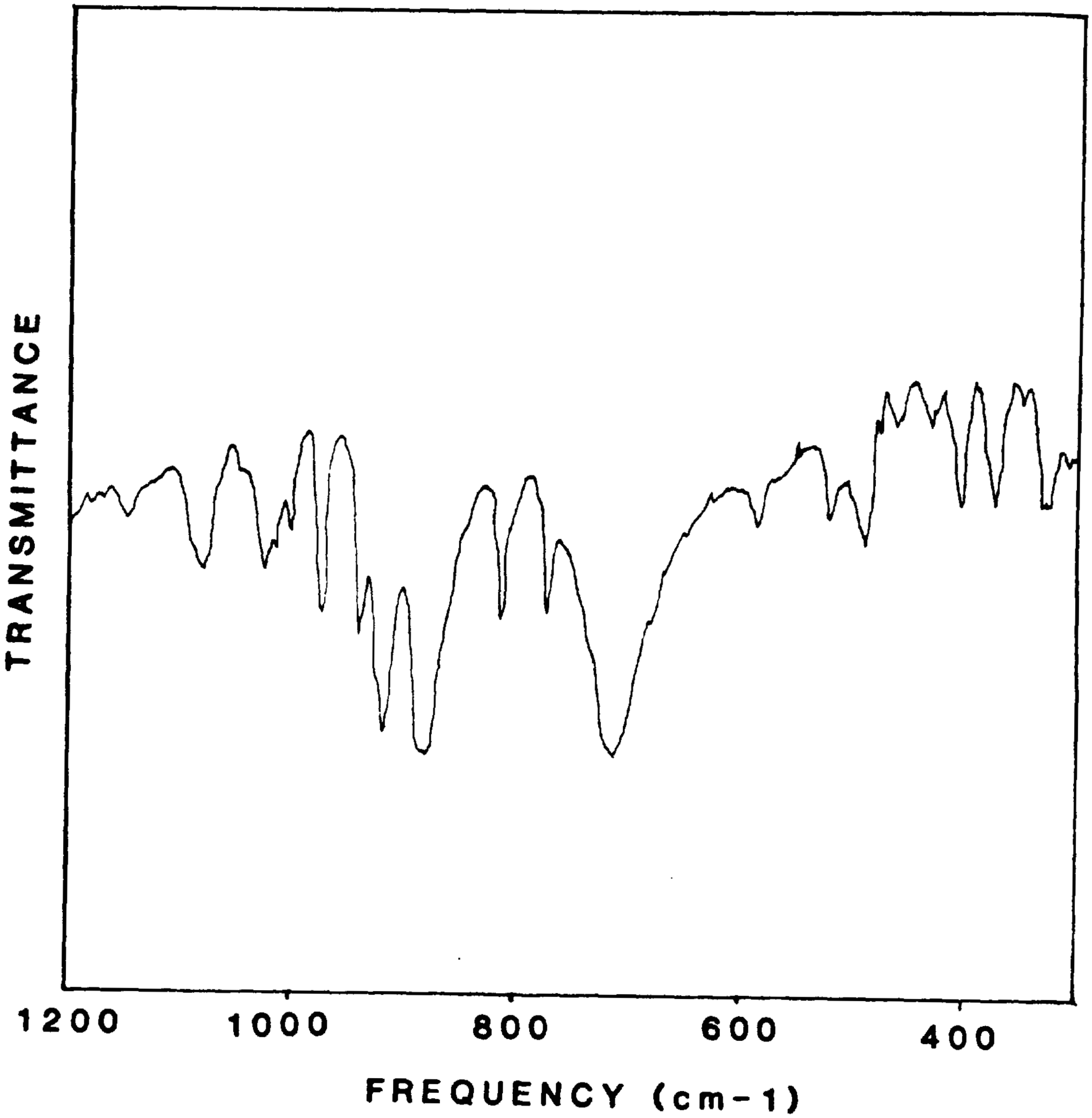

Figure I-39. Infrared spectrum of complex M.

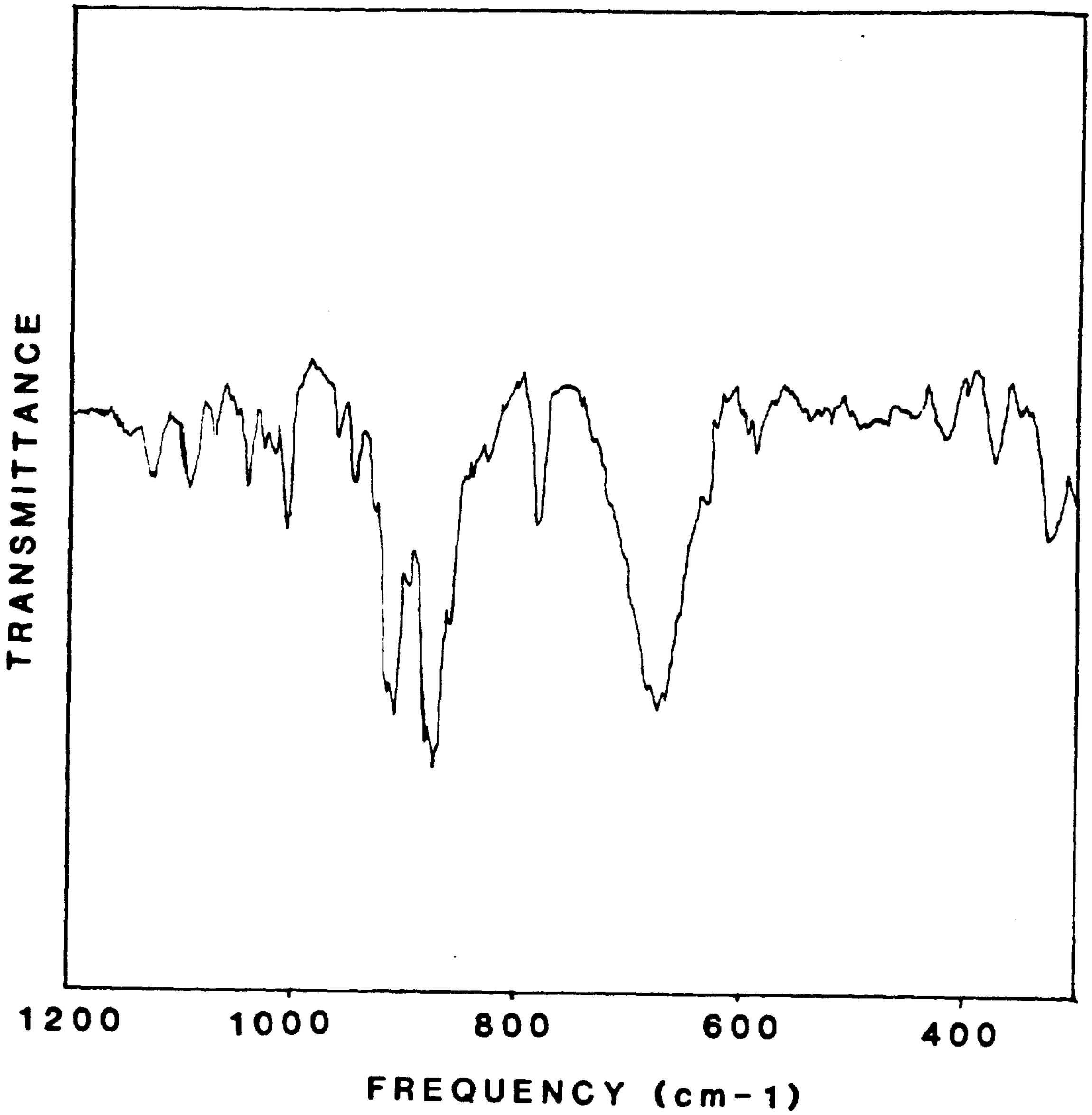

Figure I-40. Infrared spectrum of complex N.

APPENDIX II

SOLUTION RAMAN SPECTRA OF THE MOLYBDENUM COMPLEXES

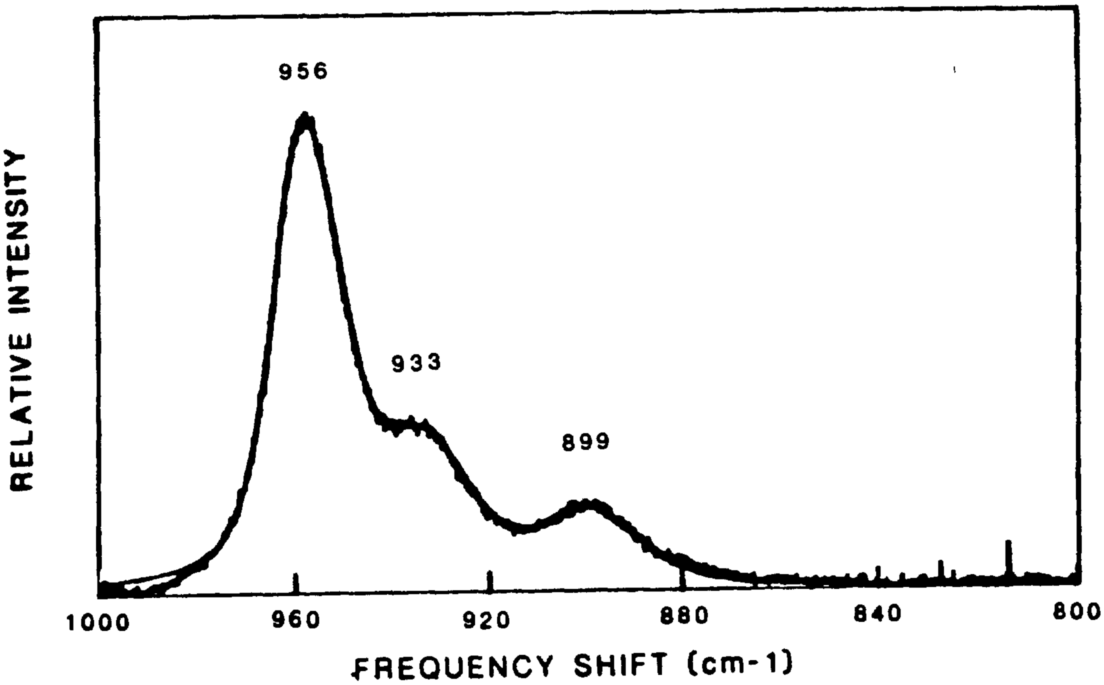

Figure II-1. Raman spectrum of dimethyl sulfoxide (DMSO) with curve fit analysis. Scan parameters: laser excitation, 457.9 nm; slitwidth, 10 cm^{-1}; scan rate, 0.25 cm^{-1}/sec; number of scans, 3; 90 degree scattering geometry; room temperature.

Peak Position	Relative Height	Width (cm^{-1})
899	188	23.6
933	344	21.5
956	1250	15.0

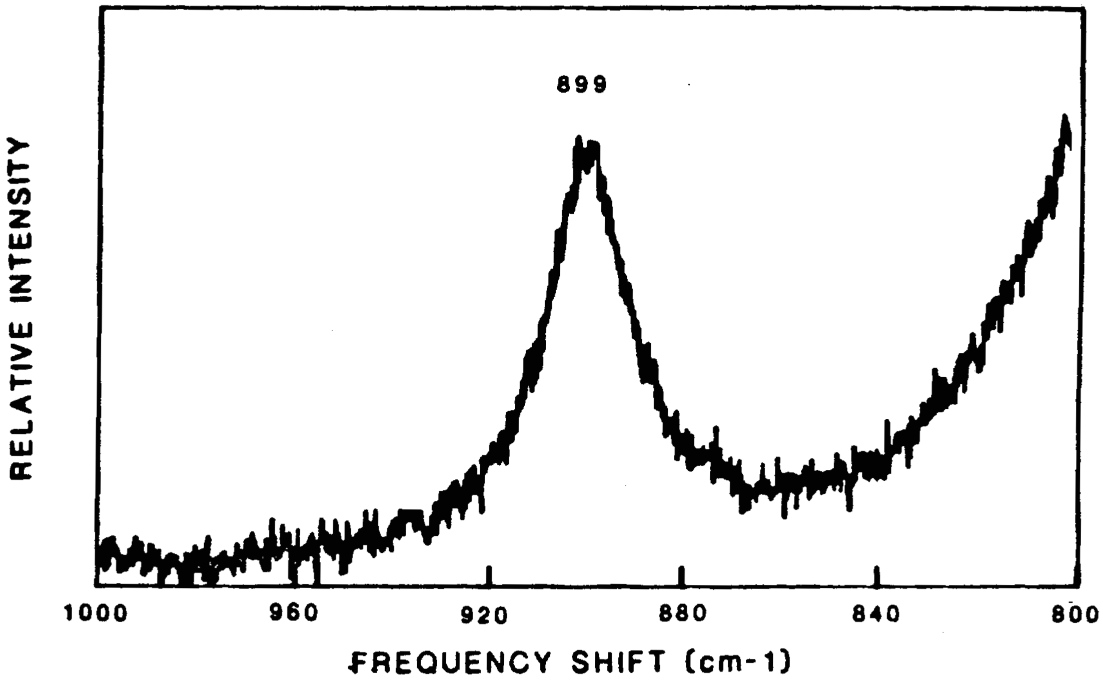

Figure II-2. Raman spectrum of CH_2Cl_2. Scan parameters: laser excitation, 457.9 nm; slitwidth, 10 cm^{-1}; scan rate, 0.25 cm^{-1}/sec; number of scans, 3; 90 degree scattering geometry; room temperature.

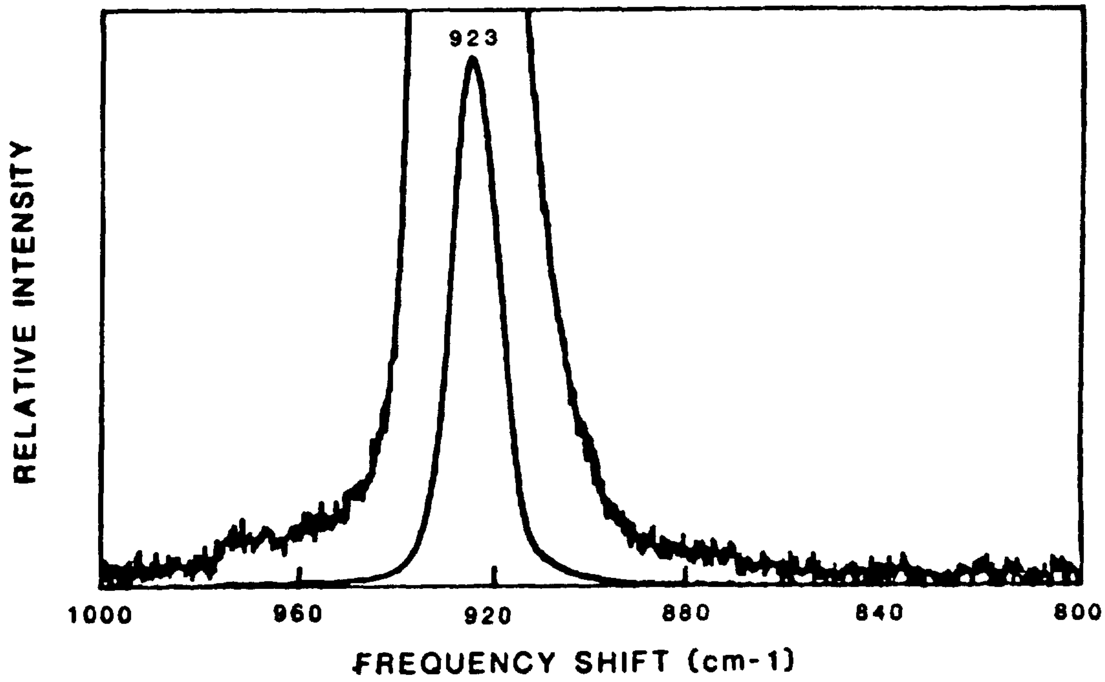

Figure II-3. Raman spectrum of CH_3CN. Scan parameters: laser excitation, 457.9 nm; slitwidth, 10 cm^{-1}; scan rate, 0.25 cm^{-1}/sec; number of scans, 3; 90 degree scattering geometry; room temperature. The upper trace is plotted at a factor of about 14 times the lower trace to display the lack of features on the low frequency shift side of the peak.

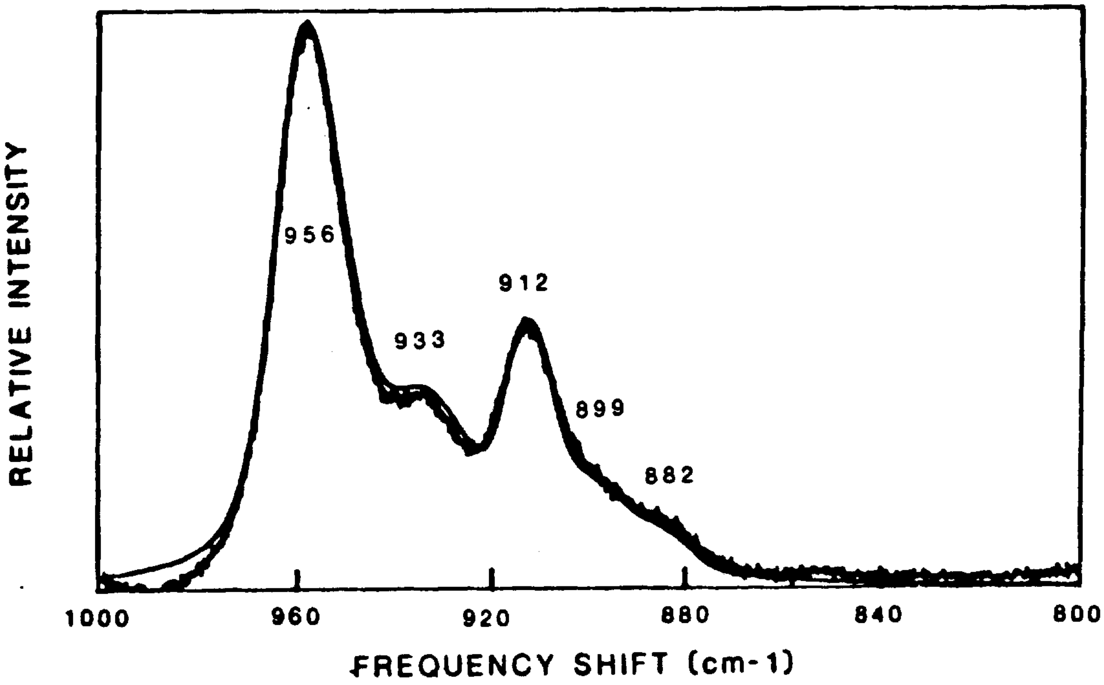

Figure II-4. Raman spectrum of complex A in DMSO with curve fitting analysis. The first three peaks of the list correspond to DMSO. Scan parameters: laser excitation, 457.9; slitwidth, 10 cm^{-1}; scan rate, 0.25 cm^{-1}/sec; number of scans, 3 ; 90 degree scattering geometry; room temperature.

Peak Position	Relative Height	Width (cm^{-1})
899	188	23.6
933	344	21.5
956	1250	15.0
912	565	7.5
882	60	6.5

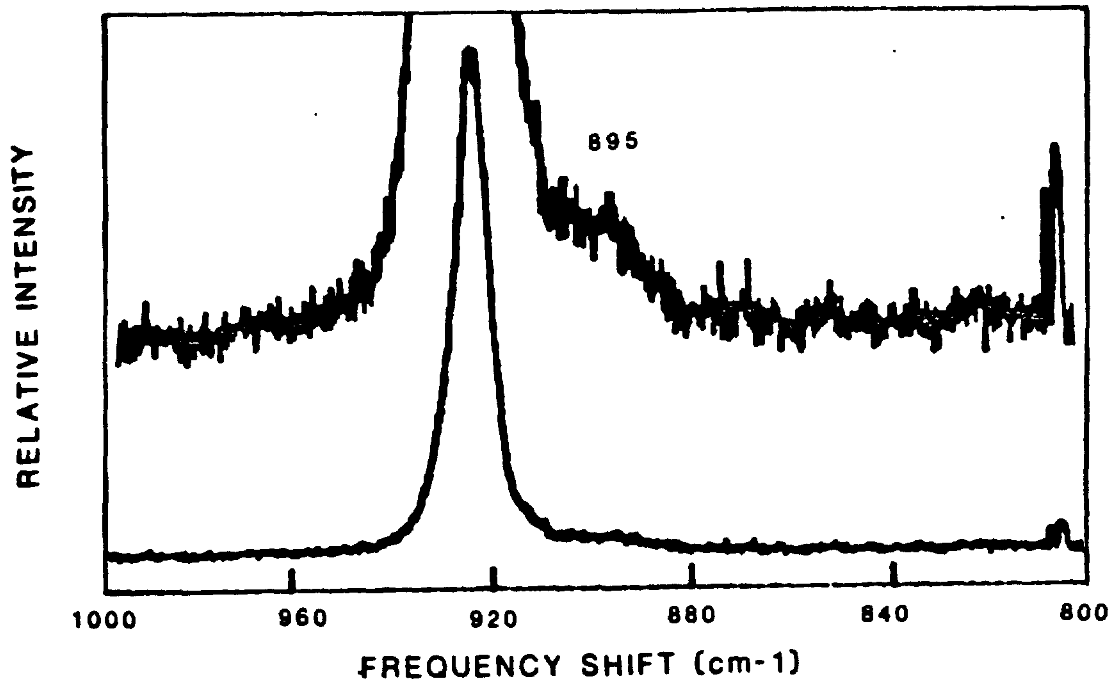

Figure II-5. Raman spectrum of complex B in CH_3CN. Scan parameters: laser excitation, 457.9 nm; slitwidth, 4 cm^{-1}; scan rate, 0.1 cm^{-1}/sec; number of scans, 2; 90 degree scattering geometry; room temperature. The upper trace is plotted at a factor of 7 times the lower trace.

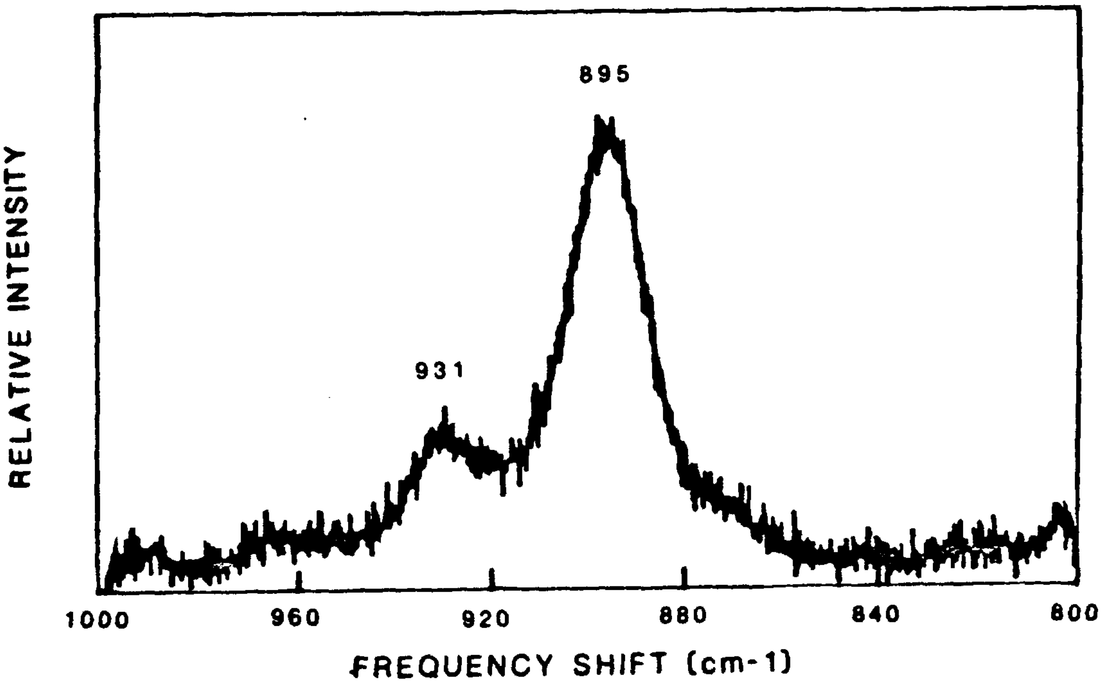

Figure II-6. Raman spectrum of complex B in CH_2Cl_2. Scan parameters: laser excitation, 457.9 nm; slitwidth, 10 cm^{-1}; scan rate, 0.25 cm^{-1}/sec; number of scans, 3; 90 degree scattering geometry; room temperature.

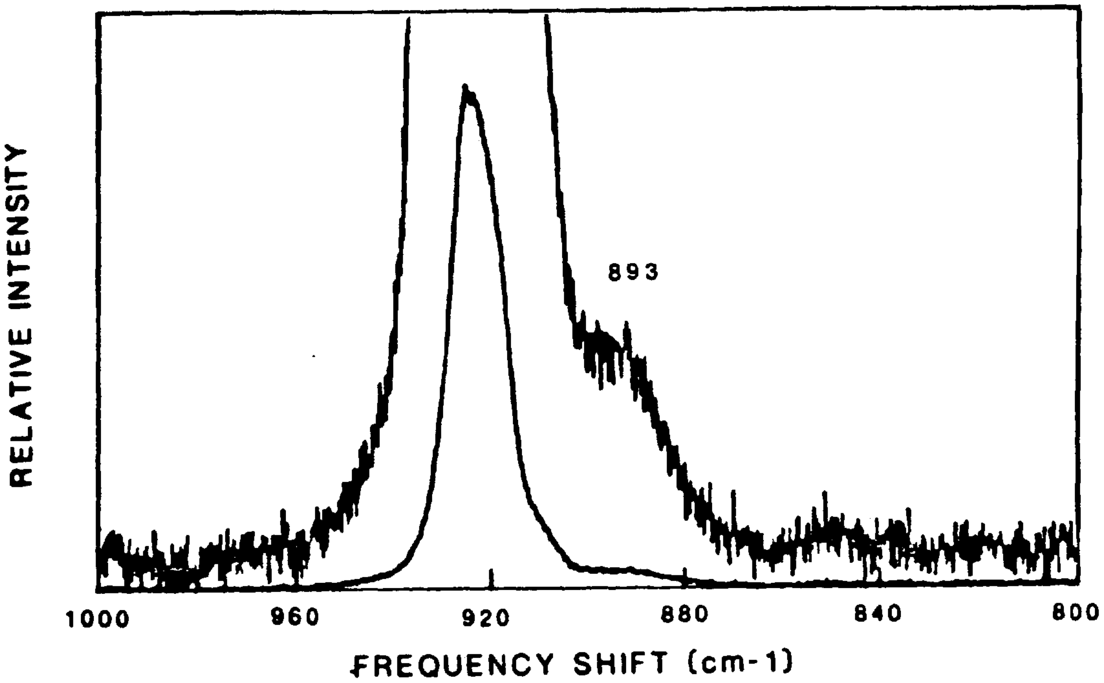

Figure II-7. Raman spectrum of complex C in CH_3CN. Scan parameters: laser excitation, 457.9 nm; slitwidth, 10 cm^{-1}; scan rate, 0.25 cm^{-1}/sec; number of scans, 3; 90 degree scattering geometry; room temperature. The upper trace is plotted at a factor of 12.5 times the lower trace.

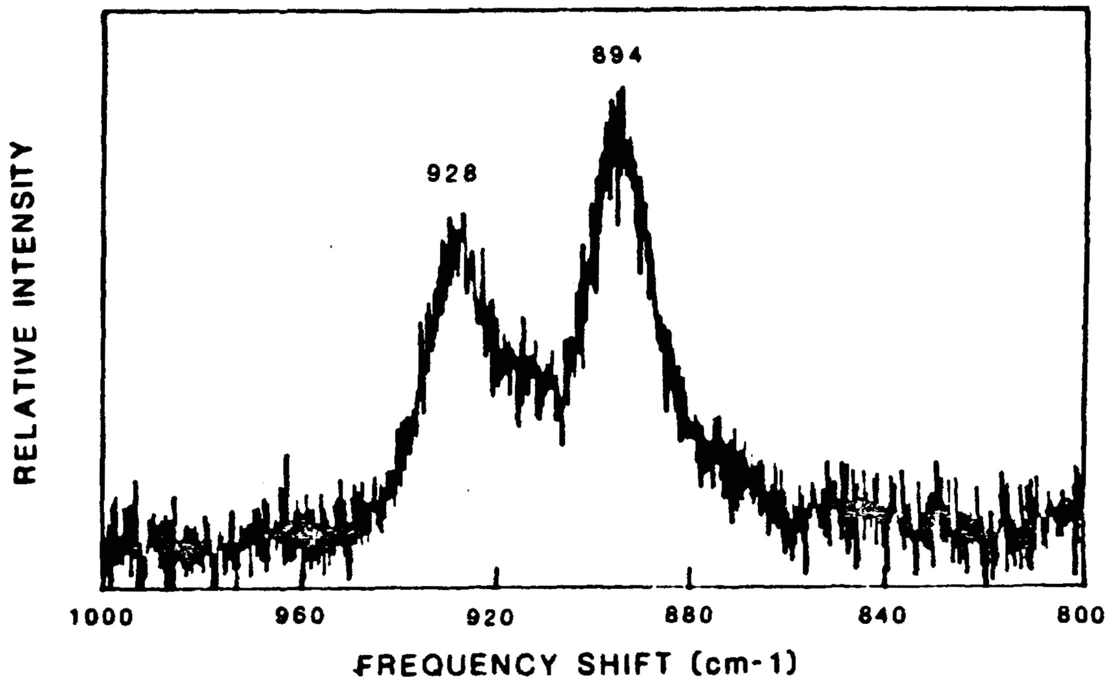

Figure II-8. Raman spectrum of complex C in CH_2Cl_2. Scan parameters: laser excitation, 457.9 nm; slitwidth, 10 cm^{-1}; scan rate, 2.5 cm^{-1}/sec; number of scans, 10; 90 degree scattering geometry; room temperature.

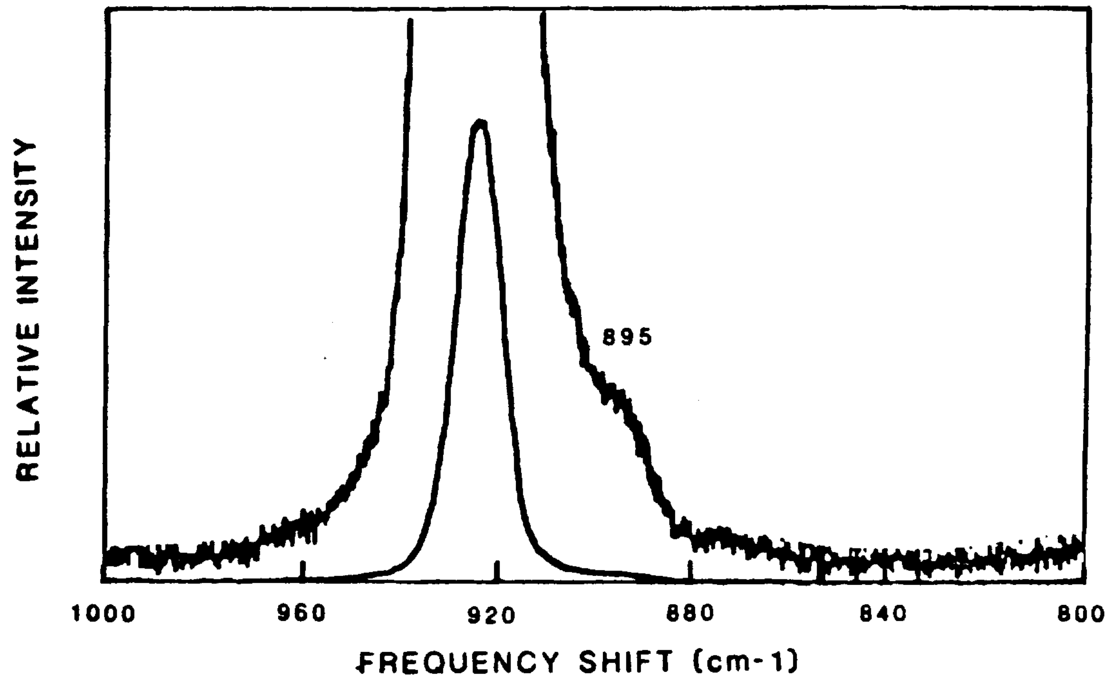

Figure II-9. Raman spectrum of complex D in CH_3CN. Scan parameters: laser excitation, 457.9 nm; slitwidth, 10 cm^{-1}; scan rate, 0.25 cm^{-1}/sec; number of scans, 3; 90 degree scattering geometry; room temperature. The upper trace is plotted at a factor of 20 times the lower trace.

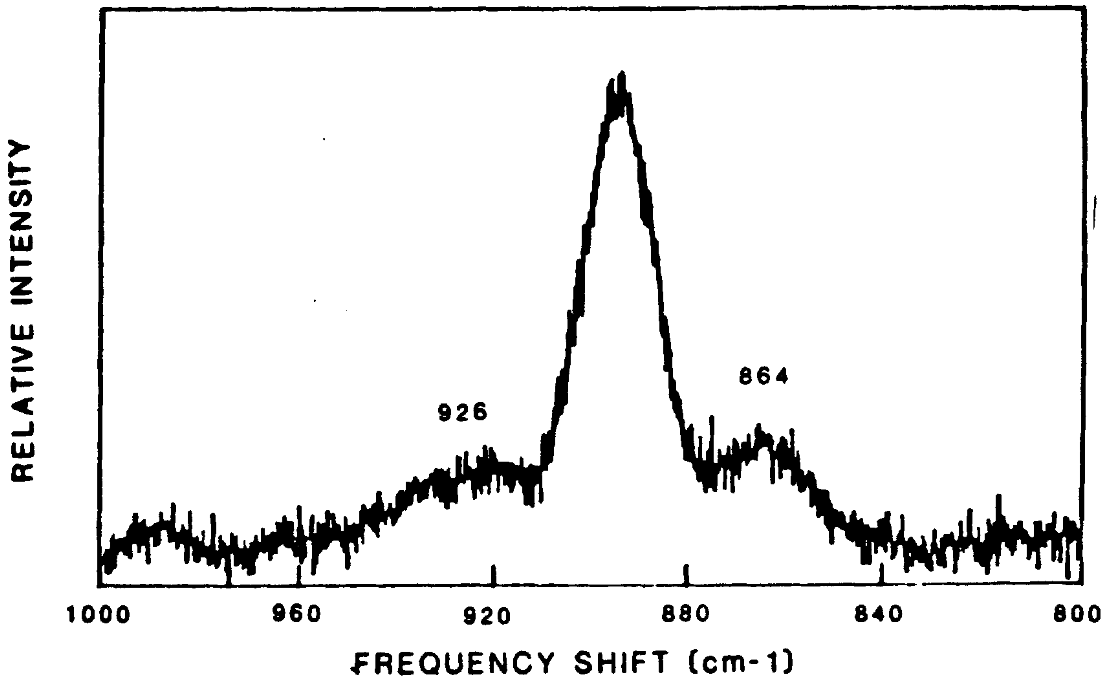

Figure II-10. Raman spectrum of complex D in CH_2Cl_2. Scan parameters: laser excitation, 457.9 nm; slitwidth, 10 cm^{-1}; scan rate, 0.25 cm^{-1}/sec; number of scans, 3; 90 degree scattering geometry; room temperature.

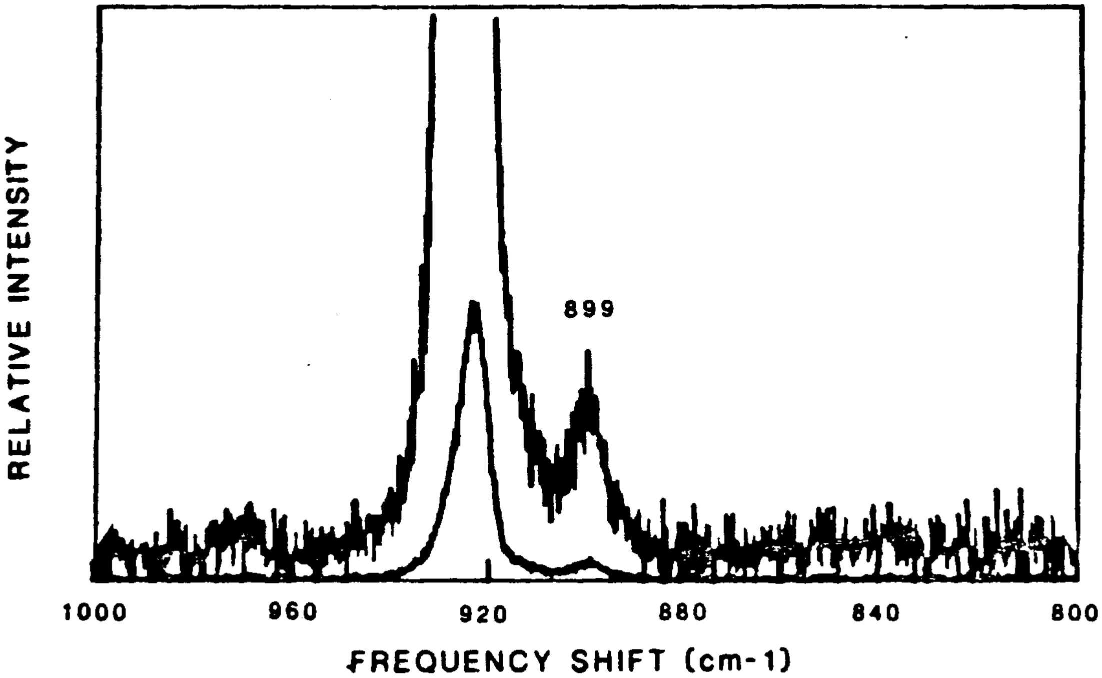

Figure II-11. Raman spectrum of complex F in CH_3CN. Scan parameters: laser excitation, 457.9 nm; slitwidth, 4 cm^{-1}; scan rate, 0.1 cm^{-1}/sec; number of scans, 1; 90 degree scattering geometry; room temperature. The upper trace is plotted at a factor of 10 times the lower trace.

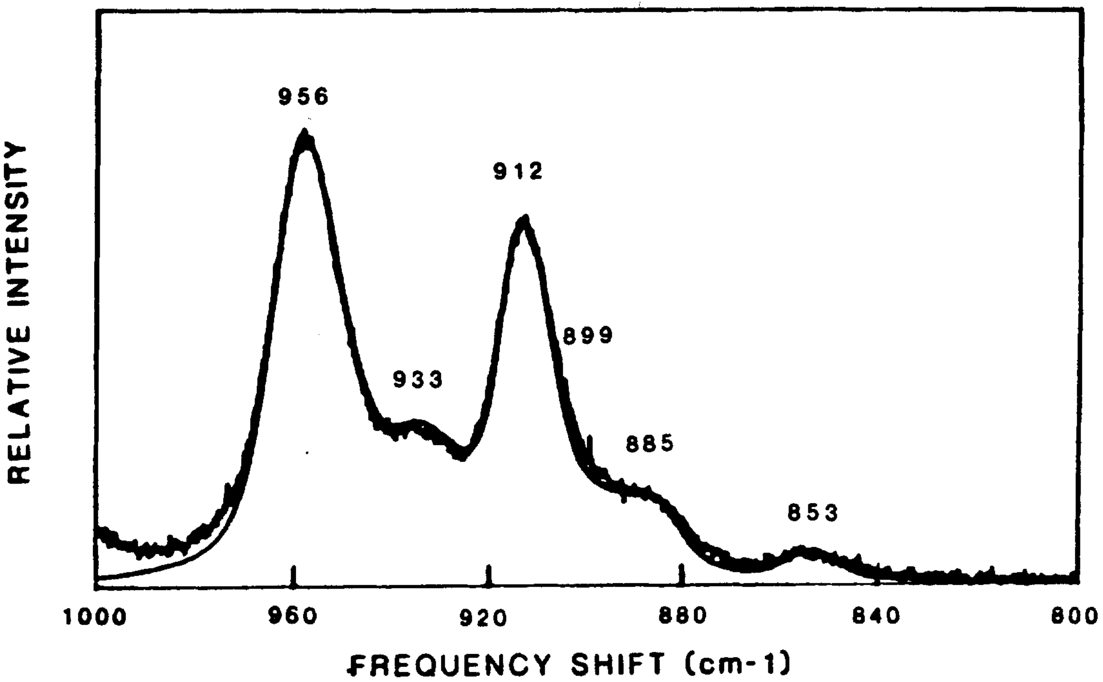

Figure II-12. Raman spectrum of complex G in DMSO with curve fitting analysis. The first three peaks of the list correspond to DMSO. Scan parameters: laser excitation, 457.9 nm; slitwidth, 10 cm^{-1}; scan rate, 0.25 cm^{-1}/sec; number of scans, 3; 90 degree scattering geometry; room temperature.

Peak Position	Relative Height	Width (cm^{-1})
899	188	23.6
933	344	21.5
956	1250	15.0
912	1040	9.0
885	157	9.0
853	92	9.0

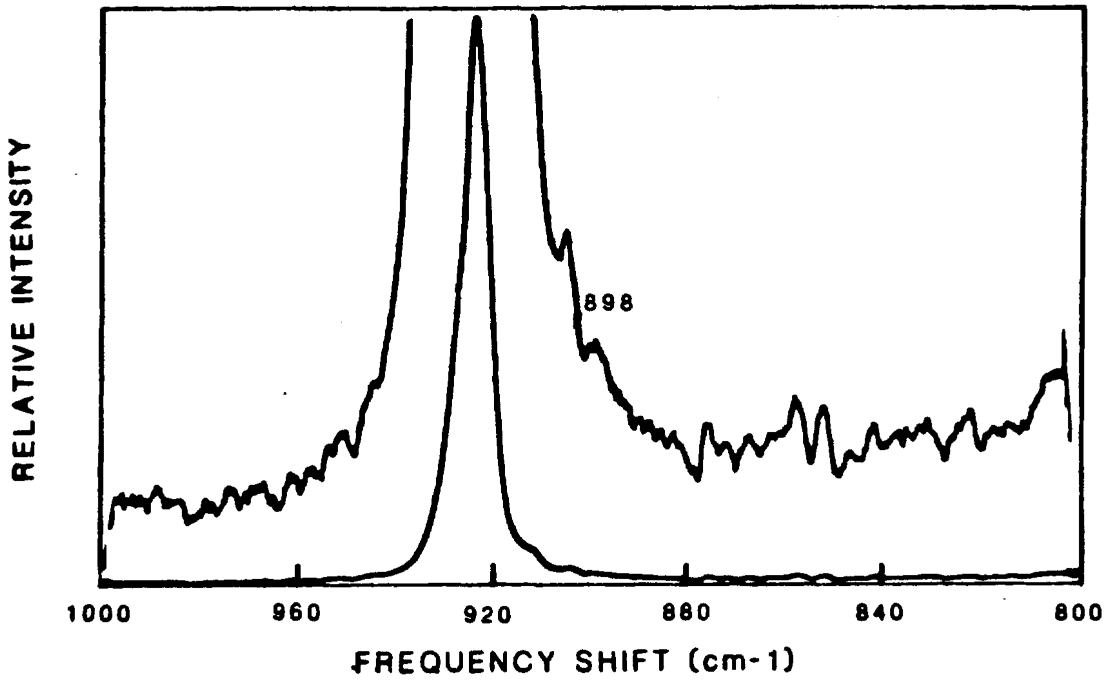

Figure II-13. Raman spectrum of complex H in CH_3CN. Scan parameters: laser excitation, 457.9 nm; slitwidth, 3 cm^{-1}; scan rate, 0.1 cm^{-1}/sec; number of scans, 3; 90 degree scattering geometry; room temperature. The data have been subjected to a 25 point smoothing routine. The upper trace is plotted at a factor of 20 times the lower trace.

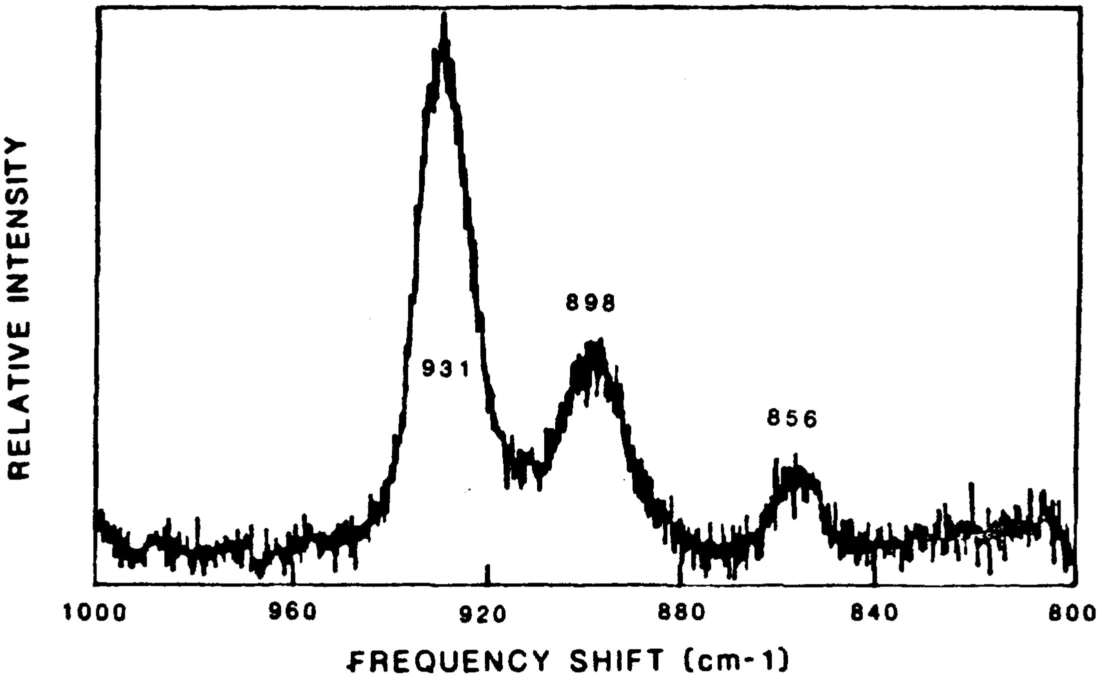

Figure II-14. Raman spectrum of complex H in CH_2Cl_2. Scan parameters: laser excitation, 457.9 nm; slitwidth, 10 cm^{-1}; scan rate, 0.25 cm^{-1}/sec; number of scans, 3; 90 degree scattering geometry; room temperature.

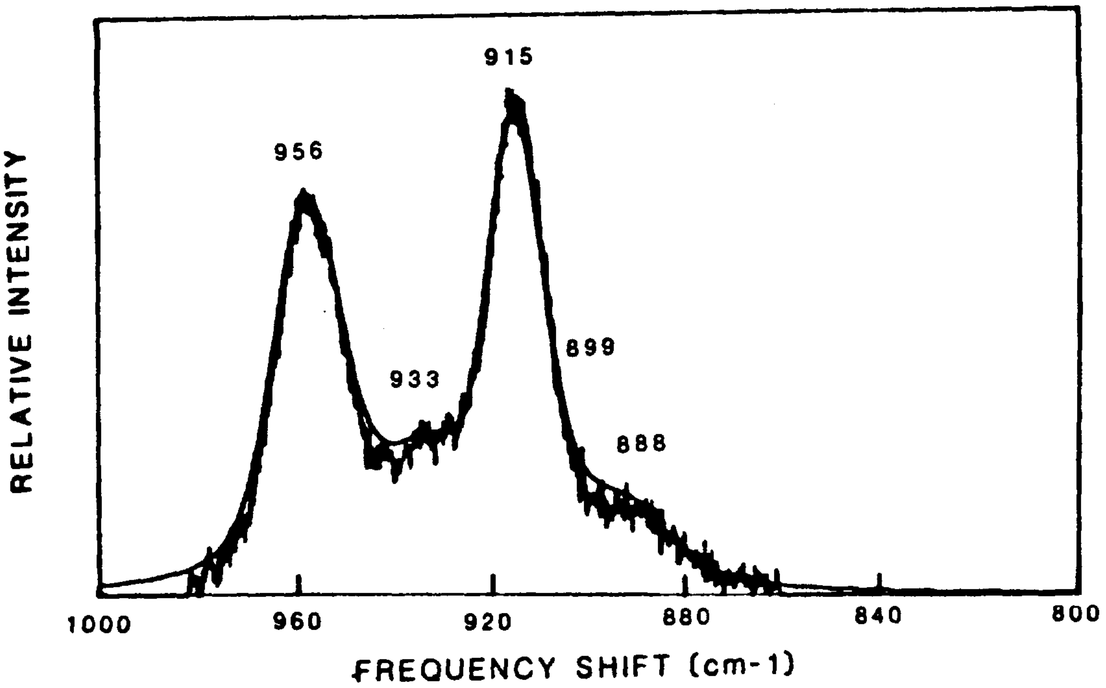

Figure II-15. Raman spectrum of complex E in DMSO with curve fitting analysis. The first three peaks of the list correspond to DMSO. Scan parameters: laser excitation, 457.9 nm; slitwidth, 10 cm^{-1}; scan rate, 0.25 cm^{-1}/sec; number of scans, 3; 90 degree scattering geometry; room temperature.

Peak Position	Relative Height	Width (cm^{-1})
899	188	23.6
934	344	21.5
957	1250	15.0
915	1535	11.0
888	120	13.0

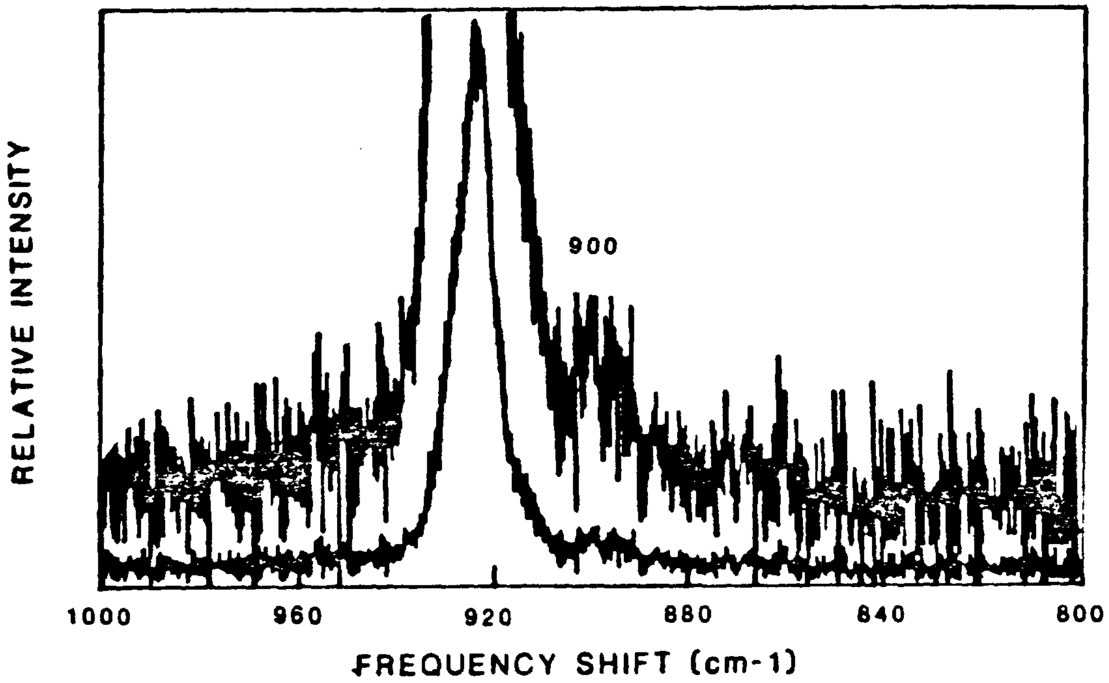

Figure II-16. Raman spectrum of complex I in CH_3CN. Scan parameters: laser excitation, 457.9 nm; slitwidth, 3 cm^{-1}; scan rate, 0.1 cm^{-1}/sec; number of scans, 2; 90 degree scattering geometry; room temperature. The upper trace is plotted at a factor of 5 times the lower trace.

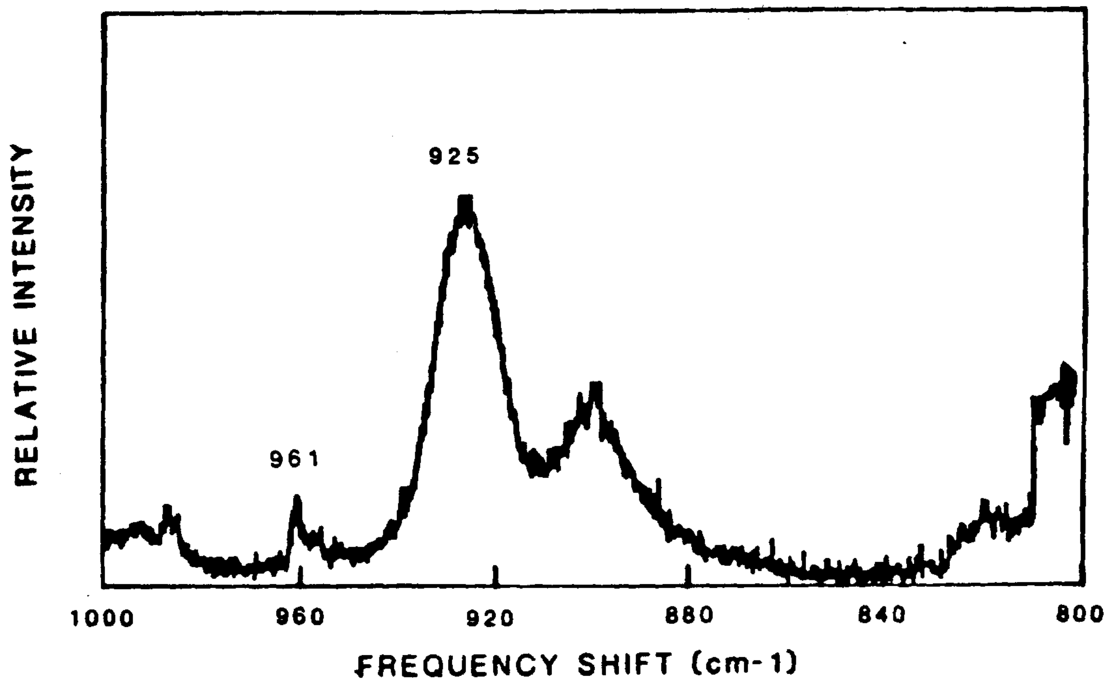

Figure II-17. Raman spectrum of complex I in CH_2Cl_2. Scan parameters: laser excitation, 457.9 nm; slitwidth, 10 cm^{-1}; scan rate, 0.1 cm^{-1}/sec; number of scans, 1; 90 degree scattering geometry; room temperature.

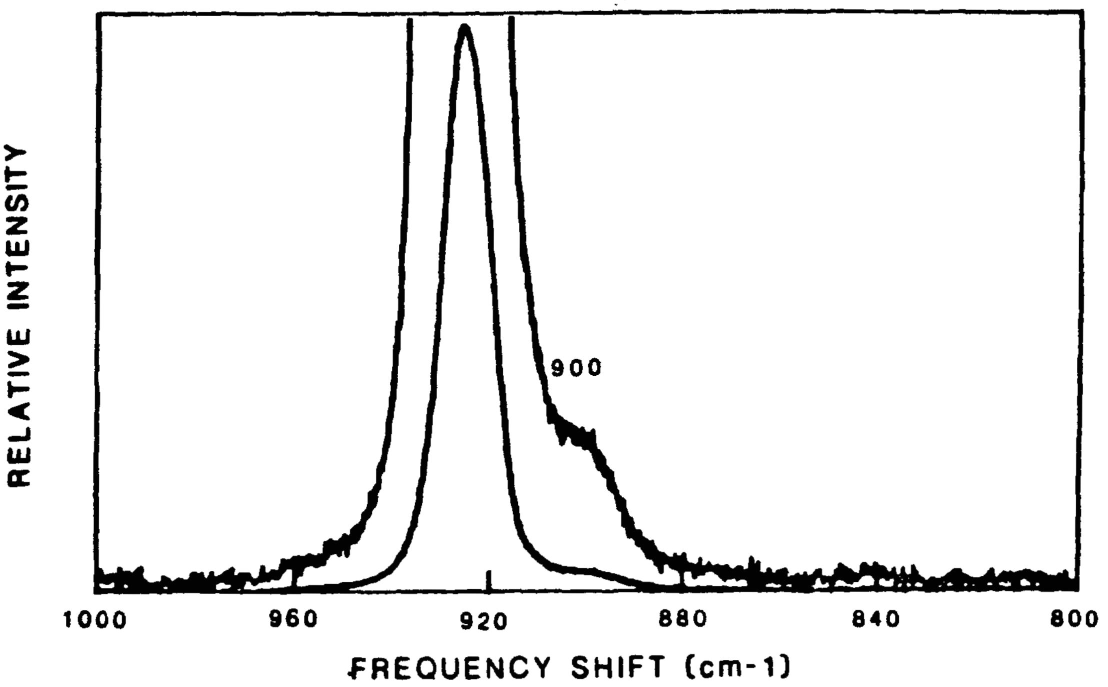

Figure II-18. Raman spectrum of complex J in CH_3CN. Scan parameters: laser excitation, 457.9 nm; slitwidth, 10 cm^{-1}; scan rate, 0.1 cm^{-1}/sec; number of scans, 1; 90 degree scattering geometry; room temperature. The upper trace is plotted at a factor of 7.3 times the lower trace.

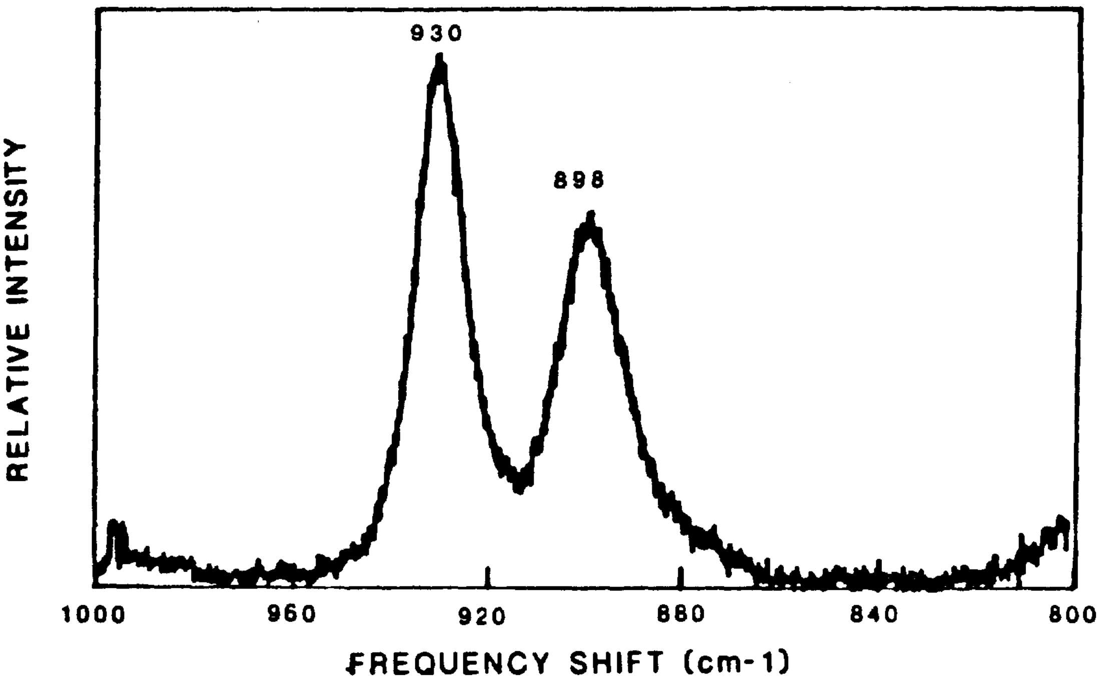

Figure II-19. Raman spectrum of complex J in CH_2Cl_2. Scan parameters: laser excitation, 457.9 nm; slitwidth, 10 cm^{-1}; scan rate, 0.1 cm^{-1}/sec; number of scans, 1; 90 degree scattering geometry; room temperature.

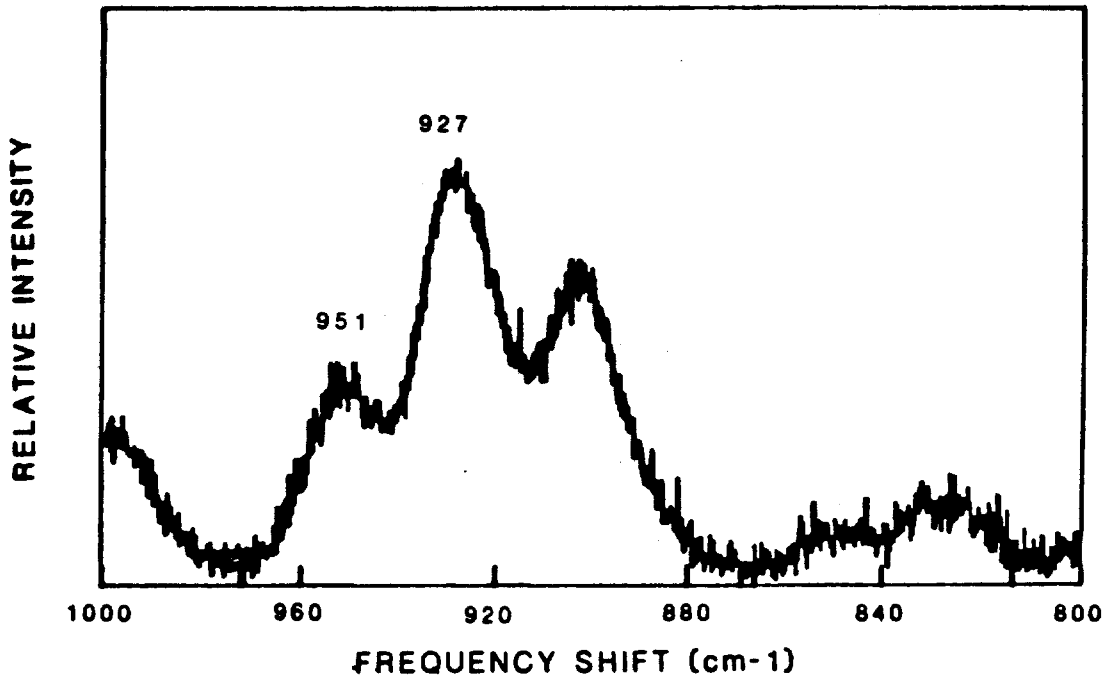

Figure II-20. Raman spectrum of complex K in CH_2Cl_2. Scan parameters: laser excitation, 457.9 nm; slitwidth, 10 cm^{-1}; scan rate, 0.1 cm^{-1}/sec; number of scans, 1; 90 degree scattering geometry; room temperature.

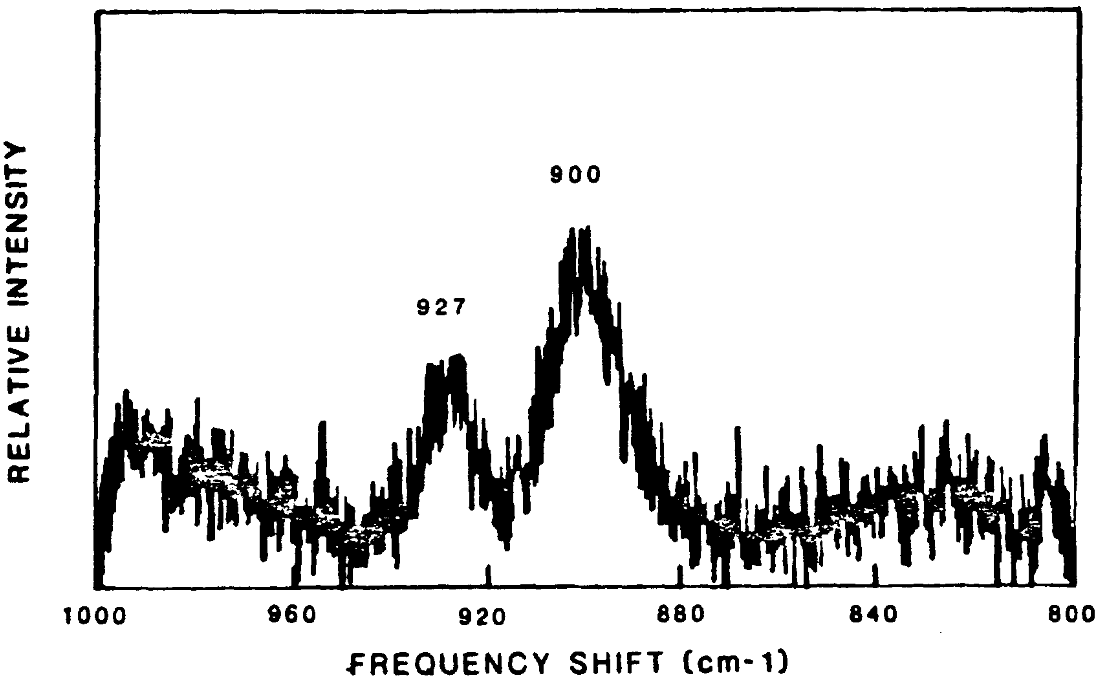

Figure II-21. Raman spectrum of complex L in CH_2Cl_2. Scan parameters: laser excitation, 457.9 nm; slitwidth, 10 cm^{-1}; scan rate, 0.5 cm^{-1}/sec; number of scans, 1; 90 degree scattering geometry; room temperature.

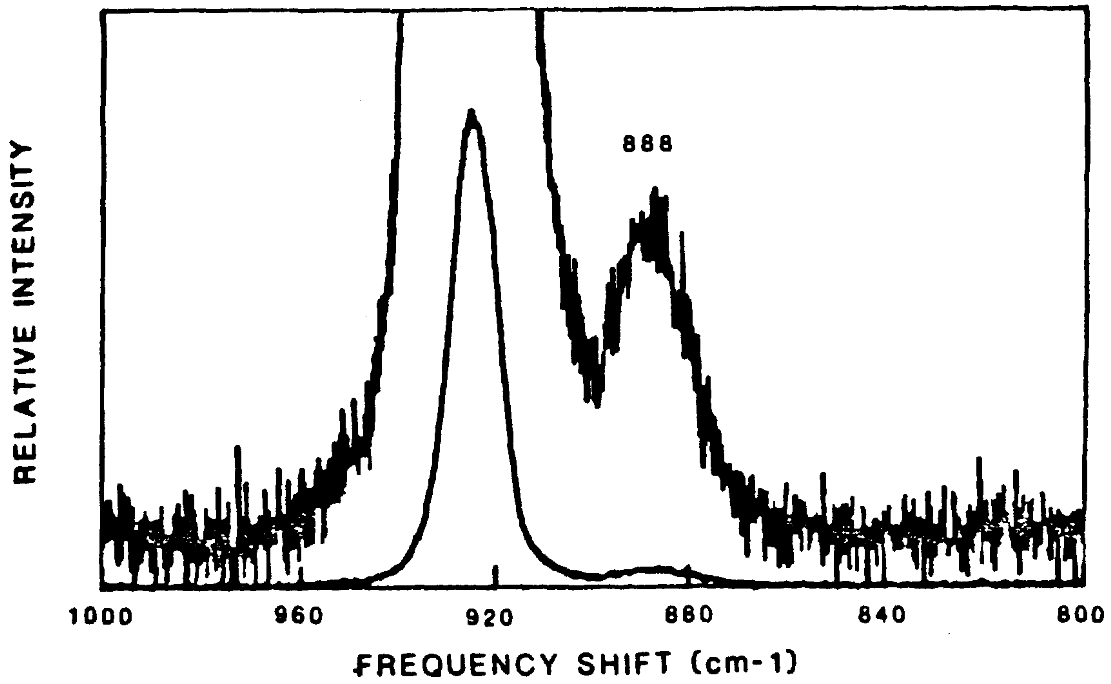

Figure II-22. Raman spectrum of complex M in CH_3CN. Scan parameters: laser excitation, 457.9 nm; slitwidth, 10 cm^{-1}; scan rate, 0.5 cm^{-1}/sec; number of scans, 1; 90 degree scattering geometry; room temperature. The upper trace is plotted at a factor of 20 times the lower trace.

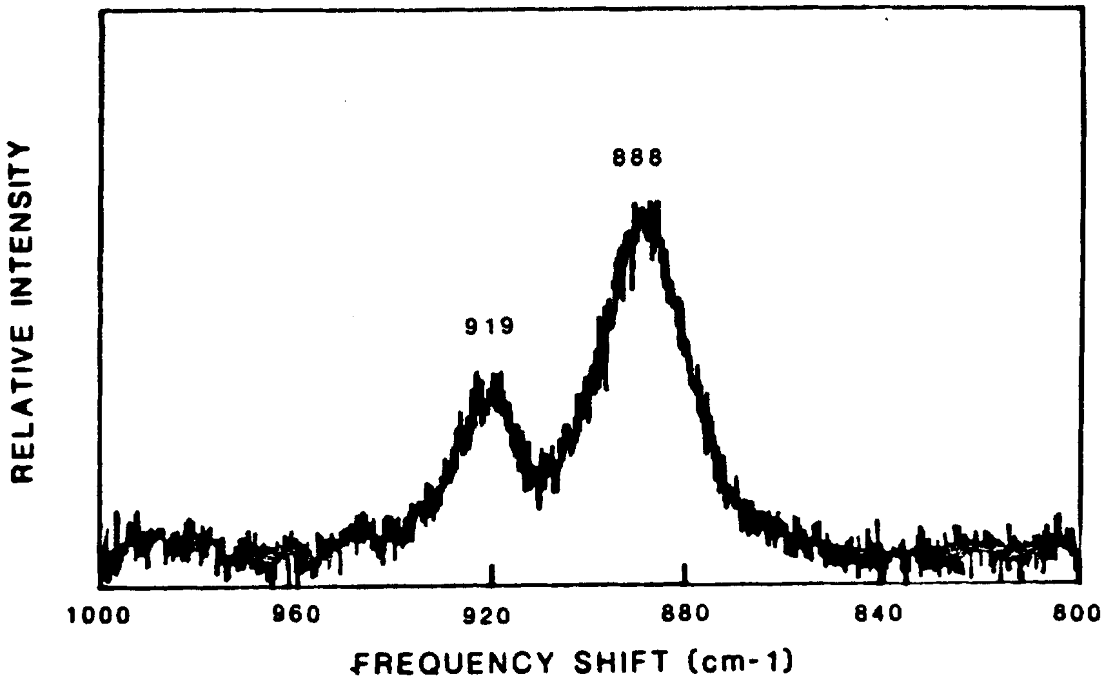

Figure II-23. Raman spectrum of complex M in CH_2Cl_2. Scan parameters: laser excitation, 457.9 nm; slitwidth, 10 cm^{-1}; scan rate, 0.5 cm^{-1}/sec; number of scans, 1; 90 degree scattering geometry, room temperature.

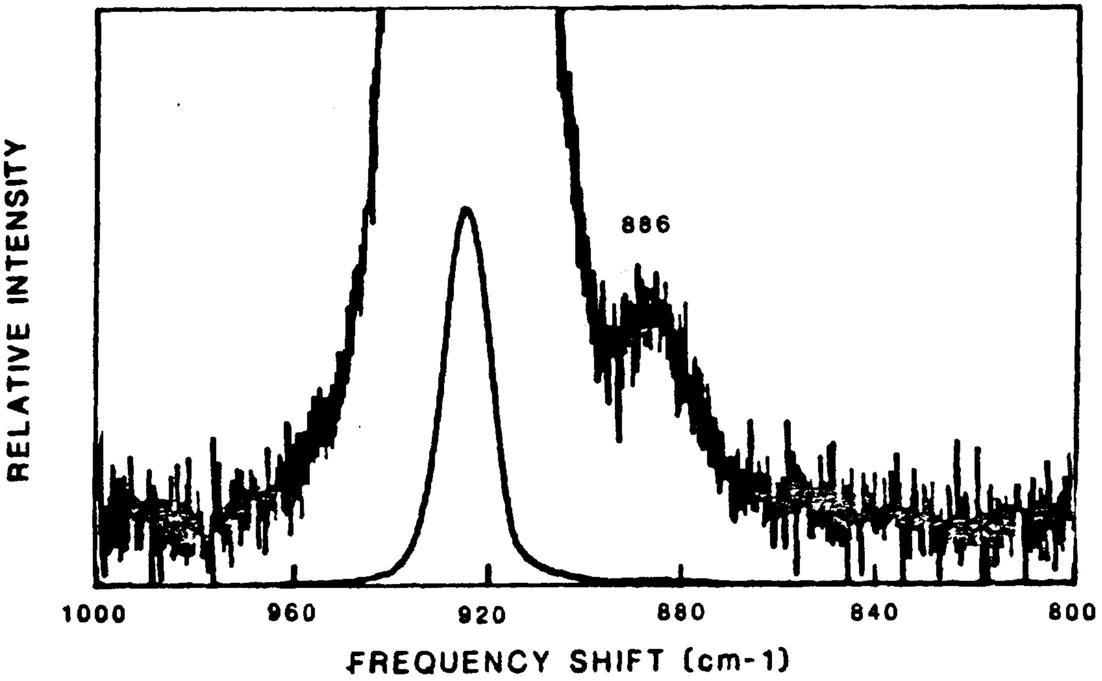

Figure II-24. Raman spectrum of complex N in CH_3CN. Scan parameters: laser excitation, 457.9 nm; slitwidth, 10 cm^{-1}; scan rate, 0.5 cm^{-1}/sec; number of scans, 2; 90 degree scattering geometry; room temperature. The upper trace is plotted at a factor of 50 times the lower trace.

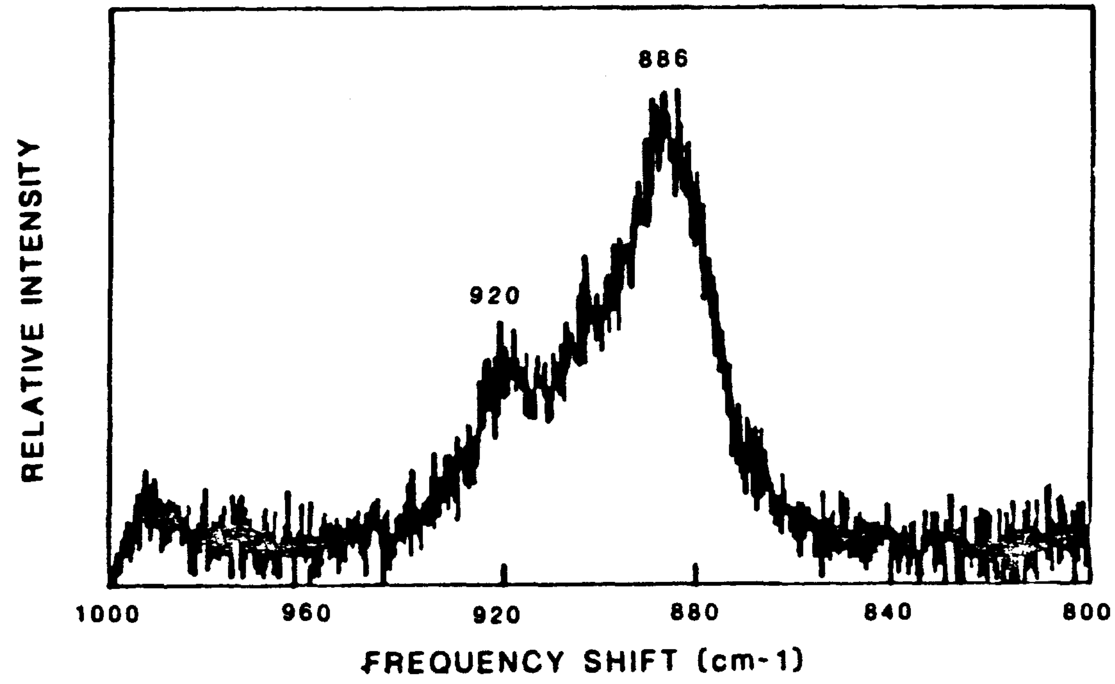

Figure II-25. Raman spectrum of complex N in CH_2Cl_2. Scan parameters: laser excitation, 457.9 nm; slitwidth, 10 cm^{-1}; scan rate, 0.5 cm^{-1}/sec; number of scans, 2; 90 degree scattering geometry; room temperature.

APPENDIX III

RESONANCE RAMAN SPECTRA OF COMPLEX K IN CH_2Cl_2 SOLUTION

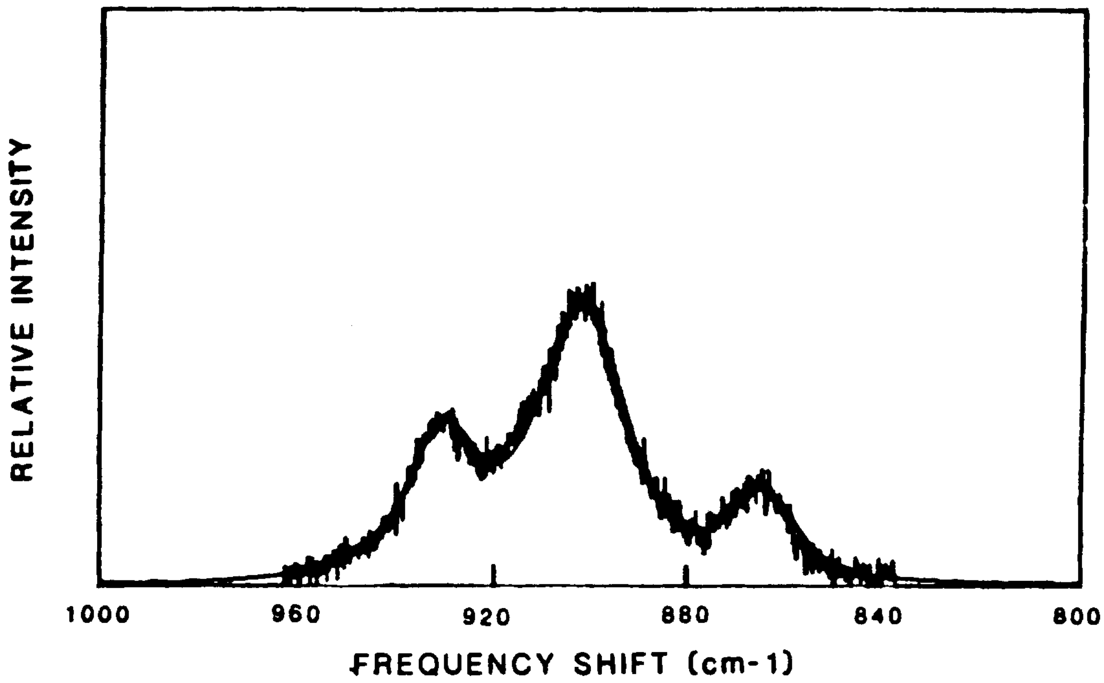

Figure III-1. Raman spectrum of ^{18}O substituted complex K in CH_2Cl_2 plotted over calculated curve. Scan parameters: laser excitation, 406.7 nm; slitwidth, 10 cm^{-1}; scan rate, 0.25 cm^{-1}/sec; number of scans, 3; 90 degree scattering geometry; room temperature.

Peak Position	Relative Height	Width (cm^{-1})
900	100	20
927	55	15
950	6	15
865	35	15
916	9	15

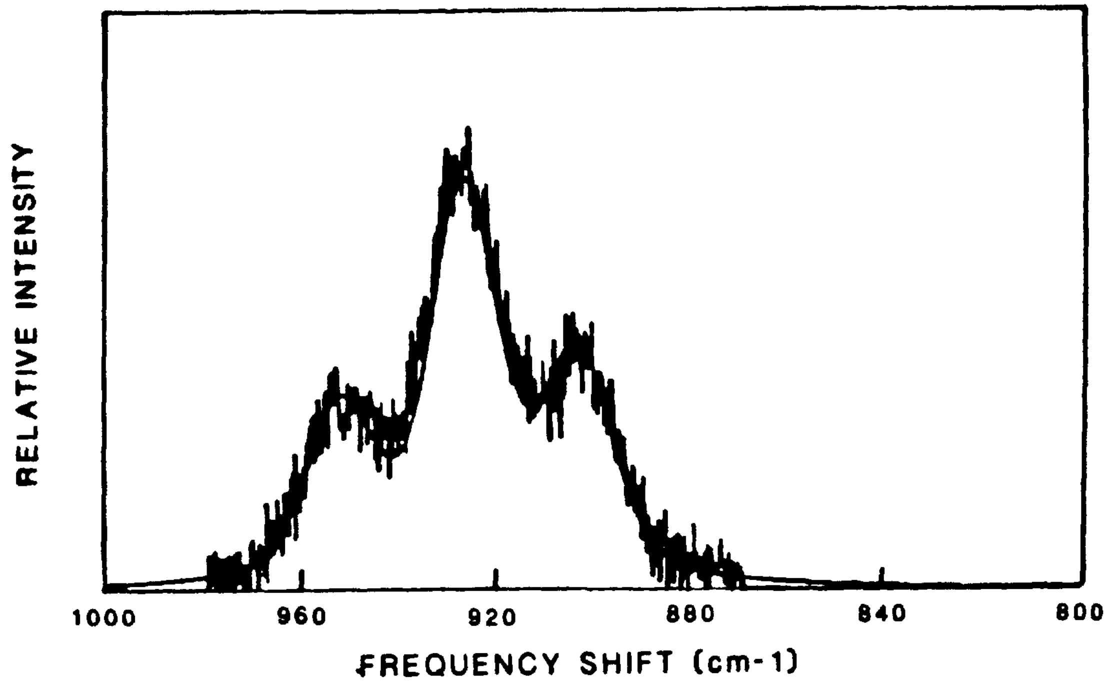

Figure III-2. Raman spectrum of ^{18}O substituted complex K in CH_2Cl_2 plotted over calculated curve. Laser excitation, 457.9 nm. Other scan parameters same as Figure III-1.

Peak Position	Relative Height	Width (cm^{-1})
900	100	20
927	178	15
950	78	15

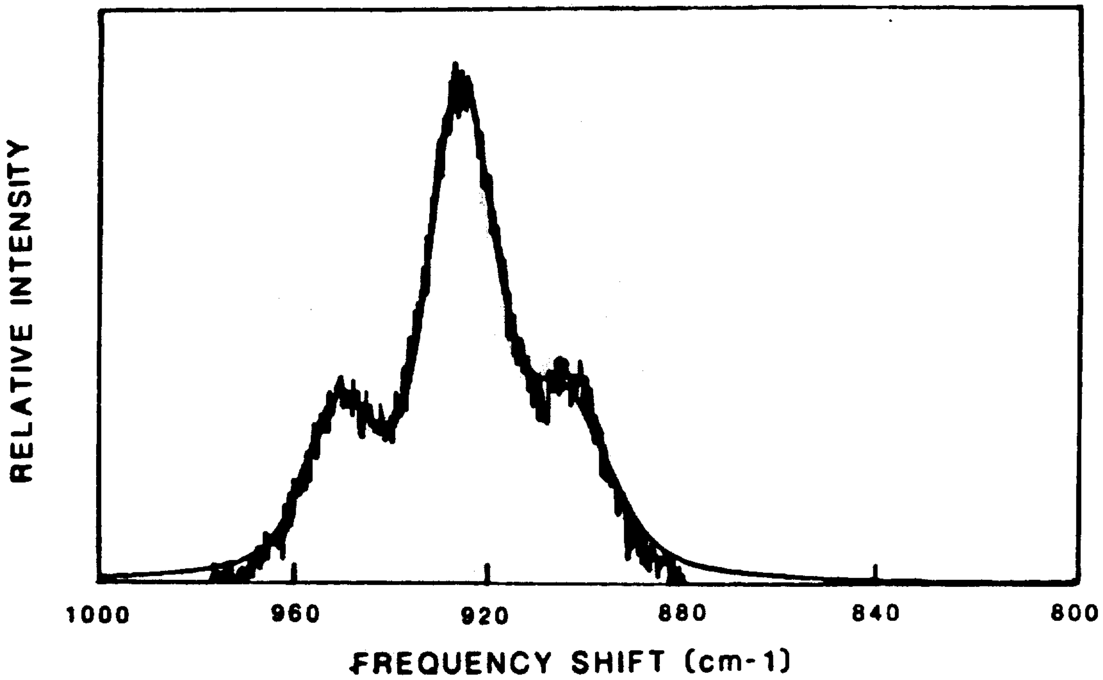

Figure III-3. Raman spectrum of ^{18}O substituted complex K in CH_2Cl_2 plotted over calculated curve. Laser excitation, 476.5 nm. Other scan parameters same as Figure III-1.

Peak Position	Relative Height	Width (cm^{-1})
900	100	20
927	300	15
950	105	15

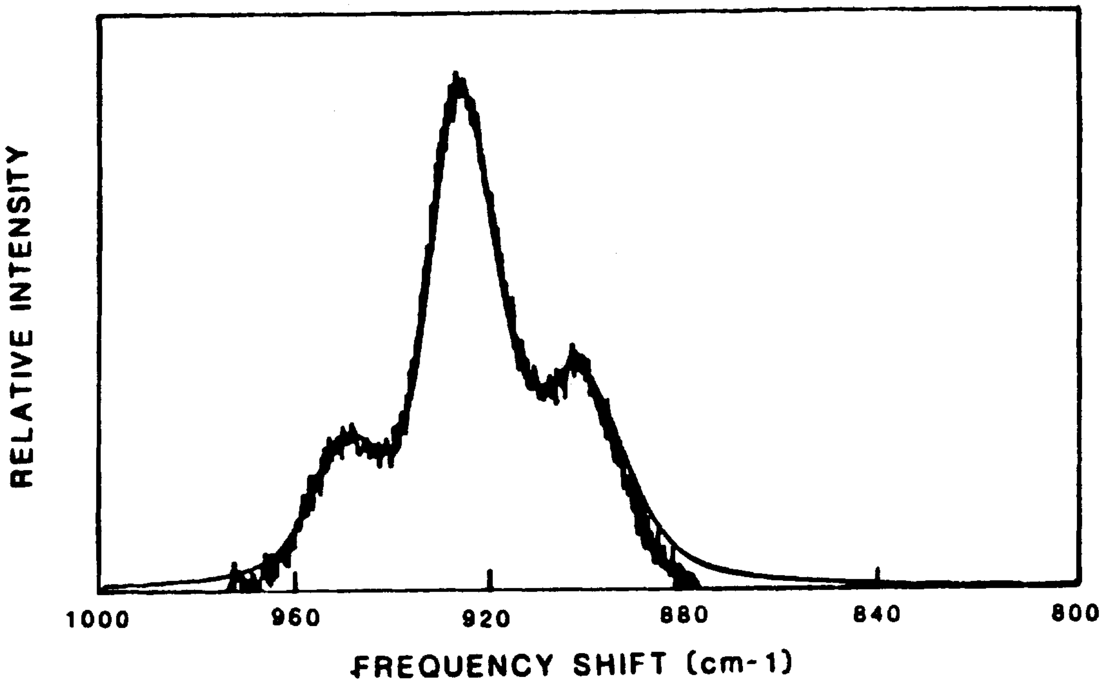

Figure III-4. Raman spectrum of ^{18}O substituted complex K in CH_2Cl_2 plotted over calculated curve. Laser excitation, 488.0 nm. Other scan parameters same as Figure III-1.

Peak Position	Relative Height	Width (cm^{-1})
900	100	20
927	254	15
950	67	15

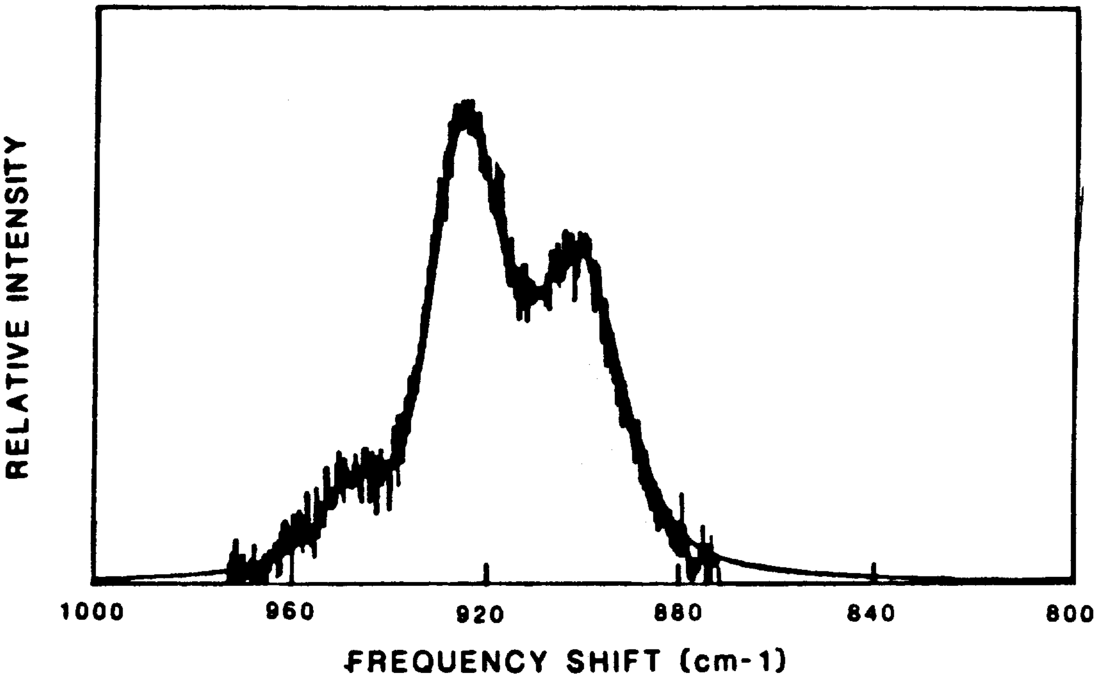

Figure III-5. Raman spectrum of ^{18}O substituted complex K in CH_2Cl_2 plotted over calculated curve. Laser excitation, 514.5 nm. Other scan parameters same as Figure III-1.

Peak Position	Relative Height	Width (cm^{-1})
900	100	20
927	144	15
950	24	15

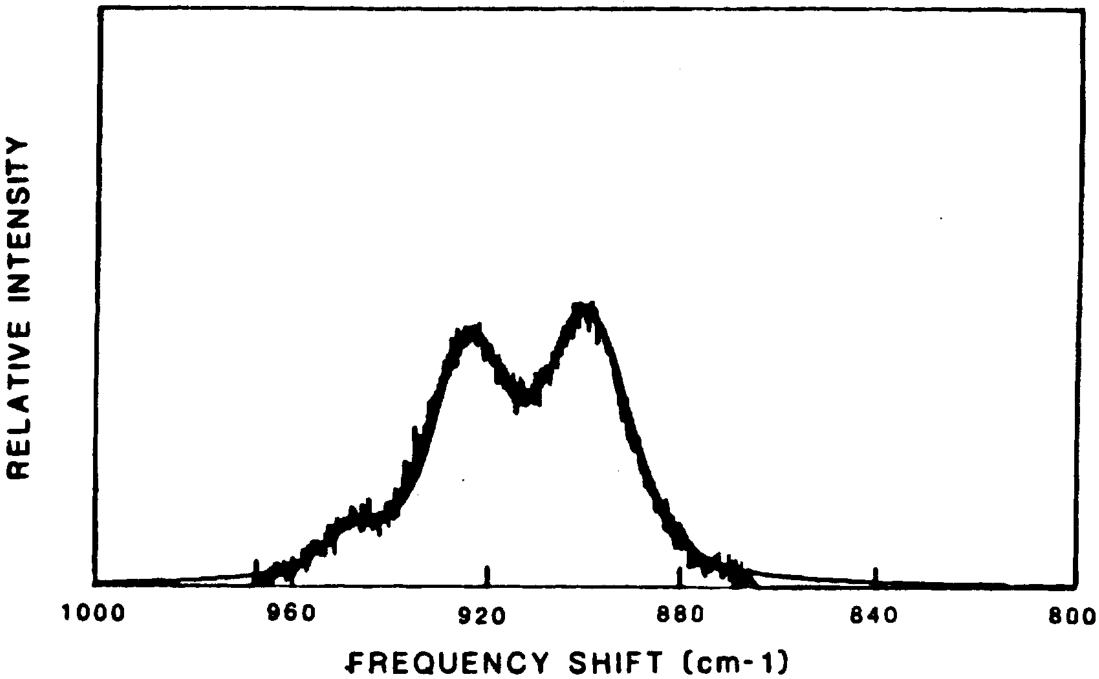

Figure III-6. Raman spectrum of ^{18}O substituted complex K in CH_2Cl_2 plotted over calculated curve. Laser excitation, 530.8 nm. Other scan parameters same as Figure III-1.

Peak Position	Relative Height	Width (cm^{-1})
900	100	20
927	89	15
950	18	15

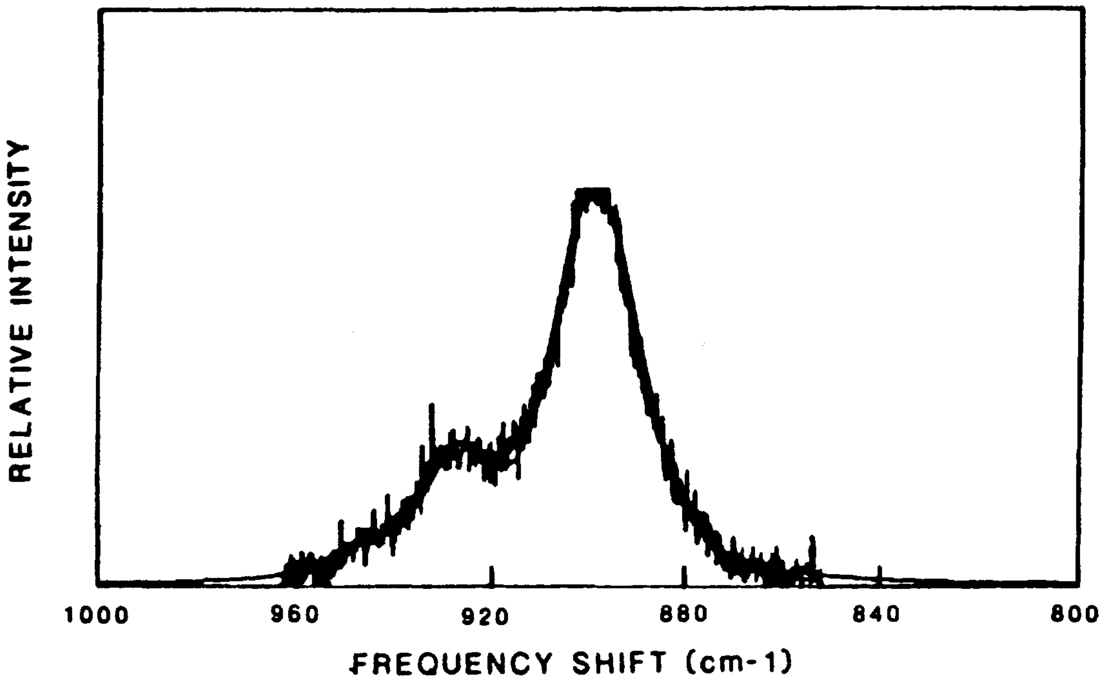

Figure III-7. Raman spectrum of ^{18}O substituted complex K in CH_2Cl_2 plotted over calculated curve. Laser excitation, 568.2 nm. Other scan parameters same as Figure III-1.

Peak Position	Relative Height	Width (cm^{-1})
900	100	20
927	30	15
950	8	15

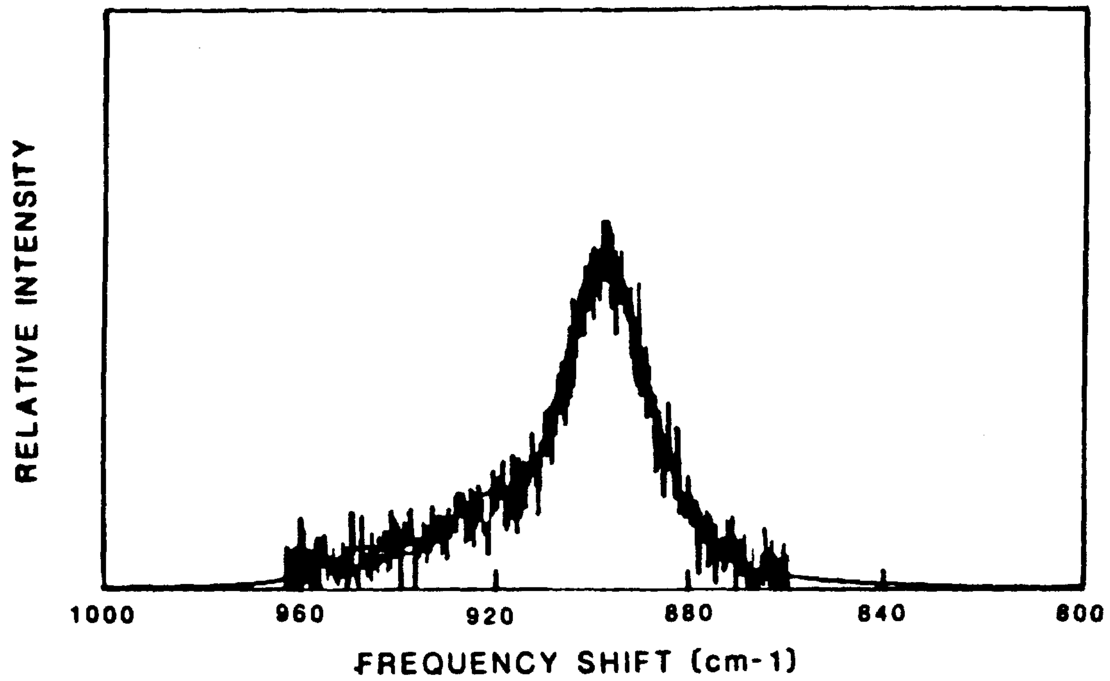

Figure III-8. Raman spectrum of ^{18}O substituted complex K in CH_2Cl_2 plotted over calculated curve. Laser excitation, 647.1 nm. Other scan parameters same as Figure III-1.

Peak Position	Relative Height	Width (cm^{-1})
900	100	20
927	20	15
950	10	15

BIOGRAPHICAL NOTE

The author was born October 27, 1948, in Portland, Oregon, the second of three children to Charles B. and E. Adele Willis. He attended grade school and high school in Gresham, Oregon. He then entered Oregon State University and received his B.S. in Chemistry in June, 1970, along with a commission as a Second Lieutenant in the U.S. Air Force.

While stationed at Holloman AFB, New Mexico, the author married Barbara Ann Zwetschke on June 19, 1971. After being stationed at Yokota AB, Japan for two years, he was released from active duty in July, 1974. He then entered Wright State University in Dayton, Ohio and was graduated with an M.S. in Chemistry in August, 1977, whereupon he enrolled at the Oregon Graduate Center to study for his Ph.D. degree in Chemistry.